Investigation of Recessed and Concealed Sprinklers Activation in Wind Tunnel Plunge Test and in BRANZFIRE Computer Model

by
Xinjun (Kevin) YU

Supervised by

Dr. Michael Spearpoint

Fire Engineering Research Report

March 2007

A thesis submitted in partial fulfilment of the requirements for the degree of
Master of Engineering in Fire Engineering

Department of Civil Engineering
University of Canterbury
Private Bag 4800
Christchurch, New Zealand

ABSTRACT

Installation of exposed fire sprinklers may cause inconvenience in areas where architectural and interior presentation is significant. In order to overcome this inconvenience, recessed and concealed sprinklers were created and are applied widely. Response Time Index (RTI) and C-factor are the thermal sensitivity (intrinsic parameters) used to characterise a sprinkler. They are also used as input parameters in computer fire models to simulate sprinkler response time. However, the RTI and C-factor are not published by the manufactures. Therefore the RTI and C-factor of the recessed and concealed sprinklers have been analysed and determined in this research.

In order to obtain the RTI of the recessed and concealed sprinklers, four of the most commonly used sprinkler models (two recessed and two concealed) in New Zealand have been investigated in plunge test experiment by using a wind tunnel in this research.

The UC3 wind tunnel used to conduct the plunge test has been fabricated in this research. This work has demonstrated that the UC3 wind tunnel could provide a very stable and uniform temperature profile in the test section. However, the velocity uniformity of the tunnel needs to be improved in the future.

The “apparent” RTI for different recessed and concealed sprinkler models (two recessed and two concealed) have been determined in the plunge test experiment. It should be noted that the “final calculated RTI” for each tested recessed and concealed sprinklers has been denoted as “apparent RTI” in this study.

BRANZFIRE computer model has been used to model the fire scenarios in the full scale fire tests conducted by Bill and Heskestad (1995). The best input fire object location, the best input sprinkler distance below the ceiling and the input “apparent C-factor” in BRANZFIRE for the flush, recessed, concealed and the recessed sidewall sprinklers have been determined in this research.

This work has generally improved the guidance available to fire safety engineers for the RTI and C-factor of the recessed and concealed sprinklers.

ACKNOWLEDGEMENTS

The research was carried out at the University of Canterbury under the guidance of Dr. Michael Spearpoint. I would like to thank and acknowledge the following people who have supported and contributed to this research.

Dr. Michael Spearpoint, my supervisor, for his professional instruction, invaluable advice and constant encouragement throughout this research project.

Ms. Colleen Wade, for her invaluable advice in this research and patience for providing me the user licence for the BRANZFIRE computer software.

Dr. Charles Fleischmann, for his invaluable advice in this research and his contribution to the fire engineering program.

Mr. Grant Dunlop and Mr. Bob Wilsea-Smith, for their skill and patience in designing and constructing the experimental apparatus.

Mr. Roger Harrison and Mr. Jerry Chang, Ph.D. students, for their concern and encouragement.

Ms. Christine Mckee and Mr. Dave Lane, for their help to find resources in the engineering library.

The New Zealand Fire Service Commission, for their funding to support the fire engineering program.

Finally, I would like to thank my spouse and my parents for their support and encouragement throughout my years of study.

TABLE OF CONTENTS

LIST OF FIGURES

LIST OF TABLES

NOMENCLATURE

Symbol	Description
A_f	Horizontal burning area of the fuel (m^2)
C	Conductivity factor of sprinkler $(m/s)^{1/2}$
d_{max}	Depth below the ceiling at the location of the occurrence of maximum ceiling jet temperature (m)
H	Height of the ceiling above the base of the fire (m)
ΔH_c	Heat of combustion (kJ/g)
$\dot{m}''$	Free burn mass loss rate ($kg/m^2.s$)
ΔP	Pressure differential reading from the pressure transducer (Pa)
$\dot{Q}$	Heat release rate (kW)
r	Radial distance from the centre of the plume (m)
RTI	Response time index of sprinkler $(m.s)^{1/2}$
t	Time (s)
t_r	Sprinkler response time in plunge test (s)
T_e	Temperature of sprinkler link/detector (K)
T_{cj}	Ceiling jet temperature (K)
T_{int}	Initial temperature (ambient temperature) (K)
T_a	Hot gas temperature in the wind tunnel (^oC)
ΔT_b	Mean (actuation temperature) operating temperature of the sprinkler minus the mount temperature (^oC)
ΔT_g	Hot gas temperature in the test section minus the mount temperature (^oC)
U	Air velocity in the test section of the wind tunnel (m/s)

U_{cj}	Ceiling jet velocity (m/s)

Greek symbol	Description
χ	Combustion efficiency

CHAPTER 1

1 INTRODUCTION

1.1 Background

In the latter part of the nineteenth century, the first sprinkler head was patented in U.S. Unlike modern sprinkler technology as we know it today, the first sprinkler was a perforated head controlling by a valve that was held closed against water pressure by a heavy spring made of low fusing material (Grant 1996). During the last century, sprinkler development was rapid, and the performance and reliability of sprinklers had been improved continually. Nowadays, the concept of an automatic sprinkler is defined as a "thermosensitive device designed to react at a predetermined temperature by automatically releasing a stream of water and distributing it in a specified pattern and quantity over a designated area" (International Standard 2004; Isman 2003).

The appearance of the installed sprinkler head may affect the aesthetics in some architecturally sensitive areas. In order to overcome this flaw, recessed and concealed sprinklers were created and are used currently. The heat-responsive element of recessed and concealed sprinklers is partially or fully hidden above the ceiling, therefore the visible part of sprinkler below the ceiling is diminished. To date, due to the aesthetic advantages of the recessed and concealed sprinkler, the use of them has become increasingly popular.

In the past, fire protection engineering applications relied on straightforward numerical equation calculations. Even though these manual approaches can provide good estimations on calculating some simple fire effects (e.g. the smoke layer height and temperature within a fire compartment), they are not suited to perform extensive tedious and lengthy calculations. Based on the limitations of manual calculation approaches, computer fire models were created and have been developed. By comparing with the manual approaches, fire models advance a more accurate, cost-effective and time effective solution, and therefore they are increasingly used by fire

professionals (e.g. designer and architect) and have become an essential part of fire protection engineering.

The background knowledge regarding sprinklers and computer fire models are described below in this section to provide fundamental information for the reader.

1.2 Sprinkler types and sprinkler operation mechanism

As described in the ISO 6182 - 1 (International Standard 2004), sprinklers can be classified by five different characteristics. These five classifications are listed as follows:

- Types of sprinkler according to type of heat-responsive element
- Types of sprinkler according to type of water distribution
- Types of sprinkler according to position
- Special types of sprinkler
- Types of sprinkler according to sprinkler sensitivity

A brief description of the different types of sprinklers is described below. It should be noted that the following descriptions are focused on sprinklers which are more commonly used in New Zealand and are mainly referenced from ISO 6182-1 (International Standard 2004). The reader can refer to ISO 6182-1 (International Standard 2004) and Isman (2003) for a full set information on all types of sprinklers.

1.2.1 Types of sprinkler according to type of heat-responsive element

Fusible element sprinklers and glass bulb sprinklers are the two different types of sprinklers classified according to their heat-responsive element. The sprinklers' definition and operation mechanism are shown below.

1.2.1.1 Fusible element sprinkler

Fusible element sprinkler is a sprinkler that operates by the melting of a fusible component under the influence of heat. Typically, when a fusible element sprinkler is exposed to the heated environment, the metal solder melts at its predetermined temperature. The melted metal solder loosens the spring-loaded element and activates the sprinkler. Figure 1.1 illustrates the structure of a typical fusible element sprinkler.

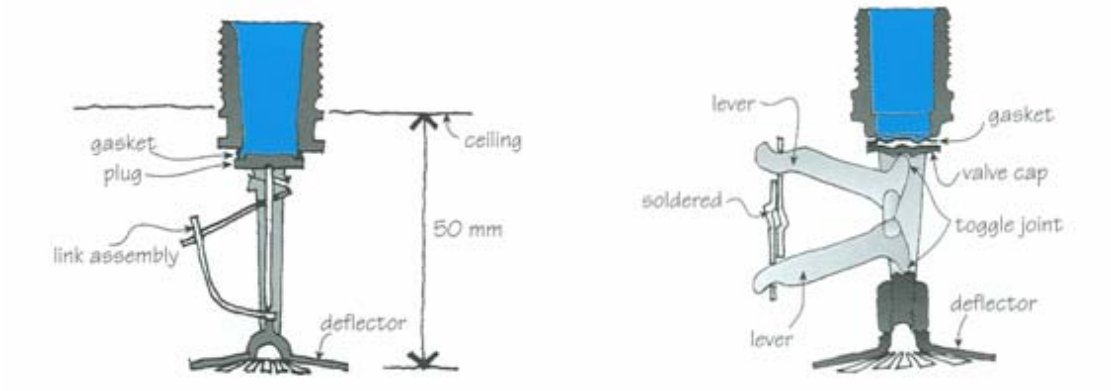

Figure 1.1: Typical fusible element sprinkler (Saunders and Conder 2002)

1.2.1.2 Glass bulb sprinkler

Glass bulb sprinklers are a sprinkler system that operates under the influence of heat by bursting the glass bulb through an increase of pressure resulting from the expansion of the fluid enclosed inside. As shown in Figure 1.2, the sprinkler glass bulb is filled with special liquid and an air bubble. When the glass bulb is heated, the liquid inside the glass bulb expands and compresses the air bubble. The pressure acts on the glass bulb and increases gradually due to heat expansion. The glass bulb bursts when the air bubble is completely absorbed by the liquid. Figure 1.2 below shows the configuration of a typical glass bulb sprinkler.

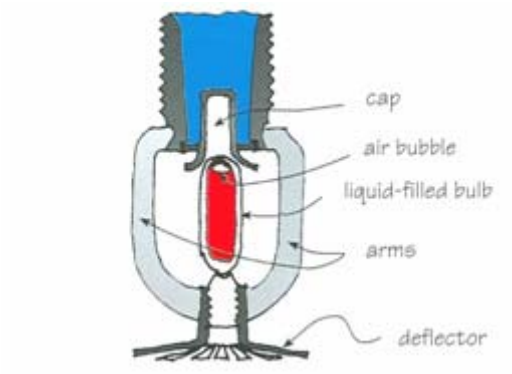

Figure 1.2: Typical glass bulb sprinkler (Saunders and Conder 2002)

1.2.2 Types of sprinkler according to type of water distribution

Based on the types of water distribution, four different types of sprinkler can be classified, which are the conventional sprinkler, spray sprinkler, sidewall sprinkler and flat spray sprinkler. The first three types of sprinkler are described as below.

1.2.2.1 Conventional sprinkler

A conventional sprinkler is a sprinkler that provides spherical water distribution directed downward and at the ceiling for a specific protection area (40 % to 60 % of the total water flow is spray downward initially). When the conventional sprinkler is activated, a large portion of water sprays and impinges onto the ceiling. The combination of the impinged water and the directed spray downward forms a spherical-shape spray pattern as shown in Figure 1.3 below.

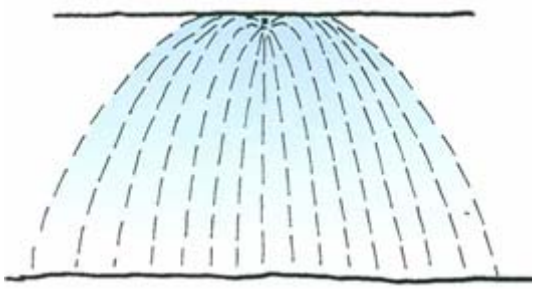

Figure 1.3: Spray pattern of a typical conventional sprinkler (Saunders and Conder 2002)

1.2.2.2 Spray sprinkler

Spray sprinklers are a sprinkler that provides a parabolic water distribution directed downward for a specific protection area (80 % to 100 % of the total water flow is spray downward initially). Thompson (1964) states that the more effective way to suppress fire is to direct all the water downward and horizontally covering the specific protection area, and therefore spray sprinklers are recognized as a more efficient sprinkler than the conventional sprinkler. Figure 1.4 shows the spray pattern of a typical spray sprinkler.

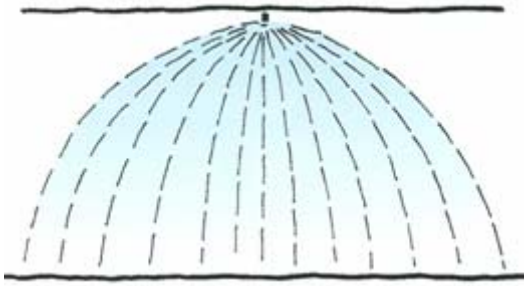

Figure 1.4: Spray pattern of a typical spray sprinkler (Saunders and Conder 2002)

1.2.2.3 Sidewall sprinkler

Sidewall sprinklers are a sprinkler that provides a half parabolic water distribution for a specific protection area. Sidewall sprinklers are normally considered to be installed in some architecturally sensitive areas where it is not desirable for the piping arrangement to be observed across the ceiling. Figure 1.5 illustrates the configuration of a typical sidewall sprinkler.

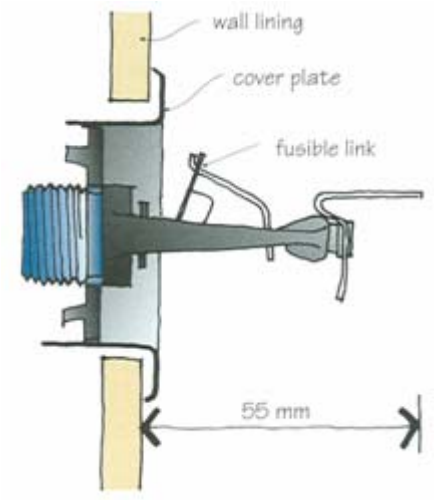

Figure 1.5: Typical sidewall sprinkler (Saunders and Conder 2002)

1.2.3 Types of sprinkler according to position

Three different types of sprinkler can be classified based on their position. These sprinklers are the upright sprinkler, pendent sprinkler and horizontal sprinkler. Descriptions are provided below (except for the horizontal sprinkler).

1.2.3.1 Upright sprinkler

The upright sprinkler is a sprinkler where the discharge orifice is arranged upwards, and therefore the water stream is directed upwards against the deflector during the sprinkler operation. Figure 1.6 shows the appearance of a typical upright sprinkler.

Figure 1.6: Typical upright sprinkler (Tyco Fire & Building Products 2006)

1.2.3.2 Pendent sprinkler

In contrast to the upright sprinkler, pendent sprinkler is a sprinkler where the discharge orifice is arranged downwards, and therefore the water stream is directed downwards against the deflector during the sprinkler operation. The appearance of a typical pendent sprinkler is shown in Figure 1.7 below.

Figure 1.7: Typical pendent sprinkler (Tyco Fire & Building Products 2006)

1.2.4 Special types of sprinkler

There are ten types of special sprinkler listed in the ISO 6182-1 (International Standard 2004), these include the dry upright sprinkler, dry pendent sprinkler, flush sprinkler, recessed sprinkler, concealed sprinkler, on/off sprinkler, multiple-orifice pendent sprinkler, coated sprinkler, sprinkler with water shield and extended-coverage sprinkler. The flush sprinkler, recessed sprinkler and concealed sprinkler are described as below.

1.2.4.1 Flush sprinkler

Flush sprinklers are a sprinkler where all or part of its heat-responsive element is exposed below the lower plane of the ceiling lining, but part or all of its body (including the shank thread – the part that connects to a pipe) is mounted above the lower plane of the ceiling lining.

Figure 1.8 below shows the configurations of a typical flush sprinkler before and after its operation. When a flush sprinkler is exposed to a fire, the heat-responsive element starts to absorb heat from its surrounding environment. The heat-responsive element

falls away (or bursts) and activates the sprinkler when it reaches the predetermined actuation temperature (operating temperature). It should be noted that the deflector of the flush sprinkler drops down to its operational position at the point when the sprinkler is activated (see Figure 1.8).

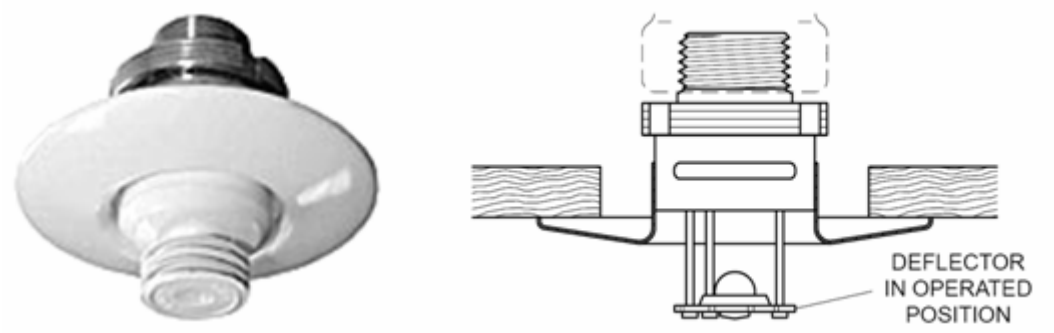

Figure 1.8: Typical flush sprinkler before and after its operation (Tyco Fire & Building Products 2006)

1.2.4.2 Recessed sprinkler

The recessed sprinkler is a sprinkler where all or part of its body (excluding the shank thread) is mounted within the recessed housing. As illustrated in Figure 1.9, a recessed sprinkler consists of its main body and a recessed escutcheon. The recessed escutcheon is a two-piece component and consists of a closure and a mounting plate (see Figure 1.9). The mounting plate can be adjusted vertically within the closure to provide a recess condition for the sprinkler head. It should be noted that the recessed sprinkler can also be classified as a recessed pendent and recessed sidewall sprinkler. The information regarding all types of recessed sprinkler are detailed in Tyco (Tyco Fire & Building Products 2006).

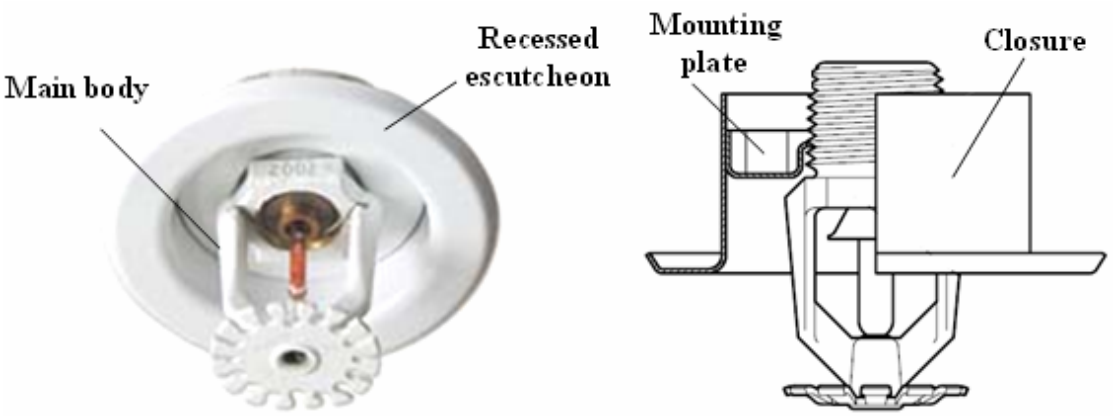

Figure 1.9: Typical recessed pendent sprinkler (Tyco Fire & Building Products 2006)

1.2.4.3 Concealed sprinkler

Concealed sprinkler is a sprinkler that can be defined as a recessed sprinkler having a cover plate. The main distinction of the concealed sprinkler is that the entire body of it is hidden above the ceiling by using a cover plate. As shown in Figure 1.10, the bottom of the cover plate is almost flush with the lower plane of the ceiling, this advantage provides the greatest visual effect for aesthetics.

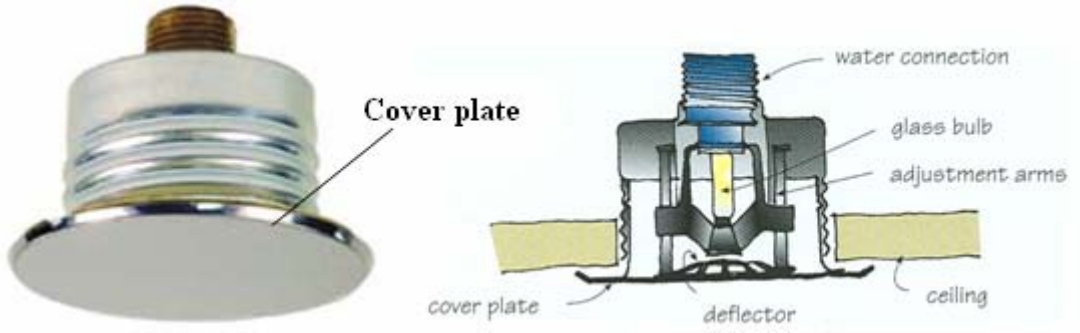

Figure 1.10: Typical concealed sprinkler (Saunders and Conder 2002; Tyco Fire & Building Products 2006)

It should be noted that concealed sprinklers are a sprinkler that approaches two stages of activation (cover plate activation and head-responsive element activation). Figure 1.11 below shows the configuration of a typical cover plate assembly of the concealed sprinkler. Essentially, the cover plate is soldered to the “retainer” at three points. When a concealed sprinkler is exposed to a fire, its solder melts at the pre-set melting temperature. The cover plate drops down when the force from the ejection spring

becomes larger than the connecting force provided by the solder. The actuation temperature of the cover plate is lower than the heat-responsive element. Hence, the heat-responsive element will be exposed to the heated environment directly and is ready to be activated after the cover plate falls away. The heat-responsive element is activated at its predetermined actuation temperature.

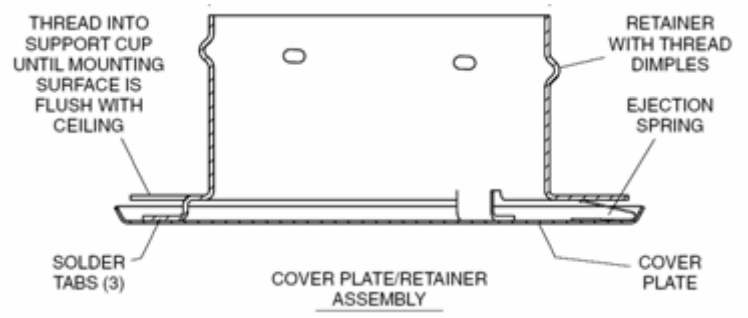

Figure 1.11: Typical cover plate assembly of concealed sprinkler (Tyco Fire & Building Products 2006)

It should be noted that the deflector of concealed sprinkler drops down to its operational position after the cover plate drops down (see Figure 1.12).

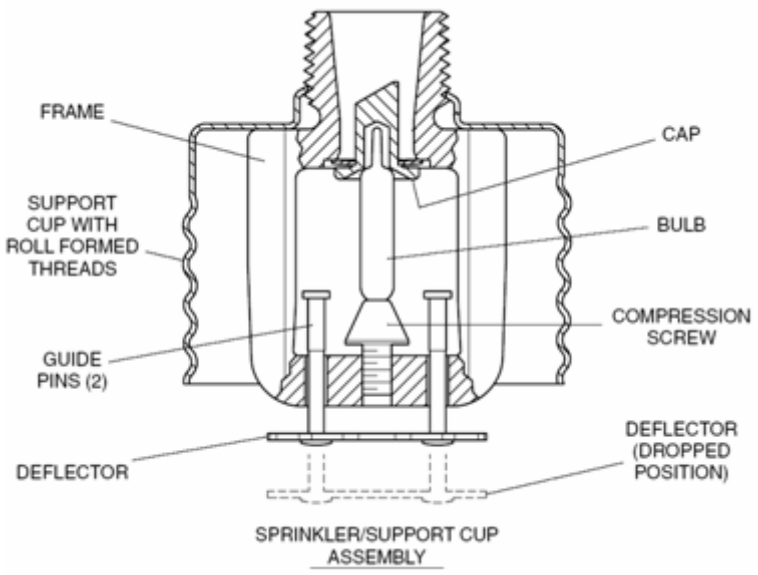

Figure 1.12: Typical sprinkler assembly of concealed sprinkler (Tyco Fire & Building Products 2006)

1.2.5 Types of sprinkler according to sprinkler sensitivity

Fast-response, special-response and standard-response sprinklers are the three types of sprinkler classified depending on their thermal sensitivity (RTI and C-factor). The definition of the RTI and C-factor are represented as follows:

Response Time Index (RTI) – A measurement that accounts for the sprinkler thermal inertia and indicates how quickly the sprinkler can absorb heat from its surroundings sufficient to cause activation (Bill and Heskestad 1995; Fleming 2003; Madrzykowski and Fleming 2003).

Conductivity factor (C-factor) – A measurement that accounts for the heat loss due to conduction between the heat-responsive element and the fitting of the sprinkler (International Standard 2004).

The combination of the RTI and C-factor can be used to determine the types of sprinkler. ISO 6182-1 (International Standard 2004) provides the RTI and C-factor range for each type of sprinkler, those thermal sensitivity ranges (limits) are also illustrated in Figure 1.13 below.

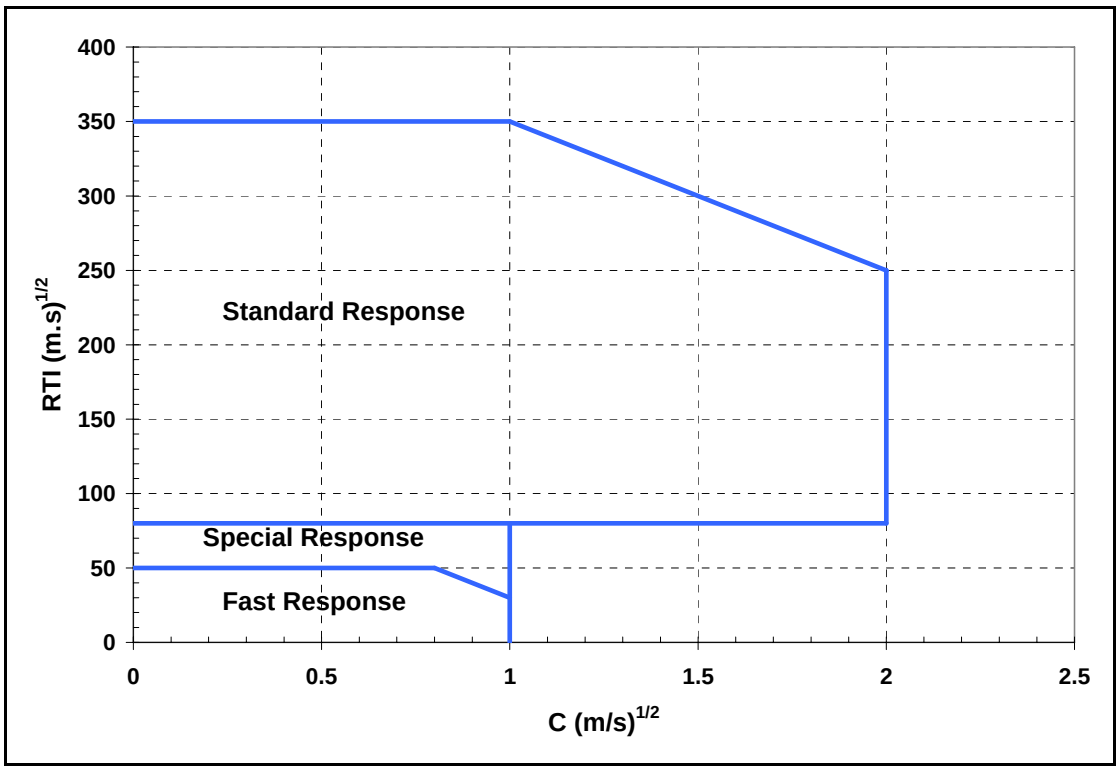

Figure 1.13: RTI and C-factor limits (International Standard 2004)

1.2.5.1 Fast, special and standard-response sprinklers

Fast-response sprinklers can be defined when its $\text{RTI} \le 50\,(\text{m}\cdot\text{s})^{1/2}$ and its C factor $\le 1\,(\text{m}/\text{s})^{1/2}$.

Special-response sprinklers can be defined when its $50\,(\text{m}\cdot\text{s})^{1/2} < \text{RTI} \le 80\,(\text{m}\cdot\text{s})^{1/2}$ and its C factor $\le 1\,(\text{m}/\text{s})^{1/2}$.

Standard-response sprinklers can be defined when its $80\,(\text{m}\cdot\text{s})^{1/2} < \text{RTI} \le 350\,(\text{m}\cdot\text{s})^{1/2}$ and its C factor $\le 2\,(\text{m}/\text{s})^{1/2}$.

1.3 Sprinkler nominal operating temperature

The nominal operating temperatures (actuation temperatures) of automatic sprinklers range from 57 ^{o}C to 343 ^{o}C and are determined by the "Test of static operation" represented in Section 7.7.1 in ISO 6182-1 (International Standard 2004). The specified nominal operating temperature of a sprinkler can be found either from its

heat-responsive element or its assembly component. For example, the nominal operating temperature of a typical fusible element sprinkler is marked on its soldered link. However, the nominal operating temperature of a typical glass bulb sprinkler is marked on its deflector.

Colour codes are also used to indicate the nominal operating temperatures of sprinklers (see Table 1.1).

Table 1.1: Nominal operating temperatures (International Standard 2004)

Fusible element sprinklers	
Nominal operating temperature range (^{o}C)	**Yoke arm colour code**
57 to 77	uncoloured
80 to 107	white
121 to 149	blue
163 to 191	red
204 to 246	green
260 to 302	orange
320 to 343	orange
Glass bulb sprinklers	
Nominal operating temperature (^{o}C)	**Liquid colour code**
57	orange
68	red
79	yellow
93	green
107	green
121	blue
141	blue
163	mauve
182	mauve
204	black
227	black
260	black
343	black

1.4 Sprinkler systems

The sprinkler system is one of the fire protection systems commonly used to safeguard people and minimise fire damage in the event of fire. It is reliable and can provide a very effective protection for occupants. Rohr (1998) states that the National Fire Protection Association (NFPA) record shows that there were no more than two people killed by a fire in a completely sprinklered public assembly, institutional, educational, or residential building where the system was operating properly. Essentially, a sprinkler system consists of sprinkler heads, monitoring valves, alarms, a piping system and a fire service inlet. The typical layout of a sprinkler system is shown in Figure 1.14.

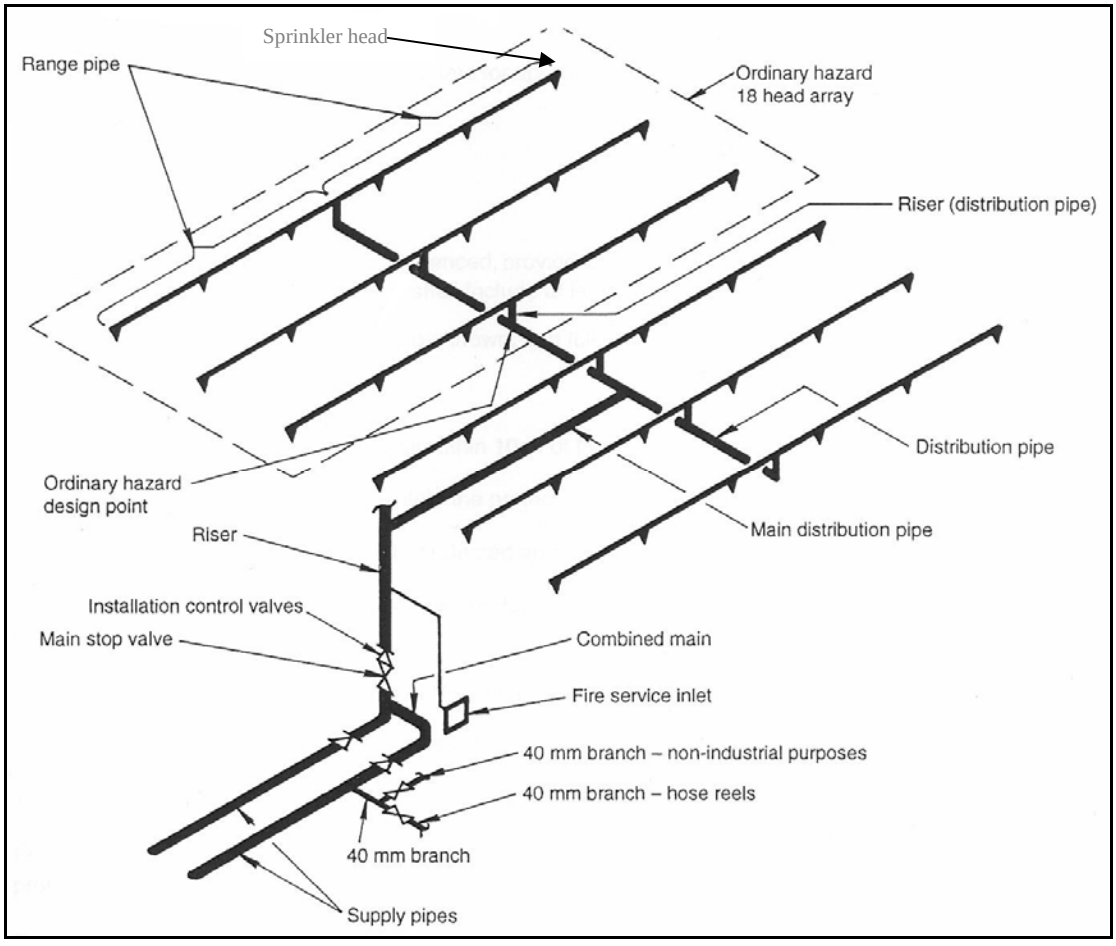

Figure 1.14: Typical layout of a sprinkler system (Standards New Zealand 2003)

As described in the automatic sprinkler systems handbook (Solomon 1994), nine types of sprinkler systems can be classified, these include wet pipe system, dry pipe

system, preaction system, deluge system, combined dry pipe-preaction system, antifreeze system, circulating closed-loop system, girded system and looped system. Wet pipe system, dry pipe system, preaction system and deluge system are considered as the four basic types of sprinkler systems, all of the others can be categorised into one of the basic four types (Fleming 2002). It should be noted that the description of all four basic types of sprinkler systems below is mainly referenced from Solomon (1994).

1.4.1 Wet pipe system

Wet pipe systems are a sprinkler system where all automatic sprinklers are installed to a piping system containing water and are connected to a water supply. Because the water contained in the system is pressurised at all times, it will discharge immediately when the sprinklers are activated. This sprinkler system is the most reliable and simplest, and has the lowest maintenance cost of all sprinkler systems. Therefore it should always be the first option for designers and it is the most recommended type of sprinkler system (Fleming 2002; Puchovsky 2003; Solomon 1994).

1.4.2 Dry pipe system

The dry pipe system is a sprinkler system where all automatic sprinklers are installed into a piping system containing air or nitrogen under pressure. Water used to suppress fire is held back by a special dry valve. When one or more sprinklers are activated, the pressure provided from the air or nitrogen can no longer handle the pressure from the water side and then the valve will open due to the water pressure. The opened valve allows the water to flow into the piping system and discharge from the activated sprinklers. This sprinkler system is recommended to be used in places where water in the piping is at risk from freezing. Therefore it is a good substitution for the wet pipe system in areas prone to freezing (Fleming 2002; Solomon 1994).

1.4.3 Preaction system

Preaction systems are a sprinkler system where all automatic sprinklers are installed to a piping system containing air which may or may not be pressurised. Water used to

suppress fire is held back by a special valve which is controlled by a separate fire detection system. After the detection system is activated, the valve is opened and allows water to flow into the sprinkler piping system. This type of sprinkler system is suitable to be used in places where there is a concern that accidental water discharge will result in damaging the contents inside the building such as computer and mechanical machinery (Fleming 2002; Solomon 1994).

1.4.4 Deluge system

The deluge system is a sprinkler system where open sprinklers are installed in a piping system connected to a water supply. Similar to the preaction system, water used to suppress a fire is held back by a special valve which is controlled by a separate fire detection system. When the detection system is activated, the valve is opened and permits water to flow into the piping system. Because open sprinklers are used, water will discharge from all sprinkler heads simultaneously. This sprinkler system is solely controlled by the fire detection system, and therefore it is recommended to be used for protection against rapid flame spreading and high hazard fires (Fleming 2002; Solomon 1994).

1.5 Computer fire model

Computer fire models are computer programs that can be used to solve a large number of arithmetic and differential (fire dynamics) equations simultaneously. They can provide a fast performance and accurate estimation for fire protection design, and therefore they have become primary tools for fire engineers. Nowadays, the two most commonly used computer fire models are the zone model and field model. They not only can be used to simulate the consequences of a fire within an enclosure but can be used to design and evaluate the activation time of sprinklers.

The zone model is an approach that solves the conservation equations for control volumes. It is assumed that there are two control volumes (homogenous zones) formed within a fire enclosure, where the upper zone contains the hot gases generated from the combustion, and the lower zone contains all space underneath the upper zone. BRANZFIRE (Wade 2004a), CFAST (Peacock et al. 2005), CCFM (Forney et al.

1990), LAVENT (Davis and Cooper 1989), and FPEtool (Nelson 1990) are typical zone models.

The field model is an approach that solves the fundamental equations (e.g. the Navier-Stokes equations) of mass, momentum, and energy conservation for many small cells divided from the space of the simulated enclosure. Fire Dynamics Simulator (FDS) (McGrattan and Forney 2004) and JASMINE (Cox and Kumar 1987) are the typical field models.

The reader is guided to references Walton (2002) and Cox and Kumar (2002) for a detail review of the zone models and field models respectively.

1.6 Impetus for the research

BRANZFIRE is one of the most popular computer models used by fire engineers in New Zealand. It is a two-layer zone model used to predict various fire phenomenon in the upper and lower layers, such as layer interface height, temperature and sprinkler/detector activation. In BRANZFIRE, the sprinkler activation sub-model is designed for the pendent sprinklers in which the sprinkler heat-responsive elements are exposed directly to the hot gas flow. However, the heat-responsive elements of recessed and concealed sprinklers may not be exposed to the hot gas flow directly. Therefore it is useful to know how BRANZFIRE can be used to predict the response sensitivity of recessed and concealed sprinklers.

In BRANZFIRE, the specification of a sprinkler depends on a few parameters, such as the RTI, the C-factor and the actuation temperature of heat-responsive element. It should be noted that the RTI and C-factor are not published by the manufacturers. The lack of information may affect the analysed outcome from BRANZFIRE and therefore it is useful to know what the RTI and C-factor are for the recessed and concealed sprinkler.

1.7 Research objectives

There are four main objectives which this work purposes to address, these objectives are described as below:

- To develop the University of Canterbury (UC) wind tunnel and characterise its performance.

  The first (UC1) and second generation (UC2) wind tunnel were developed by Chin (2002) and Tsui (2002) respectively. The UC2 wind tunnel was further developed in order to achieve the tunnel performance represented by Factory Mutual Research Corporation (FMRC). Hot gas temperature and velocity are the two main measurements used to compare with the results from other tunnels. Tsui (2004) states that the UC2 wind tunnel cannot achieve the wind tunnel criteria and therefore needs to be improved. In this study, the third generation (UC3) wind tunnel was fabricated based on the recommendations by Tsui (2004).

- To determine the RTI for different recessed and concealed sprinkler models.

  In order to obtain the RTI of the recessed and concealed sprinklers, four of the most commonly used sprinkler models (two recessed and two concealed) in New Zealand were investigated in this study. All sprinkler experiments were conducted using the developed UC3 wind tunnel. The experimental procedure and methodology were mainly referenced from Tsui (2004) and Bill and Heskestad (1995).

- To determine the flush, recessed, concealed and recessed sidewall sprinkler response time correlation between the BRANZFIRE and the full scale fire tests.

  A series of full scale fire tests with the flush, recessed, concealed, sidewall and recessed sidewall sprinkler were conducted by Bill and Heskestad (1995) at FMRC. In those fire tests, sprinkler response times were recorded. In this study, in order to find correlations between the normal sprinkler response

times predicted in BRANZFIRE and the experimental flush, recessed, concealed and recessed sidewall sprinkler response times in the full scale fire tests, BRANZFIRE was used to simulate the fire scenarios in the full scale fire tests. Sprinkler response time correlations between the BRANZFIRE and the full scale fire tests were obtained by the comparison of the predicted (BRANZFIRE) and experimental (full scale fire test) sprinkler response times.

- To determine the relationship of the sprinkler response time between the full scale fire test, wind tunnel test and BRANZFIRE modelling.

  The intention was to determine the sprinkler response time relationship between the full scale fire test, wind tunnel test and BRANZFIRE modelling. Because the full scale fire test was not conducted in this research, the experimental data used to assess the sprinkler response time relationship was obtained from the full scale fire test conducted by Bill and Heskestad at FMRC (Bill and Heskestad 1995).

1.8 Report outline

This research report consists of 12 chapters. The content of each chapter following this introductory chapter is summarised as follows:

Chapter 2 reviews the literature related to this research (e.g. development of the wind tunnel, procedure of the wind tunnel test (plunge test), simulation in BRANZFIRE and the full scale fire test for investigating the recessed and concealed sprinklers).

Chapter 3 describes the development and performance of the newly developed wind tunnel at the University of Canterbury.

Chapter 4 presents and discusses the calibration results obtained from the newly developed wind tunnel.

Chapter 5 describes the experimental apparatus, instrumentation, methodology, procedure and data analysis techniques used in the wind tunnel test (plunge test) conducted in this research.

Chapter 6 presents and discusses the sprinkler response time and RTI for the recessed and concealed sprinklers obtained from the wind tunnel test (plunge test) in the research.

Chapter 7 describes the modelling procedure, the assumptions made, the scenarios modelled and the data analysis techniques used in BRANZFIRE to simulate the fire scenarios in the full scale fire tests.

Chapter 8 illustrates and discusses the BRANZFIRE simulation results obtained in this study.

Chapter 9 describes the conclusions and findings from this research.

Chapter 10 describes the recommendations for the further research.

Finally, Chapter 11 and Chapter 12 present the references and the appendices used in this research respectively.

CHAPTER 2

2 LITERATURE REVIEW

This chapter presents the summary of the full scale fire tests and the wind tunnel tests (plunge tests) used to investigate the recessed and concealed sprinkler at FMRC (Bill and Heskestad 1995). In addition to this, a previous study (Annable 2006) was implemented to investigate the recessed and concealed sprinkler activation at Building Research Establishment (BRE). The summary of the recessed and concealed sprinklers investigated at BRE in wind tunnel tests (plunge tests) is also presented in this chapter.

As mentioned in Chapter 1, in order to determine the sprinkler response time correlation between the prediction (BRANZFIRE) and the experiment (full scale fire tests), BRANZFIRE was used to model the fire scenarios in the full scale fire tests conducted at FMRC (Bill and Heskestad 1995). It is important to know how a sprinkler is modelled in BRANZFIRE. Therefore, the assumptions and the underlying physics used to estimate the activation of sprinkler in BRANZFIRE are summarized in this chapter.

In addition, the “prolonged test” and the “ramp test” are briefly described in this chapter.

2.1 Full scale fire test

The details of the full scale fire testes conducted by Bill and Heskestad (1995) are described in this section. It should be noted that all data used to describe the full scale fire tests is referenced from Bill and Heskestad (1995).

2.1.1 Test Facility and Instrumentation

Sixteen tests were conducted by using four different test facilities in the full scale fire tests. Table 2.1 shows the test facility used in each corresponding full scale fire test. It should be noted that the identification (Test ID) of each full scale test is extracted and identical to the test notations represented by Bill and Heskestad (1995). In addition, Test 15 was the preliminarily test to Test 16 and conducted without installing sprinklers with the purpose of measuring the static pressure at the room centre after removing the south wall of the compartment.

Table 2.1: Test facility used in each full scale fire test

Test ID	Test facility
1 ~ 12	1
13	2
14	3
15, 16	4

2.1.1.1 Test facility 1

Figure 2.1 shows the configuration of Test facility 1. From this figure, it can be seen that the dimensions of the test compartment were measured as 3.66 × 7.32 × 2.44 m in height. Wood studs and 12.7 mm thick gypsum board were used as the construction materials of this compartment. There was only one ventilation opening (doorway) located at the south wall and connected to the surrounding of this compartment. The dimension of this ventilation opening was 1.18 ×2.06 m high.

A fire source was used in Test 1 ~ 12 and placed in a location 1.02 m from the north wall and 1.83 m from the east wall of the tested compartment. Heptane was the fuel contained in the fire source pan to provide a steady heat release rate. The diameter of

the fire source pan was 0.6 m for Test 7 and 0.46 m for the others, where 0.6 m was the greatest fire source diameter used in the full scale fire tests. Based on the mass loss measurements recorded by Heskestad and Bill (1987), the chemical heat release rate (HRR) was estimated to be 130 kW and 260 kW for 0.46 m and 0.6 m diameter heptane pool fire respectively.

As shown in Figure 2.1, there were two “ceiling stations” mounted on the ceiling of the tested compartment. The distance between the fire source to the near ceiling station and the far ceiling station was measured as 1.63 m and 4.55 m respectively. The tested sprinklers together with associated instruments used for measuring smoke temperature and velocity were installed at each ceiling station. In each full scale fire test, the sprinkler at the west side of the ceiling station was a pendent type sprinkler. While the sprinkler installed at the east side of each ceiling station was flush, recessed or concealed sprinkler. All tested sprinklers were fixed in location by being screwed into the steel pipes which were extended 0.3 m above the ceiling plane of the compartment. 100 ml of water was filled into each steel pipe after the sprinklers were connected to the piping system. Because a small amount of water was used for each sprinkler, the water sprays from actuated sprinkler were sufficiently weak that no significant influence of fire suppression or gas cooling took place. The water temperature inside the steel pipes during experiments was recorded by placing a thermocouple within the waterway of each sprinkler. The response time of each sprinkler was monitored and recorded by using a 3 mm diameter tube in conjunction with an electronic manometer positioned near the top of the 0.3 m long pipe above the ceiling.

In order to measure the smoke flow velocity, a bi-directional flow probe was used at the central location of each ceiling station. The sensing element of this flow probe was placed in a distance of 76 mm underneath the lower plane of the ceiling. The determination of this measuring location was based on the approximate position of the heat-responsive element of pendent sprinklers.

Along with the two sprinklers and the flow probe at each ceiling station, two thermocouples were used to record the hot smoke temperatures during the full scale fire tests. It should be noted that both the thermocouples were placed at 76 mm below

the lower plane of the ceiling in Test 1. However, the measuring location of the west and the east side thermocouple was placed at 76 mm and 6 mm beneath the lower plane of the ceiling for Test 2 ~ 16 (with the exception of Test 1).

In addition, the static pressure at the central point of the ceiling was measured by using a pressure port flushed with the surface of the ceiling.

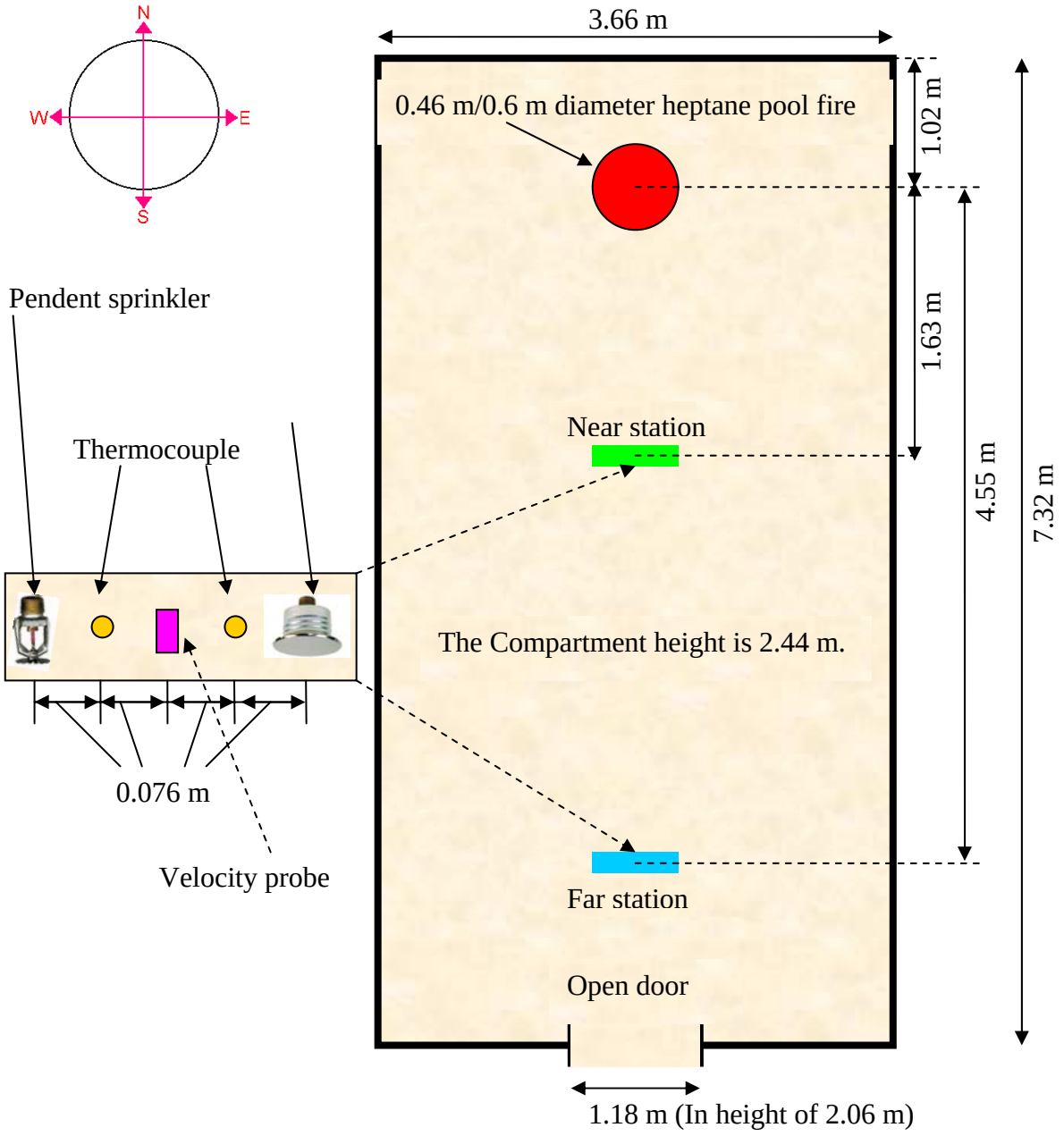

Figure 2.1: Configuration of Test facility 1

2.1.1.2 Test facility 2

Test facility 2 shown in Figure 2.2 was used to conduct Test 13 in the full scale fire tests. In this test, there were three recessed sidewall sprinklers installed on the west wall of the compartment and were installed with their deflector 100 mm below the lower plane of the ceiling. The distance between the "standard sidewall (sprinkler E)" and the north wall was 1.77 m. In addition, the gap between each installed sprinkler was measured to be 0.13 m.

It should be noted that the fire source was placed at a distance of 0.34 m away from the north wall of the compartment, which was shorter than the distance measured in Test facility 1. By changing the location of the fire source, the distance from the centre of the fire source to the "standard sidewall (sprinkler E)" and to the near ceiling station was equal to each other.

In Test 13, the flush, recessed or concealed sprinklers were not investigated. Therefore only pendent sprinklers were installed at the ceiling stations to compare the sprinkler response time obtained from the recessed sidewall sprinklers.

The distance between the vertical axis of the fire to the position of the sprinkler's sensing element (radial distance) of each sprinkler investigated in Test 13 was tabulated in Table 2.2 below.

Table 2.2: Radial distance of sprinklers tested in Test 13

Model of sprinkler	Radial distance (m)
Er	2.24
Es	2.32
Fr	2.4

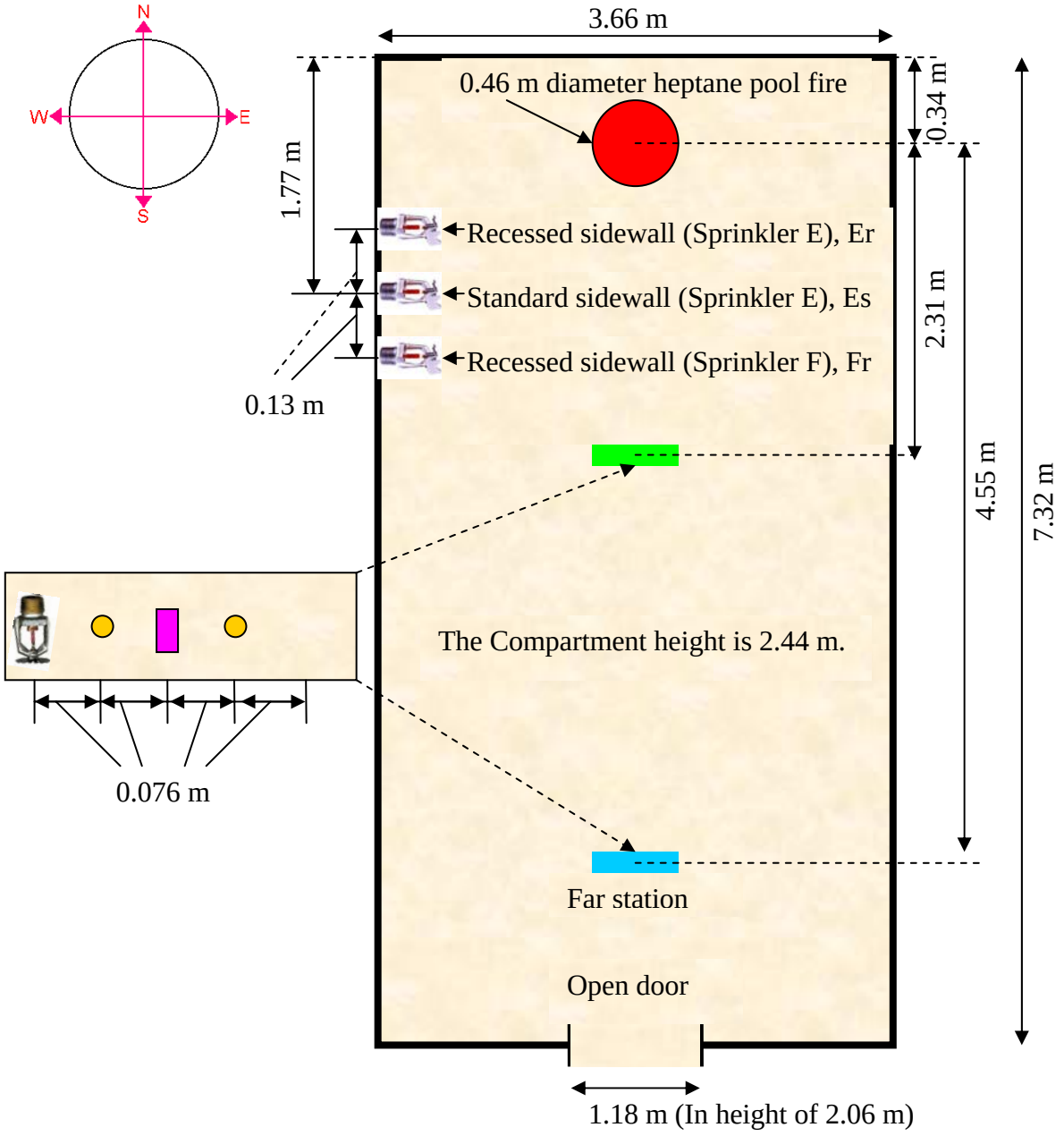

Figure 2.2: Configuration of Test facility 2

2.1.1.3 Test facility 3

Figure 2.3 shows the configuration of Test facility 3 which was used to conduct Test 14 in the full scale tests. In this test, four recessed sidewall sprinklers were tested simultaneously and installed on the south wall of the compartment. From this figure, two “standard sidewall (sprinkler E)” and two “recessed sidewall (sprinkler E)” were installed straddling the vertical centreline of the south wall. The distance between each side of the sprinklers and the vertical south wall centreline was 0.06 m. It should be noted that these sprinklers were installed at two different height levels, where one “standard sidewall (sprinkler E) and one “recessed sidewall (sprinkler E) was installed with their deflector 0.1 m below the lower plane of the ceiling. While the other recessed sidewall sprinklers were installed 0.3 m below the ceiling.

The length of the tested compartment was reduced to 4.6 m. This is because the maximum installation spacing for recessed sidewall sprinkler was 4.6 m. In addition, since the sprinklers straddled the vertical centreline of the south wall, the ventilation opening was moved to the left corner of the south wall. The dimension of this ventilation opening was 0.76×2.03 m in height.

One pendent sprinkler was installed at the near ceiling station (no sprinklers installed at the far ceiling station in Test 14). The response time of this pendent sprinkler was used to compare the activation time of the recessed sidewall sprinklers investigated in this full scale fire test.

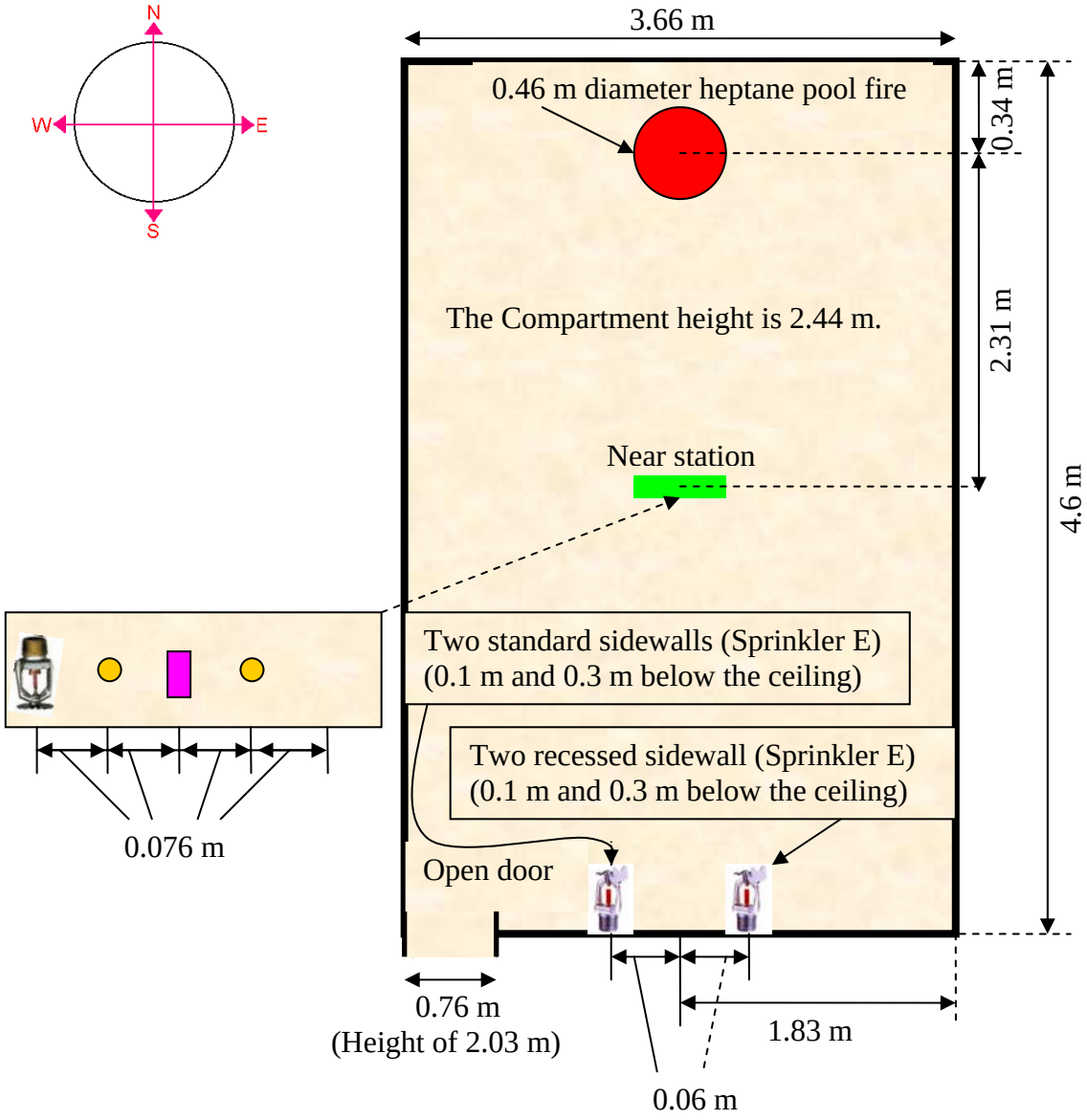

Figure 2.3: Configuration of Test facility 3

2.1.1.4 Test facility 4

Test 16 was conducted by using Test facility 4 shown in Figure 2.4 below. The geometry of Test facility 4 was similar to Test facility 1. The only difference between these two test facilities was that the south wall of Test facility 4 was removed to assess the response time of sprinkler.

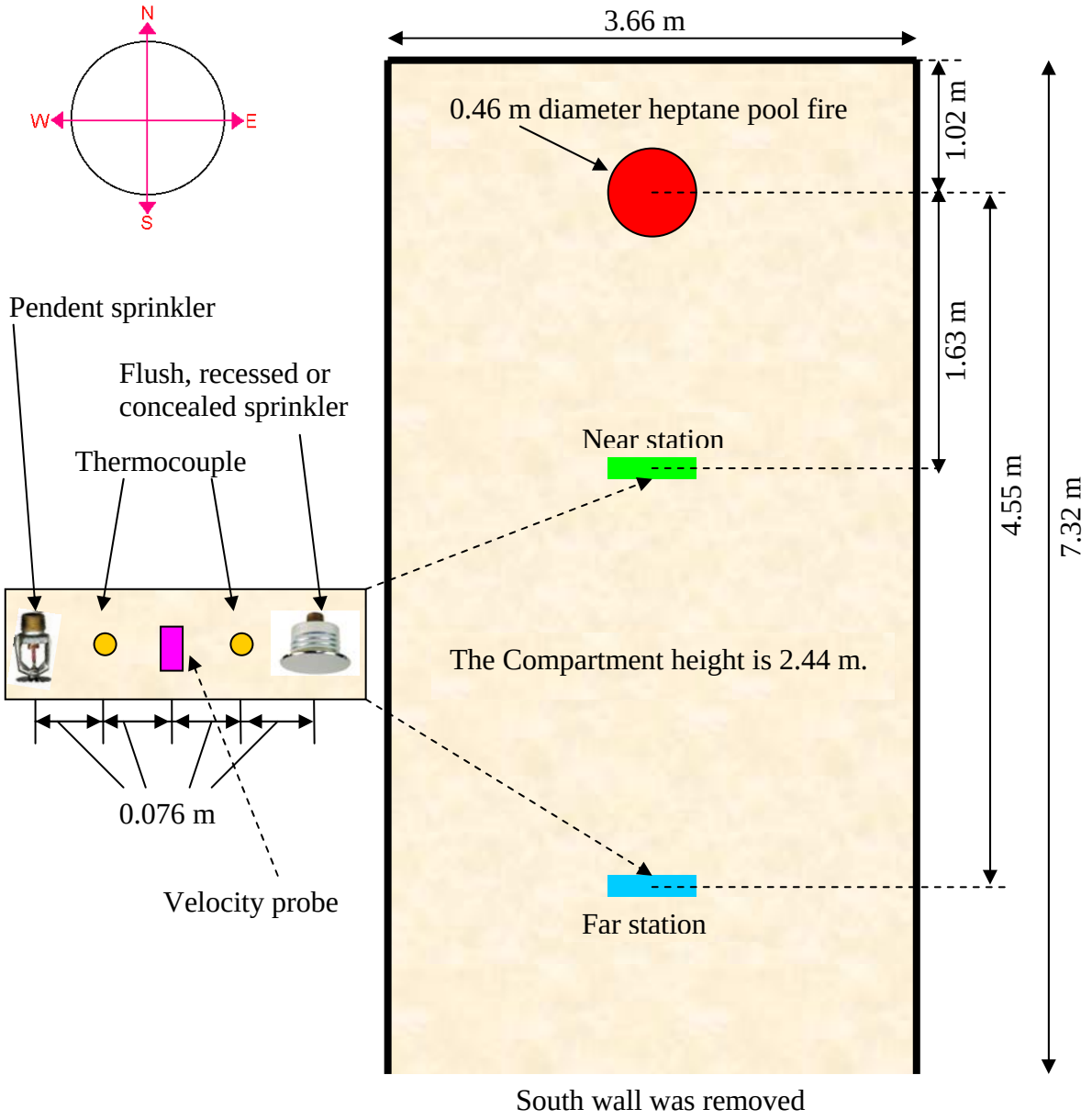

Figure 2.4: Configuration of Test facility 4

2.1.2 Description of sprinkler characteristics and test results

2.1.2.1 Sprinkler characteristics

Twelve different sprinkler models were tested in full scale fire tests, these included two pendent sprinklers, one flush sprinkler, four recessed sprinklers, three concealed sprinklers and two recessed sidewall sprinklers. The characteristics of these sprinklers are extracted from the technical report provided by Bill and Heskestad (1995) and shown in Table 2.3 below. It should be noted that the identification code (sprinkler model letter) used to specify each sprinkler model was the same as represented by Bill and Heskestad (1995).

Table 2.3: Sprinkler characteristics (Bill and Heskestad 1995)

Sprinkler Model	Type	Link Type	Nominal RTI $(m.s)^{1/2}$	* Actuation temperature (^oC)
A	Recessed pendent	3mm bulb	35	68
B	Recessed pendent	5mm bulb	135	68
C	Recessed pendent (vented)	Solder	183	74
D	Recessed pendent	Solder	183	74
E	Recessed sidewall	8mm bulb	246	68
F	Recessed sidewall	5mm bulb	135	68
G	Flush pendent	Solder	34	74
H	Concealed (vented)	Solder	203	74
I	Concealed (vented)	Solder	26	74
J	Concealed	Solder	264	74
K	Pendent	Solder	203	74
L	Pendent	Solder	26	74

(*Note: “Actuation temperature” is used to represent “Temperature rating” as presented in the report by Bill and Heskestad (1995) and indicates the temperature specified by the supplier which is marked in the sprinkler.)

2.1.2.2 Full scale fire test results

As mentioned in Section 2.1.1, sixteen full scale fire testes were carried out to obtain the sprinkler response times of the twelve different models of sprinklers. Table 2.4 below tabulates the experimental sprinkler response times recorded in the full scale fire tests.

Table 2.4: Experimental sprinkler response times in the full scale fire tests (Bill and Heskestad 1995)

Test	Model	Sprinkler response time (s)	
		at near station	at far station
1	K	178	323
	L	82	93
2	K	219	417
	I	No operation, wet link	297
3	K	216	362
	D	282	No operation
4	K	227	369
	H	331	500
5	L	63	99
	G	57	89
6	K	238	410
	C	233	377
7	K	84	117
	H	122	166
8	L	78	113
	A	77	112
9	L	59	90
	A	94	184
10	K	152	285
	J	323	506
11	K	202	390
	B	193	243
12	K	170	285
	B	192	269
16	K	217	413
	C	244	567

Test	Model	Response time (s)	Comments
13	K	231	At the near ceiling station
	E_s	156	Standard sidewall, deflector 0.1 m below ceiling
	E_r	157	Recessed sidewall, deflector 0.1 m below ceiling
	F_r	152	Recessed sidewall, deflector 0.1 m below ceiling
14	K	156	At the near ceiling station
	$E_s^{0.1}$	191	Standard sidewall, deflector 0.1 m below ceiling
	$E_r^{0.1}$	203	Recessed sidewall, deflector 0.1 m below ceiling
	$E_s^{0.3}$	179	Standard sidewall, deflector 0.3 m below ceiling
	$E_r^{0.3}$	183	Recessed sidewall, deflector 0.3 m below ceiling

(Note: In Test 9 and Test 12, the sprinklers' frame arms of the tested sprinklers (sprinkler model A and B) were orientated at 0 ^{o} (parallel) to the ceiling flow generated by the fires.)

2.2 Wind tunnel test (Plunge test)

After the full scale fire tests were conducted, the wind tunnel tests (plunge tests) were conducted to develop the plunge test methods to evaluate the thermal sensitivity and determine the plunge test conditions which would represent a wide range of fire conditions and provide response times consistent with the fire tests for the flush, recessed and concealed sprinklers at FMRC (Bill and Heskestad 1995).

It should be noted that the experimental methodology of the plunge tests used to assess the sprinkler activation and the thermal sensitivity of the flush, recessed and concealed sprinklers conducted at FMRC was developed based on the methodology of the plunge tests used to investigate the normal sprinklers (the heat-responsive element of sprinkler is entirely exposed to the surrounding environment). In order to provide the fundamental information to the reader, the standard plunge test used to investigate the normal sprinklers and the modified plunge test used to test the flush, recessed and concealed sprinklers are summarized in this chapter.

2.2.1 Standard plunge test for normal sprinklers

The earliest standard plunge test used to investigate the normal sprinklers was created and developed at FMRC in U.S. (Heskestad and Smith 1976). Since the earliest

standard plunge test was established, researchers (e.g. Heskestad and Smith (1980), Heskestad and Bill (1987), Beever (1990), and Ingason (1998)) continued to try and further develop and investigate this standard plunge test. However, it was found that the basic premise of the standard plunge test generated at FMRC was undisputed and very reliable when used to investigate the sprinkler activation and the sprinkler thermal sensitivity of the normal sprinklers. It should be noted that the standard plunge test could be also used to investigate the (fusible – link – actuated) fire vents and the smoke detectors. The relevant literature could be found from Cooper (1998) and Grosshandler (1997).

As described in Chapter 1, the (part or entire) heat-responsive element of the sprinkler (with the exception of the concealed sprinklers) was exposed to the heated environment under an event of fire in an enclosure compartment. The operation of the sprinkler's heat-responsive element mainly depends on the ceiling jet temperatures and velocities which flow through the sprinkler heat-responsive element (Karlsson and Quintiere 2000). The definition of the ceiling jet is defined as when the plume flow (smoke generated from the fire, see Figure 2.5 below) rises and impinges to the ceiling, the hot gases spread in a shallow layer underneath the lower plane of the ceiling as a momentum-driven circular jet (Alpert 2002; Karlsson and Quintiere 2000). The plume flow and the ceiling jet are also illustrated in Figure 2.5 below.

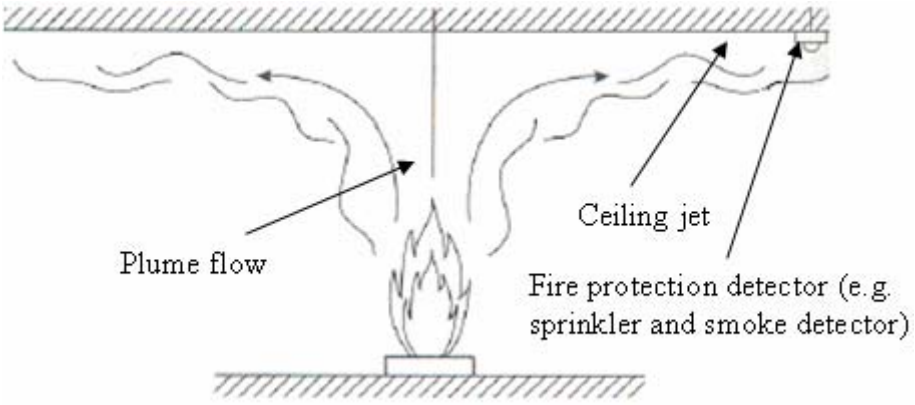

Figure 2.5: Ceiling jet flow below the lower plane of the ceiling (Alpert 2002)

The principle of a plunge test is that a sprinkler with the ambient temperature is installed in a sprinkler mounting plate and plunged into a circulating heated hot gas stream of known (pre-determined) constant temperature and velocity (Madrzykowski

and Fleming 2003). It should be noted that the plunge test conditions (pre-determined temperature and velocity) were obtained from the full scale fire tests and aimed to simulate the ceiling jet flow temperatures and velocities passed through the heat-responsive element of the sprinklers. The plunge test conditions used for investigating the normal sprinklers are detailed in the technical report presented by Heskestad and Smith (1980). In addition to this, it should be noted that the plunge test conditions presented by Heskestad and Smith (1980) are only used to determine the RTI value (excluding the C-factor). The plunge test conditions used to determine the C-factor of sprinklers is different than the test conditions used to obtain the RTI. The C-factor of a sprinkler was determined by using the "prolonged test" where it is a modified plunge test that uses the identical apparatus (wind tunnel). The "prolonged test" conditions are described by Heskestad and Bill (1987) in details.

Figure 2.6 below shows the configuration of the wind tunnel used to conduct the plunge tests at FMRC (Heskestad and Smith 1976).

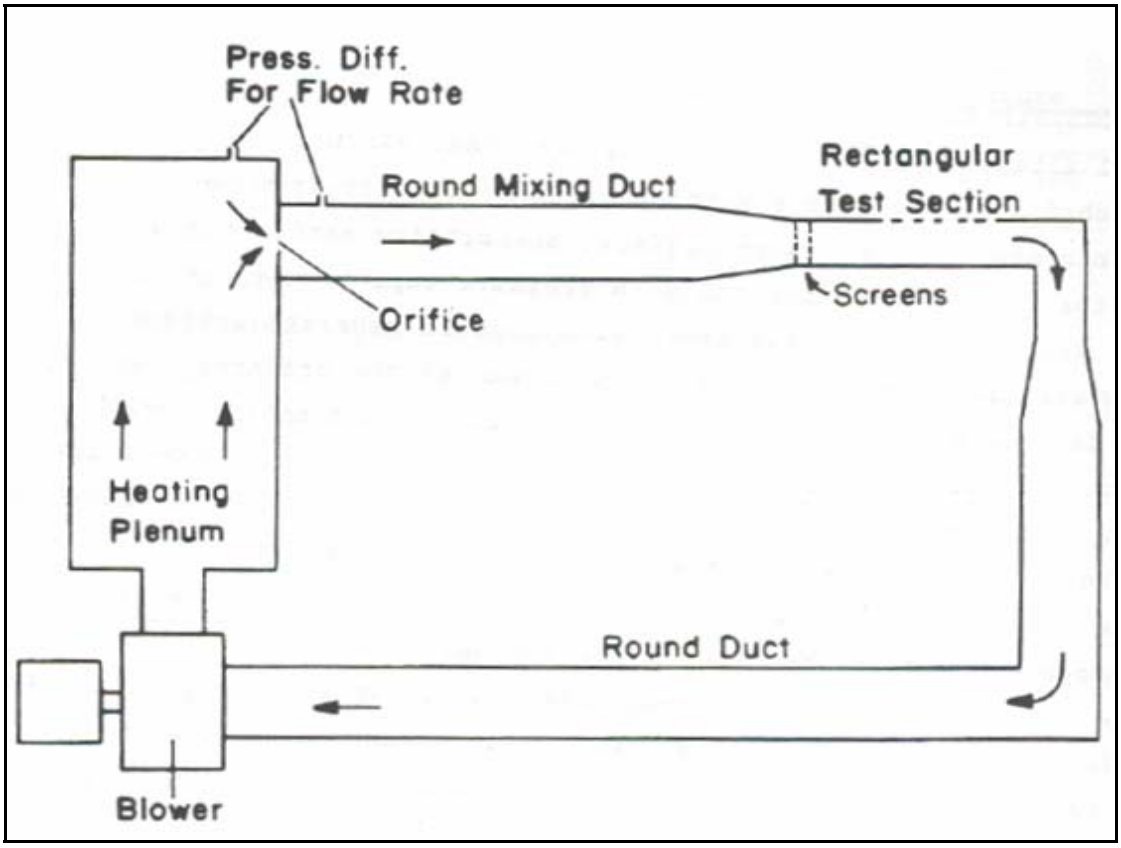

Figure 2.6: Configuration of the wind tunnel used to conduct the plunge tests at FMRC (Heskestad and Smith 1976)

Apart from the wind tunnel generated at FMRC shown in figure above, there is another type of wind tunnel commonly used to assess the sprinkler activation (the thermal sensitivity of sprinkles) and designed at the Fire Research Station (FRS) in U.K. The configuration of the wind tunnel constructed at FRS is shown in Figure 2.7 below and referenced from Theobald (1987).

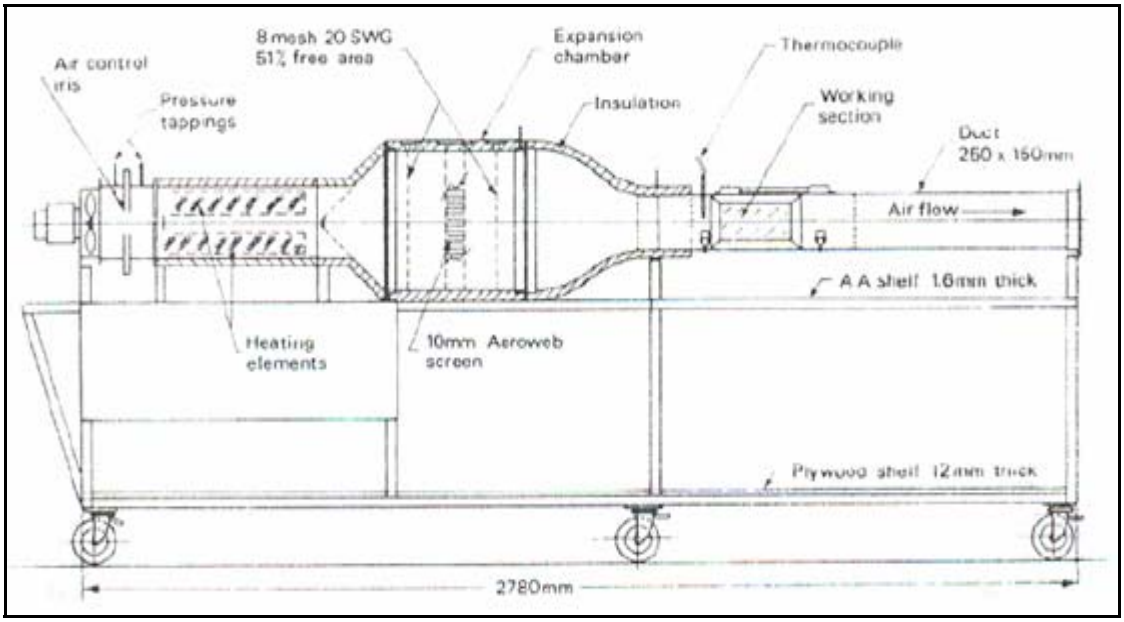

Figure 2.7: Configuration of the wind tunnel fabricated at FRS (Theobald 1987)

From this figure, it can be seen that the air stream inside the wind tunnel is generated at the left end of the tunnel by controlling the evolution frequency of the fan motor and flows out of the tunnel from the opening located at the right end of the tunnel. The sprinkler tests conducted using this wind tunnel are called “ramp test”. As mentioned previous in this section, the hot gas temperature and velocity (plunge test condition) are pre-determined to be constant during the FMRC plunge tests. However, the hot gas temperature inside the FRS wind tunnel is not constant and is set to be raised with a constant increase rate during the ramp tests. Readers could refer to references (Theobald 1987) and (International Standard 2004) for more details regard the performance and the test conditions of the ramp test by using the FRS wind tunnel.

2.2.2 Modified plunge test for flush, recessed and concealed sprinklers at FMRC

After the full scale fire tests were conducted by Bill and Heskestad (1995) at FMRC, the methodology and plunge test conditions used to assess the activation and thermal sensitivity of the flush, recessed and concealed sprinklers were established by comparing the experimental results obtained from the full scale fire tests and the plunge tests. It should be noted that the C-factor was not determined by Bill and Heskestad in their plunge test experiments. The conclusions found between the full scale fire tests and the plunge tests are listed below and extracted from Bill and Heskestad (1995).

- By comparing the full scale fire test results with the plunge test results, it was found that the air pressures below the ceiling were larger than the air pressure measured above the ceiling. The pressure differentials generated the hot gas flow which passed through and resulted in heating of the heat-responsive element of the flush, recessed and concealed sprinklers and significantly influenced the activation time of these sprinklers. Therefore, the ceiling pressures generated by the fires are important and needed to be simulated in the plunge tests.

- In order to simulate the installation location of the flush, recessed and concealed sprinklers (part or entire body of the sprinkler is hidden above the ceiling) in the actual ceiling installation, a special plate was fabricated to mount the flush, recessed and concealed sprinklers in the plunge test wind tunnel. The front view and the configuration of the special mounting plate are shown in Figure 2.8 and Figure 2.9 below and referenced from Bill and Heskestad (1995).

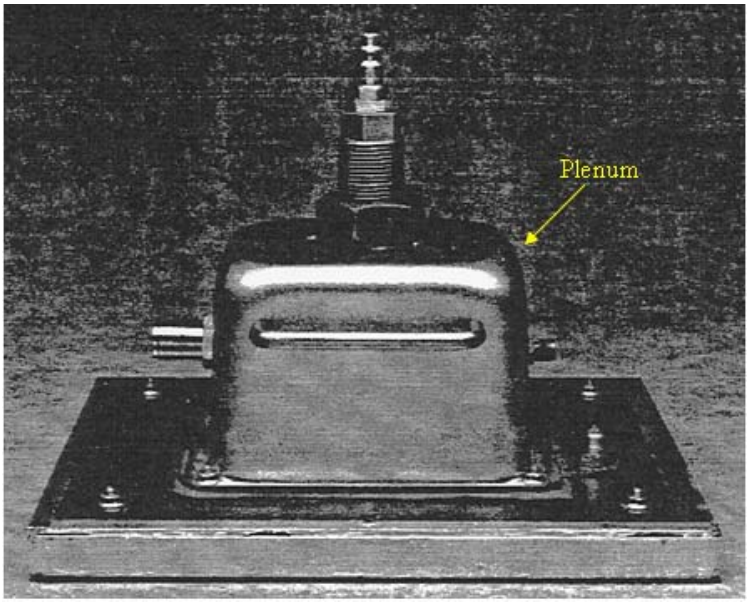

Figure 2.8: Front view of the special mounting plate (Bill and Heskestad 1995)

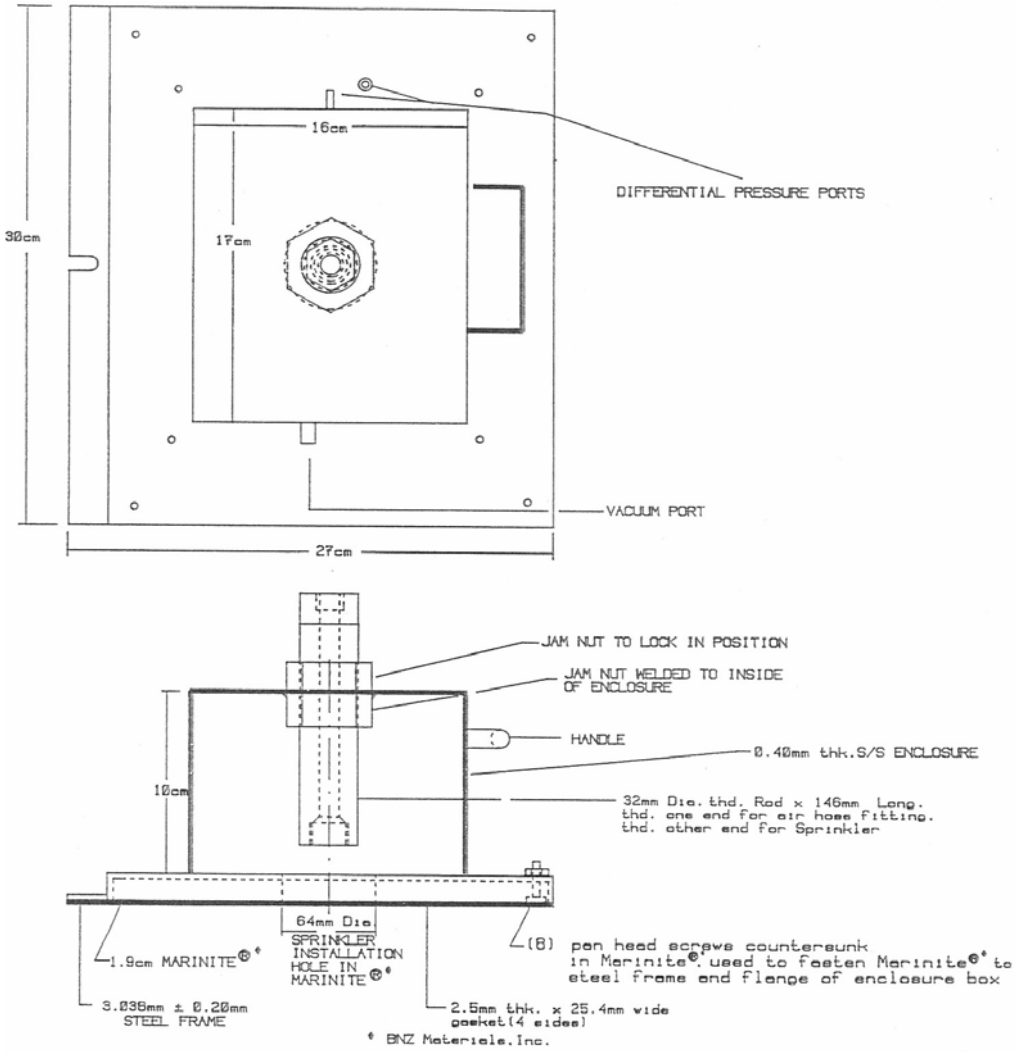

Figure 2.9: Configuration of the special mounting plate (Bill and Heskestad 1995)

- The simulation of the pressure differences (hot gas flows through the plenum) between the space below and above the ceiling was accomplished by evacuating the plenum of the mounting plate by using a vacuum pump connected to the vacuum port shown in Figure 2.9.

- The measurement of the pressure difference between the plenum of the special mounting plate and the wind tunnel test section was read from the pressure transducer connected to the two differential pressure ports show in Figure 2.9.

- From the plunge test results, it was found that the recessed and concealed sprinklers failed to operate if the vacuum was not applied on the special mounting plate during the plunge tests.

- Nine plunge test conditions used to investigate the activation time and the thermal sensitivity (RTI) of the flush, recessed and concealed sprinklers were determined by comparing the full scale fire test results and the plunge test results (Bill and Heskestad 1995). These nine plunge test conditions are shown in Table 2.5 below and extracted from Bill and Heskestad (1995).

Table 2.5: Plunge test conditions used for the flush, recessed and concealed sprinklers

Plunge test condition	Gas temperature	Gas velocity	Applied vacuum
1	128 ^{o}C	1 m/s	0.007 mm Hg
2	128 ^{o}C	2.56 m/s	0.007 mm Hg
3	128 ^{o}C	3.48 m/s	0.007 mm Hg
4	199 ^{o}C	1 m/s	0.01 mm Hg
5	197 ^{o}C	2.56 m/s	0.01 mm Hg
6	197 ^{o}C	3.48 m/s	0.01 mm Hg
7	301 ^{o}C	1 m/s	0.013 mm Hg
8	290 ^{o}C	2.56 m/s	0.013 mm Hg
9	289 ^{o}C	3.48 m/s	0.013 mm Hg

2.2.3 Modified plunge test for recessed and concealed sprinklers at BRE

The plunge tests of the recessed and concealed sprinklers were conducted by Annable at BRE (Annable 2006). In this research, the BRE wind tunnel and the BRE modified mounting plate was used to conduct the plunge tests for the recessed and concealed sprinkler. The configuration of the BRE wind tunnel and the arrangement of the BRE modified mounting plate are illustrated in Figure 2.10 and Figure 2.11.

Figure 2.10: Configuration of the BRE wind tunnel (Annable 2006)

Figure 2.11: Arrangement of the BRE modified mounting plate (Annable 2006)

Seven sprinkler models (1 pendent, 1 recessed and 5 concealed) were tested in the plunge tests at BRE. The characteristics of the investigated sprinklers were tabulated in Table 2.6 below and referenced from Annable (2006).

Table 2.6: Characteristics of the tested sprinklers in the plunge tests at BRE (Annable 2006)

Sprinkler ID	Type	K factor UK (K factor US)	*Actuation temperature of sprinkler (cover plate) (^oC) (^oC)	Details of concealer plate and recess cup	Manufacturer's recommended recessing details	
					Recess distance MAX.	Recess distance MIN
A_P	Pendent	71 (4.9)	68 (not applicable) glass bulb	N/A	N/A	N/A
B_R	Recessed	62 (4.3)	68 (not applicable) glass bulb	N/A	Deflector 41 mm below ceiling	Deflector 22 mm below ceiling
C_C	Concealed	70 (4.9)	68 (57) glass bulb	Domed plate, vented cup	Concealer adjustment of 12.7 mm	Concealer adjustment of 4.7 mm
D_C	Concealed	60.5 (4.2)	71 (57) solder link	Flat plate, vented cup	Deflector 12.7 mm below ceiling	Deflector 25.4 mm below ceiling
E_C	Concealed	71 (4.9)	68 (57) glass bulb	Domed plate, vented cup	Deflector 9.5 mm below ceiling	Deflector 22.2 mm below ceiling
F_C	Concealed	59 (4.1)	60 (57) solder link	Flat plat, unvented cup	Distance between ceiling and sprinkler thread fitting of 65 mm	Distance between ceiling and sprinkler thread fitting of 52.4 mm
G_C	Concealed	62 (4.3)	74 (57)	Flat plat, vented cup	Concealer adjustment of 12.7 mm	Concealer adjustment of 4.7 mm

(*Note: "Actuation temperature of sprinkler" is used to represent "Nominal operating temperature of sprinkler" as presented in the report by Annable (2006) and indicates the temperature specified by the supplier which is marked in the sprinkler.)

It should be noted that the identification (sprinkler ID) used to specify each sprinkler model in this table was the same as presented in report provided by Annable (2006).

The thermal sensitivity (both the RTI and C-factor) of the tested recessed and concealed sprinklers was determined in the investigation conducted by Annable. The average RTI and the average C-factor of the investigated sprinklers in each corresponding plunge (or ramp) test condition at BRE are shown in Table 2.7 and summarized from the data provided by Annable (2006). It should be noted that the RTI and the C-factor were obtained from the plunge test and the ramp test respectively. Therefore, the RTI (C-factor) was not determined and shown as "N/A" in Table 2.7 for the ramp test (plunge test).

In Table 2.7, "Frame arm orientated 90 ^{o} to the oncoming flow" and "Frame arm orientated 0 ^{o} to the oncoming flow" indicates the sprinkler's frame arm orientated at 90 ^{o} (perpendicular to the flow) and 0 ^{o} (parallel to the flow) to the oncoming hot gas flow in the wind tunnel respectively.

It should be noted that the concealer plate, (the cover plate for the concealed sprinkler) retainer orientation and the lug position was examined in the research conducted by Annable at BRE. The "Favourable concealer plate" shown in Table 2.7 indicates that the location of the lug of the concealer plate does not obstructed the oncoming hot gas flow to the heat-responsive element of the sprinklers during the plunge tests. In contrast, the "Unfavourable concealer plate" results in the lug of the concealer plate obstructing the oncoming flow to the heat-responsive element of the sprinklers during the plunge tests. Figure 2.12 below illustrates the lug of the concealer plate.

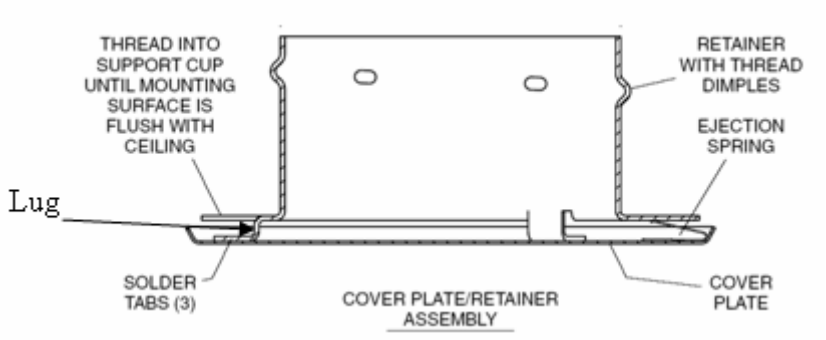

Figure 2.12: Lug of the concealer plate (Tyco Fire & Building Products 2006)

Table 2.7: Average RTI and C-factor of the sprinklers tested at BRE (Annable 2006)

Test setup	Sprinkler	Test method	Frame arm orientated (Degrees) to the oncoming flow	Recess distance	Concealer plate	Nominal			Average	
						Air temperature (^oC)	Air velocity (m/s)	Pressure difference (Pa)	RTI $(m.s)^{1/2}$	C-factor $(m/s)^{1/2}$
1	A_P	Ramp	90	N/A	N/A	68 + 1/min	1	N/A	N/A	0.53
2	A_P	Plunge	90	N/A	N/A	135	1.75	N/A	27.8	N/A
3	B_R	Ramp	90	Max.	N/A	68 + 1/min	1.75	N/A	N/A	0.89
4	B_R	Plunge	90	Max.	N/A	135	1.75	N/A	42.4	N/A
5	B_R	Plunge	0	Max.	N/A	135	1.75	N/A	62.5	N/A
6	C_C	Ramp	90	Min.	Favourable	57 + 1/min	1	1.33	N/A	0.52
7	C_C	Plunge	90	Min.	Favourable	135	2.5	1.33	104.1	N/A
8	C_C	Plunge	0	Max.	Unfavourable	197	2.5	1.33	166.8	N/A
9	D_C	Ramp	90	Min.	Favourable	57 + 1/min	1	1.33	N/A	2.37
10	D_C	Plunge	90	Min.	Favourable	197	2.5	1.33	284.3	N/A
11	E_C	Ramp	90	Min.	Favourable	57 + 1/min	1	1.33	N/A	0.46
12	E_C	Plunge	90	Max.	Favourable	135	2.5	1.33	88.3	N/A
13	E_C	Plunge	25	Max.	Favourable	135	2.5	1.33	97.6	N/A
14	E_C	Plunge	0	Max.	Favourable	135	2.5	1.33	143.6	N/A
15	E_C	Plunge	90	Min.	Favourable	135	2.5	1.33	71.9	N/A
16	E_C	Plunge	90	Max.	Unfavourable	135	2.5	1.33	94.1	N/A
17	E_C	Plunge	90	Max.	Favourable	Hotter (197)	2.89	1.33	93.6	N/A
18	E_C	Plunge	90	Max.	Favourable	135	Slower (1.8)	1.33	92.8	N/A
19	E_C	Plunge	90	Max.	Favourable	135	1.75	Higher (3.5)	67.9	N/A
20	F_C	Ramp	90	Min.	Favourable	57 + 1/min	1	1.33	N/A	0.71
21	F_C	Plunge	90	Min.	Favourable	197	2.5	2.5	114.9	N/A
22	F_C	Plunge	0	Max.	Unfavourable	197	2.5	0	410	N/A
23	G_C	Ramp	90	Min.	Favourable	57 + 1/min	1	1.33	N/A	0.96
24	G_C	Plunge	90	Min.	Favourable	197	2.5	1.33	130.1	N/A
25	G_C	Plunge	0	Max.	Unfavourable	197	2.5	1.33	192.8	N/A

2.3 BRANZFIRE zone model

BRANZFIRE is a fire computer zone model that can be used to predict the fire phenomenon (e.g. visibility, toxicity of combustion products, heat release rate from the combustion and sprinkler actuation) in an event of fire. As mentioned in Chapter 1, one of the main objectives in this research was to determine the flush, recessed, concealed and recessed sidewall sprinkler response time correlations between BRANZFIRE and the full scale fire tests. Therefore, it is important to know the assumptions and the underlying physics upon which the sprinkler actuation model in BRANZFIRE is based. It should be noted that all the assumptions and the underlying physics of the BRANZFIRE shown in this section are obtained and referenced from the "BRANZFIRE technical reference guide" (Wade 2004b). For more detailed information regarded to the sprinkler actuation model or other prediction models in BRANZFIRE, readers can refer to literature "BRANZFIRE technical reference guide" provided by Wade (2004b).

2.3.1 Sprinkler actuation

In BRANZFIRE, there are two algorithms (JET algorithm and Alpert's correlations) used to predict the sprinkler actuation (Wade 2004b). The assumptions and the underling physics of these two algorithms are described as follows.

2.3.1.1 JET algorithm

The JET algorithm was developed by Davis at the NIST (Davis 1999). By using this algorithm, the centreline temperature of the plume, the ceiling jet temperature and the ceiling jet velocity produced by a single fire plume can be calculated (Wade 2004b). In addition to this, the ceiling jet temperature and velocity can be calculated at different depths beneath the lower plane of the ceiling by using this algorithm. Equation 2.1 (Wade 2004b) shown below is used to calculate the depth below the ceiling at the location of the occurrence of the maximum ceiling jet temperature.

$$d_{\max} = 0.023H\left(r/H\right)^{0.9} \qquad \text{for } \frac{r}{H} > 0.2 \qquad \textbf{Equation 2.1}$$

Where:

d_{max} = depth below the ceiling at the location of the occurrence of maximum ceiling jet temperature (m)

r = radial distance from the centre of the plume (m)

H = height of the ceiling above the base of the fire (m)

It should be noted that the ceiling jet temperature predicted in this case is not a constant. The ceiling jet temperature increases from the temperature at the surface of the ceiling to the maximum ceiling jet temperature at a certain depth below the lower plane of the ceiling (d_{max}). The ceiling jet temperature would start to reduce when the distance below the ceiling (depth) beyond d_{max} and decrease until it equals to the upper layer temperature at the layer interface height (Wade 2004b).

2.3.1.2 Alpert's correlations

The Alpert's correlations (Evans 1998) used to calculate the ceiling jet temperature and velocity are presented in this section. It should be noted that the Alpert's correlations shown below are used to calculate the maximum temperature and velocity of an unconfined ceiling jet. Therefore, the Alpert correlations are only valid for predicting sprinklers located at the distance below the ceiling which experience the maximum ceiling jet temperature and velocity (Wade 2004a). This also implies that the ceiling jet temperature is a constant value as a function of the depth underneath the ceiling (Wade 2004a). As a result, by selecting the "Alpert's correlations" option in BRANZFIRE, the location of the heat-responsive element of the modelled sprinkler in BRANZFIRE is assumed at the location where the maximum ceiling jet temperature and velocity occur.

Equations shown below are the Alpert's correlations incorporated to predict the sprinkler actuation in BRANZFIRE.

$$T_{cj} - T_{\text{int}} = \frac{16.9\dot{Q}^{2/3}}{H^{5/3}} \quad \text{for } \frac{r}{H} \le 0.18 \qquad \textbf{Equation 2.2}$$

$$T_{cj} - T_{\text{int}} = \frac{5.38\left(\dot{Q}/r\right)^{2/3}}{H} \quad \text{for } \frac{r}{H} > 0.18 \qquad \textbf{Equation 2.3}$$

$$U_{cj} = 0.96\left(\frac{\dot{Q}}{H}\right)^{1/3} \quad \text{for } \frac{r}{H} \le 0.15 \qquad \textbf{Equation 2.4}$$

$$U_{cj} = \frac{0.195 Q^{1/3} H^{1/2}}{r^{5/6}} \quad \text{for } \frac{r}{H} > 0.15 \qquad \textbf{Equation 2.5}$$

Where:

T_{cj} = ceiling jet temperature (K)

T_{int} = initial temperature (ambient temperature) (K)

$\dot{Q}$ = heat release rate (kW)

H = height of the ceiling above the base of the fire (m)

r = radial distance from the centre of the plume (m)

U_{cj} = ceiling jet velocity (m/s)

2.3.1.3 Sprinkler activation time

The differential equation shown below is incorporated into BRANZFIRE to calculate the sprinkler activation time and was derived by Heskestad and Bill (1988).

$$\frac{dT_e}{dt} = \frac{\sqrt{U_{cj}}\left(T_{cj} - T_e\right)}{RTI} - \frac{C\left(T_e - T_{\text{int}}\right)}{RTI} \qquad \textbf{Equation 2.6}$$

Where:

T_e = temperature of sprinkler link/detector (K)

t = time (s)

U_{cj} = ceiling jet velocity (m/s)

T_{cj} = ceiling jet temperature (K)

RTI = response time index of sprinkler $((m.s)^{1/2})$

C = C-factor of sprinkler $((m/s)^{1/2})$

T_{int} = initial temperature (ambient temperature) (K)

CHAPTER 3

3 WIND TUNNEL DEVELOPMENT and PERFORMANCE

3.1 UC wind tunnel development

As mentioned in Chapter 1, the UC2 wind tunnel was further developed in order to achieve the tunnel performance represented by the Factory Mutual Research Corporation (FMRC), this resulted in the UC3 tunnel. Previous studies were carried out at the University of Canterbury where the performance of sprinklers at the lower end of the nominal operating temperature scale (Table 1.1 in Chapter 1) were investigated using the UC wind tunnel. Literature such as Heskestad and Smith (1976, 1980), Heskestad and Bill (1987), Bill and Heskestad (1995), FM Approval Standard (2002), and International Standard (2004) describe the plunge test conditions used to test different types of sprinklers in the FM Approvals wind tunnel. From the above research, the commonly used test conditions of the plunge test for low actuation temperature (operating temperature) sprinklers can be summarised as follows:

- The hot gas temperature can be heated up to 300 ^{o}C.
- During the plunge test in the test section (sprinkler location), the selected hot gas temperature should remain constant with an accuracy of $\pm$ 1 ^{o}C for the hot gas temperature ranging from 129 ^{o}C to 141 ^{o}C and within $\pm$ 2 ^{o}C for all other hot gas temperatures.
- The hot gas velocity can be calibrated up to 2.6 m/s.
- During the plunge test in the test section (sprinkler location), the selected hot gas velocity should be maintained at a constant speed to an accuracy of $\pm$ 0.03 m/s for hot gas velocity ranging from 1.65 m/s to 1.85 m/s and from 2.4 m/s to 2.6 m/s.

In order to meet the criteria represented above, the UC wind tunnel was modified and developed from its first generation to its third generation. The first (UC1) and second

(UC2) generation wind tunnel were developed by Chin (2002) and Tsui (2002) respectively at University of Canterbury and are briefly described in the next sections. While, the newly developed (UC3) wind tunnel was fabricated based on the recommendations from Tsui (2004) and is described in details below.

3.1.1 UC1 wind tunnel

Figure 3.1: UC1 wind tunnel

Figure 3.1 above shows the configuration of the UC1 wind tunnel. In this wind tunnel, a flow straightener was used to reduce the turbulence level of the hot gas flow in the test section. It was inserted vertically within the hot gas flow and across the whole cross-section at the upstream side of the tunnel test section. Figure 3.2 below illustrates the configuration of the flow straightener inside the wind tunnel.

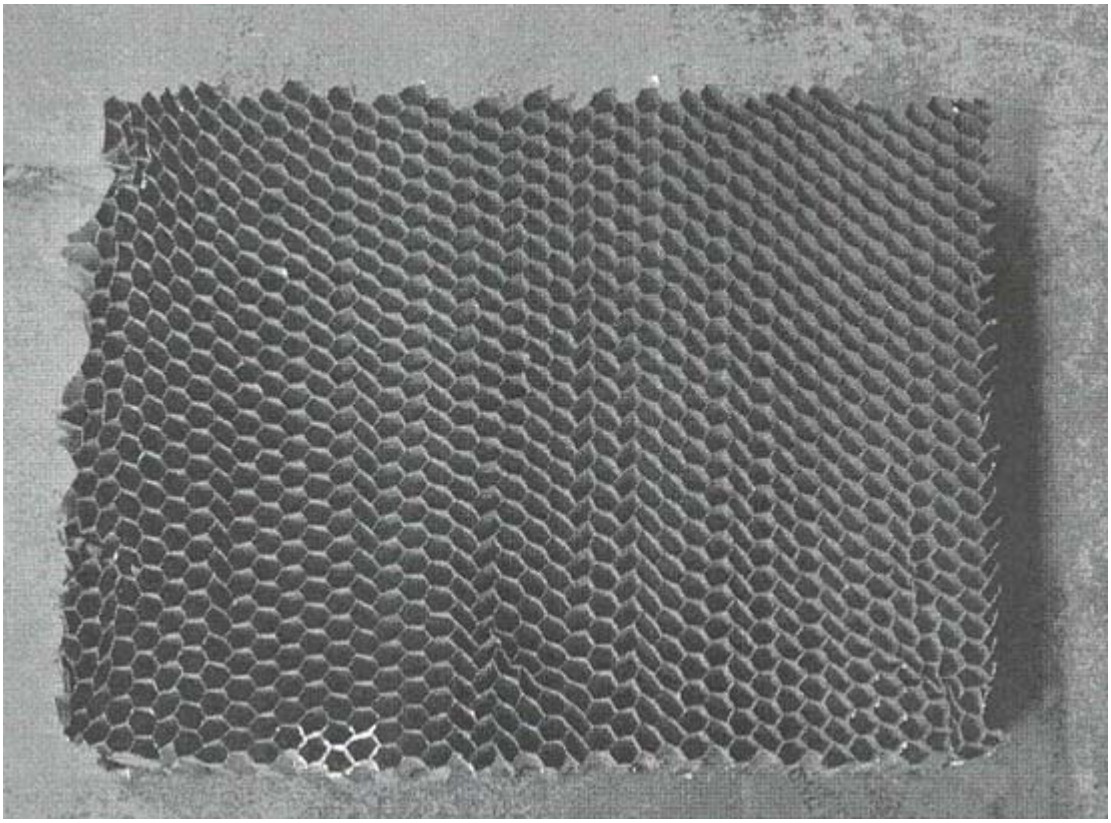

Figure 3.2: Flow straightener inside the wind tunnel

3.1.1.1 Limitations

It was found that the hot gas flow was still beyond the laminar flow limit required by the FMRC after the flow straightener was installed. Another limitation found using the flow straightener was that the configuration of the flow straightener significantly reduced the flow rate of the hot gas flow passing through it.

In addition to this, the hot gas temperature and velocity could not be calibrated to achieve the plunge test criteria represented by the FMRC.

Based on the limitations from the UC1 wind tunnel, the UC2 wind tunnel was designed and developed by Tsui (2002).

3.1.2 UC2 Wind Tunnel

3.1.2.1 Improvement

Figure 3.3: UC2 Wind Tunnel

Figure 3.3 above shows the appearance of the UC2 wind tunnel. In order to improve the performance and energy efficiency of the wind tunnel, there were a few modifications implemented on the UC1 wind tunnel. Those modifications are summarized as follows:

- The fan motor used to control the hot gas velocity was replaced with a multi speed unit which can be adjusted by varying the frequency of the fan revolution.
- The heating element used to heat up the hot gas temperature was controlled by a digital thermostat.
- All external steel surfaces (except the fan motor and the window of the test section) of the tunnel were insulated with glass wool fibre blankets to reduce the heat loss between the tunnel and the surroundings.

- All gaps were sealed with high temperature flexible gaskets to diminish the hot gas escape out from the tunnel.

The following points summarized the performance that was achieved by the UC2 wind tunnel:

- Hot gas temperature can be heated up to 120 ^{o}C.
- Hot gas velocity can be performed up to 3.5 m/s.

3.1.2.2 Limitations

By comparing the calibration results of the hot gas temperature and velocity measurements (Tsui 2004) to the FMRC wind tunnel criteria, it was found that some limitations still existed in the UC2 wind tunnel and these are listed below as follows:

- The hot gas velocity profile was not uniform in the cross-section of the tunnel test section at the sprinkler location and the variation level of the hot gas flow was larger than the requirements in the FMRC criteria.
- Even though the hot gas temperature profile was fairly uniform at the sprinkler location in the cross-section of the tunnel test section, it still did not achieve the FMRC requirements.

3.1.3 UC3 wind tunnel

Recommendations to further improve the wind tunnel were suggested by Tsui (2004). This is aimed to eliminate the limitations found from the UC2 wind tunnel and are represented as follows:

- The fan outlet should be centralized to provide a more uniform velocity distribution in the test section.
- The fan and motor should be relocated further upstream from the test section to provide more space to mix and reduce the fluctuating level of the oncoming flow.

- The heating element should be replaced with a high output unit so that sprinklers can be tested under a higher temperature plunge test conditions.
- The fan blade should be replaced and made from materials that can perform under a high temperature environment.

Based on the above recommendations, the UC3 wind tunnel was fabricated. It should be noted that the UC3 wind tunnel had a first and second model. The configuration and calibration results of the first model are shown in Figure 3.4 and Appendix A respectively. From the calibration results, the maximum hot gas velocity was recorded as 1.56 m/s in the test section at the sprinkler location (25 mm below the tunnel ceiling). Therefore, the velocity performance of the tunnel did not comply with the FMRC criteria. However, it was observed that the hot gas velocity in the lower zone of the test section was large and could be achieved up to 3 m/s. From these results, it was judged that a large proportion of the flow generated from the fan was impinged and flowed along with the bottom confining boundary of the tunnel. As a further means to overcome this problem, the fan should be shifted to the lower corner instead of the upper corner of the wind tunnel. This is because the new location of the fan allowed the generated flow to impinge and flow along with the upper confining boundary of the wind tunnel. This would result in an increase in the hot gas velocity at the sprinkler location in the test section. It was observed that the flow strength in the upper zone of the test section was stronger than before and the maximum hot gas velocity could be calibrated to reach the tunnel criteria from the FMRC after arranging the fan and motor to the lower corner of wind tunnel.

The configuration of the second model of UC3 wind tunnel is shown in Figure 3.5. It should be noted that the second model of UC3 wind tunnel was adopted to perform all calibrating tests and plunge tests in this study and was simply denoted as “UC3 wind tunnel” throughout the rest of this report. The calibration results of this modified wind tunnel are discussed in Chapter 4.

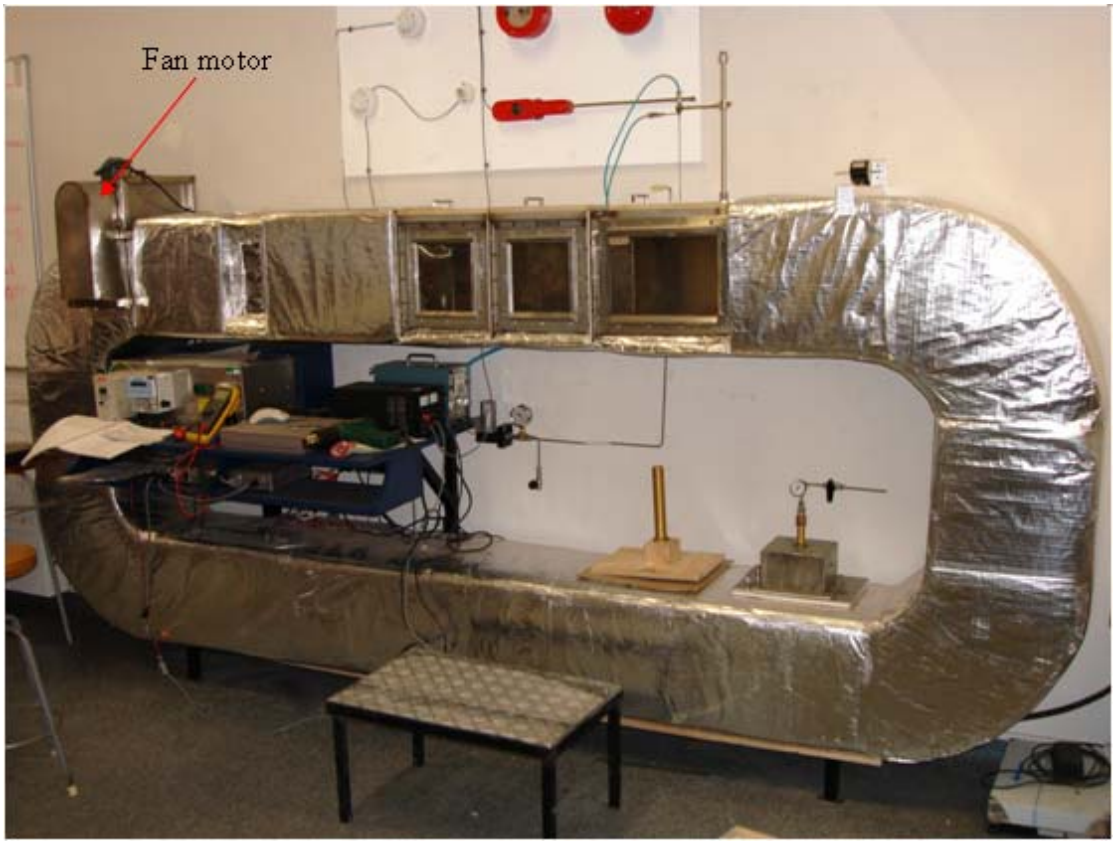

Figure 3.4: First model of the UC3 wind tunnel with fan in original location

Figure 3.5: Second model of the UC3 wind tunnel with fan relocated

3.1.3.1 Improvement

Improvements to the UC3 wind tunnel were carried out and are described as follows:

Dimensions of UC3 wind tunnel

By comparing with the UC2 wind tunnel, the length of the UC3 wind tunnel was extended by 1m and aimed to provide more space to mix the flow prior to the tunnel test section is reached. The dimensions of the wind tunnel and test section are tabulated in Table 3.1 below.

Table 3.1: Dimensions of the UC3 wind tunnel and the tunnel test section

	Length (m)	Width (m)	Depth (m)
Wind Tunnel	3.45	0.3	0.3
Test Section	0.36	0.3	0.3

Fan motor

As mentioned before, the fan motor was relocated in the lower corner of the wind tunnel to provide a stronger flow velocity in the upper zone of the test section. Additionally, the fan outlet was positioned at the centre of wind tunnel cross-section, with the aim of distributing the flow more uniformly inside the tunnel.

Flow divider

The main feature of this wind tunnel was that there were two flow dividers installed inside the wind tunnel. They were installed between the fan outlet and the upstream of the test section with the intention of distributing the hot gas flow more uniformly across the cross-section of the test section. The configuration and arrangement of the two flow dividers are sketched as below:

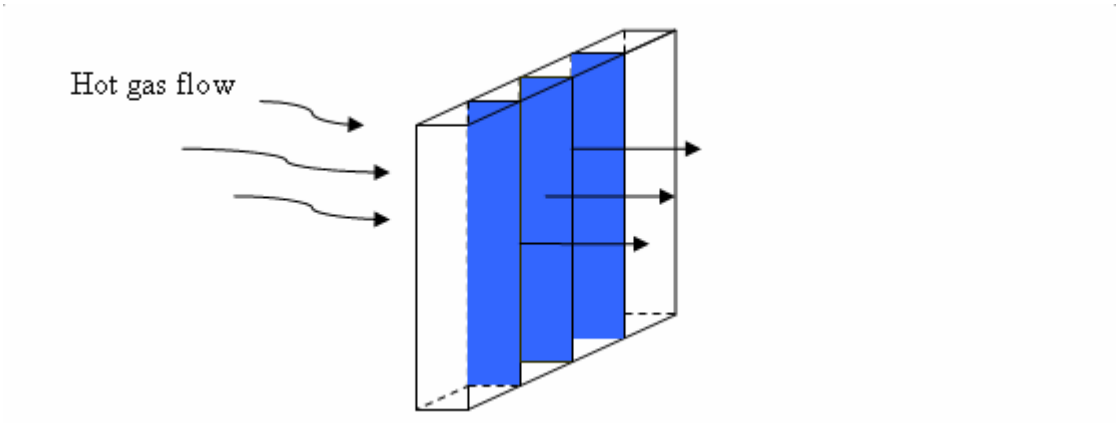

Figure 3.6: First flow divider

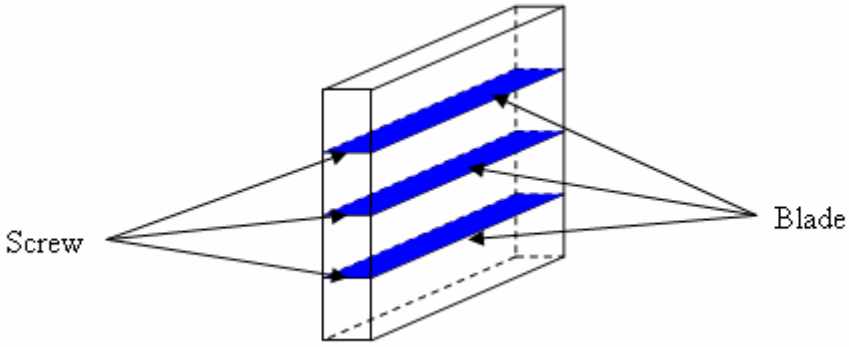

Figure 3.7: Second flow divider

It should be noted that the sketches shown above are placed in sequence, which means that the hot gas will flow through the first flow divider and then into the second. From Figure 3.6 and Figure 3.7, it can be seen that each flow divider consists of three blades. These blades can be rotated to a desired angle against the flow by turning the screws at the side of flow dividers. The blades' layout of these two flow dividers is different. For the first flow divider, the blades were orientated to divide the flow stream in the vertical direction. For the second divider, the blades were orientated to distribute the hot gas flow horizontally in the tunnel. The combination of these blades formed a "lattice" shape filter and efficiently distributed the flow in the wind tunnel.

Heating Element

A new heating element was used in this wind tunnel. The maximum power output of this heating element was 9 kW, which is similar to the heating element output of the

FMRC Approvals wind tunnel. By using this high performance heating element, the gas can be heated up to 300 ^{o}C inside the tunnel.

Fan blade

The fan blades in this tunnel were made from stainless steel. During the experiment, it was shown that they could perform well under the maximum hot gas temperature (300 ^{o}C).

Insulating Material

Similar to the UC2 wind tunnel, glass wool fibre blankets were used as the insulating material and covered the entire wind tunnel (except the fan motor and the window of test section). However, the thickness of the wool fibre blanket was twice the size as the product used in the UC2 wind tunnel.

Summary

The performance of the UC3 wind tunnel was summarized and is shown below, the figures were obtained from the wind tunnel calibration results represented in Chapter 4.

- Hot gas temperature can be heated up to 300 ^{o}C.
- At the sprinkler location in the test section, the selected hot gas temperature maintained a constant temperature with an accuracy of $\pm$ 1 ^{o}C for the hot gas temperature ranging from 129 ^{o}C to 141 ^{o}C and within $\pm$ 2 ^{o}C for all other hot gas temperatures.
- Hot gas velocity can be created up to 2.94 m/s.

3.1.3.2 Limitations

From the summary above, it can be seen that the accuracy of the calibrated temperature and the maximum calibrated temperature and velocity generated from the UC3 wind tunnel met the FMRC tunnel criteria set for this study. However, based on

the calibration results described in Chapter 4, limitations still existed in this tunnel and need to be considered in the future. These limitations are mentioned as follows:

- The glue (used to glue the gaskets to the gaps between the wind tunnel sections) melted under the maximum calibrated hot gas temperature (300 ^{o}C). The maximum safely calibrated temperature was determined to be 200 ^{o}C, and therefore 200 ^{o}C was the highest temperature that was used in wind tunnel calibrating tests and plunge tests.
- At the sprinkler location in the test section, the selected hot gas velocity was constant with an accuracy of ± 0.20 m/s for range from 1 m/s to 2.94 m/s. Apparently, it could not achieved the FMRC criteria (± 0.03 m/s).

The recommendations used to further improve the UC3 wind tunnel are described in Chapter 10 in this report.

3.2 Instrumentation

3.2.1 Gas temperatures

The gas temperatures inside the wind tunnel and the ambient temperature were measured by using 0.5 mm bead diameter chromel/alumel (Type K) thermocouples. The thermocouple used to measure the ambient temperature during tests was placed at a convenient location which was not affected by the heated wind tunnel apparatus.

In order to measure the temperatures as a function of depth in the wind tunnel, a thermocouple tree was fabricated and used. The thermocouple tree consisted of 21 thermocouples, the interval between each thermocouple is 5 mm for the first 40 mm (from the top to bottom of wind tunnel) and it increased to 200 mm thereafter. Figure 3.8 below shows the thermocouple tree used in this study.

Figure 3.8: Thermocouple tree placed inside the wind tunnel

Figure 3.9: Temperature control panel

Figure 3.9 shows the temperature control panel of the wind tunnel, it was used to adjust the hot gas temperature.

3.2.2 Gas velocities

The gas velocity in the wind tunnel was measured using a Pitot-static tube. The Pitot-static tube was used in conjunction with a pressure transducer (See Figure 3.10), this allowed a direct measurement of dynamic pressure which can be used to calculate the gas velocity in the wind tunnel.

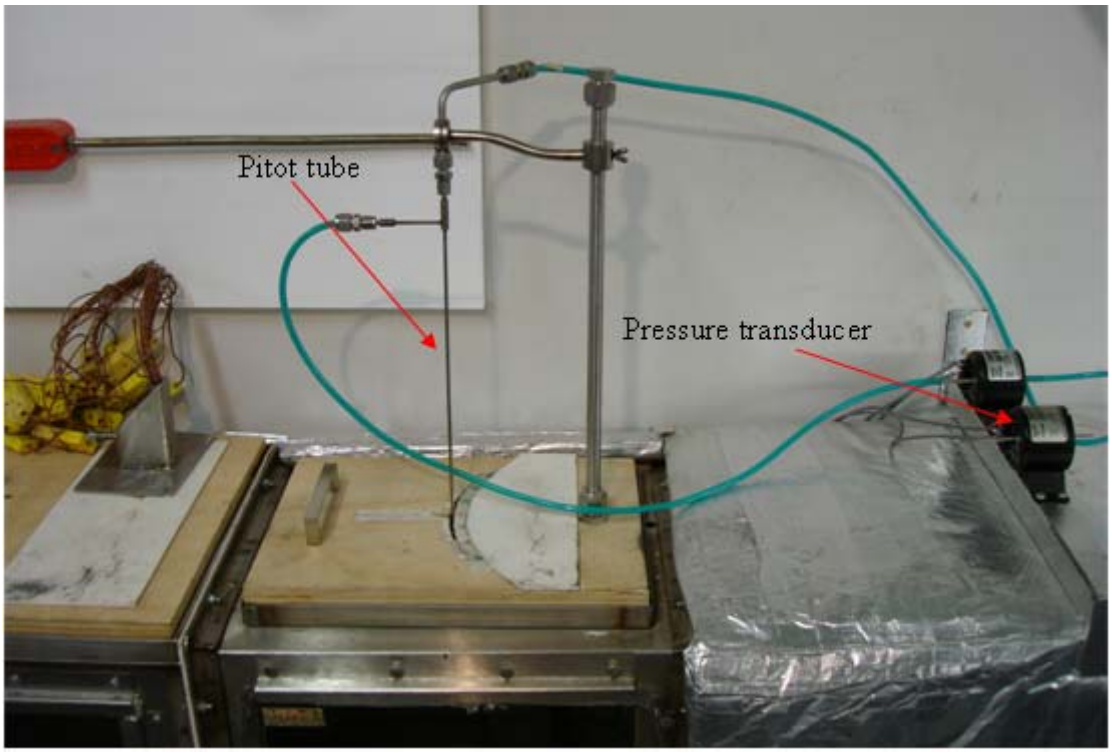

Figure 3.10: Pitot-static tube and pressure transducer

The hot gas velocity in the tunnel was controlled by the speed of the fan. Figure 3.11 shows the fan revolution speed controller for the wind tunnel.

Figure 3.11: Fan revolution speed controller

The hot gas velocity can be calculated by using the equation represented below:

$$U = \sqrt{\frac{\Delta P \times 2 \times (273 + T_a)}{353}} \qquad \text{Equation 3.1}$$

Where:

U = hot gas velocity in the wind tunnel (m/s)

ΔP = pressure differential reading from the pressure transducer (Pa)

T_a = hot gas temperature in the wind tunnel (^{o} C)

3.2.3 Vacuum Pump

As described in Chapter 2, a vacuum pump was used to generate flow through the sprinkler housing of the mounting plate for both recessed and concealed sprinklers. Figure 3.12 below shows the vacuum pump for the wind tunnel. The rate of vacuum can be adjusted by loosening/tightening the valve as shown in Figure 3.12.

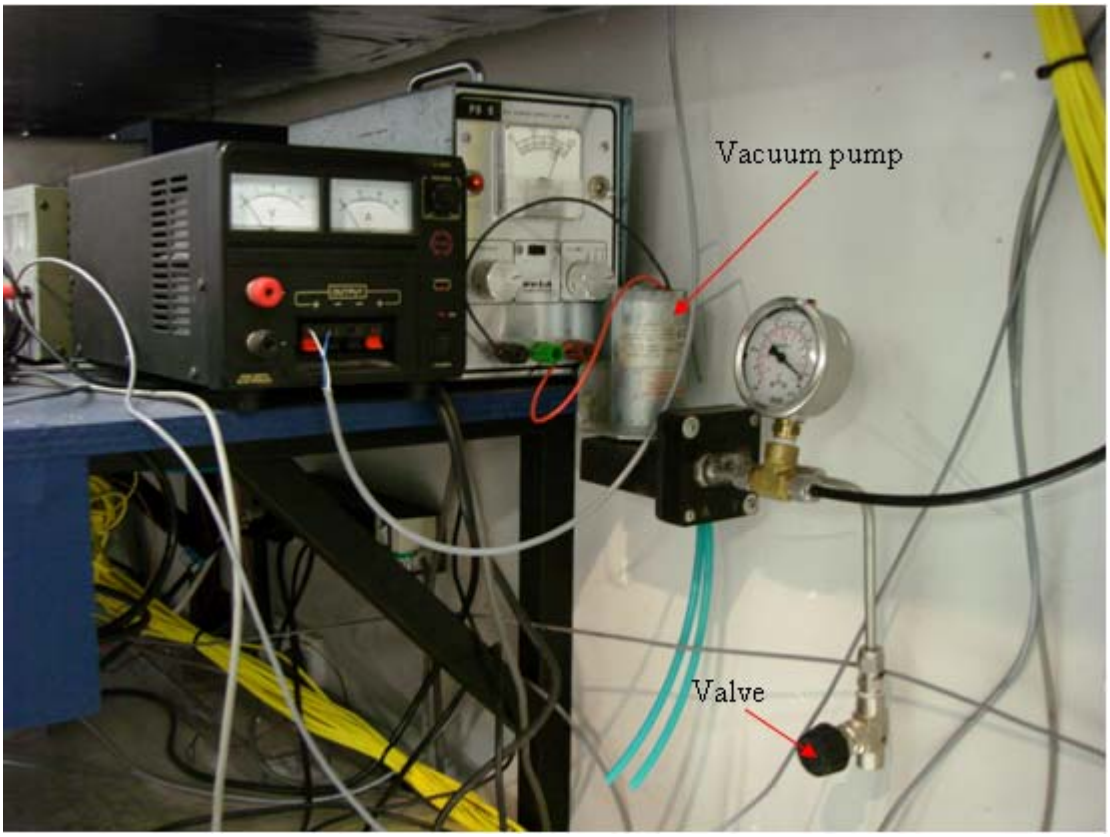

Figure 3.12: Vacuum pump

3.2.4 Data recording

All of the instrument readings were recorded by using the Universal Data Logging (UDL) computer software. The UDL transferred all the received data in the form of an EXCEL spreadsheet and then stored them in a computer, from which the data could be processed to perform further analysis.

3.3 UC3 wind tunnel calibrating approach

The calibrating approach used to determine the stability, uniformity and consistency of hot gas temperature and velocity in the UC3 wind tunnel is shown in this section.

3.3.1 Velocity calibration

3.3.1.1 Blade (flow divider) orientation

In order to obtain a more uniform flow distribution in the wind tunnel test section, the optimum orientation of blades was determined. The measuring locations of velocities were distributed across the mid cross-section of the wind tunnel test section. In addition to this, the gas velocities were measured under three different temperatures, which were 20 ^{o}C, 128 ^{o}C and 200 ^{o}C. 20 ^{o}C was assumed as the ambient temperature. Other tested temperatures were selected based on the plunge test conditions for recessed and concealed sprinklers represented by Bill and Heskestad (1995). The maximum fan revolution frequency was recorded as 45 Hz and used at each test condition. The optimum orientation of blades was determined when it provided the most stable and uniform flow distribution for all test conditions. It should be noted that this task was the preliminary calibrating test and the optimum blades' orientation was fixed and used to perform all wind tunnel calibrating tests and plunge tests after the orientation was determined.

- Test duration: 600 s (at each test location)
- Test location: distribute at the mid cross-section of the test section
- Test condition: three different sets (See Table 3.2)

Table 3.2: Test conditions for testing blade orientation

	Test condition 1	Test condition 2	Test condition 3
Temperature (^{o}C)	20	128	200
Fan revolution frequency (Hz)	45	45	45

3.3.1.2 Velocity stability

The maximum response time of recessed and concealed sprinklers was recorded as 867 s in plunge tests (Bill and Heskestad 1995), and therefore the selected duration (1200 s) allowed a sufficient margin for testing of the sprinkler's response time. The test location was chosen based on the approximate position of the heat-responsive element of sprinklers. Test condition 1 (200 ^{o}C and 45 Hz) was the upper operating limit of this wind tunnel. It was assumed that if the wind tunnel could perform well under this ultimate test condition, then it would be able to perform well for hot gas temperatures and velocities which were smaller than the upper operating limit of the wind tunnel.

- Test duration: 1200 s
- Test location: mid span (width) and 25 mm below the bottom of cover plate
- Test condition: See Table 3.3

Table 3.3: Test condition for testing velocity stability

	Test condition 1
Temperature (^{o}C)	200
Fan revolution frequency (Hz)	45

3.3.1.3 Fan blades' stability

A prolonged test (3600 s) was conducted to examine the fan blades' condition and integrity when they were exposed to a prolonged high temperature environment. The test location and condition was identical to the test in the previous section.

- Test duration: 3600 s
- Test location: mid span (width) and 25 mm below the bottom of cover plate
- Test condition: the same as Table 3.3

3.3.1.4 Velocity uniformity

The velocity uniformity of the wind tunnel was determined by obtaining the velocity profile at the mid cross-section of the test section. In order to establish the velocity profile, velocities were measured at 49 different locations in each test condition. In Table 3.4, the term "7 mm" in depth implies the measuring location was below the bottom of cover plate at a distance of 7 mm. The "0 mm" in width indicates the mid-span point at the short span direction of the cover plate. Negative width value meant that the corresponding point was located at the left hand side of the mid-span point. Test condition 1 was extracted and identical to the test condition used by Tsui (2004), and therefore the calibration results could be used to compare the results obtained by Tsui.

- Test duration: 600 s
- Test location: 49 different locations (See Table 3.4)
- Test condition: two different sets (See Table 3.5)

Table 3.4: Measuring locations

Location	Depth (mm)	Width (mm)	Location	Depth (mm)	Width (mm)
1	7	-75	**26**	27	0
2	12	-75	**27**	32	0
3	17	-75	**28**	37	0
4	22	-75	**29**	7	25
5	27	-75	**30**	12	25
6	32	-75	**31**	17	25
7	37	-75	**32**	22	25
8	7	-50	**33**	27	25
9	12	-50	**34**	32	25
10	17	-50	**35**	37	25
11	22	-50	**36**	7	50
12	27	-50	**37**	12	50
13	32	-50	**38**	17	50
14	37	-50	**39**	22	50
15	7	-25	**40**	27	50
16	12	-25	**41**	32	50

17	17	-25	**42**	37	50
18	22	-25	**43**	7	75
19	27	-25	**44**	12	75
20	32	-25	**45**	17	75
21	37	-25	**46**	22	75
22	7	0	**47**	27	75
23	12	0	**48**	32	75
24	17	0	**49**	37	75
25	22	0			

Table 3.5: Test conditions for testing velocity uniformity

	Test condition 1	Test condition 2
Temperature (^{o}C)	120	200
Fan revolution frequency (Hz)	45	45

3.3.1.5 Velocity reproducibility (consistency)

The velocity reproducibility of the wind tunnel was assessed on two different days using the same test condition. The objective of this test was achieved when the results from both tests were similar.

- Test duration: 600 s
- Test location: mid span (width) and 25 mm below the bottom of cover plate
- Test condition: See Table 3.6

Table 3.6: Test condition for testing velocity reproducibility

	Test condition in day 1	Test condition in day 2
Temperature (^{o}C)	200	200
Fan revolution frequency (Hz)	45	45

3.3.2 Temperature calibration

3.3.2.1 Temperature stability

Temperatures inside the wind tunnel were recorded using the thermocouple tree, where data collected from six different thermocouples (Table 3.7) was used to compare the calibration results obtained by Tsui (2004).

- Test duration: 1200 s
- Test location: 6 different locations (See Table 3.7)
- Test condition: the same as Table 3.5

Table 3.7: Test for testing temperature stability

Location	Depth (mm)	Width (mm)
1	0	0 (at the mid span)
2	5	0 (at the mid span)
3	10	0 (at the mid span)
4	15	0 (at the mid span)
5	100	0 (at the mid span)
6	280	0 (at the mid span)

3.3.2.2 Temperature uniformity

In order to obtain the temperature profile of the wind tunnel, tests were carried out to record temperatures at different locations in the test section. The thermocouple tree was used to record temperatures inside the wind tunnel.

- Test duration: 600 s
- Test location: 3 different locations (See Table 3.8)
- Test condition: the same as Table 3.5

Table 3.8: Test locations for testing temperature uniformity

Location	Depth (mm)	Width (mm)
1	Thermocouple tree	- 50
2	Thermocouple tree	0 (at the mid span)
3	Thermocouple tree	50

3.3.2.3 Temperature reproducibility

Similar to the velocity reproducibility tests, the temperature reproducibility was examined by conducting two tests with identical test conditions on two different days. The test location for both tests was arranged at the mid-span (width) of the cover plate.

- Test duration: 600 s
- Test location: mid span (width) with thermocouple tree
- Test condition: the same as Table 3.6

3.3.3 Thermocouple tree location for plunge tests

Tests were carried out to determine the thermocouple tree location for plunge tests. The determination of the thermocouple tree depended on two conditions, which were:

1. The temperatures at this location were similar to the temperatures at the mid-span point of the cover plate.
2. The location of the thermocouple tree would not influence the oncoming hot gas velocity at the sprinkler location in the test section.

- Test duration: 600 s
- Test location: tested around the mid-span point of the cover plate
- Test condition: the same as Table 3.3

3.3.4 Calibrating procedure

The calibrating procedure used to characterise the stability, uniformity and reproducibility of hot gas temperature and velocity in the wind tunnel is described as follows:

1. The initial ambient temperature was recorded.
2. The Pitot-static tube and thermocouple tree were placed at the desired measuring locations.
3. The temperature was set by using the temperature control panel.
4. The velocity was set by adjusting the fan revolution speed controller.
5. The cover plate was checked and ensured to be closed.
6. The tunnel condition was stabilized for a minimum period of 30 minutes after the pre-set hot gas temperature and velocity were reached.
7. The stop watch was reset.
8. The stop watch and the UDL were turned-on simultaneously.
9. The test and the UDL were stopped when the test duration was reached.

CHAPTER 4

4 WIND TUNNEL CALIBRATION RESULTS AND DISCUSSION

The results from calibrating the UC3 wind tunnel to examine the velocity and temperature performance are given and analysed below. The calibration results obtained from the UC2, FMRC Approvals and FRS wind tunnel are also presented to compare the performance of the UC3 wind tunnel in this chapter.

4.1 Velocity calibration

4.1.1 Blade (flow divider) orientation

A large number of tests were conducted to assess the optimum blades' orientation for the UC3 wind tunnel. The best calibration results were obtained when the blade's orientation of the first and second flow divider were arranged as shown in Figure 4.1. All blades of the first flow divider were arranged parallel to the flow streams and worked to divide the hot gas flow evenly across the width of the wind tunnel. For the second flow divider, the first and third blades and the second blade were rotated to an angle of 15 ^{o} and 30 ^{o} respectively.

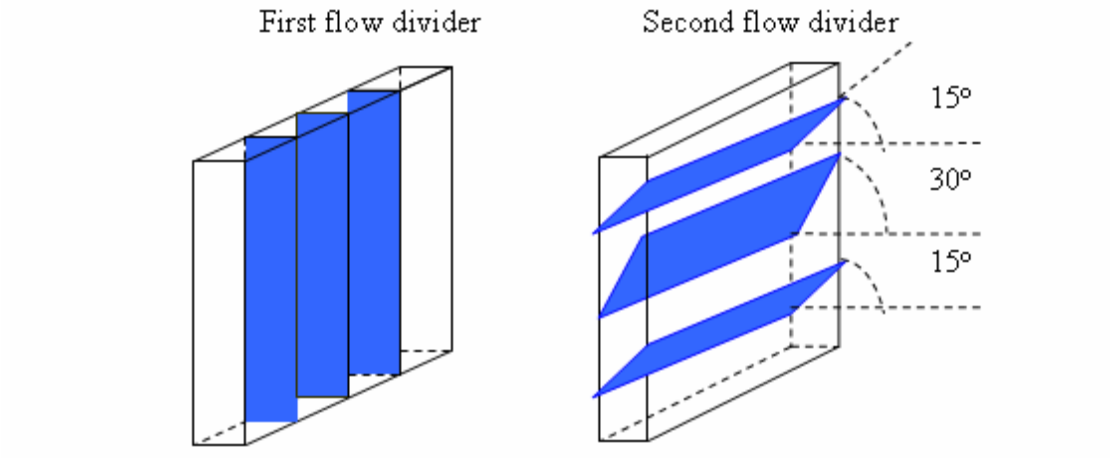

Figure 4.1: Optimum blades' orientation

The calibration results from the horizontal blades' orientation was also illustrated in this section and used to compare the results obtained from the optimum blades' orientation. For the horizontal blades' orientation, the blades' orientation of the first flow divider was the same as the optimum blades' orientation. However, all blades of the second flow divider were set horizontal to the flow in the tunnel (0 ^{o} to the flow direction). Figure 4.2 and Figure 4.3 show the maximum velocity comparison and velocity variation range comparison respectively for the horizontal and optimum blades' orientation.

As mentioned in Chapter 3, the maximum velocity criterion set for this study was 2.6 m/s. Apparently, the maximum velocities provided from both blades' orientation achieved this criterion. However, it was observed that the velocity variation ranges of the optimum blades' orientation were smaller than the horizontal blades' orientation (all other tests), and therefore this orientation was considered to be the best blades' orientation of this wind tunnel.

Appendix B shows the calibration results used to plot Figure 4.2 and Figure 4.3.

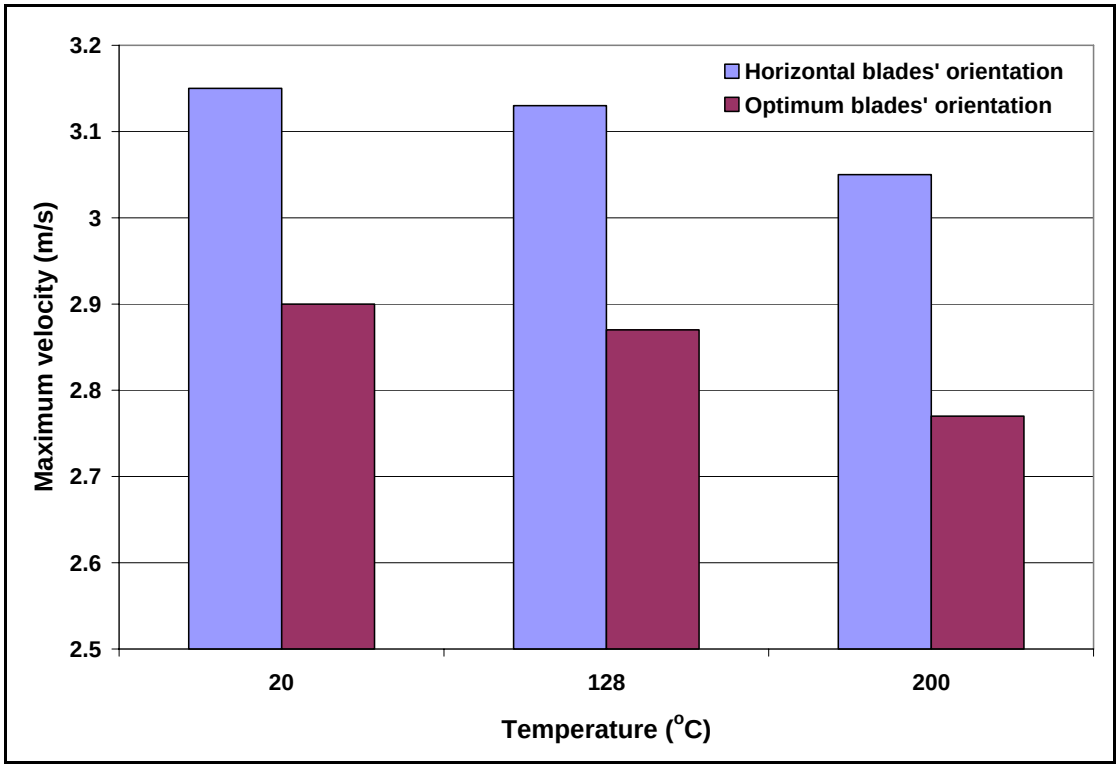

Figure 4.2: Maximum velocity of the horizontal and optimum blades' orientation

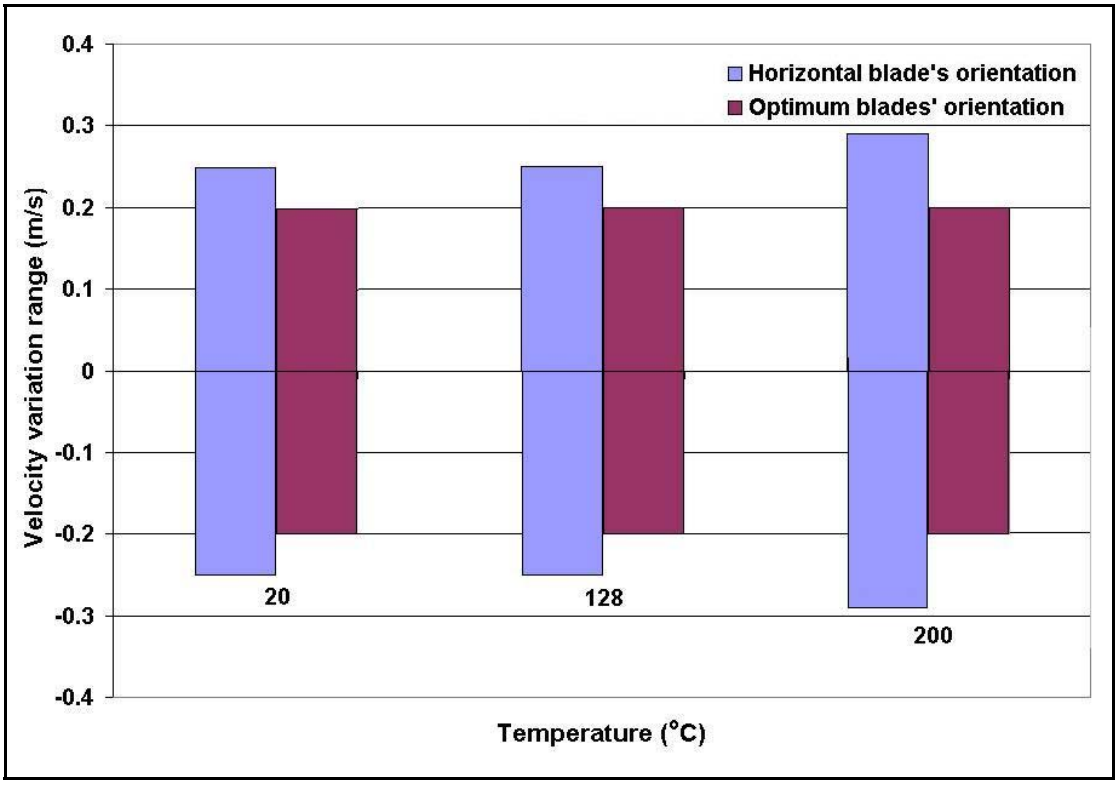

Figure 4.3: Velocity variation range of the horizontal and optimum blades' orientation

4.1.2 Velocity stability

Figure 4.4 shows the velocity record for a duration of 1200 s at the sprinkler location of the test section under the upper operating limit (200 ^{o}C and 45 Hz) of the wind tunnel. It can be seen that the hot gas velocities were averaged at 2.78 m/s and fluctuated within ± 0.2 m/s. From the FMRC criteria, the hot gas velocity shall be maintained constant to an accuracy of ± 0.03 m/s for hot gas velocity ranges from 1.65 m/s to 1.85 m/s and from 2.4 m/s to 2.6 m/s. The FMRC criteria were not satisfied for the velocity stability of this wind tunnel and needs to be improved in the future. However, it was the best result that could be obtained from the UC3 wind tunnel, and therefore plunge tests were conducted despite this limitation.

In order to develop the UC3 wind tunnel, it was considered that the thickness of the flow straightener should be increased to reduce the velocity variation level. However, this will result in a significant reduction of the hot gas velocity in the wind tunnel. As a result, a more powerful fan motor will be needed if a thicker flow straightener is installed in the wind tunnel.

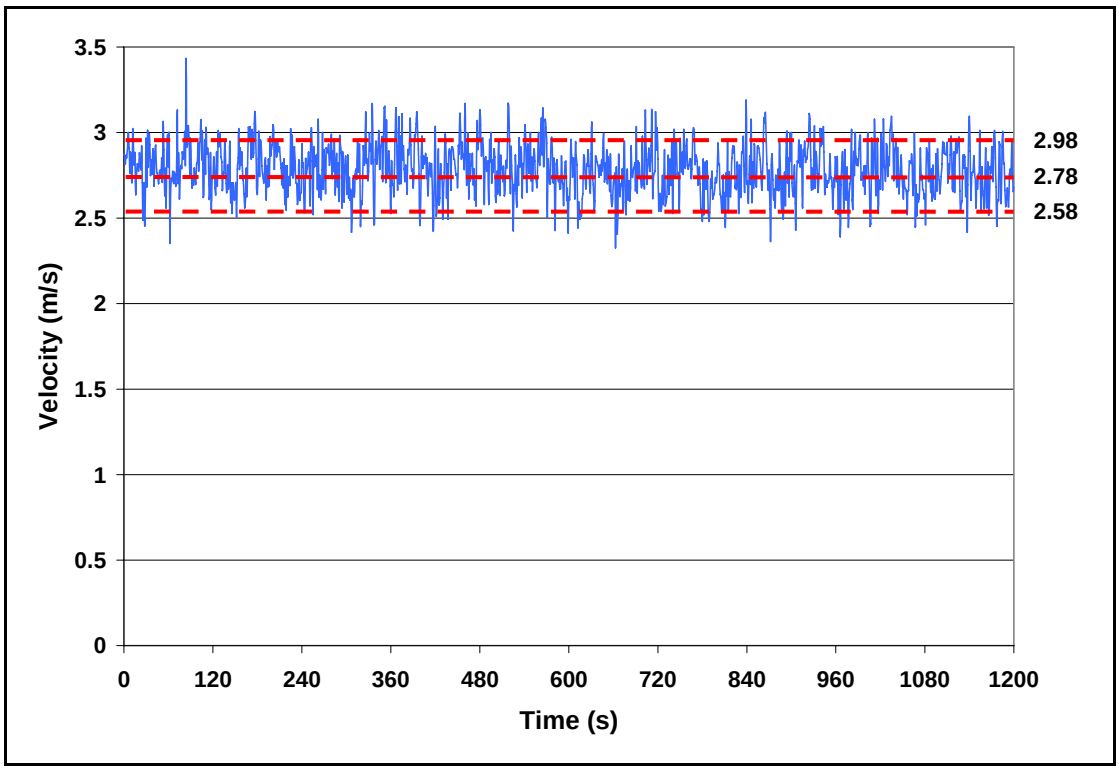

Figure 4.4: Velocity stability (200 ^{o}C and 45 Hz)

4.1.3 Fan blades' stability

Figure 4.5 shows the velocity record for assessing the stability of the fan blades. It can be seen that the fan blades were able to maintain stable operation under the upper operating limit of the wind tunnel for a long duration.

Based on the results shown in this figure, it was also reasonable to assume that the hot gas velocity can be maintained in a stable condition for a long period of time after the predetermined velocity was reached in the wind tunnel.

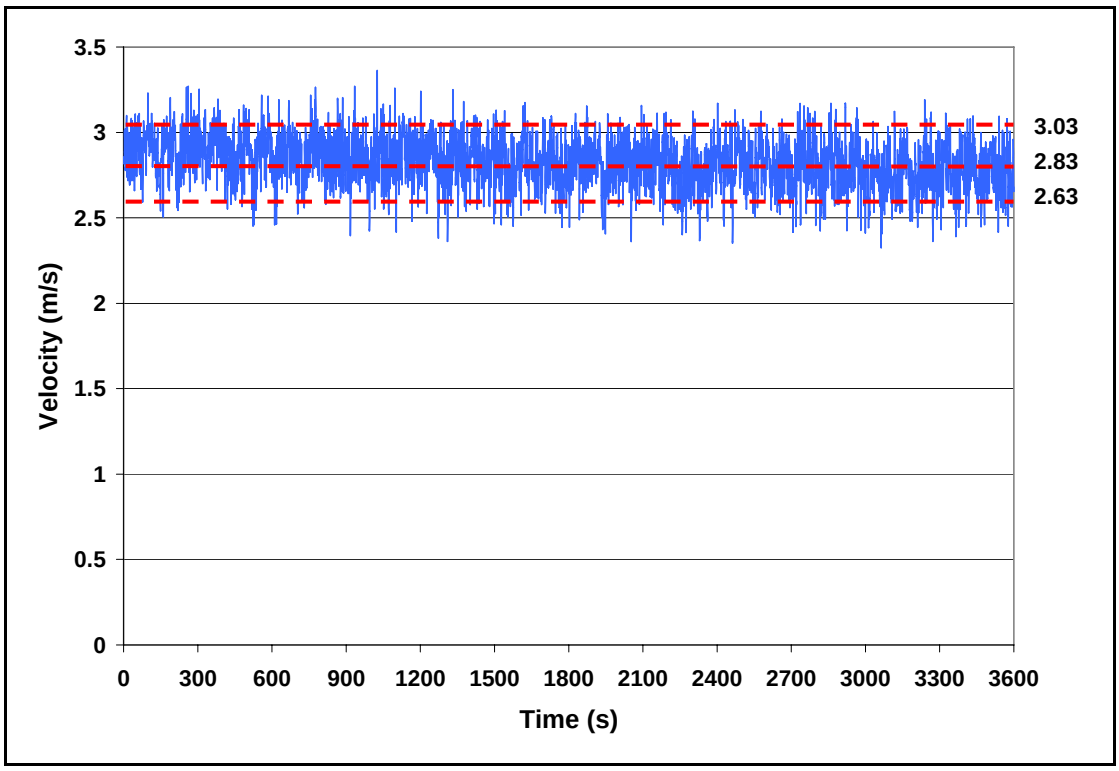

Figure 4.5: Fan blades' stability (200 ^{o}C and 45 Hz)

4.1.4 Velocity uniformity

Figure 4.6 shows the velocity profile at the mid cross-section of the wind tunnel test section under the upper operating limit of the tunnel. The velocity profile obtained at tunnel condition of 120 ^{o}C and 45 Hz are shown in Section 4.4.2 and were used to compare the velocity profile of the UC2, FMRC and FRS wind tunnel. It should be noted that the arrows sketched at the bottom of these figures indicate the hot gas flow direction in the wind tunnel. This also means that the velocity profile was rotated 90 ^{o} from its original orientation and purposed to aid the visualisation of the results. The negative notations shown in figures indicate the locations on the left of the mid-span point of the tunnel.

From this figure, it was observed that the velocity profile was not uniform in both the depth and width direction. In the depth direction, the velocities decreased gradually from "37 mm" to "0 mm". In the width direction, the maximum velocities were measured at "50 mm" and "- 50 mm". It was considered that two flow dividers were not sufficient to distribute the flow evenly in the wind tunnel. Hence, it is recommended that more flow dividers should be installed at the upstream side of the

test section. Additionally, the number of blades contained in one flow divider should be increased to distribute the hot gas flow more efficiently.

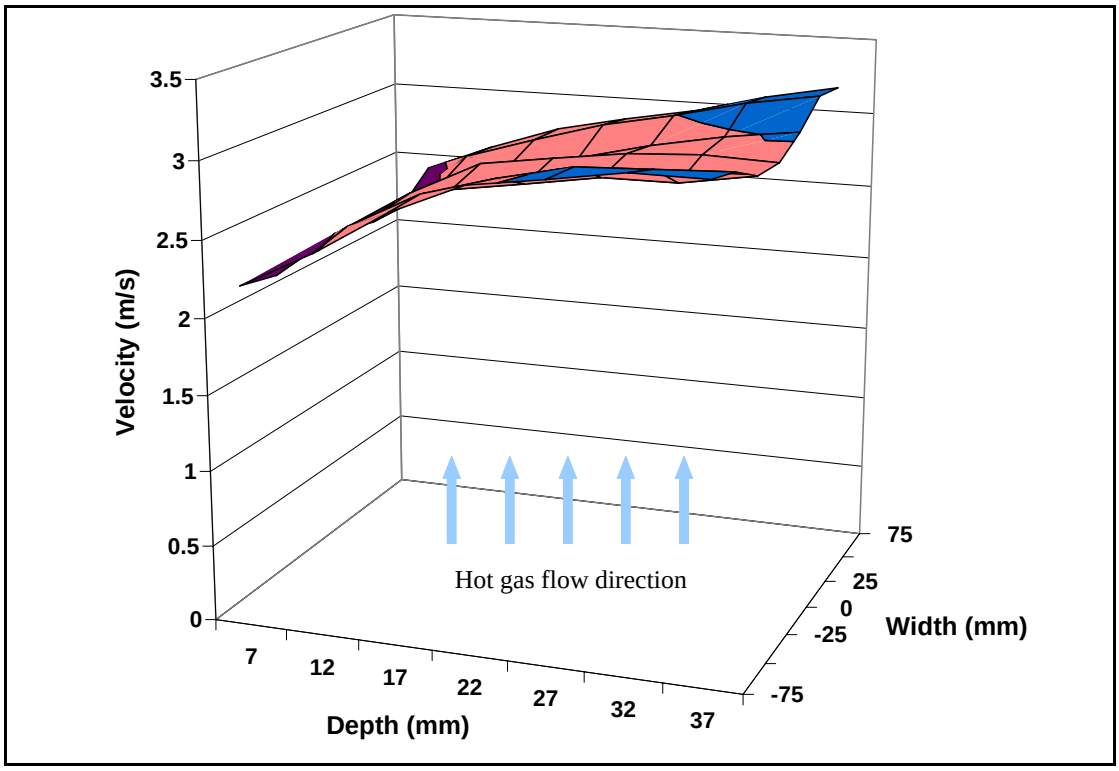

Figure 4.6: Velocity profile at the mid cross-section of the test section (200 ^{o}C and 45 Hz)

4.1.5 Velocity reproducibility (consistency)

Figure 4.7 below shows the velocities recorded at two different days under identical tunnel conditions. From this figures, it was obvious that the velocities recorded for both days were very similar. The similarity of these results implied that the wind tunnel was reliable and could produce consistence outcomes at different times by setting the using the same tunnel conditions.

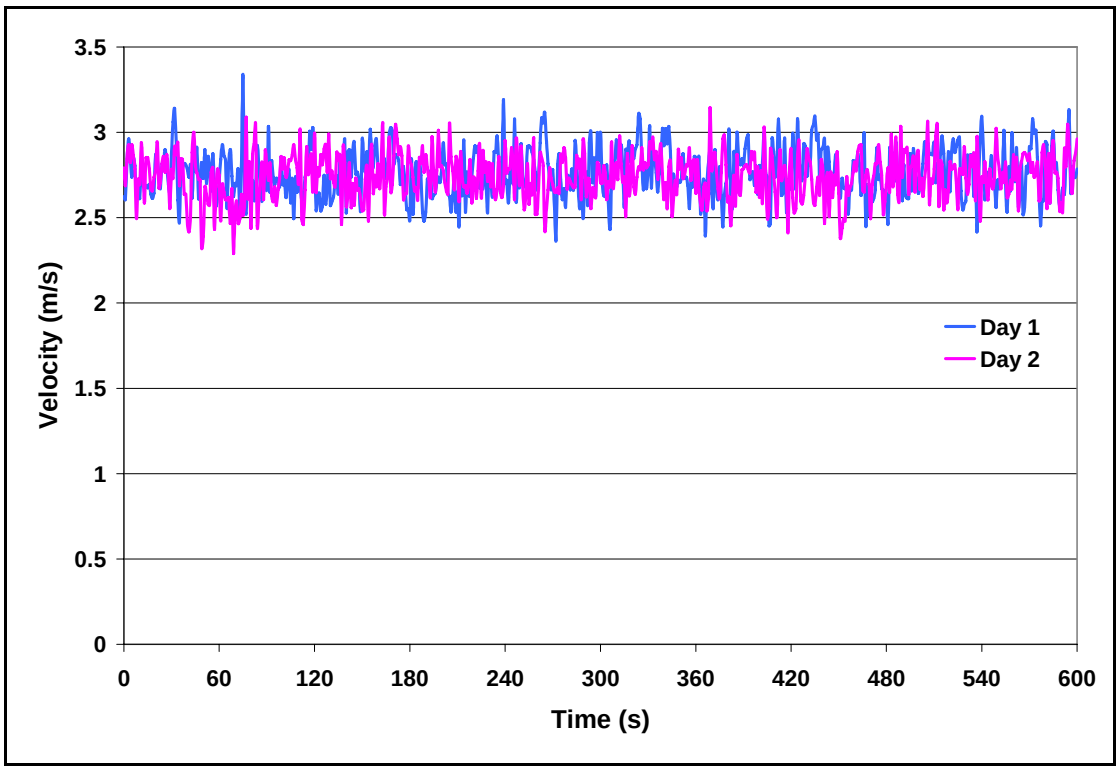

Figure 4.7: Velocity records at day 1 (200 ^{o}C and 45 Hz) and day 2 (200 ^{o}C and 45 Hz)

4.2 Temperature calibration

4.2.1 Temperature stability

Figure 4.8 shows the temperature records for a duration of 1200 s at the mid-span (width) of the tunnel test section. “0 mm” indicated the location at the bottom of the cover plate/ceiling of the tunnel test section. From this figure, the maximum temperatures were recorded at a distance of 100 mm below the ceiling of the test section. The lowest temperatures were measured at “0 mm,” this is because the temperatures at this location were affected by the boundary layer formed along the ceiling of the wind tunnel.

The temperature profiles shown in this figure were represented as wavy lines and repeated as periods across the recorded duration. It is considered that they were affected by the hysteresis of the heating system of the wind tunnel. The Hysteresis of the heating system means that the gas temperatures were affected slowly when the operating stage of the heating system was changed (switched on or off).

The occurrence of the hysteresis of the heating system was unavoidable, and therefore it was considered that the temperatures in the wind tunnel were very stable.

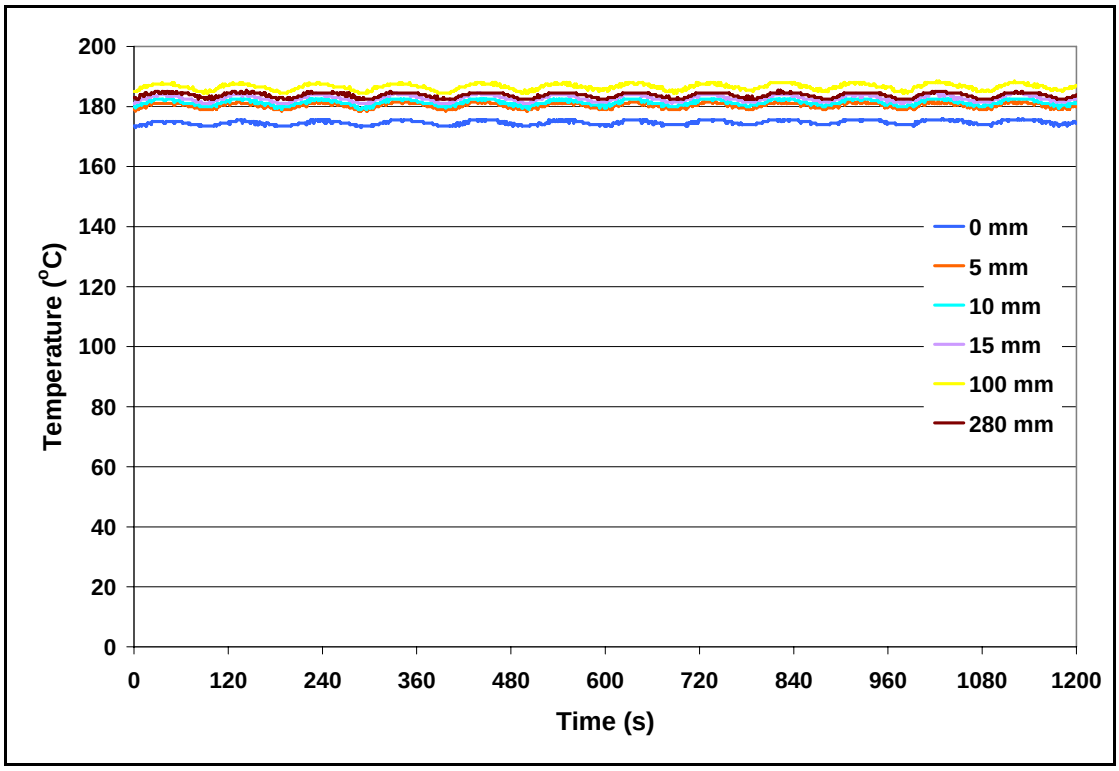

Figure 4.8: Temperature stability (200 °C and 45 Hz)

4.2.2 Temperature uniformity

Figure 4.9 below shows the temperature profile at the mid cross-section of the wind tunnel test section under the tunnel condition of 200 °C and 45 Hz. The temperature profile obtained at a lower temperature tunnel condition (120 °C and 45 Hz) is presented in Section 4.4.2 and used to compare the temperature profiles obtained from the UC2, FMRC and FRS wind tunnel.

From this figure, it can be seen that the temperatures were fairly uniform across the mid cross-section of the tunnel test section below 10 mm depth. Due to the influence of the boundary flow layer, the temperatures decreased progressively from 10 mm to 0 mm below the ceiling of the wind tunnel. The results from this figure also implied that the output of the heating element was sufficient to support and maintain high temperatures for the flow in the tunnel.

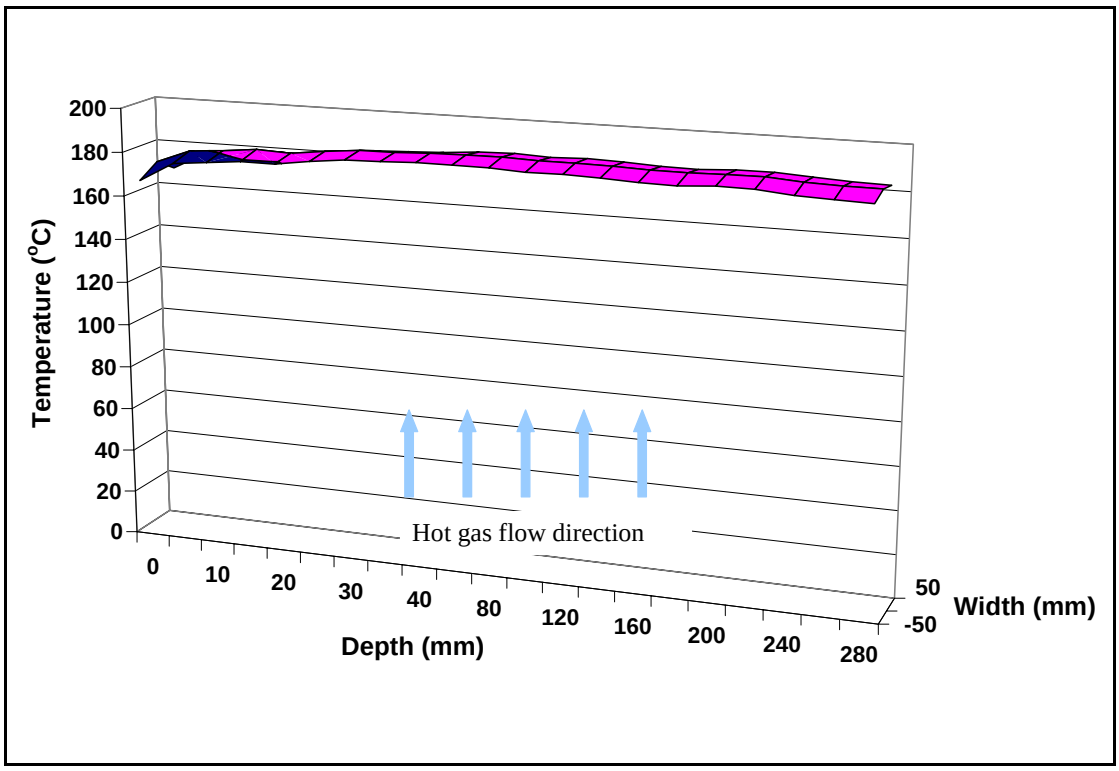

Figure 4.9: Temperature profile at the mid cross-section of the test section (200 °C and 45 Hz)

4.2.3 Temperature reproducibility

Figure 4.10 shows the temperature recorded on two different days by using the thermocouple tree. The values shown in the x-axis of this figure indicated the locations of thermocouples which were mounted in the thermocouple tree. It can be seen that temperatures recorded on both days at each thermocouple location gave similar results. The maximum temperature difference at a single measuring location was only 1% and occurred at the "0 mm" location. The similarity of the results obtained on both days implied that the wind tunnel can generate consistent temperature results at different times by setting identical tunnel test conditions. As a conclusion, it was recognized that this wind tunnel had excellent temperature reproducibility.

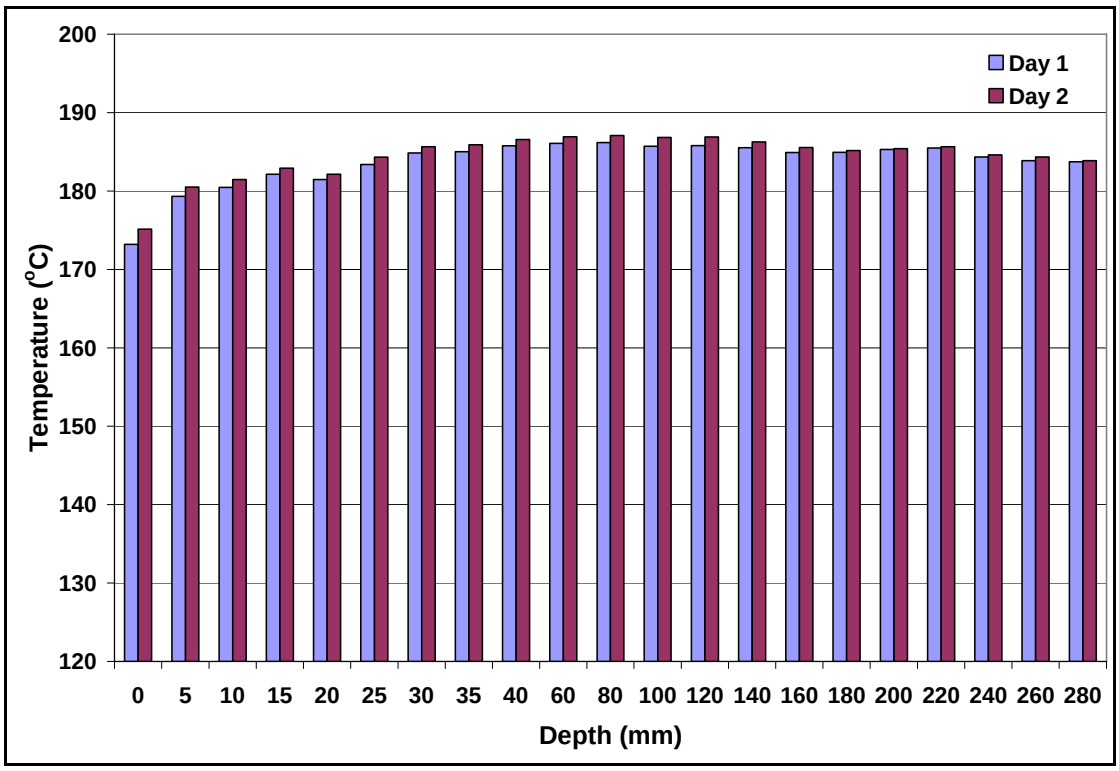

Figure 4.10: Temperature records on day 1 and day 2 (200 °C and 45 Hz)

4.3 Thermocouple tree location for plunge test

Figure 4.11 shows the location of the thermocouple tree for plunge test. The distance between the thermocouple tree and the mid-span (width) of the cover plate was measured as 0.3 m.

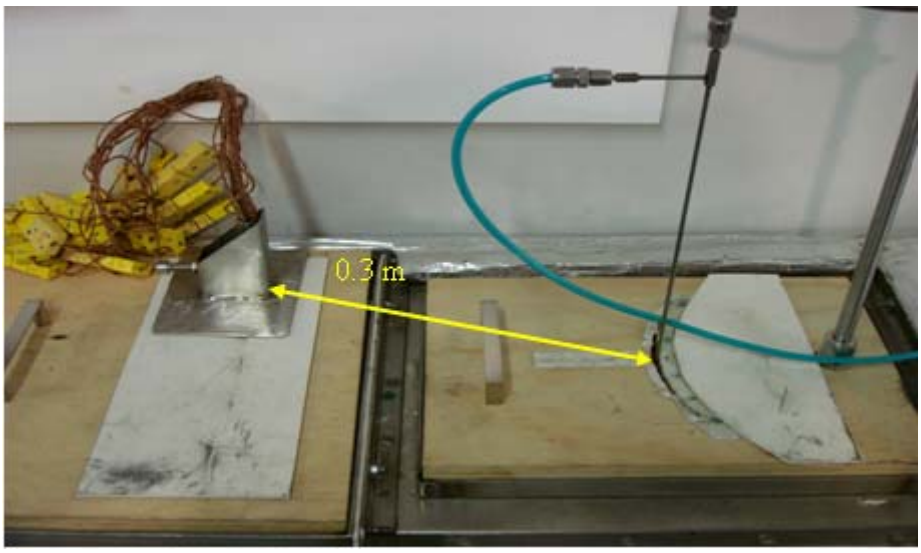

Figure 4.11: Thermocouple tree location for plunge test

Figure 4.12 shows the temperatures recorded at both the mid-span (width) of cover plate and the thermocouple tree location under the same tunnel condition. From this figure, the temperatures recorded at the thermocouple tree location were similar and slightly greater than the mid-span (width) of the cover plate. The maximum temperature difference between these two locations was calculated as 1.7%.

Figure 4.13 shows the comparison of velocities obtained from two different tests. The blue lines represent the velocities measured at the sprinkler location of the test section but without inserting the thermocouple tree in the wind tunnel. In contrast, the purple lines represent the velocities recorded when the thermocouple tree was used at the thermocouple tree location. Based on the comparison of the results, the velocities of both tests were consistence and had very similar average velocities.

From the analysis above, it can be concluded that the thermocouple tree could be placed in the thermocouple tree location to measure the temperature profile during plunge test by without affecting the oncoming flow at the sprinkler location of the test section.

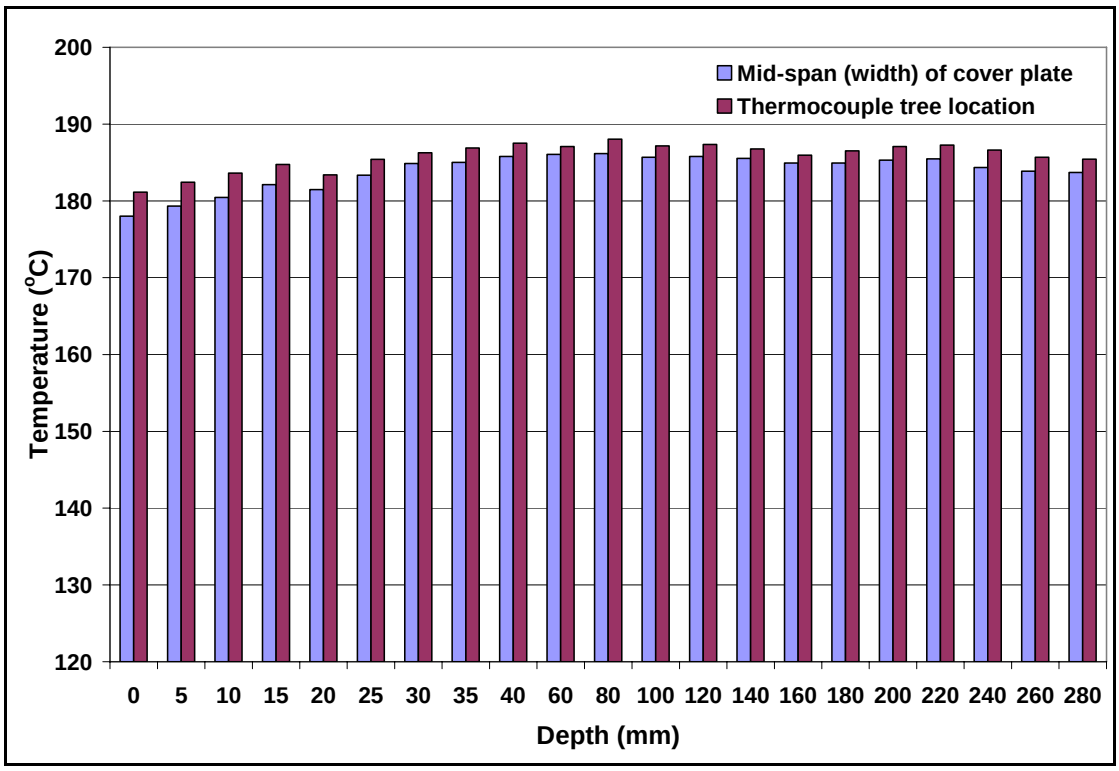

Figure 4.12: Temperature records at the mid-span (width) of cover plate and thermocouple tree location (200 °C and 45 Hz)

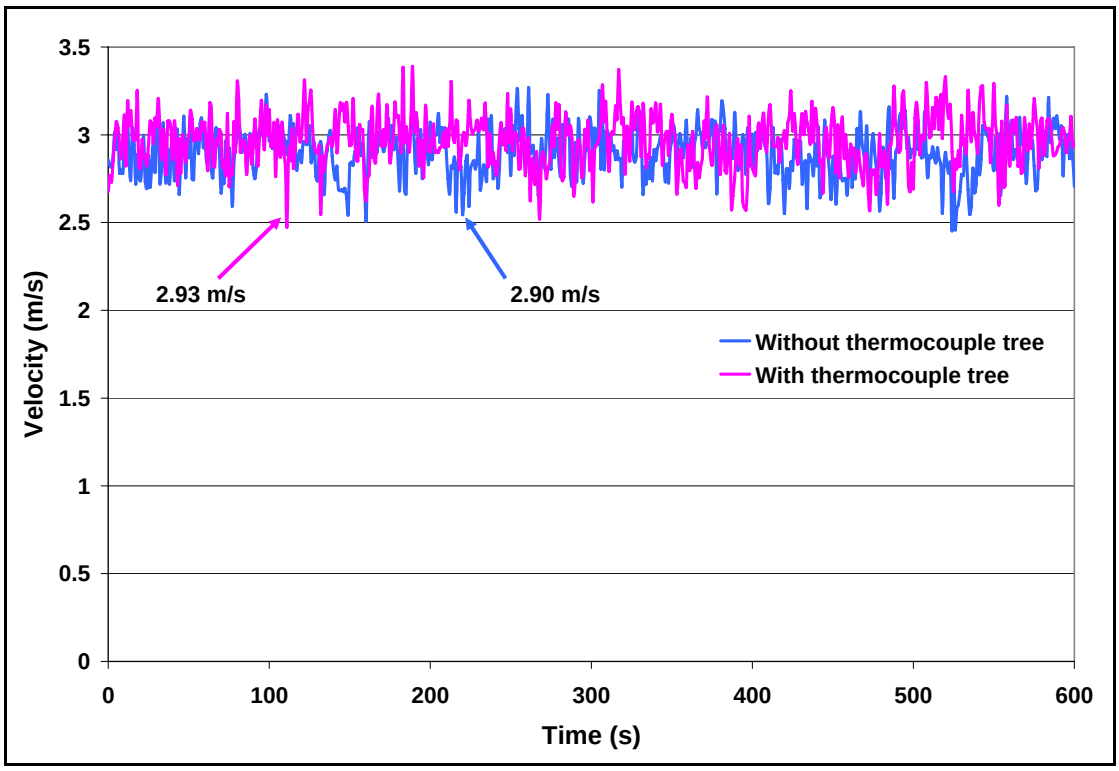

Figure 4.13: Velocity records with and without thermocouple tree (200 ^{o}C and 45 Hz)

4.4 Comparisons

In this section, comparisons were conducted to compare the performance results obtained from the UC3 wind tunnel with those generated from the UC2, FMRC, and FRS wind tunnel. The performance of the UC2, FMRC and FRS wind tunnel were referenced from Tsui (2004), Heskestad and Smith (1976) and Theobald (1987) respectively.

4.4.1 Temperature stability comparison

Figure 4.14 and Figure 4.15 show the temperatures recorded from the UC3 and UC2 wind tunnel respectively. The test conditions for both tests were identical and pre-set as 120 ^{o}C and 45 Hz. By comparing these two figures, it can be seen that both tunnels gave a very stable temperature result through the recorded duration. Despite the temperatures recorded at the “0 mm” and “100 mm” at both figures, the temperature difference between each measuring location of the UC3 wind tunnel was smaller than the UC2 wind tunnel. This result implied that the UC3 wind tunnel could provide a more uniform temperature profile than the UC2 wind tunnel in the tunnel test section.

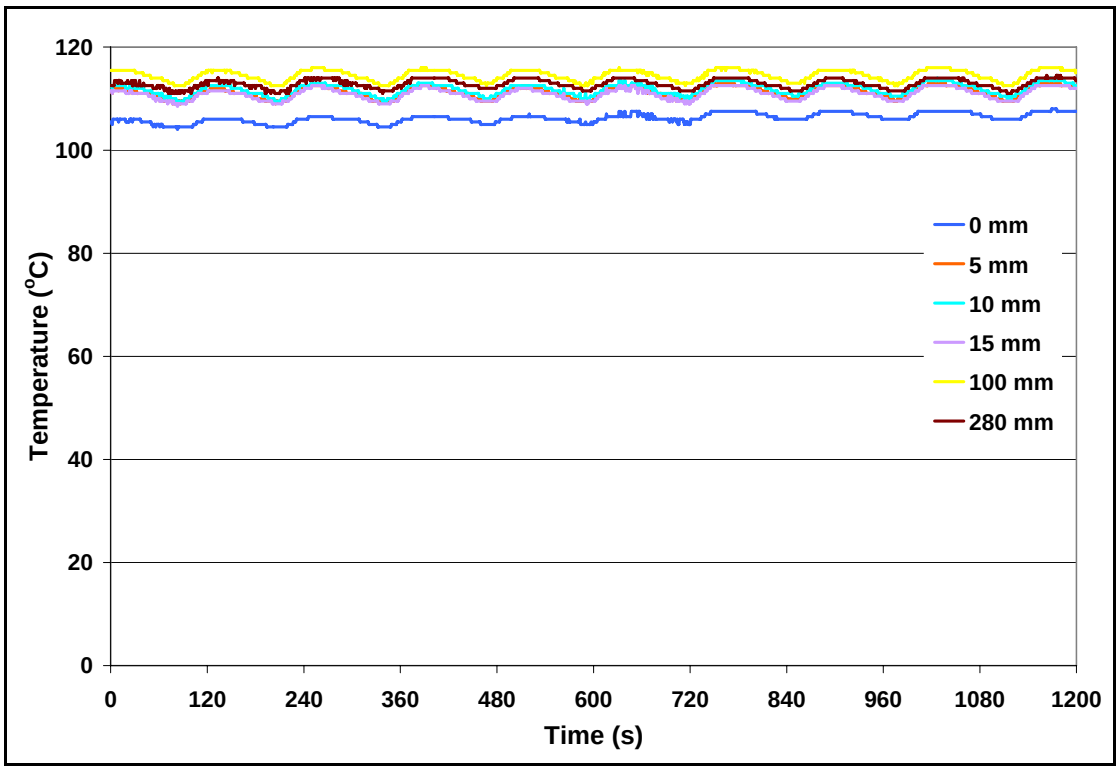

Figure 4.14: Temperature record from the UC3 wind tunnel (120 °C and 45 Hz)

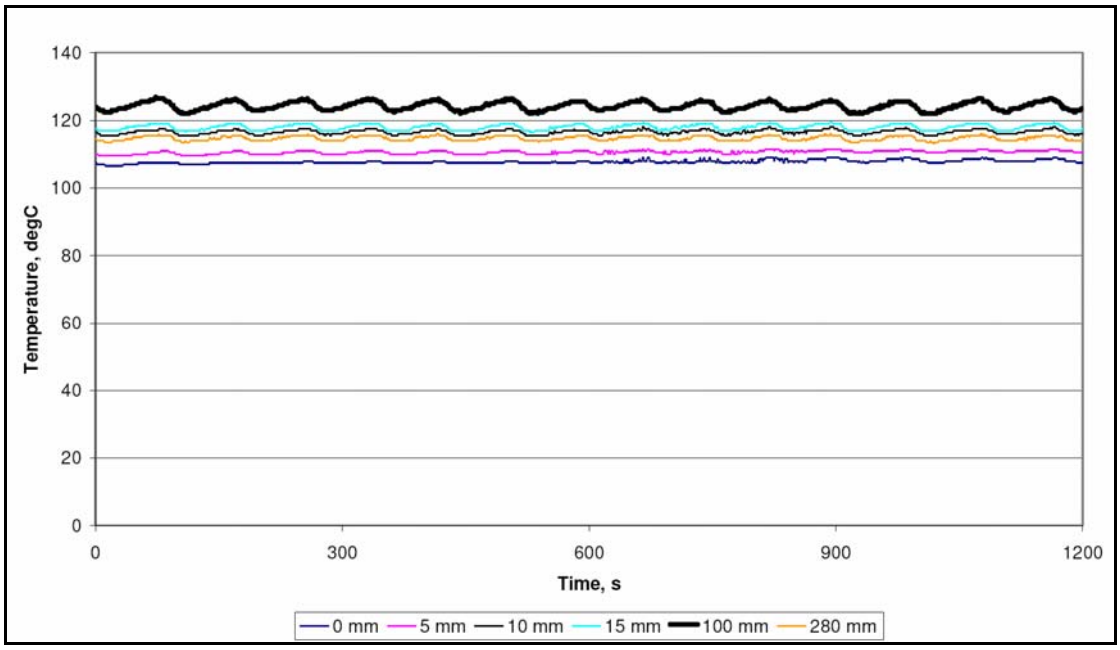

Figure 4.15: Temperature record from the UC2 wind tunnel (120 °C and 45 Hz)

4.4.2 Velocity and temperature uniformity comparison

Figure 4.16 shows comparisons of the velocity profile among the UC3, UC2, FMRC and FRS wind tunnel. In this figure, the axis scales of the velocity profile from each wind tunnel are different, because they are reproduced from the data available from their respective reports (raw data were not provided). In addition, it should be noted that the axis and flow orientation of the velocity profiles as shown in Figure 4.16 are the same for each wind tunnel.

By comparing the velocity profile of the UC3 and UC2 wind tunnel, the former presented a more uniform velocity profile than the latter. For the velocity profile obtained from the UC2 wind tunnel, it can be seen that the maximum and minimum velocity were measured at location (37 mm, 75 mm) and (0 mm, -75 mm) respectively. The velocity difference between those two points was approximately 2 m/s. However, the velocity difference between the maximum and minimum measurements was about 1 m/s from the UC3 wind tunnel. Further to this, the velocities obtained from the UC3 wind tunnel were symmetrical with the centreline in the width direction of the test section.

For the FRS wind tunnel, the velocities were uniformly distributed in the central region of the tunnel test section. However, velocities decreased rapidly at locations around the central region.

From the velocity profile of the FMRC wind tunnel, it was observed that there was no significant velocity variation across the tunnel test section in the range of 10 mm to 140 mm (depth). By comparing the velocity profile among the UC3, FRS and FMRC wind tunnel, the FMRC wind tunnel provided the best velocity uniformity across the test section. The approaches recommended to improve the UC3 wind tunnel are represented in Chapter 10 of this thesis.

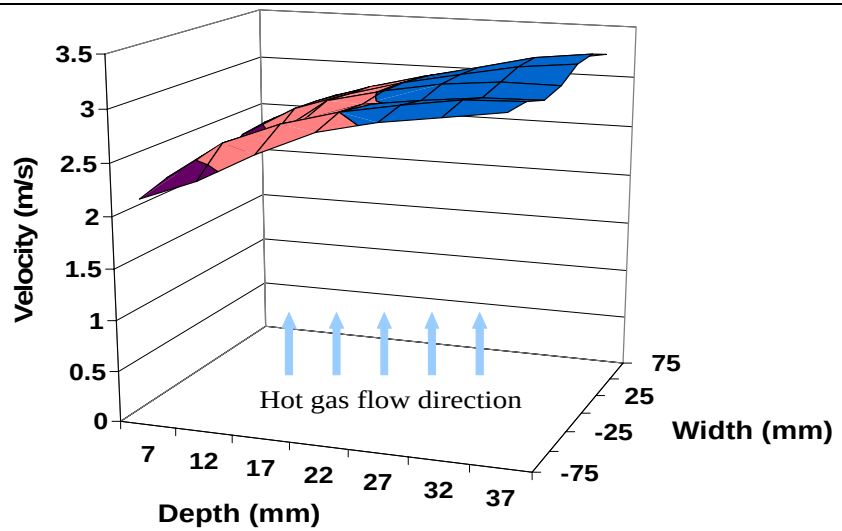

(a) UC3 wind tunnel performance (120 °C and 45 Hz)

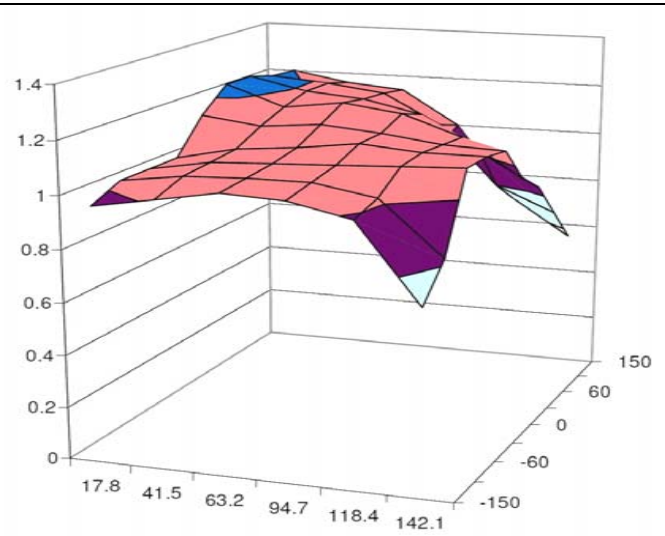

(b) FRS wind tunnel performance

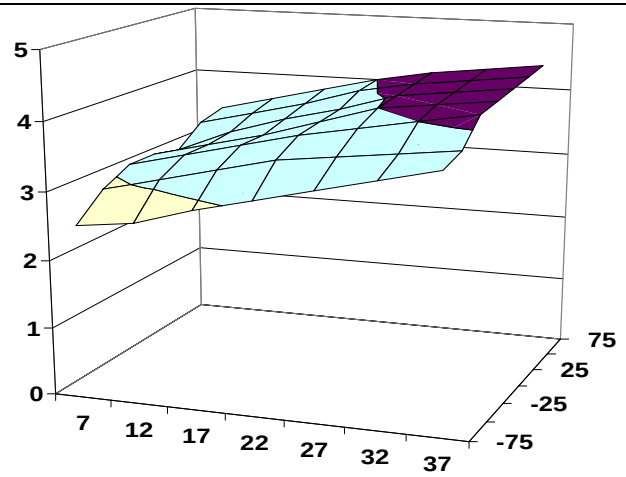

(c) UC2 wind tunnel performance (120 °C and 45 Hz)

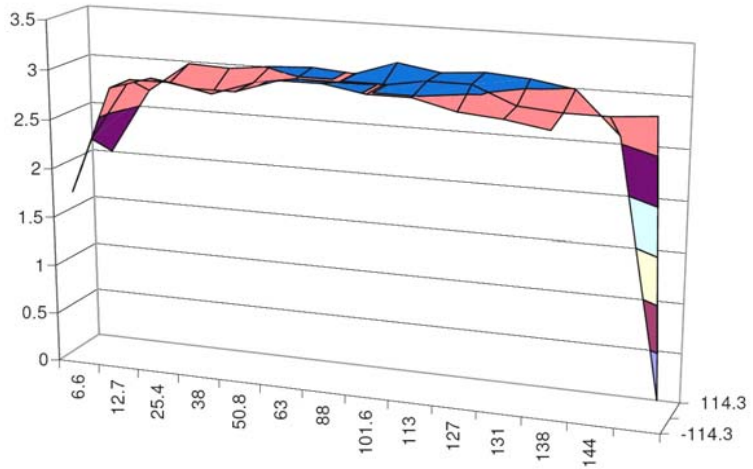

(d) FMRC wind tunnel performance

Figure 4.16: Velocity uniformity comparison

The temperature profile comparisons of the UC3, UC2, FMRC and FRS wind tunnel were shown in Figure 4.17. In this figure, the axis scales of the temperature profile from each wind tunnel are different, because they were reproduced from their respective reports (raw data were not provided). In addition, it should be noted that the axis and flow orientation of the temperature profiles as shown in Figure 4.17 are the same for each wind tunnel.

From the comparison of the UC3 and UC2 wind tunnel, the temperature profile formed in the test section of the former was flatter than the latter. The temperature profile generated from the UC2 wind tunnel was fairly uniform except at the location of "280 mm", and this was assumed to be caused by the low power output (3 kW) from the heating element of the wind tunnel. As mentioned in Chapter 3, a 9 kW heating element was used in the UC3 wind tunnel. This improvement did reduce the temperature variable level at locations nearby the tunnel boundaries and then provided a smooth temperature profile of the UC3 wind tunnel.

By comparing graph (a), (b), and (d) in Figure 4.17, the temperature distribution in the test section of the UC3 and FMRC wind tunnel was more uniform than the FRS tunnel. The maximum temperature variation at the temperature profile of the UC3, FMRC and FRS wind tunnel were 7 ^{o}C, 19 ^{o}C and 37 ^{o}C respectively. From this result, it showed that the temperature uniformity provided from the UC3 wind tunnel was slightly better than the FMRC wind tunnel.

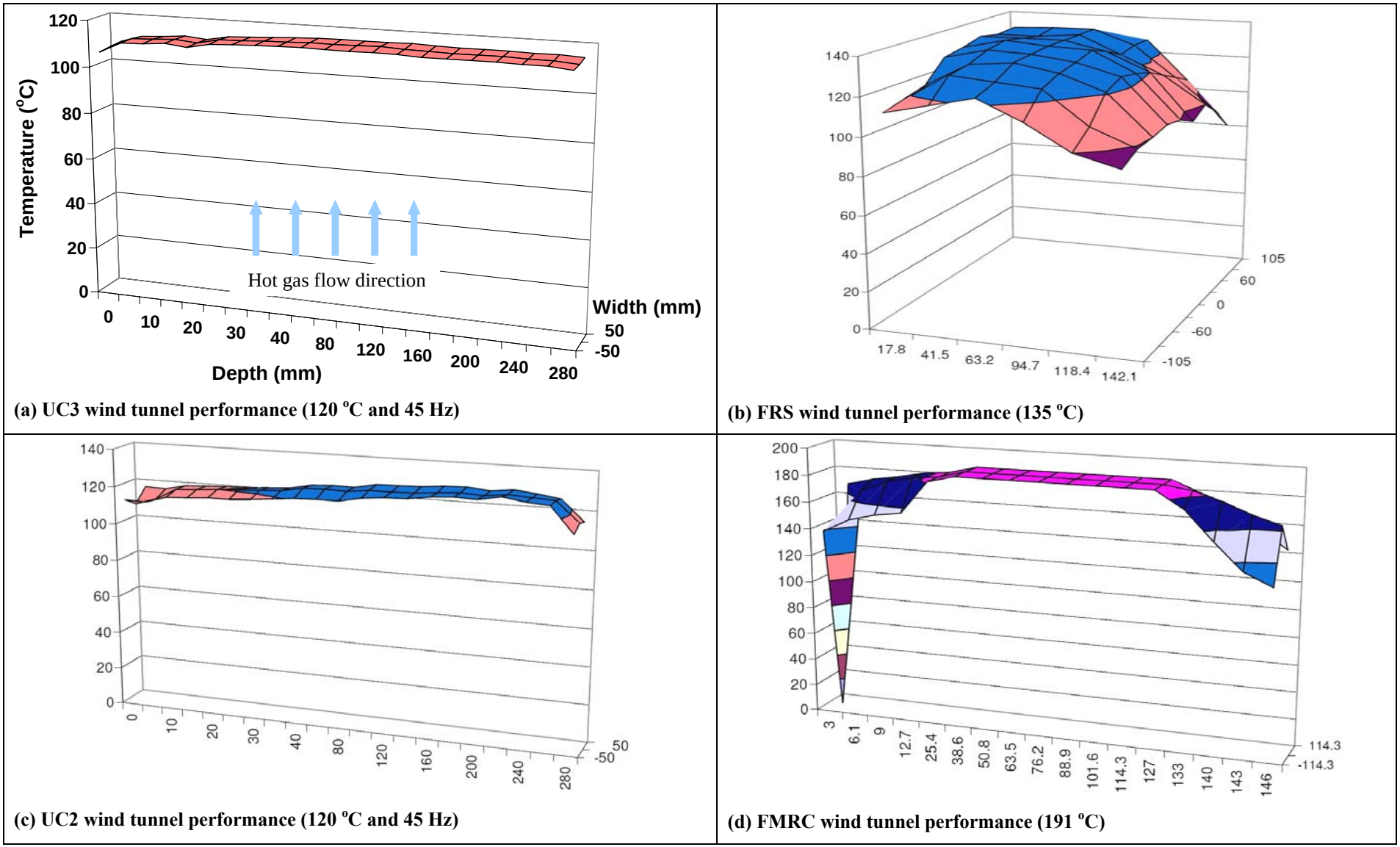

(a) UC3 wind tunnel performance (120 °C and 45 Hz)

(b) FRS wind tunnel performance (135 °C)

(c) UC2 wind tunnel performance (120 °C and 45 Hz)

(d) FMRC wind tunnel performance (191 °C)

Figure 4.17: Temperature uniformity comparison

4.5 General discussion

In general, the UC3 wind tunnel could provide a very stable and uniform temperature profile in the test section. In addition, the UC3 wind tunnel could produce consistent temperature and velocity results at different times by setting identical tunnel test conditions. However, the velocity uniformity of the tunnel needs to be improved in the future.

The comparisons demonstrated good agreement between the calibration results in the experiment in this research, FMRC and the FRS in terms of temperature and velocity. Therefore, it was considered that the UC3 wind tunnel was reliable and could be used to conduct the plunge test for the sprinklers.

CHAPTER 5

5 PLUNGE TEST (EXPERIMENTS): APPARATUS AND METHODOLOGY

Plunge tests were conducted to obtain the sprinkler response time and the RTI for the recessed and concealed sprinklers in this research. The experimental apparatus, instrumentation, methodology and data analysis techniques are described in this chapter. In addition to this, the types (models) of the recessed and concealed sprinklers used in the plunge test are described below.

5.1 Plunge test apparatus

5.1.1 Experimental facility

The UC3 wind tunnel was used as the experimental apparatus for the plunge test. The configuration and the performance of this newly developed wind tunnel is described in Chapter 3 and Chapter 4 respectively.

5.1.2 UC modified mounting plate

In this research, two identical UC modified mounting plates were fabricated for testing the recessed and concealed sprinklers in the UC3 wind tunnel. They were developed based on the design of the mounting plate for the recessed and concealed sprinklers represented at FMRC (Bill and Heskestad 1995).

Figure 5.1 and Figure 5.2 below show the top and bottom view of one of the UC modified mounting plates respectively.

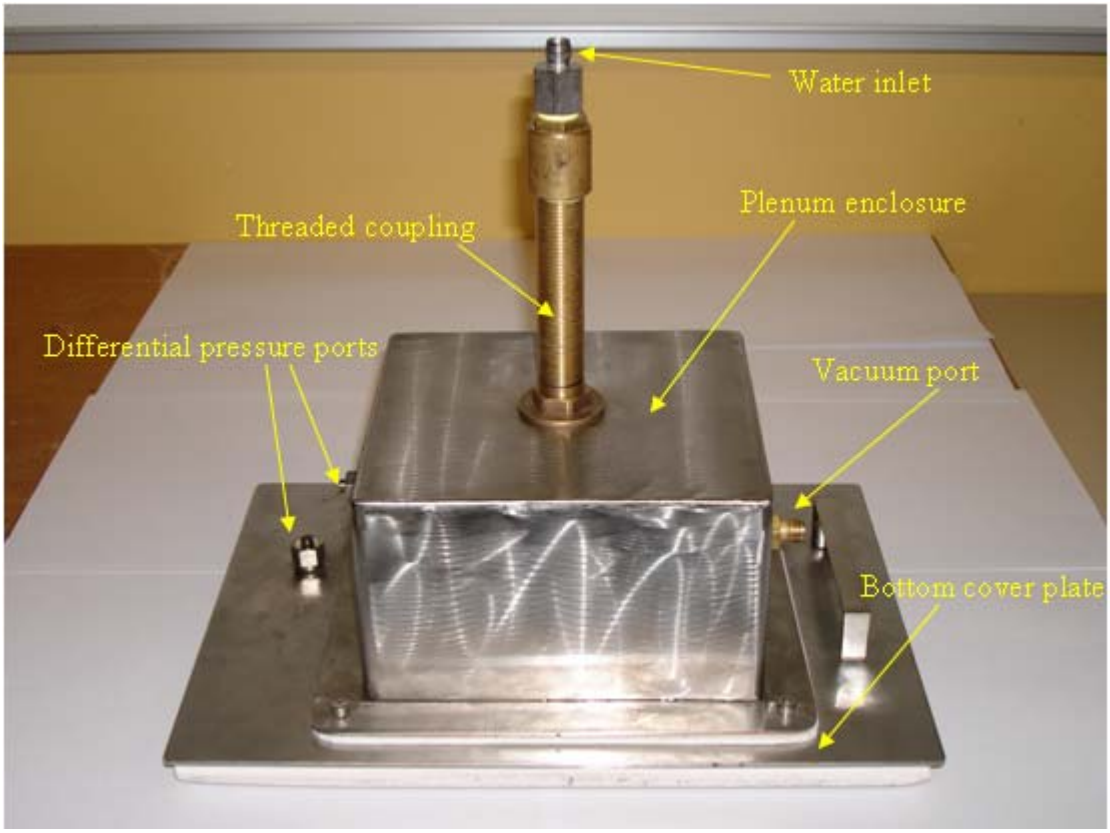

Figure 5.1: Top view of the special mounting plate

Figure 5.2: Bottom view of the special mounting plate

Table 5.1 tabulates the dimensions of the plenum enclosure and the bottom cover plate of the UC modified mounting plates. These dimensions are very similar to the dimensions of the mounting plates used at FMRC (Bill and Heskestad 1995).

Table 5.1: Dimensions of the special mounting plate

	Length (m)	Width (m)	Height / Thickness (m)
Plenum enclosure	0.170	0.160	0.100
Bottom cover plate	0.325	0.232	0.016

In addition, the features of the UC modified mounting plates are similar to the FMRC mounting plates (Bill and Heskestad 1995). These main features are summarized as follows:

- The vacuum port as shown in Figure 5.1 was connected to the vacuum pump by using a plastic tube to generate hot gas flow through the plenum enclosure from the wind tunnel during each plunge test.
- The two pressure ports were connected to a pressure transducer to measure the pressure difference between the wind tunnel and the plenum enclosure.
- The length of the threaded coupling inside the plenum enclosure was adjusted vertically to accommodate different types of recessed and concealed sprinklers installed through the sprinkler installation hole.
- Water was added to the sprinkler waterway (threaded coupling) through the water inlet after installing the tested sprinkler.
- The water in the sprinkler waterway was pressurized by using a pressure gauge (valve) and a pressure spray.

5.1.3 UC modified mounting plate arrangement

(a): Before placing the UC modified mounting plate

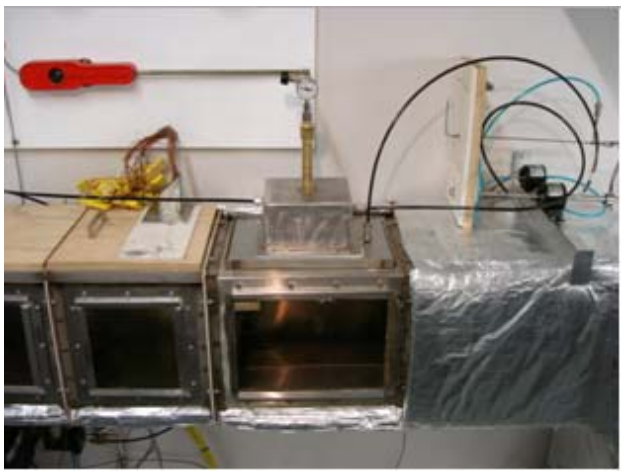

(b): after placing the UC modified mounting plate

Figure 5.3: UC modified mounting plate arrangement

Figure 5.3 (a) and (b) above show the UC3 wind tunnel before and after placing the UC modified mounting plate. It was unavoidable that hot gas would escape out of the opening of the tunnel test section when the cover plates were being changed and into the surrounding environment. Therefore, the duration used to change the cover plates remained as short as possible to minimize the hot gas escape from the wind tunnel.

5.1.4 Pressure gauge (valve)

The pressure added to the water in the sprinkler waterway (read from the pressure gauge attached to the water inlet of the UC modified mounting plate) was within a range of 35 kPa to 40 kPa (See Figure 5.4). The valve was closed to maintain the water pressure when the pressure had reached the pre-determined range. It should be noted that the magnitude (range) of the pressure added to the water in the sprinkler waterway was referenced from Heskestad and Smith (1980).

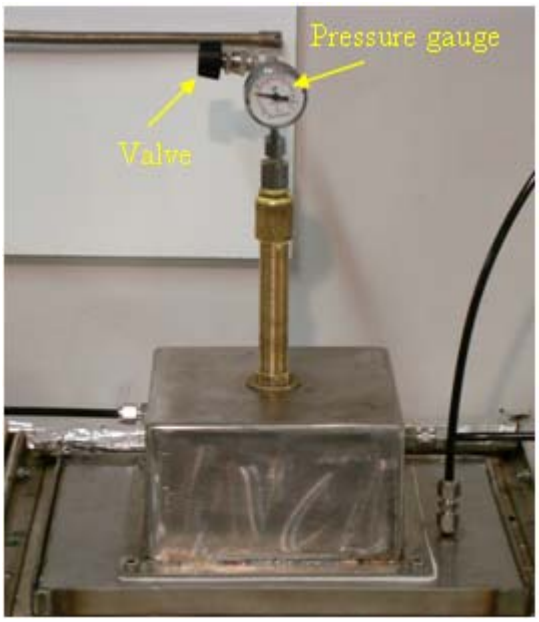

Figure 5.4: Pressure gauge attached to the water inlet

5.2 Instrumentation and data recording

The instruments used to measure temperatures and velocities in the wind tunnel and generate hot gas flow through the plenum enclosure of the cover plate are detailed in Chapter 3 and are not repeated here.

The Universal Data Logging (UDL) computer software was used to record all of the instrument readings.

5.3 Experimental methodology

As mentioned in Chapter 2, the plunge test for the recessed and concealed sprinklers were both conducted by Bill and Heskestad (1995) and Annable (2006). The experimental methodology used in this study was mainly based on the methodology represented by Bill and Heskestad (1995) and described as below.

5.3.1 Determination of thermal sensitivity

In this research, the RTI values of the recessed sprinklers were determined by using both the “simple” RTI equation (without C-factor, Equation 5.1) and the “comprehensive” RTI equation (with C-factor, Equation 5.2) as shown below.

However, the RTI values of the concealed sprinklers were only calculated by the "comprehensive" RTI equation.

5.3.1.1 Determination of RTI for recessed sprinkler

Equation 5.1 ("simple" RTI equation) was used to calculate the RTI without using the C-factor and referenced from Tsui (2004). This equation could be used to calculate the RTI values for sprinklers with the heat-responsive element are entirely exposed to the heated environment. Since the heat-responsive element of the recessed sprinklers is partially exposed below the ceiling, it is interested to investigate the RTI of the recessed sprinklers by using the "simple" RTI equation (without C-factor).

$$RTI = \frac{-t_r U^{1/2}}{\ln\left(1-\Delta T_b / \Delta T_g\right)} \qquad \text{Equation 5.1}$$

Where:

t_r = sprinkler response time in plunge test (s)

U = air velocity in the test section of the wind tunnel (m/s)

ΔT_b = mean actuation temperature (operating temperature) of the sprinkler minus the mount temperature (^oC)

ΔT_g = hot gas temperature in the test section minus the mount temperature (^oC)

The equation (Equation 5.2) used to determine the RTI for the recessed sprinklers at FMRC (Bill and Heskestad 1995) was the same as the BRE (Annable 2006). However, it should be noted that the C-factor is taken into account for calculating the RTI in this equation.

$$RTI = \left(\frac{-t_r U^{1/2}}{\ln\left[1-\Delta T_b\left(1+C/\left(U\right)^{1/2}\right)/\Delta T_g\right]}\right)\cdot\left[1+C/U^{1/2}\right] \qquad \text{Equation 5.2}$$

Where:

C = conductivity factor $(m/s)^{1/2}$

5.3.1.2 Determination of RTI for concealed sprinkler

The RTI values of the concealed sprinklers tested in this study were only determined by using Equation 5.2 (with C-factor). The heat-responsive element of the concealed sprinklers is hidden above the ceiling (for the entire period in the plunge test) and covered by the cover plate in the initial stage (before the activation of the cover plate), therefore it is more accurate to calculate the RTI of the concealed sprinklers with the C-factor. Equation 5.2 was also used by Bill and Heskestad (1995) and Annable (2006) to calculate the RTI for their tested concealed sprinklers.

5.3.1.3 Determination of C-factor for recessed and concealed sprinklers

The C-factor can be either obtained from the "Prolonged plunge test" or the "Prolonged exposure ramp test". For the prolonged plunge test, the hot gas velocity in the wind tunnel test section at the sprinkler location is required to be maintained within 0.03 m/s of the selected velocity (FM Approval Standard 2002). For the prolonged exposure ramp test, the hot gas temperature in the wind tunnel test section shall be increased at rate of (1 ± 0.25) ^{o}C per minute until the sprinkler activates (International Standard 2004). However, the performance of the UC3 wind tunnel cannot meet the criteria as required above, and therefore the C-factor was not determined in this study. The appropriate C-factor used to calculate the RTI of the recessed and concealed sprinklers in this research was obtained from the experimental results provided from the BRE (Annable 2006).

It was considered that the use of C factor from BRE (results from other experiments) to calculate the RTI of recessed and concealed sprinklers in this work may affect the accuracy of the RTI results. However, the C factor provided by BRE (Annable 2006) is the only data available to calculate the RTI at the time of the plunge test experiments in this research. In addition, the sprinkler characteristics of tested

sprinklers at the BRE (Annable 2006) are similar to the tested sprinklers in this study. Therefore, the C factor from BRE (Annable 2006) was considered to be sufficiently reliable.

An error analysis investigating the consequences of using inherently linked parameters (e.g. C factor) whose absolute values have been derived from different experimental sources is important. Similar works were carried out at University of Canterbury by Tsui (2004) to investigate statistical analyses of sprinkler RTI and C factor using plunge test for pendent sprinklers. Further investigation will be needed to fully assess the accuracy of the RTI of recessed and concealed sprinklers by using the C factor from other experiments.

5.3.2 Sprinkler models tested

Four of the most commonly used sprinkler models (two recessed and two concealed) in New Zealand were investigated in the plunge test by using the UC3 wind tunnel. The configuration and characteristic of these sprinklers are described in this section. It should be noted that all tested sprinklers in this research were purchased at the same time from the same manufacturer. However, all sprinklers obtained may not have come from the same batch.

Table 5.2 shows the sprinkler characteristics (i.e. type and actuation temperature of sprinkler heat-responsive element) of the recessed and concealed sprinklers which were tested in the experiment. It should be noted that both the glass bulb and fusible solder link concealed sprinklers were tested. However, only glass bulb recessed sprinklers were investigated in this research. The subscripts R and C shown in this table denote the recessed sprinkler and concealed sprinkler respectively. The maximum (minimum) recess distance and the model number of sprinklers are referenced from the sprinkler manufacturer (Tyco Fire & Building Products 2006).

Table 5.2: Sprinkler characteristics

Sprinkler model	Type (Model number)	Actuation temperature of sprinklers (cover plate for concealed sprinkler)	K factor UK K factor US	Recess distance (Referenced from the manufacturer)	
				Maximum	Minimum
M_R	Recessed (TY3251)	68 ^oC – 5 mm glass bulb (N/A)	80.6 LPM/bar$^{1/2}$ 5.6 GPM/psi$^{1/2}$	Deflector 22.3mm below ceiling	Deflector 35mm below ceiling
N_R	Recessed (TY3231)	68 ^oC – 3 mm glass bulb (N/A)	80.6 LPM/bar$^{1/2}$ 5.6 GPM/psi$^{1/2}$	Deflector 22.3mm below ceiling	Deflector 35mm below ceiling
O_C	Concealed (TY2596)	71 ^oC – Fusible solder link (57 ^oC)	60.5 LPM/bar$^{1/2}$ 4.2 GPM/psi$^{1/2}$	Deflector 12.7mm below ceiling	Deflector 25.4mm below ceiling
P_C	Concealed (TY3531)	68 ^oC – 3 mm glass bulb (57 ^oC)	80.6 LPM/bar$^{1/2}$ 5.6 GPM/psi$^{1/2}$	Deflector 4.8mm below ceiling	Deflector 17.5mm below ceiling

(a) At the maximum recess distance **(b) At the minimum recess distance**

Figure 5.5: Sprinkler N_R at the maximum and minimum recess distance

Figure 5.5 (a) and (b) show the configurations of the sprinkler N_R at its maximum and minimum recess distance. Recess distance is a parameter used to indicate how deep the sprinkler heat-responsive element is mounted above or below the lower plane of the ceiling. From Figure 5.5 (a), it can be seen that the smallest portion of the

sprinkler head is exposed outside the recess housing when the recessed sprinkler was installed at the maximum recess distance.

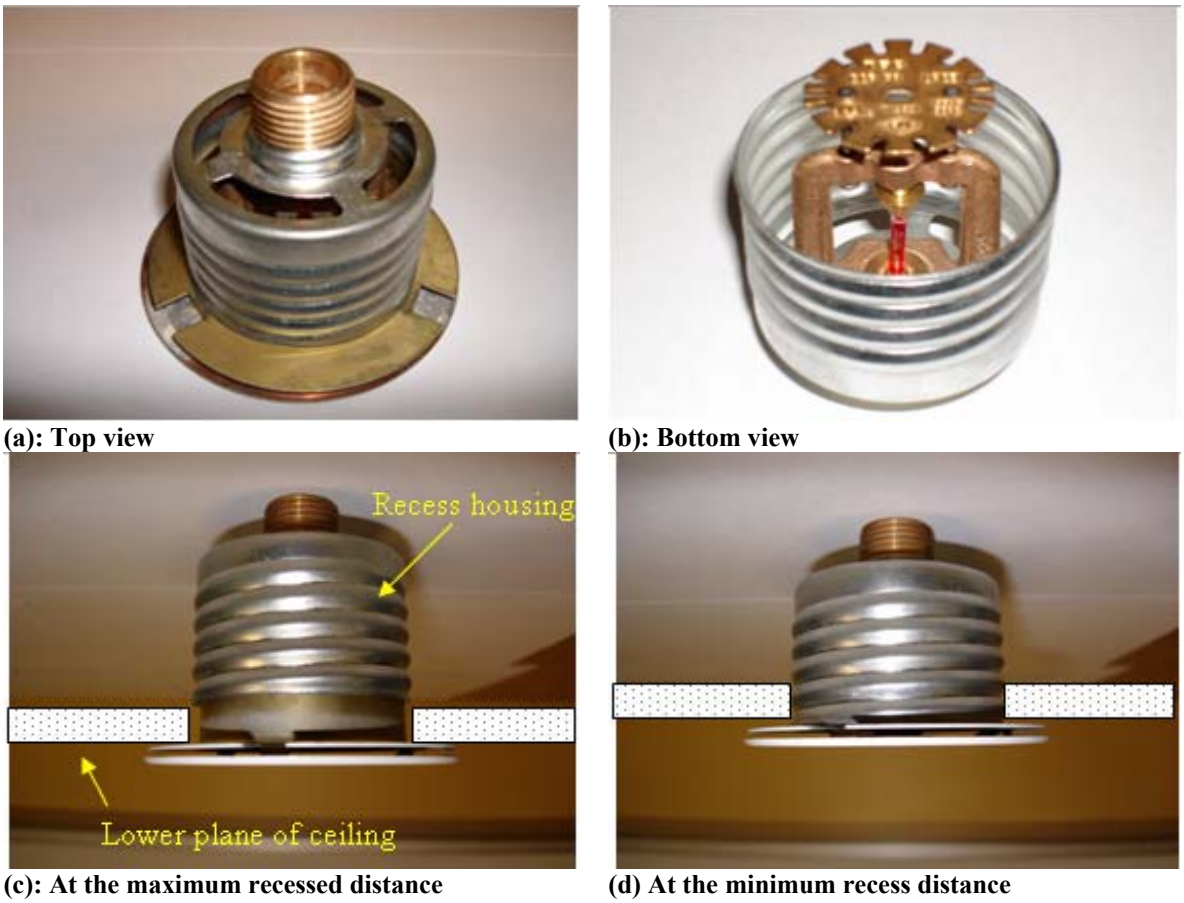

(a): Top view **(b): Bottom view**

(c): At the maximum recessed distance **(d) At the minimum recess distance**

Figure 5.6: Sprinkler P_C at the maximum and minimum recess distance

Figure 5.6 (a) and (b) show the top and bottom view of the sprinkler P_C. In addition, the illustrations of the sprinkler P_C installed at its maximum and minimum recess distance are shown in Figure 5.6 (c) and (d) respectively.

From Figure 5.6 (d), it can be seen that the concealed sprinkler installed at the minimum recess distance is achieved when the cover plate is totally screwed into the recess housing and installed flush with the lower plate of the ceiling. This also implies that the position of the heat-responsive element of the concealed sprinkler is closest to the compartment space below the lower plane of the ceiling when it was installed at the minimum recess distance.

The configurations of other sprinklers investigated in this study are shown in Appendix C.

5.3.3 Plunge test conditions

As described in Chapter 2, nine plunge test conditions were investigated by Bill and Heskestad (1995) at FMRC. However, due to the limitations of the UC3 wind tunnel, only four of the test conditions investigated by Bill and Heskestad could be performed in this work. Table 5.3 below shows the plunge test conditions conducted in the experiment. It should be noted that the "Applied vacuum" shown in this table indicates the pressure difference measured between the wind tunnel and the plenum enclosure of the UC modified mounting plate during the plunge test.

Table 5.3: Plunge test conditions

Test condition	Gas temperature (^{o}C)	Gas velocity (m/s)	Applied vacuum (mm Hg)
1	128	1	0.007
2	128	2.56	0.007
3	199	1	0.01
4	197	2.56	0.01

5.3.4 Parameters measured in plunge test

The parameters listed below were recorded in each plunge test and used to calculate the RTI of the recessed and concealed sprinklers.

- Sprinkler response time
- Hot gas temperature and velocity in the test section of the wind tunnel
- Sprinkler fitting temperature

5.3.4.1 Sprinkler response time

In each plunge test, visual observations were carried out to record the sprinkler activation time for the recessed and concealed sprinklers by using a stopwatch. It should be noted that there were two operation times needed to be recorded in the plunge tests with concealed sprinklers. These included the operation time of the cover plate of the concealed sprinkler and the response time of the heat-responsive element of the concealed sprinkler. The maximum recorded time was set to 1000 s for each plunge test and referenced from FMRC (Bill and Heskestad 1995).

5.3.4.2 Hot gas temperature and velocity in the test section of the wind tunnel

The hot gas temperatures during each plunge test were measured by using a thermocouple tree placed at the “thermocouple tree location”. The description of the “thermocouple tree location” is found in Chapter 4. The average of the temperatures recorded from the upper five thermocouples from the thermocouple tree during each plunge test was used to calculate the RTI for the recessed and concealed sprinklers.

As shown in Figure 5.3, the Pitot-static tube was removed from the tunnel test section after placing the UC modified mounting plate in the UC3 wind tunnel during the plunge test. This implies that the hot gas velocities during the plunge test could not be measured in the wind tunnel. However, it was found that the hot gas velocities were very similar by comparing the velocities measured before and after each plunge test. Therefore, it was assumed that the average of the velocities measured before and after each plunge test could be used to calculate the RTI of the recessed and concealed sprinklers.

5.3.4.3 Sprinkler fitting temperature

The sprinkler fitting temperature in each plunge test was calculated by averaging the ambient temperature and the water temperature added in the sprinkler waterway. 40 ml of water was added to the sprinkler waterway after installing the tested

sprinkler in each plunge test. The amount of water used in the plunge test was identical and referenced from the BRE (Annable 2006).

In addition, the temperature of the water added to the sprinkler waterway should be similar to the ambient temperature and this was accomplished by allowing the water to sit in the laboratory overnight before use in the plunge tests.

5.3.5 Parameter variation

Some of the parameters of interest which may affect the sprinkler response time (and the RTI) are listed as follows:

- Applied vacuum for the recessed sprinkler
- Sprinkler frame arm orientation
- Recess distance

5.3.5.1 Applied vacuum for the recessed sprinkler

Annable (2006) suggests that "the pressure difference between the wind tunnel and the mounting plate plenum box applied only to the concealed residential sprinklers". However, Bill and Heskestad (1995) suggest that the vacuum should be applied to both the recessed and concealed sprinklers. Therefore, a sensitivity analysis was conducted to examine the influence of the applied vacuum for the recessed sprinklers. In this sensitivity analysis, twelve recessed sprinklers were operated in four different plunge test conditions where either a vacuum was or was not applied. The test conditions used in this sensitivity analysis are presented in Section 5.3.6 of this chapter.

5.3.5.2 Sprinkler frame arm orientation

In order to assess the influence of the sprinkler frame arm orientation for the recessed and concealed sprinklers, each model of sprinkler in the experiment was tested both in the sprinkler frame arm orientated at 90 ^{o} and 0 ^{o} to the oncoming hot gas flow in the wind tunnel. It should be noted that "standard orientation" and "worst orientation" are

used to denote the sprinkler frame arm orientated at 90 ^{o} and 0 ^{o} respectively to the oncoming hot gas flow in the rest of this report.

5.3.5.3 Recess distance

The sensitivity analysis of the recess distance for the concealed sprinkler was conducted by Annable (2006). Annable (2006) found that the RTI of the concealed sprinkler was significantly increased when the sprinkler was installed at the maximum recess distance compared with the minimum recess distance. This result implied that the sprinkler response time of the concealed sprinklers installed at the minimum recess distance was significantly shorter than at the maximum recess distance. Therefore, the concealed sprinkler installed at the minimum recess distance was considered to be the most favourable installation position for safeguarding the occupants. In this research, the concealed sprinklers were only tested at the minimum recess distance.

For aesthetic reasons, the recessed sprinkler is more likely to be installed at the maximum recess distance rather than at the minimum recess distance. Hence, the recessed sprinklers were only investigated at the maximum recess distance in this study. It should be noted that the recessed sprinklers were also only tested at the maximum recess distance by Annable (2006).

5.3.6 The series of tests

In this research, 108 sprinkler heads (60 recessed sprinklers and 48 concealed sprinklers) were tested in the plunge tests.

Test 1 ~ 12 was conducted to examine the influence of the applied vacuum for the recessed sprinklers.

Table 5.4 below shows the plunge test conditions for Test 1 ~ 12.

Table 5.4: Plunge test condition for Test 1 ~ 12

Test	Sprinkler model	Frame arm orientation	Nominal hot gas temperature	Nominal hot gas velocity	Applied vacuum
1	M_R	90° to the hot gas flow	128 °C	1 m/s	Not applied
2					
3					
4	M_R	90° to the hot gas flow	128 °C	1 m/s	0.007 mmHg
5					
6					
7	M_R	90° to the hot gas flow	197 °C	2.56 m/s	Not applied
8					
9					
10	M_R	90° to the hot gas flow	197 °C	2.56 m/s	0.010 mmHg
11					
12					

Test 13 ~ 108 were conducted to assess the sprinkler response time and RTI for the sprinkler M_R, N_R, O_C, and P_C. For each model of sprinkler, three sprinkler heads were tested in each sprinkler frame arm orientation under each plunge test condition.

Table 5.5 below tabulates the plunge test conditions for testing sprinkler M_R (Test 13 ~ 36). The plunge test conditions for sprinkler N_R, O_C, and P_C are shown in Appendix D.

Table 5.5: Plunge test conditions for testing sprinkler M_R (Test 13 ~ 36)

Test	Sprinkler model	Frame arm orientation	Nominal hot gas temperature	Nominal hot gas velocity	Applied vacuum
13	M_R	90° to the hot gas flow	128°C	1 m/s	N/A
14					
15					
16	M_R	90° to the hot gas flow	128°C	2.56 m/s	N/A
17					
18					

19 20 21	M_R	90° to the hot gas flow	199°C	1 m/s	N/A
22 23 24	M_R	90° to the hot gas flow	197°C	2.56 m/s	N/A
25 26 27	M_R	0° to the hot gas flow	128°C	1 m/s	N/A
28 29 30	M_R	0° to the hot gas flow	128°C	2.56 m/s	N/A
31 32 33	M_R	0° to the hot gas flow	199°C	1 m/s	N/A
34 35 36	M_R	0° to the hot gas flow	197°C	2.56 m/s	N/A

5.4 Experimental procedure

The experimental procedure for the plunge tests conducted to assess the sprinkler response time and RTI of the recessed and concealed sprinklers were as follows:

1. The tested sprinklers were placed overnight in the laboratory before testing in order to pre-condition them to the laboratory ambient temperature.
2. The required plunge test hot gas temperature was set by using the temperature control panel.
3. The differential pressure from the required plunge test hot gas temperature and velocity was calculated by using the Bernoulli equation "$\Delta p = \frac{\rho \cdot u^2}{2}$".
4. The required plunge test hot gas velocity was set by adjusting the fan revolution speed controller to the pressure calculated in Step 3.
5. A 30 minute time period was allowed to stabilize the tunnel test condition after the required plunge test condition was reached in the wind tunnel.
6. The wind tunnel hot gas velocity was recorded for a duration of 5 minutes.

7. The tested sprinkler was installed in the UC modified mounting plate (ensuring the required sprinkler recess distance and frame arm orientation was maintained in this step).
8. The cover plate was installed for the concealed sprinkler. (Not applicable for recessed sprinkler)
9. 40 ml of water was added to the sprinkler waterway through the water inlet.
10. The pressure gauge (valve) was attached to the water inlet.
11. The pressure spray was attached to the pressure gauge.
12. The water in the sprinkler waterway was pressurized to a range of 35 kPa to 40 kPa.
13. The pressure valve was closed to maintain the water pressure.
14. The vacuum pump was switched on.
15. The rate of vacuum was adjusted to achieve the required “Applied vacuum” in the plunge test condition. (The rate of vacuum can be adjusted by loosing/tightening the valve as shown in Figure 3.12. The “Applied vacuum” can be read from the pressure gauge as shown in Figure 3.12.)
16. 10 minutes were allowed to stabilize the vacuum condition after the rate of vacuum was set.
17. The instrumentation was checked.
18. The timer (stopwatch) was reset and the UDL software was run.
19. The cover plate was replaced by the UC modified mounting plate (as fast as possible).
20. The time was started (recorded using a stopwatch) when the sprinkler was plunged into the wind tunnel.
21. The response time of the sprinkler (and the operation time of the cover plate for the concealed sprinkler) was recorded.
22. The UDL was stopped and all the tested data was recorded.
23. The UC modified mounting plate was replaced by the cover plate.

24. The hot gas velocity in the wind tunnel was recorded for a duration of 5 minutes.
25. The experimental procedure was repeated from Step 2 for the next plunge test.

CHAPTER 6

6 PLUNGE TEST (EXPERIMENTS) RESULTS AND DISCUSSION

The experimental results used to examine the sprinkler response time and the RTI values for the recessed and concealed sprinklers are given and analysed below. In addition, the comparison of the RTI between the experiment in this research and those carried out at FMRC and the BRE are presented in this chapter.

6.1 Applied vacuum for the recessed sprinkler

In this sensitivity analysis, twelve M_R (recessed, 68 ^oC, 5 mm glass bulb) sprinkler heads were conducted under four different plunge test conditions to examine the influence of the applied vacuum to the recessed sprinklers. It should be noted that the tested tunnel hot gas temperature and velocity were the same between the former two of the test conditions (or the latter two of the test conditions) as shown in Figure 6.1. The only difference between them was that the vacuum was only applied on one of the test conditions.

Figure 6.1 below shows the sprinkler response times obtained from Test 1 ~ 12. From this figure, it can be seen that the sprinkler response times of the sprinkler M_R were similar in each of the four specific plunge test conditions (where each test has a triplicate sample). The similarity of the results implied that the UC modified mounting plate and the UC3 wind tunnel provided consistent test conditions for testing sprinklers at different times by setting and using the same tunnel conditions. The discrepancies of sprinkler response time recorded under each of the four specific test conditions might be caused by the non-uniformity of the sprinkler glass bulb. Tsui (2004) suggests that the variations of the sprinkler glass bulb may influence the sprinkler response time. This is because the thickness of the glass bulb and the amount of liquid filled in the glass bulb between the same types of sprinklers could be different.

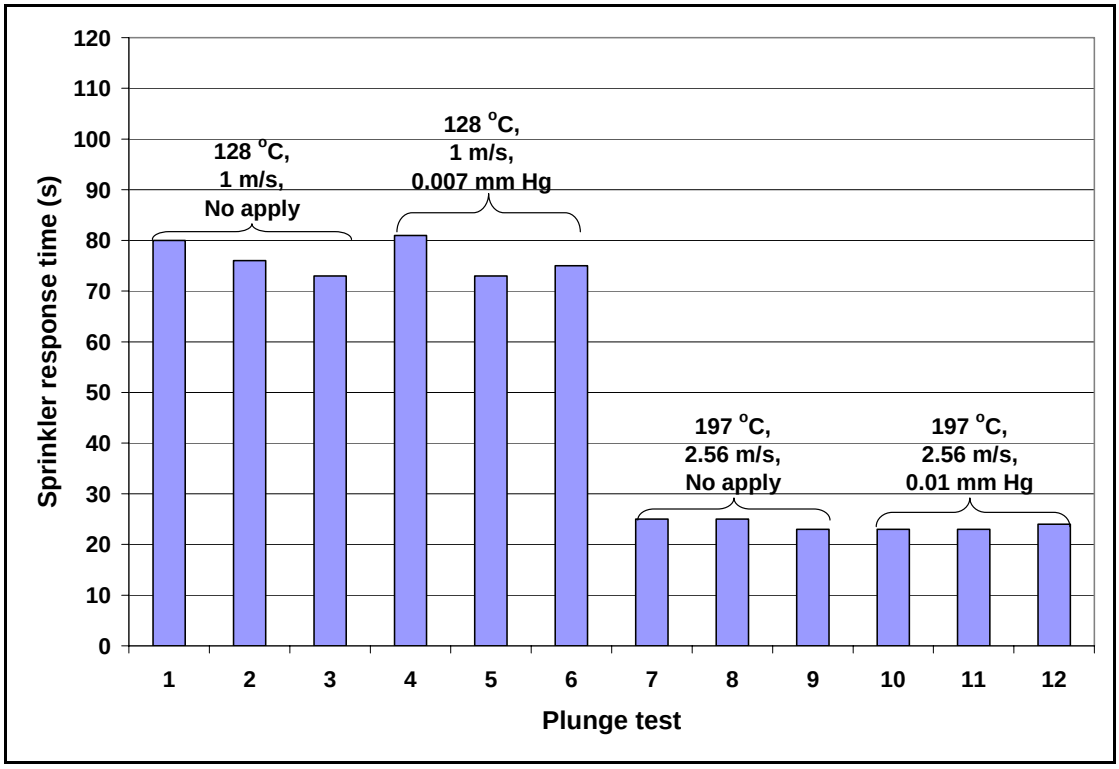

Figure 6.1: Sprinkler response time for Test 1 ~ 12

Table 6.1 shows the average sprinkler response time and the standard deviation in each test condition for Test 1 ~ 12.

Table 6.1: Average sprinkler response time for Test 1 ~ 12

Test condition	Average sprinkler response time (s)	Standard deviation
128 °C, 1 m/s, no apply	76	4
128 °C, 1 m/s, 0.007 mm Hg	76	4
197 °C, 2.56 m/s, no apply	24	1
197 °C, 2.56 m/s, 0.01 mm Hg	23	1

For the former pair of the test conditions as shown in this table, both the average sprinkler response times and the standard deviations were identical. In addition, the average sprinkler response time obtained from the third and the fourth test condition was very similar (identical standard deviations). These results implied that the sprinkler response times were not effected by the application of a vacuum during the plunge tests for the recessed sprinklers (as suggested by Annable (2006)). Hence, a vacuum was not applied to test the recessed sprinklers in the rest of the experiments.

6.2 Sprinkler response time

In this section, the sprinkler response times of the recessed and concealed sprinklers investigated in this study are presented and discussed. The full set of the experimental record data is shown in Appendix E.

6.2.1 Sprinkler M_R (recessed, 68 ^oC, 5 mm glass bulb)

Figure 6.2 shows the sprinkler response times of the sprinkler M_R from the plunge tests. It should be noted that the recessed sprinklers were tested with two different sprinkler frame arm orientations in the wind tunnel. As seen from this figure, the sprinkler response times represented at the left side of the dotted centreline was obtained from the plunge tests in the standard orientation (sprinkler frame arm 90 ^{o} to the flow). In contrast, the results shown in the other side of the dotted centreline were recorded in the worst orientation (sprinkler frame arm 0 ^{o} to the flow).

From the results shown in this figure, it was found that the sprinkler response times were similar under each of the four specific plunge test conditions in both the standard and the worst orientation. In addition to this, the fastest and slowest sprinkler response time was recorded at the upper ultimate limit test condition (197 ^{o}C and 2.56 m/s) and lower ultimate limit test condition (128 ^{o}C and 1 m/s) respectively in both the sprinkler frame arm orientations.

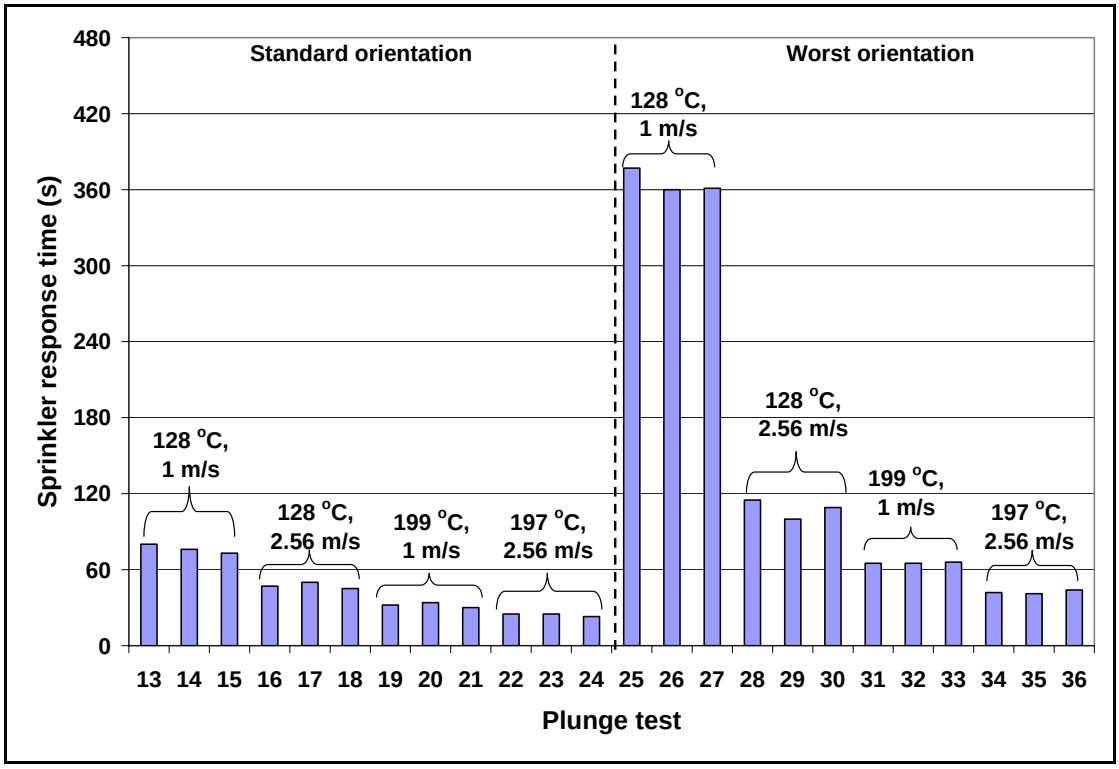

Figure 6.2: Sprinkler response time of sprinkler M_R for Test 13 ~ 36

Figure 6.3 below shows the comparison of the average sprinkler response times in the standard and the worst orientation under each of the four specific plunge test conditions. It should be noted that the average sprinkler response time obtained from each test condition and sprinkler frame arm orientation is represented as a single number and placed on the top of each column as shown in Figure 6.3.

From this figure, the results show that the average sprinkler response times recorded in the worst orientation were larger than in the standard orientation. This is because when the sprinkler was orientated in the worst orientation, the oncoming hot gas flowed to the sprinkler heat-responsive element was obstructed by the sprinkler frame arm. The obstructed hot gas flow affected the temperature increase rate of the sprinkler heat-responsive element. Therefore a longer time period was needed to increase the temperature of the heat-responsive element to the sprinkler actuation temperature when the sprinkler was installed in the worst orientation.

In addition, the differences of the sprinkler response time between the standard and the worst orientation were found to decrease in sequence from the lower ultimate limit test condition (128 ^{o}C and 1 m/s) to the upper ultimate limit of the test condition

(197 ^{o}C and 2.56 m/s). This result implied that the sprinkler response time could be significantly influenced by the sprinkler orientation at the low hot gas temperature and velocity test conditions. High gas temperature and velocity test conditions did not have as much an influence on the sprinkler response time.

From Figure 6.3, the average sprinkler response times of sprinkler M_R at plunge test condition (199 ^{o}C, 1 m/s) and (197 ^{o}C, 2.56 m/s) are similar in both the standard and worst orientation. This implies that the activation time of sprinkler M_R is independent of hot gas velocity in the wind tunnel at 199 ^{o}C. Furthermore, the similar activation times of sprinkler M_R under these two test conditions implies that the thermally sensitivity elements (RTI and C factor) of sprinkler M_R are possibly not subjected to the hot gas velocity when it is tested under high temperature (199 ^{o}C) in the wind tunnel.

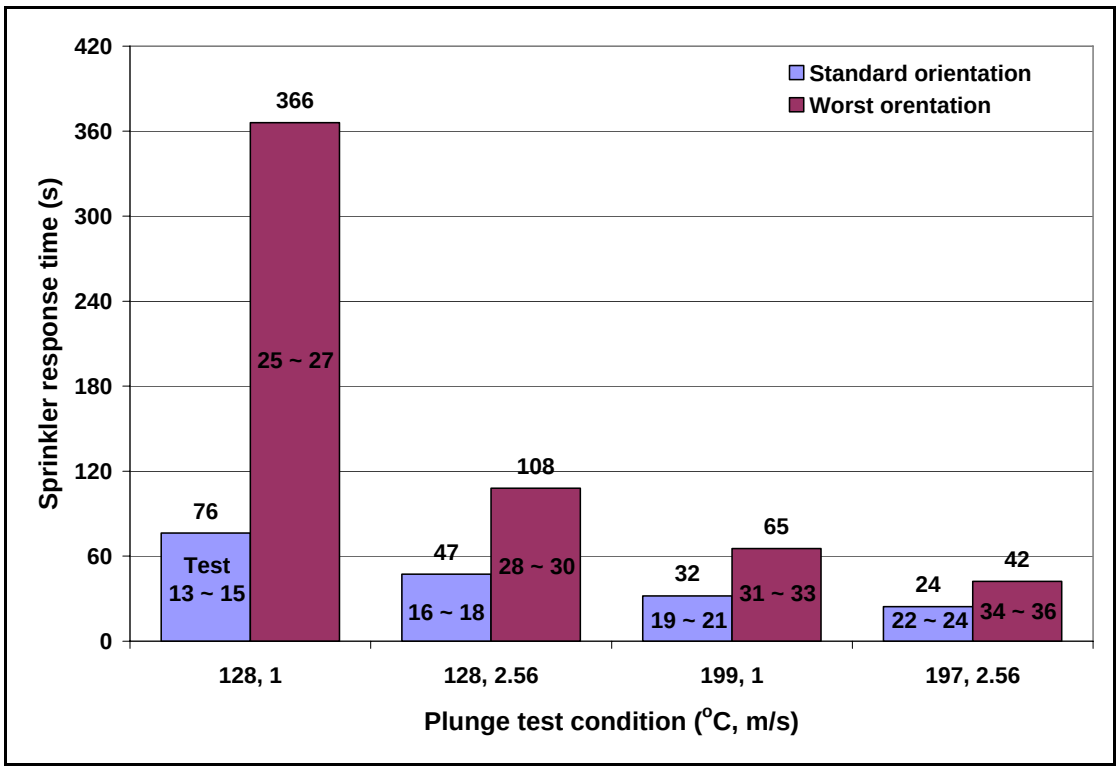

Figure 6.3: Comparison of the average sprinkler response time in both the sprinkler orientations

6.2.2 Sprinkler N_R (recessed, 68 ^oC, 3 mm glass bulb)

Figure 6.4 shows the sprinkler response times of the sprinkler N_R from the plunge tests. The result represented in this figure shows that the sprinkler response times were similar under each of the four specific plunge test conditions for the sprinkler N_R.

By comparing the maximum sprinkler response time of the sprinkler N_R and M_R in the standard sprinkler orientation, it was found that the former was smaller than the latter. The actuation temperature of the sprinkler heat-responsive element was the same for both the sprinklers. However, the size of the glass bulb of the sprinkler N_R (3 mm) was smaller than the sprinkler M_R (5 mm). For a larger glass bulb, more energy was needed to be absorbed to reach the sprinkler actuation temperature. Therefore, the sprinkler N_R gave a faster response time than the sprinkler M_R in the standard sprinkler orientation.

In addition, it was observed that the sprinkler M_R (5 mm) was faster to operate than sprinkler N_R (3 mm) at plunge test condition 1 m/s and 128 ^oC in the worst sprinkler orientation. When the sprinkler is orientated to its worst orientation (sprinkler frame arm is parallel to the oncoming hot gas flow) in the plunge test, the activation of the sprinkler is influenced by the sprinkler frame arm design. For a smaller diameter sprinkler glass bulb (lower thermal mass), the frame arm shadow had a greater impact on sprinkler activation.

Furthermore, the significance of sprinkler frame arm design relative to sprinkler thermal sensitivity and what impact this might have in respect of modelling are important issues to be investigated in the future.

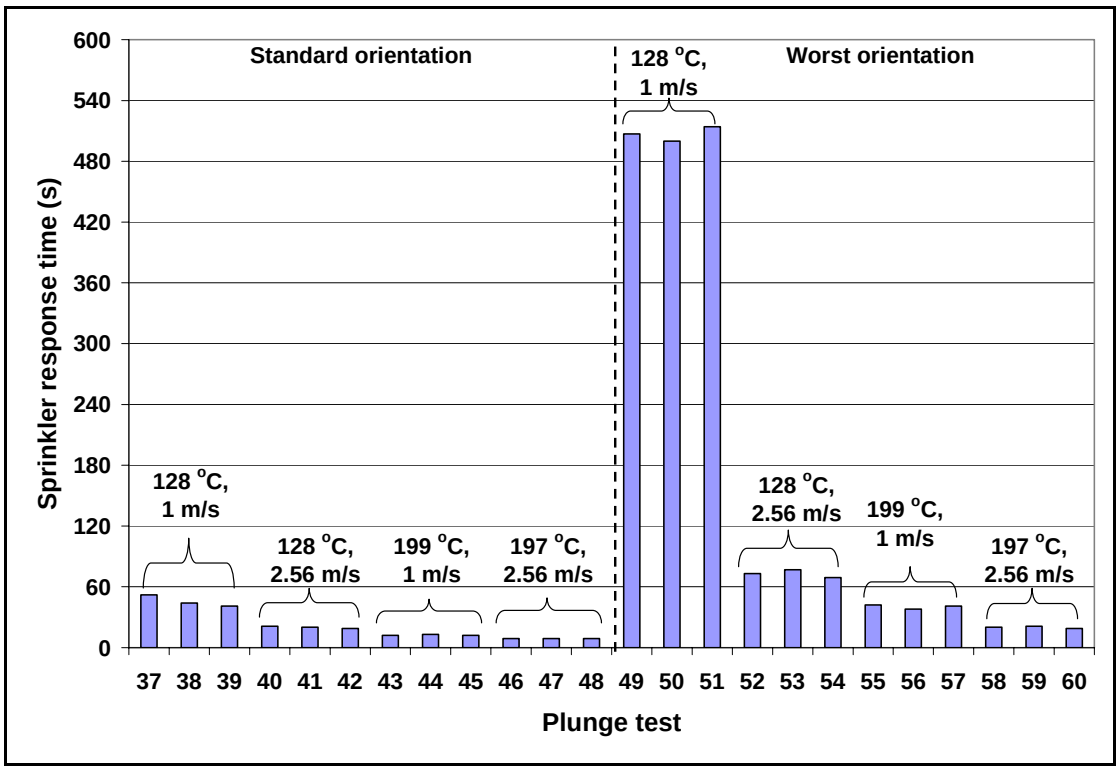

Figure 6.4: Sprinkler response time of sprinkler N_R for Test 37 ~ 60

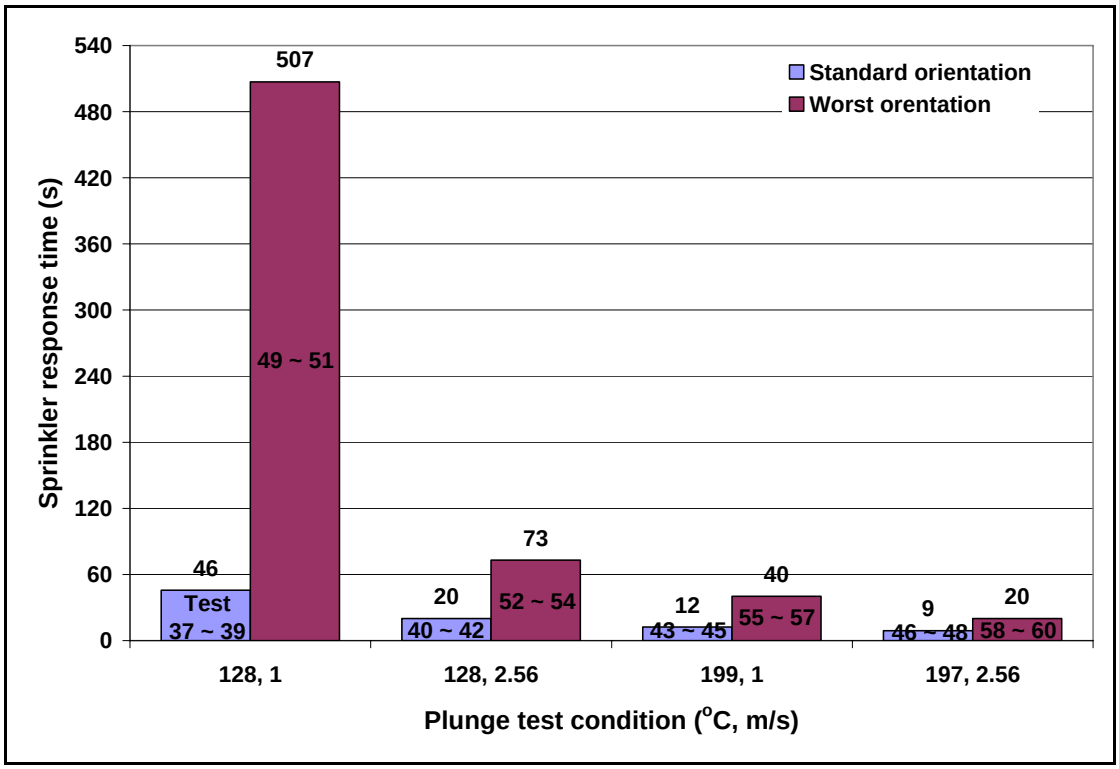

Figure 6.5: Comparison of the average sprinkler response time in both the sprinkler orientations

Figure 6.5 shows the comparison of the average sprinkler response times of the sprinkler N_R in the standard and the worst sprinkler orientation. This comparison of results shows the similarities to the comparison result as discussed for the sprinkler M_R in the previous section.

6.2.3 Sprinkler O_C (concealed, 71 ^oC, fusible solder link)

Figure 6.6 shows the sprinkler response times of the sprinkler O_C recorded in the experiment. The recorded duration was 1000 s in each plunge test. Therefore, "no operation" indicates the sprinkler was not activated within 1000 s in the wind tunnel.

From the results, as shown in this figure, the sprinkler response times recorded in each of the four specific plunge test conditions were very similar. The results show that the settings of the UC3 wind tunnel and the arrangement of the UC modified mounting plate provided consistent plunge test conditions for testing the concealed sprinklers.

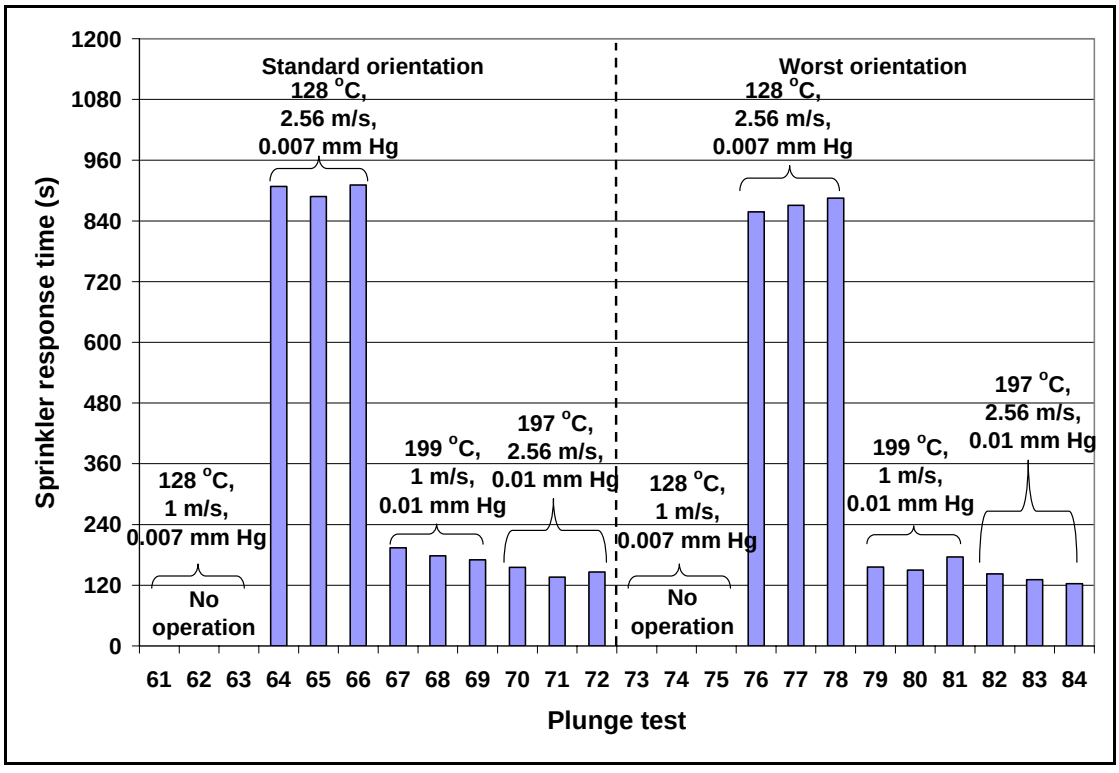

Figure 6.6: Sprinkler response time of sprinkler O_C for Test 61 ~ 84

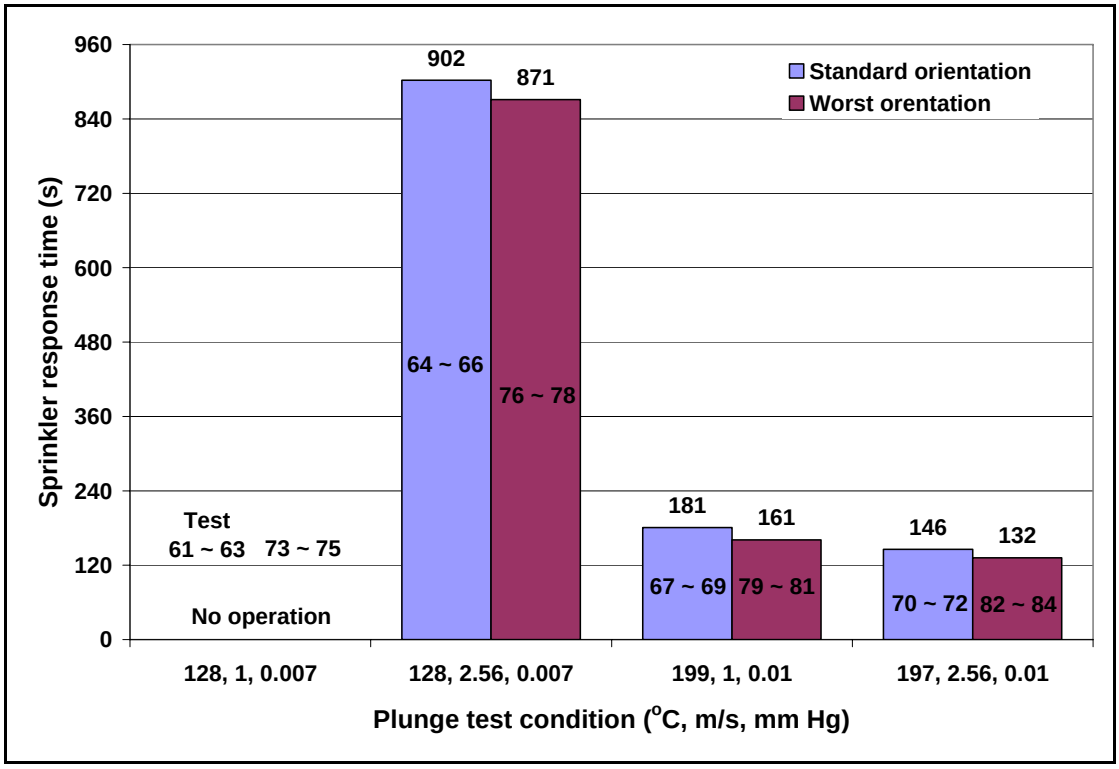

Figure 6.7: Comparison of the average sprinkler response time in both the sprinkler orientations

Figure 6.7 above shows the comparison of the average sprinkler response times under each of the four specific test conditions in both the standard and the worst orientation.

As seen from this figure, the differences between the average sprinkler response time recorded in the standard and the worst orientation under each of the four specific test conditions were small. This result implied that the sprinkler response time of a fusible solder link concealed sprinkler was not significantly influenced by the orientation of the sprinkler frame arm.

From Figure 6.7, it can be seen that the average sprinkler response times of sprinkler O_C at plunge test condition (199 ^oC, 1 m/s, 0.01 mm Hg) and (197 ^oC, 2.56 m/s, 0.01 mm Hg) are similar in both the standard and worst orientation. This implies that the activation time of sprinkler O_C is independent of hot gas velocity in the wind tunnel at 199 ^oC. Furthermore, the similar activation times of sprinkler O_C under these two test conditions implies that the thermally sensitivity elements (RTI and C factor) of sprinkler O_C are possibly not subjected to the hot gas velocity when it is tested under high temperature (199 ^oC) in the wind tunnel.

In addition to this, it was found that the average sprinkler response time under each of the four specific test conditions in the standard orientation was greater than the worst orientation. This result indicates that the sprinkler O_C gave a faster response in the "worst orientation" than in the "standard orientation".

(a): Standard orientation **(b): Worst orientation**

Figure 6.8: Standard and worst orientation of the sprinkler O_C

Figure 6.8 shows the standard and the worst orientation of the sprinkler O_C installed in the UC modified mounting plate. The arrows sketched along the bottom of the ceiling indicate the hot gas flow direction inside the wind tunnel.

By comparing the installation position of the sprinkler O_C in the standard (Figure 6.8 (a)) and the worst orientation (Figure 6.8 (b)), it was found that the portion of sprinkler exposed below the ceiling is similar in both the sprinkler orientations. Since the sprinkler O_C gave a faster response in the worst orientation than in the standard orientation, it is possible that the combination of heat transfer and flow pattern between the sprinkler O_C (a fusible solder link concealed sprinkler) and the tunnel hot gas in the worst orientation is more "efficient" than in the standard orientation. However, it should be noted that it is the only explanation that could be drawn from this research. Further investigation shall be conducted to confirm and fully explain this finding.

Figure 6.9 below shows the comparison of the average operation times of the cover plate of the sprinkler O_C obtained in both the standard and the worst sprinkler orientation. The comparison results show that the differences between the average

operation times of the cover plate recorded in the standard and the worst orientation were very small under each of the four specific plunge test conditions.

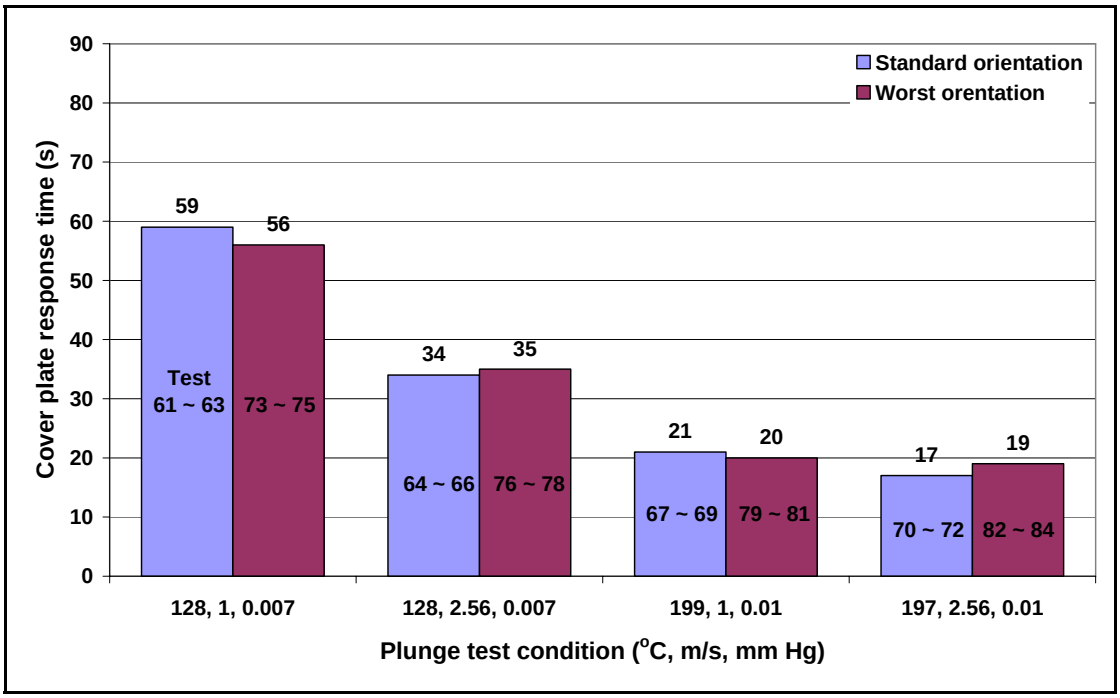

Figure 6.9: Comparison of the average cover plate response time in both the sprinkler orientations

6.2.4 Sprinkler P_C (concealed, 68 °C, 3 mm glass bulb)

Figure 6.10 and Figure 6.11 show the sprinkler response times and the comparison of the sprinkler response times of the sprinkler P_C in both the standard and the worst orientation respectively.

Unlike the analysed results for the sprinkler O_C (fusible solder link concealed sprinkler) as discussed in the previous section, the average sprinkler response times of the sprinkler P_C (glass bulb concealed sprinkler) recorded in the standard orientation were smaller than the worst orientation. This is because the sprinkler frame arm obstructed the hot gas flowed through the glass bulb when it was installed in the worst orientation.

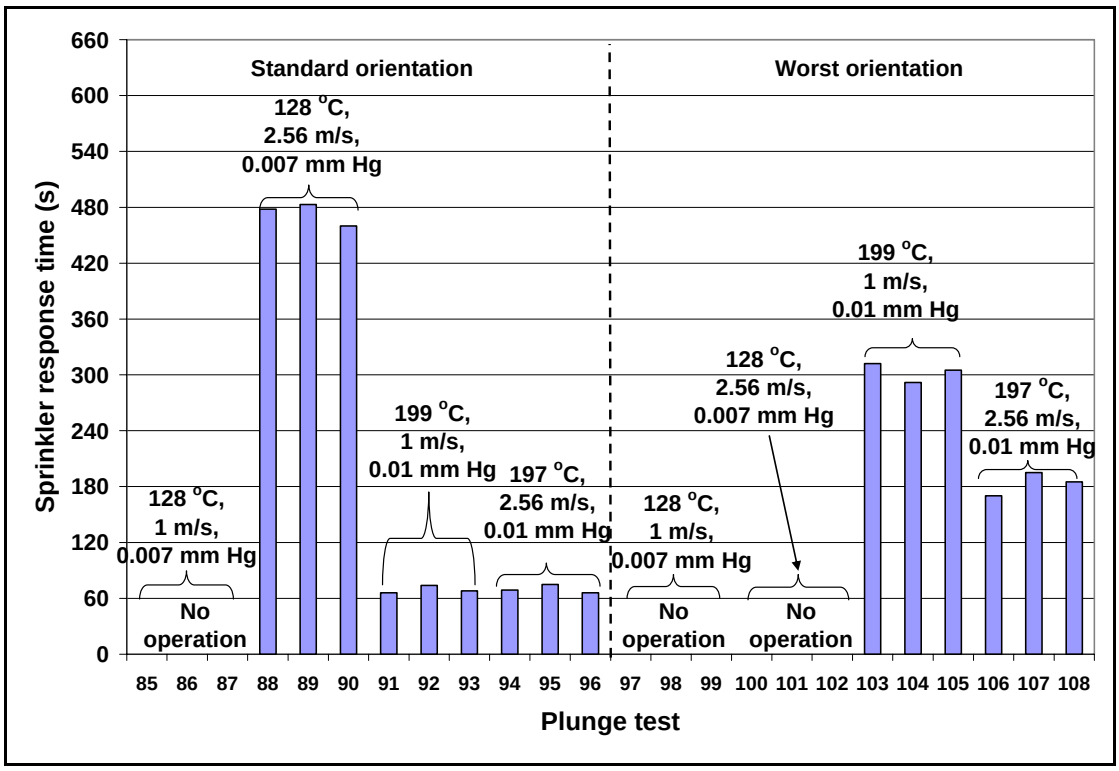

Figure 6.10: Sprinkler response time of sprinkler P_C for Test 85 ~ 108

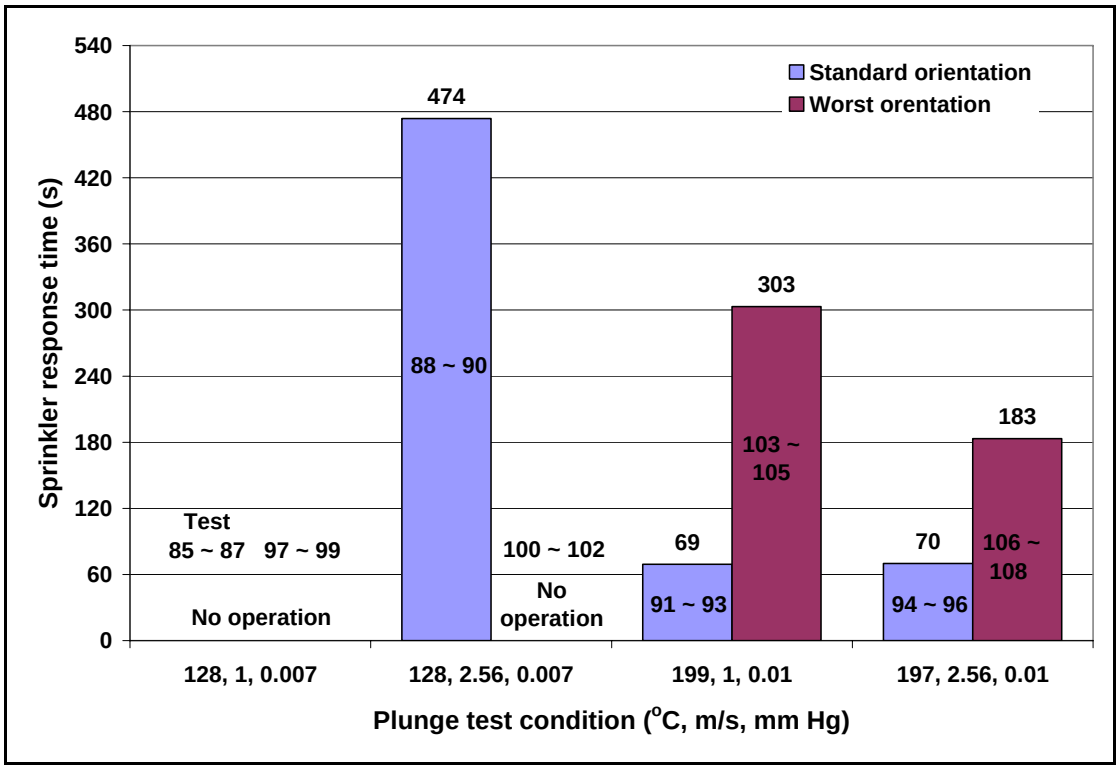

Figure 6.11: Comparison of the average sprinkler response time in both the sprinkler orientations

From Figure 6.11, the average sprinkler response times of sprinkler P_C at plunge test condition (199 ^oC, 1 m/s, 0.01 mm Hg) and (197 ^oC, 2.56 m/s, 0.01 mm Hg) are similar in the standard orientation. This implies that the activation time of sprinkler P_C is independent of hot gas velocity in the wind tunnel at 199 ^oC. Furthermore, the similar activation times of sprinkler P_C under these two test conditions implies that the thermally sensitivity elements (RTI and C factor) of sprinkler P_C are possibly not subjected to the hot gas velocity when it is tested under high temperature (199 ^oC) in the wind tunnel.

6.3 RTI

The RTI of the recessed and concealed sprinklers investigated in study were presented in this section. As mentioned in Chapter 5, the RTI of the recessed sprinklers were determined by using both the "simple" RTI equation (without C-factor) and the "comprehensive" RTI equation (with C-factor). In contrast, the RTI of the concealed sprinklers were calculated by the "comprehensive" RTI equation.

6.3.1 Sprinkler M_R (recessed, 68 ^oC, 5 mm glass bulb)

Figure 6.12 shows the calculated RTI of the sprinkler M_R in the standard and the worst orientation by using both the "simple" RTI equation (without C-factor) and the "comprehensive" RTI equation (with C-factor). As shown in this figure, the first and the second column of each pair of columns represents the RTI calculated by the "simple" RTI equation and the "comprehensive" RTI equation respectively. It should be noted that the C-factor used to calculate the RTI in the "comprehensive" equation for the sprinkler M_R was assumed to be 0.89 $(m/s)^{1/2}$ and referenced from Annable (2006).

The glass bulb sizes of tested sprinklers at the BRE were not provided in their report (Annable 2006). Based on the lack of knowledge of the glass bulb sizes of the tested sprinklers at the BRE, the C factors used to calculate the RTI in the "comprehensive" equation for each type of tested sprinkler in this work were assumed to be identical, based on the similarity of the actuation temperature and link type (glass bulb or fusible solder link) parameters in both experiments.

As tabulated in Table 2.6, the actuation temperature and link type of sprinkler B_R are identical to sprinkler M_R. Therefore, the C factor of sprinkler B_R (Annable 2006) as shown in Table 2.7 was used to calculate the RTI for sprinkler M_R.

From Figure 6.12, it can be seen that the RTI obtained in the worst orientation is much larger than in the standard orientation under each of the four specific plunge test conditions (for both the RTI equations).

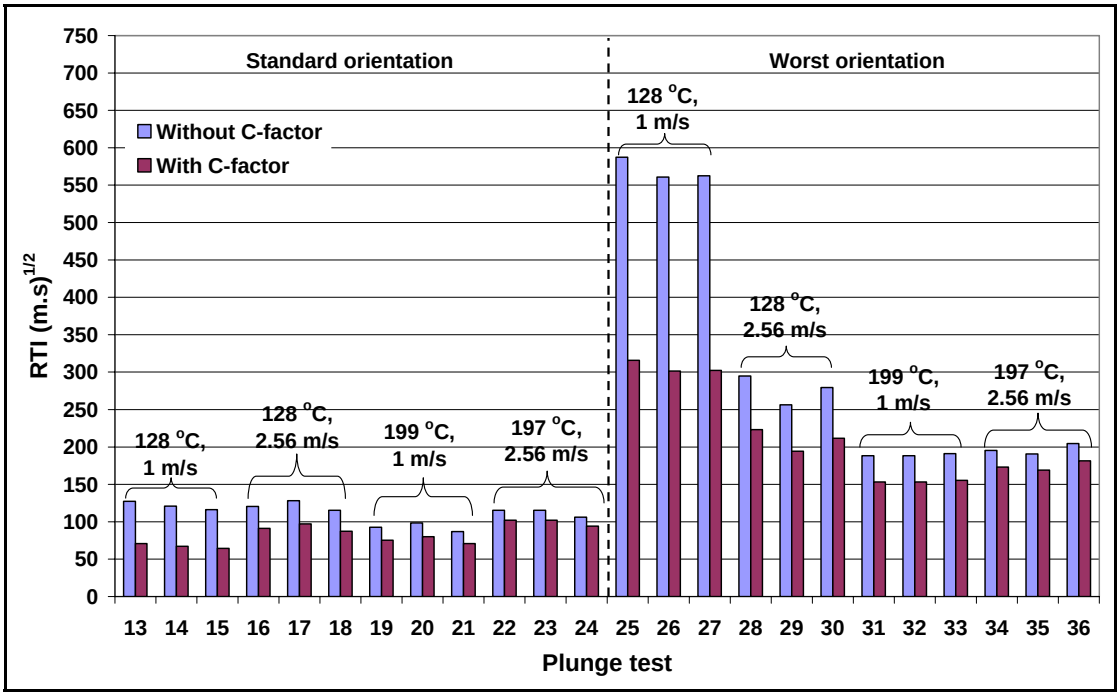

Figure 6.12: RTI of sprinkler M_R for Test 13 ~ 36

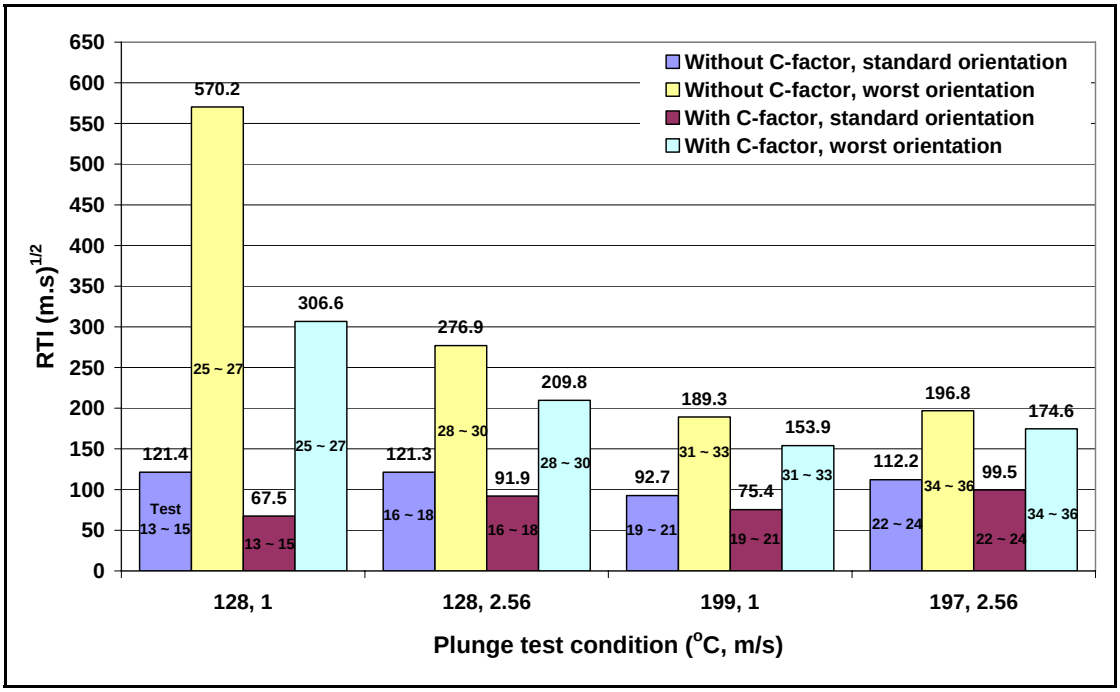

Figure 6.13: Comparison of the average RTI in both the sprinkler orientations

Figure 6.13 shows the comparison of the average RTI of the sprinkler M_R in both the sprinkler orientations for the "simple" RTI equation (without C-factor) and the "comprehensive" RTI equation (with C-factor). From this figure, the differences between the average RTI calculated from the four different plunge test conditions were found to be small in the standard orientation (for both the RTI equations). However, the variations of the average RTI calculated from the four different plunge test conditions became larger in the worst orientation (for both the RTI equations). In addition to this, it was found that the differences between the average RTI calculated by using the "simple" RTI equation were larger than the "comprehensive" RTI equation under each of the four specific plunge test conditions (for both the standard and the worst orientation).

6.3.2 Sprinkler N_R (recessed, 68 ^oC, 3 mm glass bulb)

Figure 6.14 and Figure 6.15 show the RTI and the average RTI of the sprinkler N_R obtained from the experiment.

From Figure 6.15, it can be seen that the differences of the average RTI from the four different plunge test conditions determined by using the "comprehensive" RTI

equation (with C-factor) in the standard orientation were smaller than the "simple" RTI equation (without C-factor). For the worst orientation, the variations of the average RTI from the four different plunge test conditions calculated by the "simple" RTI equation were larger than the "comprehensive" RTI equation.

It should be noted that the actuation temperature and link type of sprinkler N_R is the same as sprinkler B_R (Annable 2006), therefore the C-factor used to calculate the RTI in the "comprehensive" equation for the sprinkler N_R was assumed to be 0.89 $(m/s)^{1/2}$ (Annable 2006).

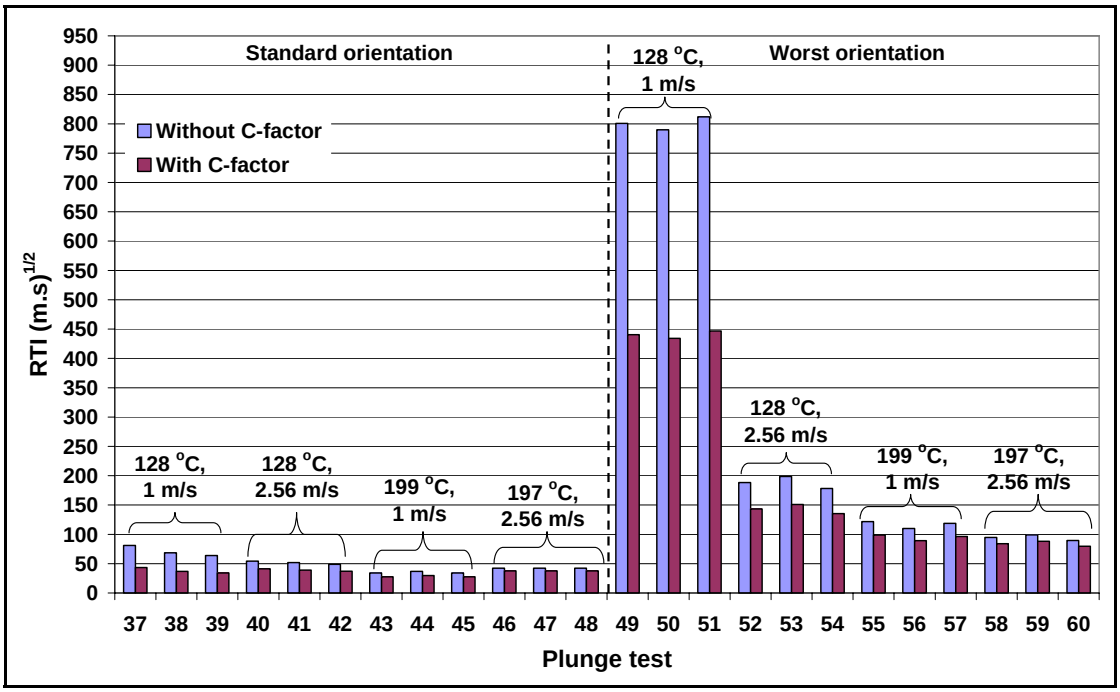

Figure 6.14: RTI of sprinkler N_R for Test 37 ~ 60

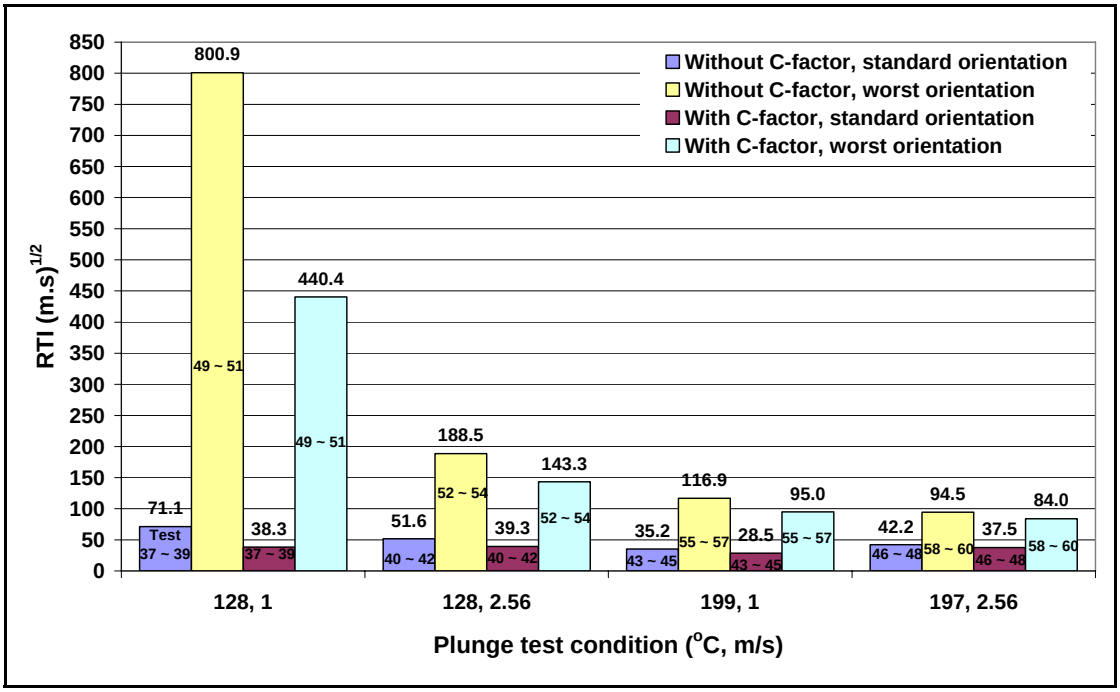

Figure 6.15: Comparison of the average RTI in both the sprinkler orientations

6.3.3 Sprinkler O_C (concealed, 71 °C, fusible solder link)

Figure 6.16 shows the calculated RTI of the sprinkler O_C in the standard and the worst orientation by using the "comprehensive" RTI equation (with C-factor). Because the actuation temperature and link type of sprinkler O_C are identical to sprinkler D_C (Annable 2006), the C factor used to calculate the RTI in the "comprehensive" equation for the sprinkle O_C was assumed to be 2.37 $(m/s)^{1/2}$ (Annable 2006). Figure 6.17 shows the comparison of the average RTI of the sprinkler O_C in both the standard and the worst orientation. From this figure, it was found that the average RTI calculated in the worst orientation is smaller than in the standard orientation.

It should be noted that the specific parameters used in the term $(1-\Delta T_b\left(1+C/(U)^{1/2}\right)/\Delta T_g)$ in the "comprehensive" RTI equation gave rise to negative values whose natural logarithm are meaningless for the RTI of the sprinkler O_C under the plunge test conditions (128 °C, 2.56 m/s, 0.007 mm Hg and 199 °C, 1 m/s, 0.01 mm Hg). Therefore, the RTI of the sprinkler O_C under these two plunge test conditions are shown as "N/A" in Figure 6.16 and Figure 6.17. In addition to this, the sprinkler O_C were not activated in the plunge test condition (128 °C, 1.0 m/s, 0.007 mm Hg), therefore the RTI was also shown as "N/A" in Figure 6.16 and Figure 6.17.

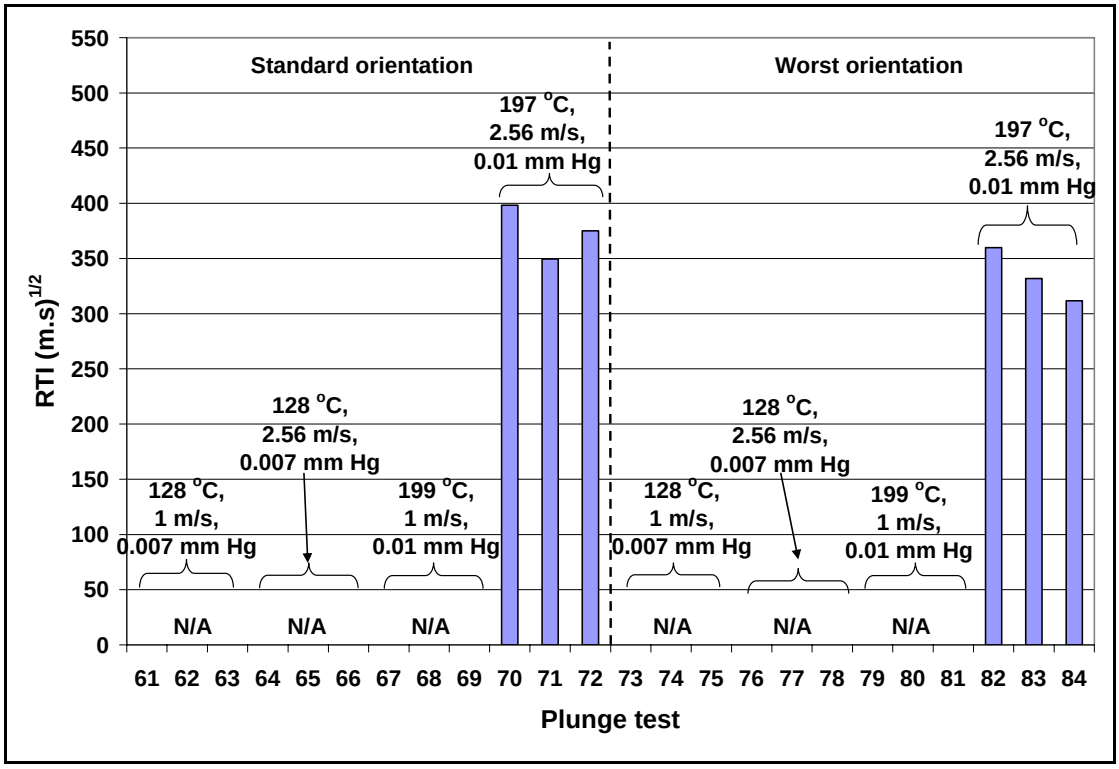

Figure 6.16: RTI of sprinkler O_C for Test 61 ~ 84

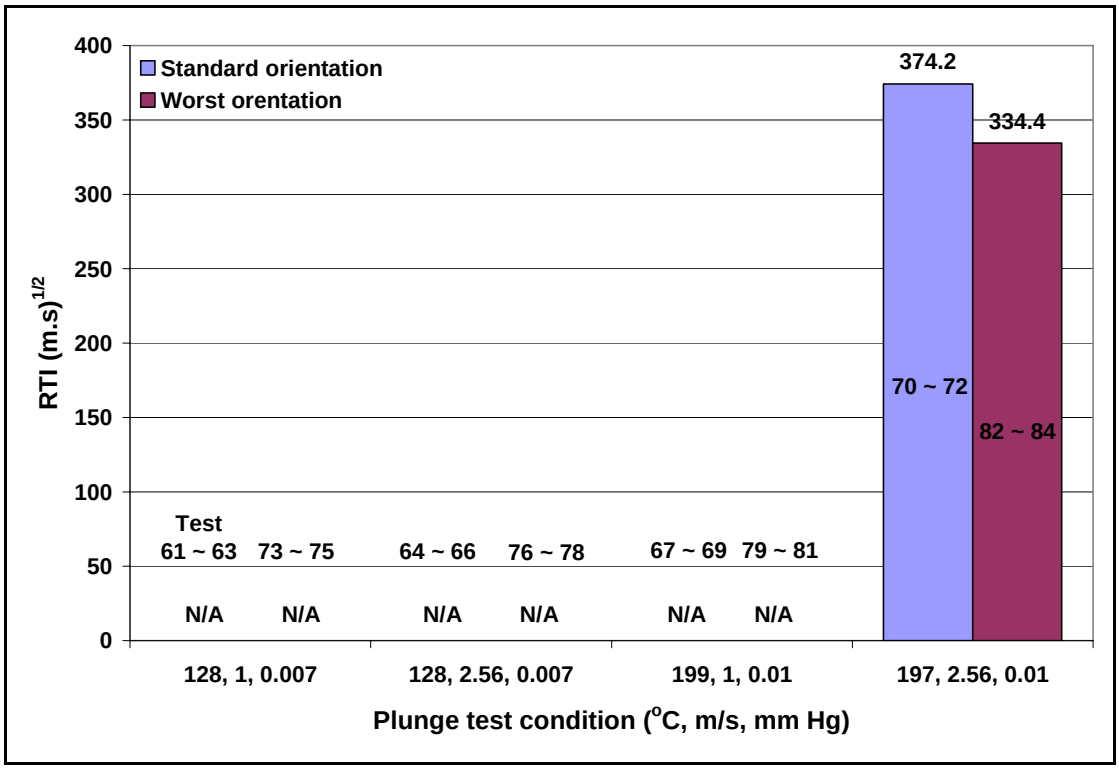

Figure 6.17: Comparison of the average RTI in both the sprinkler orientations

6.3.4 Sprinkler P_C (concealed, 68 ^oC, 3 mm glass bulb)

Figure 6.18 shows the RTI of the sprinkler P_C calculated by using the "comprehensive" RTI equation (with C-factor) in both the standard and the worst orientation. It should be noted that the actuation temperature and link type of sprinkler P_C are identical to sprinkler C_C and E_C (Annable 2006), therefore the C-factor used to calculate the RTI for the sprinkler P_C was assumed to be 0.49 $(m/s)^{1/2}$ and was the average of the C-factor of the sprinkler C_C and E_C as shown in Table 2.7 in Chapter 2.

Figure 6.19 shows the average RTI of the sprinkler P_C in the standard and the worst orientation. The "N/A" shown in Figure 6.18 and Figure 6.19 indicates that the tested sprinkler P_C were not activated in the plunge test experiments.

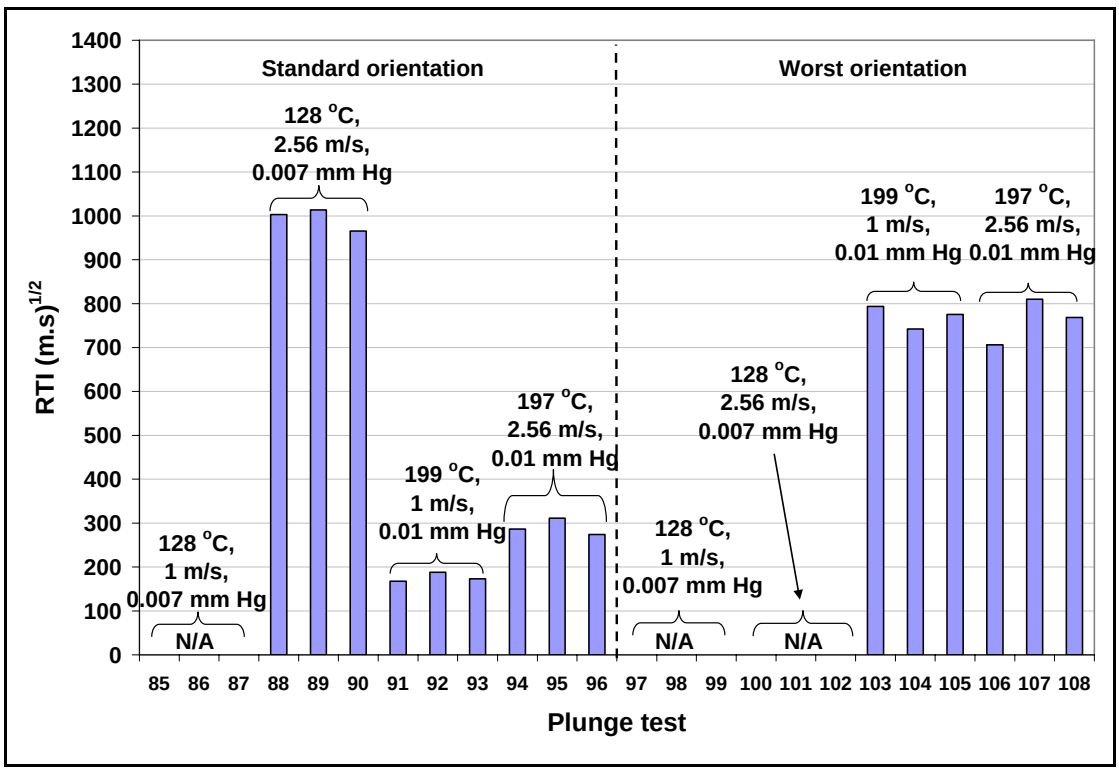

Figure 6.18: RTI of sprinkler P_C for Test 85 ~ 108

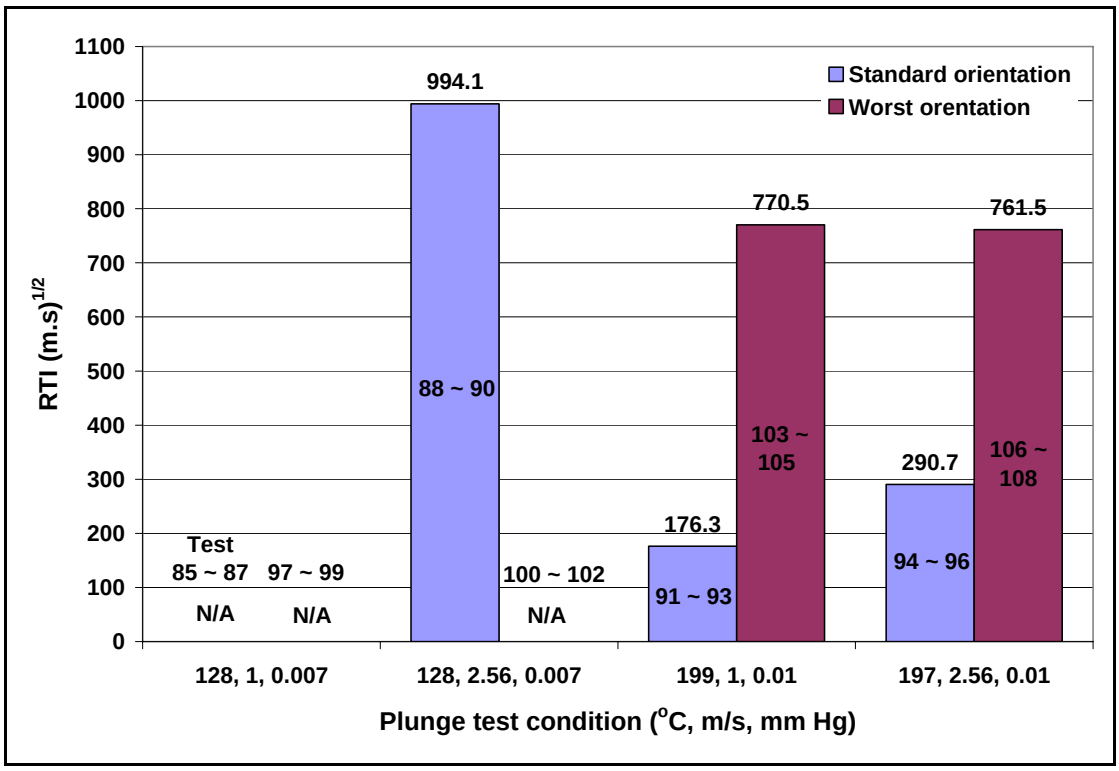

Figure 6.19: Comparison of the average RTI in both the sprinkler orientations

6.4 Determination of the apparent RTI (Comparison)

The "final calculated RTI" for each tested recessed and concealed sprinklers in each particular sprinkler frame arm orientation was determined in this section. It should be noted that the "final calculated RTI" was denoted as "apparent RTI" in this study.

The apparent RTI of the recessed and concealed sprinklers were not investigated at FMRC (Bill and Heskestad 1995). Therefore, the approach used to determine the apparent RTI of the recessed and concealed sprinklers tested in this research were developed based on the approach used at the BRE (Annable 2006) and presented as follows:

- At the BRE (Annable 2006), the apparent RTI of each type of tested sprinklers was determined by averaging the RTI obtained from one unique plunge test condition (135 ^{o}C, 1.75 m/s for the recessed sprinklers; 135 ^{o}C, 2.5 m/s, 0.01 mm Hg or 197 ^{o}C, 2.5 m/s, 0.01 mm Hg for the concealed sprinklers) in the particular sprinkler orientation (standard or worst sprinkler frame arm orientation).

- As illustrated in Section 6.3 (Figure 6.13, Figure 6.15 and Figure 6.19), the differences between the average RTI from some of the different plunge test conditions were found to be small. Therefore, it was considered that the apparent RTI is more accurate by averaging the similar RTI obtained from different plunge test conditions in the particular sprinkler orientation rather than averaging the RTI from one unique plunge test condition.

- The apparent RTI of the recessed and concealed sprinklers investigated in this study were determined by averaging the similar RTI obtained from different plunge test conditions in the particular sprinkler orientation.

In an attempt to provide further confidence in the apparent RTI found from this work, a comparison was also made with the results produced by Bill and Heskestad (1995) and Annable (2006).

6.4.1 Sprinkler M_R (recessed, 68 ^oC, 5 mm glass bulb)

The apparent RTI of the sprinkler M_R in the standard and the worst orientation (for both the RTI equations) are tabulated in Table 6.2 below. It should be noted that the average RTI calculated under test condition (128 ^oC, 1 m/s) in the worst orientation by using the “simple” RTI equation (without C-factor) was significantly larger than the other test conditions (as shown in Figure 6.13). Therefore, this average RTI value (570.2 $(m.s)^{1/2}$) was not incorporated to calculate the apparent RTI for the sprinkler M_R in the worst orientation (the “simple” RTI equation). With the exception of the apparent RTI calculated in the worst orientation (the “simple” RTI equation), all of the apparent RTI shown in Table 6.2 were calculated by averaging all the average RTI from the four different plunge test conditions in the corresponding sprinkler frame arm orientation (as illustrated in Figure 6.13).

Table 6.2: Apparent RTI of the sprinkler M_R

	Standard orientation	Worst orientation
The "simple" RTI equation (without C-factor)	111.9 $(m.s)^{1/2}$	221 $(m.s)^{1/2}$
The "comprehensive" RTI equation (with C-factor)	83.6 $(m.s)^{1/2}$	211.2 $(m.s)^{1/2}$

Figure 6.20 displays the comparison of the apparent RTI of the sprinkler M_R between the experiment, FMRC (Bill and Heskestad 1995) and the BRE (Annable 2006). As mentioned in Section 6.4, the apparent RTI of the recessed and concealed sprinklers were not determined by Bill and Heskestad (1995). However, the "nominal" RTI of each tested sprinklers was provided in the technical report (Bill and Heskestad 1995). It was considered that the "nominal" RTI was the only data that could be obtained from the literature to specify the sprinklers tested at FMRC (Bill and Heskestad 1995). Therefore, the "nominal" RTI from FMRC were used to compare the apparent RTI obtained from the experiment in this research and the BRE. It should be noted that the type and size of the heat-responsive element and the actuation temperature of the sprinkler B (as shown Table 2.3, Chapter 2) tested at FMRC were identical to the sprinkler M_R. Therefore, the "nominal" RTI of the sprinkler B was used to plot Figure 6.20.

As tabulated in Table 2.6 (Chapter 2), only one type of the recessed sprinkler (sprinkler B_R, glass bulb, 68 ^oC) was tested at the BRE (Annable 2006). The apparent RTI of the sprinkler B_R was used to compare the apparent RTI of the sprinkler M_R and the "nominal" RTI of the sprinkler B. However, the size of the heat-responsive element (glass bulb) of the sprinkler B_R was not given by Annable (2006). Due to the difference in glass bulb size, the results only provide an approximate comparison.

It should be noted that the "N/A" in Figure 6.20 (and its occurrence within figures in the rest of this chapter) indicates that the RTI value was not determined by Bill and Heskestad (1995) or Annable (2006).

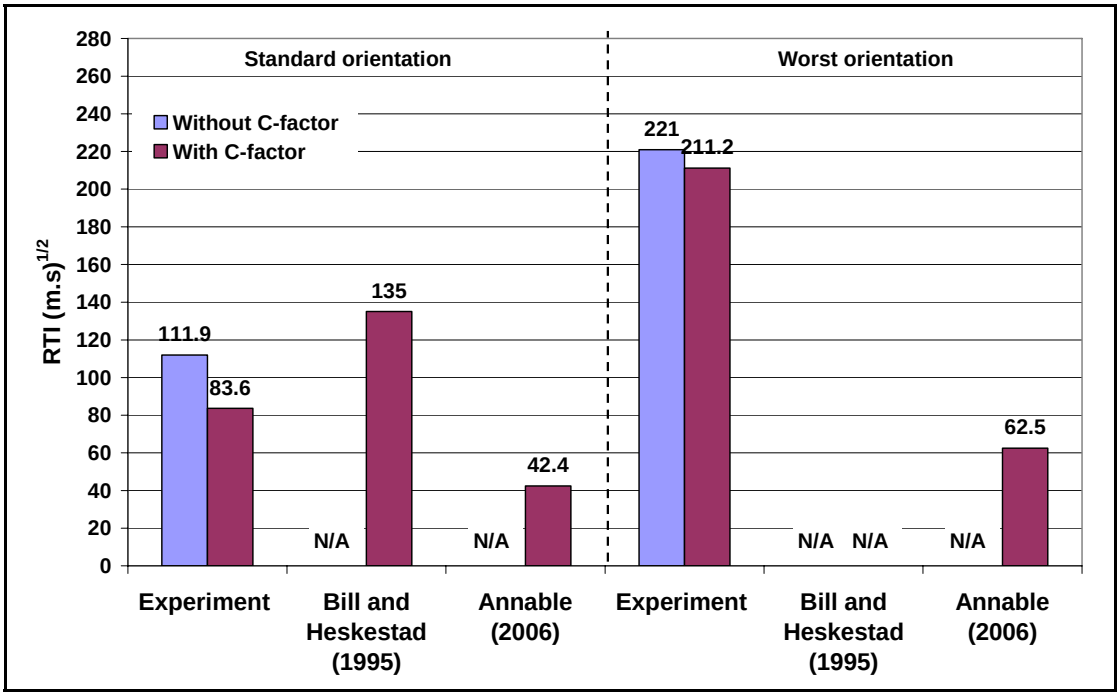

Figure 6.20: Comparison of the apparent RTI of the sprinkler M_R between the experiment, FMRC (Bill and Heskestad 1995) and the BRE (Annable 2006)

From Figure 6.20, it can be seen that the apparent RTI values do not agree with each other between the different experiments. In the standard orientation, the apparent RTI calculated by the "comprehensive" equation (with C-factor) approximately equates to the average of the RTI from Bill and Heskestad (1995) and Annable (2006). However, the apparent RTI in the worst orientation obtained from the experiment was much greater than the apparent RTI provided by Annable (2006).

In addition, it was found that the apparent RTI of the sprinkler M_R calculated by using the "comprehensive" RTI equation (with C-factor) was smaller than the apparent RTI calculated by the "simple" RTI equation (without C-factor) in both the standard and the worst orientation.

6.4.2 Sprinkler N_R (recessed, 68 ^oC, 3 mm glass bulb)

Table 6.3 below shows the apparent RTI of the sprinkler N_R in the standard and the worst orientation (for both the RTI equations). The apparent RTI in the standard and the worst orientation (for both the RTI equations) were calculated by averaging the average RTI from all plunge test conditions and three different plunge test conditions

(128 ^{o}C, 2.56 m/s; 199 ^{o}C, 1 m/s and 197 ^{o}C, 2.56 m/s) respectively (as shown in Figure 6.15).

Table 6.3: Apparent RTI of the sprinkler N_R

	Standard orientation	Worst orientation
The "simple" RTI equation (without C-factor)	50.0 $(m.s)^{1/2}$	133.3 $(m.s)^{1/2}$
The "comprehensive" RTI equation (with C-factor)	35.9 $(m.s)^{1/2}$	107.4 $(m.s)^{1/2}$

Figure 6.21 illustrates the comparison of the apparent RTI of the sprinkler N_R between the experiment, FMRC (Bill and Heskestad 1995) and the BRE (Annable 2006). The type and size of the heat-responsive element and the actuation temperature of the sprinkler A (as shown in Table 2.3, Chapter 2) tested at FMRC were the same as the sprinkler N_R. Therefore, the “nominal” RTI of the sprinkler A was used to compare the apparent RTI of the sprinkler N_R obtained in this study. As mentioned in Section 6.4.1, the size of the heat-responsive element of the sprinkler B_R was not clarified by Annable (2006). Therefore, the apparent RTI of the sprinkler B_R was also used to compare the apparent RTI of the sprinkler N_R.

From Figure 6.21, it was found that the apparent RTI calculated by using both the RTI equations were very similar to the RTI provided by Bill and Heskestad (1995) and Annable (2006) in the standard orientation. In addition to this, the apparent RTI determined by the “comprehensive” RTI equation (with C-factor) was almost identical to the RTI given by Bill and Heskestad (1995) in the standard orientation.

For the worst orientation, the apparent RTI (for both the RTI equations) were larger than the apparent RTI provided by Annable (2006).

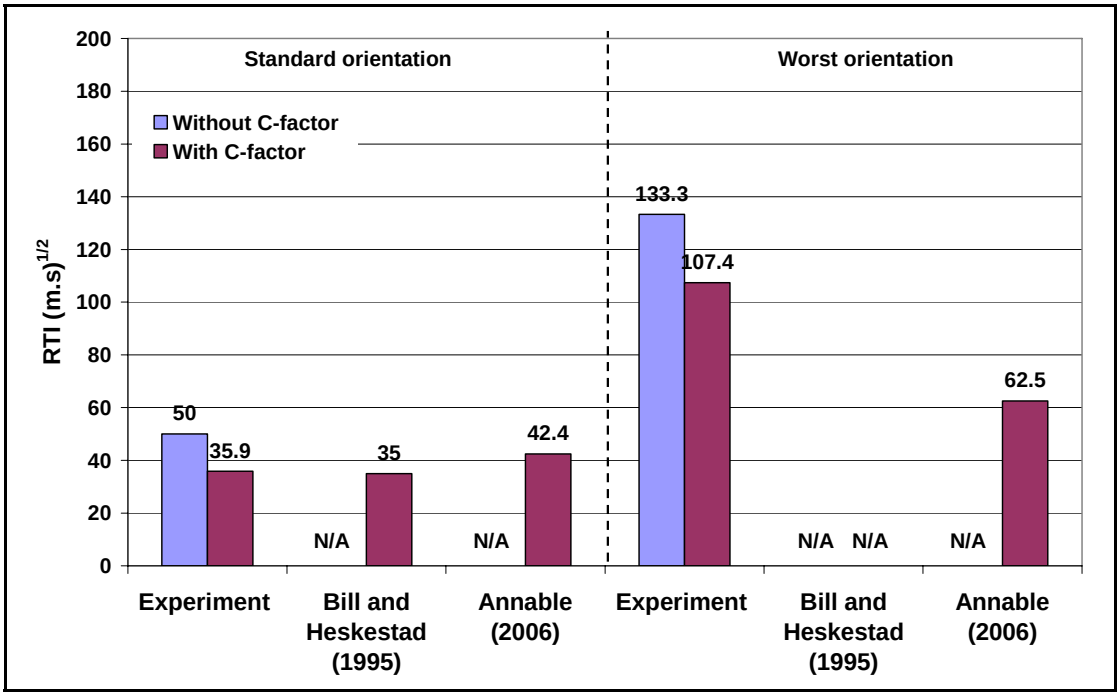

Figure 6.21: Comparison of the apparent RTI of the sprinkler N_R between the experiment, FMRC (Bill and Heskestad 1995) and the BRE (Annable 2006)

6.4.3 Sprinkler O_C (concealed, 71 ^oC, fusible solder link)

The apparent RTI of the sprinkler O_C calculated by using the "comprehensive" RTI equation (with C-factor) in the standard and the worst orientation were tabulated in Table 6.4 below. As shown in Figure 6.17, the average RTI were only available in the ultimate upper plunge test condition (197 ^oC, 2.56 m/s, 0.01 mm Hg). Therefore, the apparent RTI of the sprinkler O_C were the average RTI in the test condition (197 ^oC, 2.56 m/s, 0.01 mm Hg) at the corresponding sprinkler frame arm orientation.

Table 6.4: Apparent RTI of the sprinkler O_C

	Standard orientation	Worst orientation
The "comprehensive" RTI equation (with C-factor)	374.2 $(m.s)^{1/2}$	334.4 $(m.s)^{1/2}$

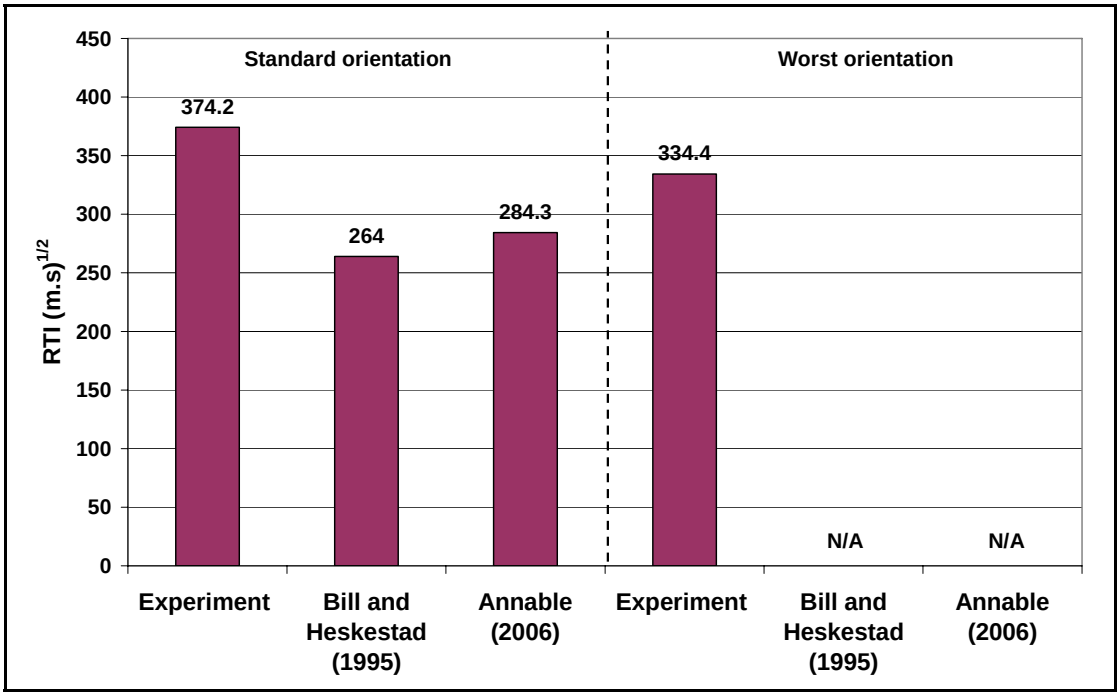

Figure 6.22: Comparison of the apparent RTI of the sprinkler O_C between the experiment, FMRC (Bill and Heskestad 1995) and the BRE (Annable 2006)

Figure 6.22 shows the comparison of the apparent RTI of the sprinkler O_C between the experiment, FMRC (Bill and Heskestad 1995) and the BRE (Annable 2006). The "nominal" RTI of the sprinkler J (Table 2.3 in Chapter 2) from FMRC and the apparent RTI of the sprinkler D_C (Table 2.7 in Chapter 2) from the BRE were used to plot Figure 6.22. It should be noted that the types of the heat-responsive element (fusible solder link) of the sprinkler O_C, J and D_C were identical. However, the actuation temperature of the sprinkler J (74 ^oC) was different and slightly higher than the sprinkler O_C and D_C (71 ^oC).

From the comparison shown in this figure, the RTI provided by Bill and Heskestad (1995) and Annable (2006) were smaller than the apparent RTI obtained from the experiment in the standard orientation. Since the concealed sprinklers with the fusible solder link were not investigated at FMRC and the BRE in the worst orientation, the comparison was not made between the experiment, FMRC and the BRE.

6.4.4 Sprinkler P_C (concealed, 68 ^oC, 3 mm glass bulb)

Table 6.5 shows the apparent RTI of the sprinkler P_C calculated by using the "comprehensive" RTI equation (with C-factor) in both the standard and the worst orientation. It should be noted that the apparent RTI in the standard and the worst orientation was calculated by averaging the average RTI in the test conditions (199 ^oC, 1 m/s, 0.01 mm Hg and 197 ^oC, 2.56 m/s, 0.01 mm Hg) as shown in Figure 6.19.

Table 6.5: Apparent RTI of the sprinkler P_C

	Standard orientation	Worst orientation
The "comprehensive" RTI equation (with C-factor)	233.5 $(m.s)^{1/2}$	766 $(m.s)^{1/2}$

The glass bulb type concealed sprinklers were not investigated by Bill and Heskestad (1995). Therefore the comparison was made between the apparent RTI from the experiment in this work and the BRE (Annable 2006) and shown in Figure 6.23. The apparent RTI from the BRE shown in this figure was the data from the sprinkler C_C (Table 2.7 in Chapter 2). It should be noted that the type of the heat-responsive element and the actuation temperature of the sprinkler C_C was the same as the sprinkler P_C. However, the size of the heat-responsive element of the sprinkler C_C was an unknown and not given by Annable (2006).

From this figure, the comparison shows that the apparent RTI determined from this study was larger than the BRE (Annable 2006) in both the standard and the worst orientation.

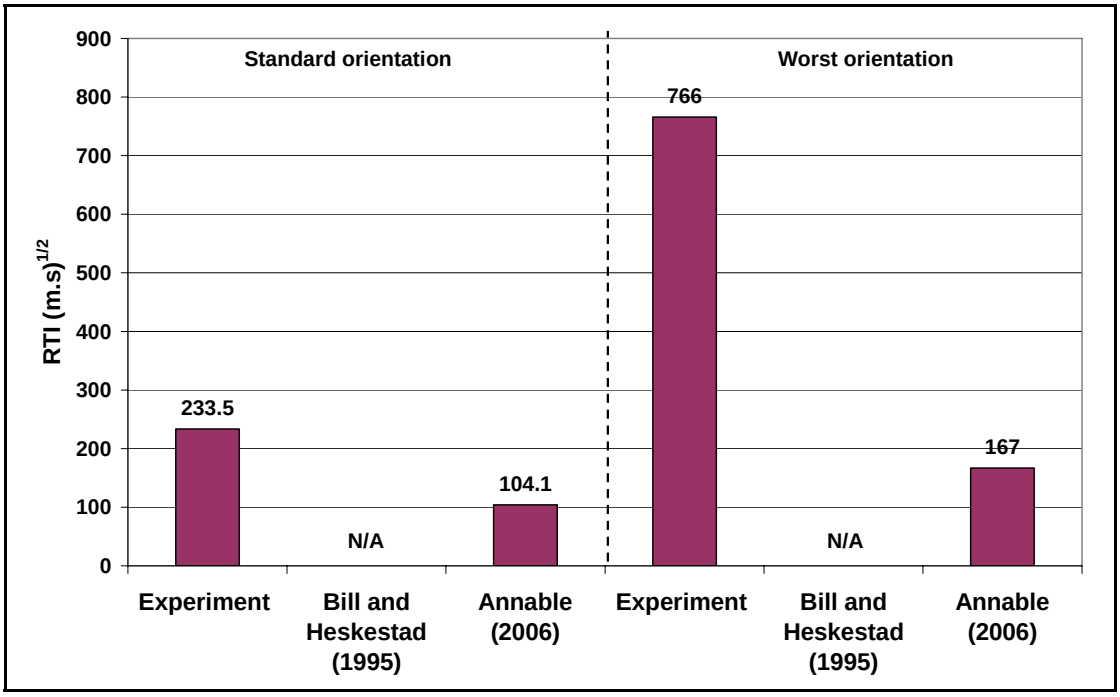

Figure 6.23: Comparison of the apparent RTI of the sprinkler P_C between the experiment, FMRC (Bill and Heskestad 1995) and the BRE (Annable 2006)

6.4.5 Summary

From the comparisons shown in Section 6.4.1 ~ Section 6.4.4, with the exception of the apparent RTI for the sprinkler N_R in the standard orientation, the apparent RTI determined in this study were different than the "nominal" RTI and the apparent RTI provided by Bill and Heskestad (1995) and Annable (2006) respectively. The differences of the RTI for the recessed and concealed sprinklers between the experiment in this research, FMRC and the BRE might cause by the factors listed below:

- The configurations of the sprinklers tested in this research, FMRC and the BRE were different.
- The performance of the wind tunnel used in this research, FMRC and the BRE was different.
- The wind tunnel test conditions conducted in this research, FMRC and the BRE were different.

- The ambient temperatures during the plunge tests in this research, FMRC and the BRE were different.

6.5 General discussion

In general, by comparing the apparent RTI obtained from the experiments in this study with the RTI provided from FMRC (Bill and Heskestad 1995) and the BRE (Annable 2006), the results show significantly differences. However, the comparisons demonstrated good agreement between the apparent RTI in this study, FMRC and the BRE for the sprinkler N_R in the standard orientation.

The apparent RTI of the recessed sprinklers investigated in this research were calculated by using both the "simple" RTI equation (without C-factor) and the "comprehensive" RTI equation (with C-factor). It was found that the apparent RTI calculated by the former RTI equation were larger than the latter RTI equation.

The RTI is a parameter used to indicate how quickly the sprinkler can absorb heat from its surroundings sufficient to cause activation, and therefore the sprinkler response would be faster with a smaller RTI value for a given sprinkler. However, it should be noted that a larger RTI should be used to produce a conservative result for fire engineering design purposes.

As discussed in Section 6.3.1 ~ 6.3.4, the glass bulb sizes of tested sprinklers at the BRE were not provided in their report (Annable 2006). Therefore, the C factors used to calculate the RTI in the "comprehensive" equation for each type of tested sprinkler in this work were assumed to be identical, based on the similarity of the actuation temperature and link type (glass bulb or fusible solder link) parameters in both experiments. However, it should be noted that the sprinkler B_R (Annable 2006) was subsequently discovered to be a 3 mm glass bulb sprinkler after completion of the majority of the work reported here. In addition, the C factor from the sprinkler B_R (Annable 2006) was the only data available to calculate the "comprehensive" RTI for recessed sprinklers. Therefore, the C factor from the sprinkler B_R was used to calculate the "comprehensive" RTI for sprinkler M_R and N_R in this research.

CHAPTER 7

7 BRANZFIRE MODELLING: PROCEDURE AND SCENARIOS

As described in Chapter 1, in order to find correlations between the normal sprinkler response times predicted in BRANZFIRE and the experimental flush, recessed, concealed and the recessed sidewall sprinkler response times in the full scale fire tests, BRANZFIRE was used to simulate the fire scenarios in the full scale fire tests. The description of the modelling procedure, the assumptions made, the scenarios modelled and the data analysis techniques used are described in this chapter.

7.1 BRANZFIRE modelling procedure

The BRANZFIRE modelling procedure and the assumptions made are described in details in this section. The input file of the BRANZFIRE used for a particular simulation (Simulation 12) is given as an example and attached in Appendix F.

7.1.1 BRANZFIRE room specification

7.1.1.1 Compartment geometry

Table 7.1 below shows the input room dimensions used in BRANZFIRE. These dimensions are also illustrated in Chapter 2. It should be noted the identification of each test shown in this table is identical to the test notation represented in Bill and Heskestad (1995).

Table 7.1: Input room dimensions in BRANZFIRE

Test	Room dimension (m)				
	Width	Length	Max. stud height	Min. stud height	Floor elevation
1 ~ 13, 16	3.66	7.32	2.44	2.44	0
14	3.66	4.6	2.44	2.44	0

Figure 7.1 shows the user interface in BRANZFIRE for inputting the compartment dimensions.

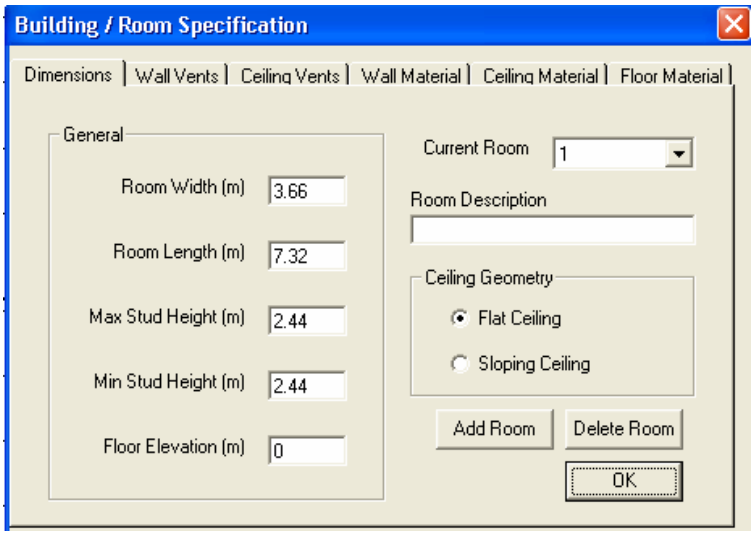

Figure 7.1: User interface for inputting the compartment dimensions

7.1.1.2 Ventilation opening

Table 7.2 and Figure 7.2 show the input parameters used to specify the ventilation opening and the user interface in BRANZFIRE respectively. The ventilation opening was unobstructed over the duration of the experiment in each full scale fire test, therefore the "vent opening time" and the "vent closing time" were specified as "zero" second in BRANZFIRE.

Table 7.2: Ventilation opening specification in BRANZFIRE

Test	Wall vent specification			
	Width (m)	Height (m)	Vent sill height (m)	Vent opening and closing time (s)
1 ~ 13	1.18	2.06	0	0
14	0.76	2.03	0	0
16	3.66	2.44	0	0

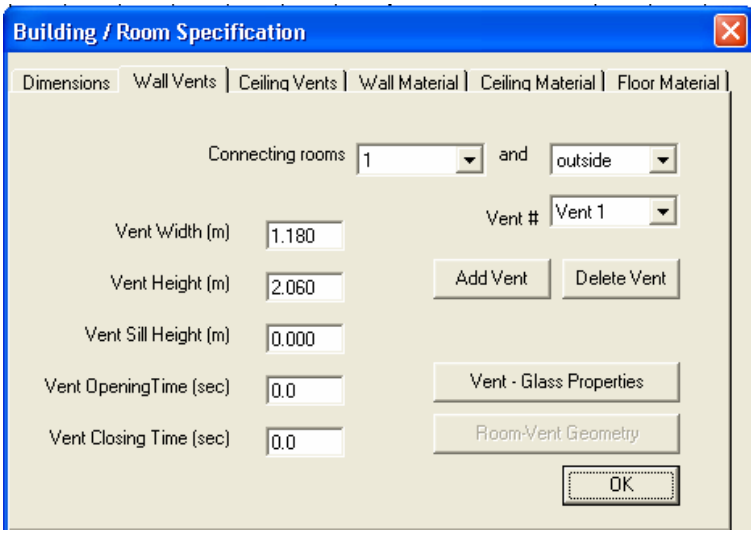

Figure 7.2: User interface for specifying the ventilation opening

7.1.1.3 Wall, ceiling and floor materials

As described in Chapter 2, the compartment used in the full scale fire tests was made from wood studs and 0.5 inch (12.7 mm) thick gypsum board. Hence, it was assumed that the wall and ceiling lining material were 12.7 mm thick plasterboard (painted gypsum) in BRANZFIRE. It should be noted that the plasterboard (painted gypsum) was selected from the material database provided in BRANZFIRE. In addition, the construction material for the floor was not given by Bill and Heskestad (1995). Therefore it was assumed that the floor was a 100 mm thick concrete slab.

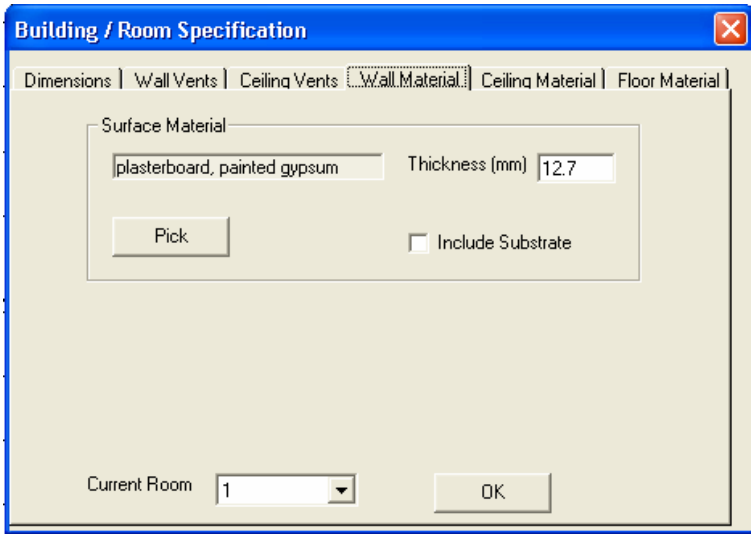

Figure 7.3: User interface for wall, ceiling and floor material specification in BRANZFIRE

7.1.2 BRANZFIRE options

7.1.2.1 General

The maximum sprinkler response time was recorded as 567 s in full scale fire tests (Bill and Heskestad 1995). In order to provide sufficient time to simulate the sprinklers activation, the maximum simulation time was assumed to be 3000 s in all simulations in BRANZFIRE (See Figure 7.4).

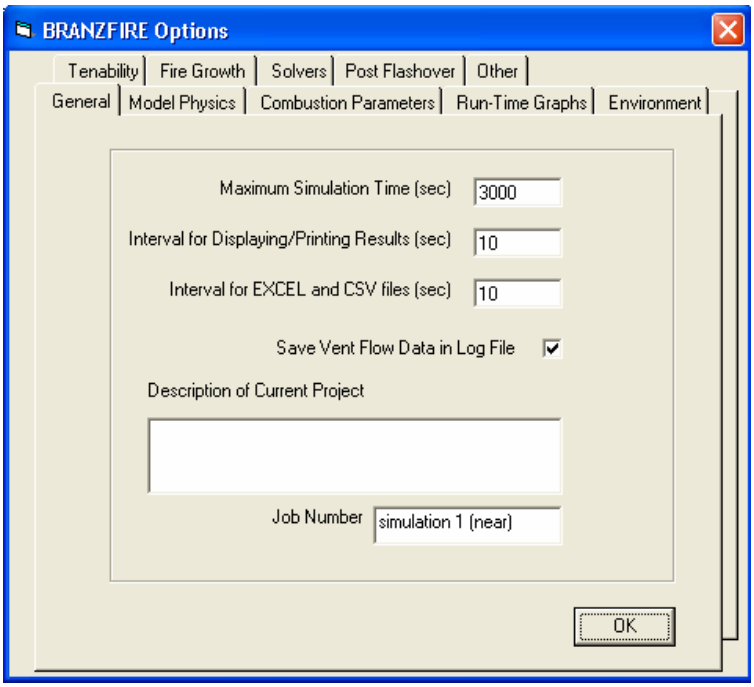

Figure 7.4: User interface for "General" option

7.1.2.2 Model physics

The McCaffrey's correlation is recommended to be used by Wade (2004a), therefore this correlation was selected as the plume model used to simulate all full scale fire tests in this study.

The NIST Jet model was chosen as the ceiling jet model in BRANZFIRE for all simulations. This is because this model is more appropriate and recommended to be used to predict the sprinkler response time in a small room (Tsui 2004; Wade et al. 2006). The dimensions of the small room were approximate 8 × 4 × 2.4 m high, which are similar to the compartment dimensions used in the full scale fire tests.

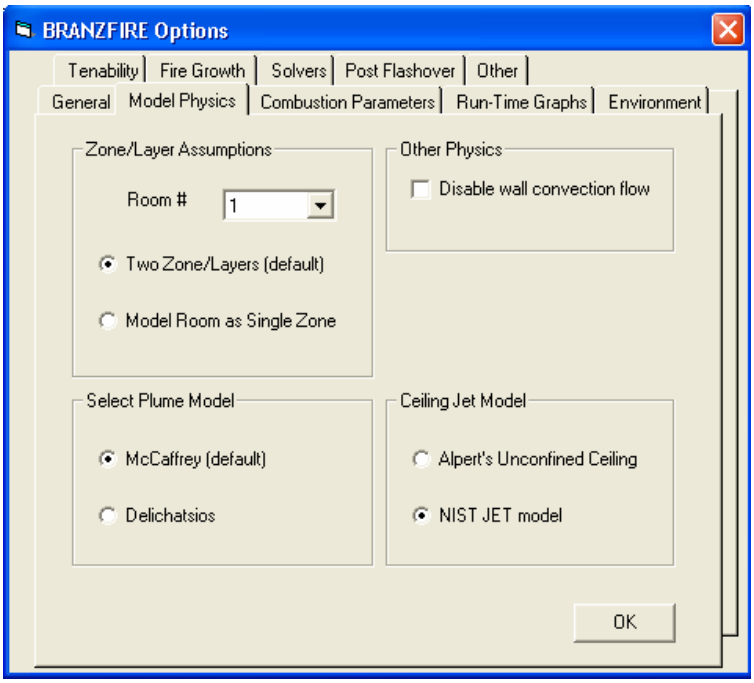

Figure 7.5: User interface for "Model physics" option

7.1.2.3 Combustion parameters

The ignition of the walls and the ceiling lining materials was not mentioned in the full scale fire tests by Bill and Heskestad (1995). Therefore, it was assumed that the major combustible material of the full scale fire test was heptane (fire source). However, "heptane" is not incorporated in the "Fuel type" drop-down list box in BRANZFIRE (See Figure 7.6). Hence, the specification of the heptane was accomplished by inputting various parameters in BRANZFIRE by selecting the "user defined" option.

The mass loss per unit area of the heptane was calculated by using Equation 7.1 (Karlsson and Quintiere 2000) shown below.

$$\dot{m}'' = \frac{\dot{Q}}{A_f \chi \Delta H_c} \qquad \text{Equation 7.1}$$

Where:

$\dot{m}''$ = free burn mass loss rate (kg/m^2.s)

$\dot{Q}$ = heat release rate (kW)

A_f = horizontal burning area of the fuel (m^2)

χ = combustion efficiency

ΔH_c = heat of combustion (kJ/g)

The procedure of calculating the mass loss rate of the heptane is detailed in Appendix G. Table 7.3 below shows the input mass loss rate per unit area for each full scale test in BRANZFIRE.

Table 7.3: Input mass loss per unit area of each test

Test	Mass loss per unit area (kg/m^2.s)
1 ~ 6, 8 ~ 16	0.021
7	0.024

The radiant loss fraction is recommended to be 0.4 for hydrocarbon fuel which consists of five or more carbon atoms in one mole of fuel in Table 3 – 11.12 (Beyler 2002). The chemical formula of heptane is C_7H_{16}, and therefore 0.4 was assumed as the input radiant loss fraction for heptane in BRANZFIRE.

Wakatsuki (2005) suggests that the soot absorption characteristics of heptane is qualitatively identical to propane. The defaulted soot absorption coefficient of propane is shown as 13.32 m^{-1} in BRANZFIRE. Therefore the soot absorption coefficient of heptane was assumed to be 13.32 m^{-1} in this study.

Parameters such as “soot yield alpha” and “epsilon constants” were used to estimate the soot yield in fires (Wade 2004a). In zone models, soot yield is an important factor used to calculate the visibility through smoke (Buchanan 2001). The soot particles generated from fires are irritant to the respiratory tract by inhalation (Purser 2005).

Therefore the characteristics of soot are more likely used to assess the tenability limit of occupants. The main purpose of this task was to evaluate the sprinkler activation time, and thus it was considered that the input of “soot yield alpha” and “epsilon constants” were not important. The soot yield alpha and the epsilon constants of heptane were assumed to be 2.5 and 1.2 respectively, where they are the defaulted values of propane in BRANZFIRE.

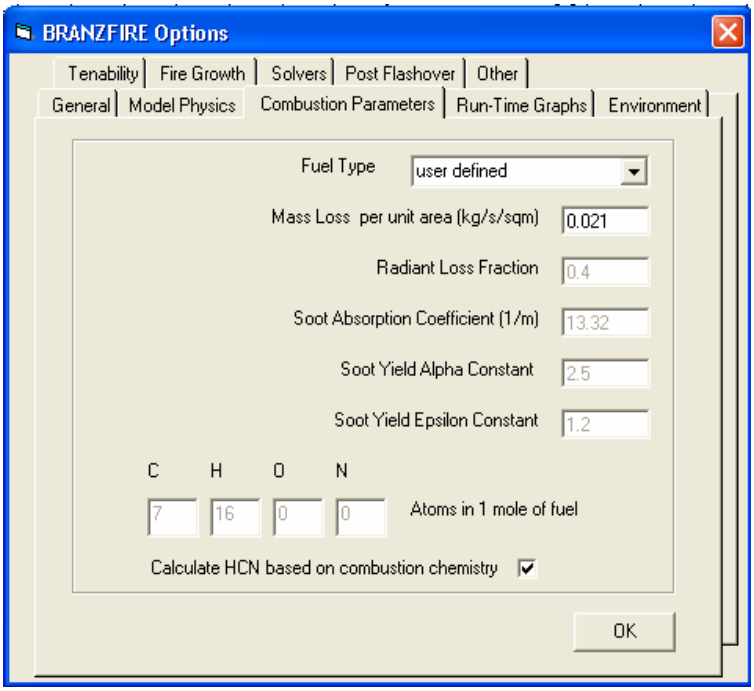

Figure 7.6: User interface for “combustion parameters” option

7.1.2.4 Fire growth

“Flame spread model” is used to model flame spread on wall and ceiling lining materials in BRANZFIRE. As mentioned before, the ignition of the walls and the ceiling lining materials in the full scale fire tests was not reported by Bill and Heskestad (1995). Therefore, “Flame spread model” was off in BRANZFIRE simulations in this research.

Taking the square root of the horizontal surface area of the fire source, the input “Burner width” was calculated to be 0.408 m and 0.532 m for 0.46 m and 0.6 m diameter fire source respectively.

7.1.2.5 Post-Flashover

The post-flashover mode incorporated in BRANZFIRE only takes effect after the incident radiant heat flux on the floor reaches or exceeds 20 kW/m^2 (Wade 2004a). In addition, Karlsson and Quintiere (2000) suggest that flashover normally occurs when the upper layer temperature reaches 500 ^{o}C to 600 ^{o}C in an enclosure. In this study, sprinklers with low actuation temperature (below 75 ^{o}C) were modelled in BRANZFIRE. Therefore, it was reasonable to assume that the sprinklers were activated in the early burning stage of a fire and prevented the occurrence of the flashover. As a result, the post-flashover mode was not used in BRANZFIRE simulations (See Figure 7.7).

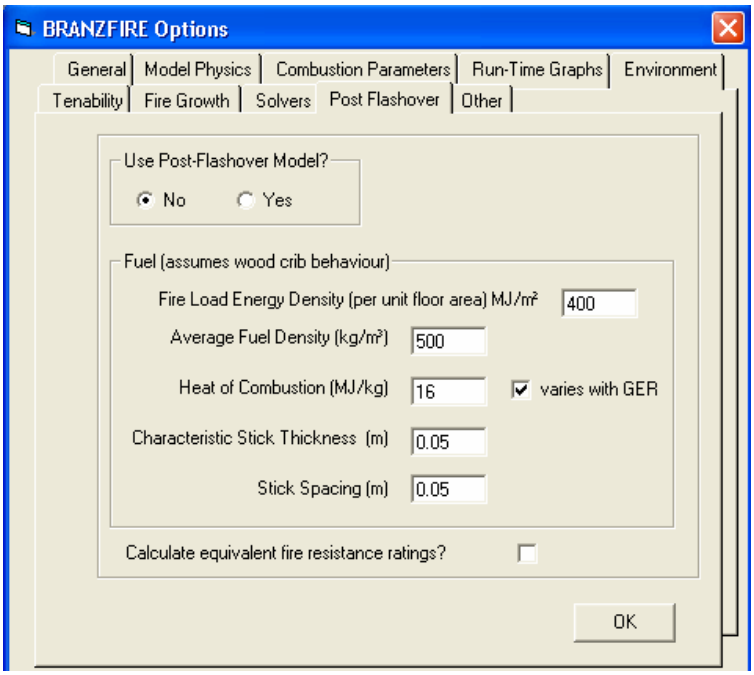

Figure 7.7: User interface for "post-flashover" option

7.1.2.6 Others

Other options such as "environment" and "tenability" are briefly described in this section. It should be noted that the parameters not mentioned in this section were assumed to be used their default values as represented in BRANZFIRE.

The ambient temperature and the humidity in the full scale fire tests were not given by Bill and Heskestad (1995). Hence, it was assumed that the ambient temperature (both interior and external) and the humidity were 20 ^{o}C and 65 % (the defaulted values shown in BRANZFIRE).

The tenability option in BRANZFIRE was used to assess the tenability limit of occupants involved in the fire environment. There was no occupant involved in the full scale fire tests, therefore tenability was not considered in this study.

7.1.3 Fire specification (input fire)

In BRANZFIRE, there are three "object location" options for users to specify the location of the fire source, these includes "centre", "wall" and "corner". According to the BRANZFIRE user's guide (Wade 2004a), the "wall" option can be selected when the fire source is placed against a wall. However, the fire source in the full scale fire tests was either placed a distance of 1.02 m or 0.34 m away from the north wall of the tested compartment. Therefore, the input location of the fire source (wall or centre) in BRANZFIRE needed to be verified. The sensitivity analysis methodology used to specify the fire source location is presented in Section 7.2.2.2 of this chapter. In addition to this, the sensitivity analysis result is discussed in Chapter 8 of this report.

The fire source in the full scale fire tests was placed directly on the floor, therefore the "Fire height above the floor" in BRANZFIRE was input as 0 m.

As mentioned in Chapter 2, the chemical heat release rate (HRR) was estimated to be 130 kW and 260 kW for the 0.46 m and 0.6 m diameter heptane pool fire respectively. The chemical HRR is the sum of the radiant and convective HRR (Tewarson 2002), it is the result of the product of the total HRR and combustion efficiency. Since the combustion efficiency is not accounted separately in BRANZFIRE, the chemical HRR was recommended to be used (Wade 2006).

BRANZFIRE requires the input of the heat release rate versus time history for the fire object. This can be accomplished by clicking the "replace fire" and then "add new" option. The HRR from the heptane pool fire was set to remain constant at 130 kW or

260 kW during the full scale fire tests (Bill and Heskestad 1995). Therefore, the HRR as a function of time input in BRANZFIRE was a straight line as shown in Figure 7.8. The input duration of HRR was 3000 s (the full simulation period).

Heptane was selected as the combustible material from the "Fuel type' drop-down list box under the "add new" option in BRANZFIRE.

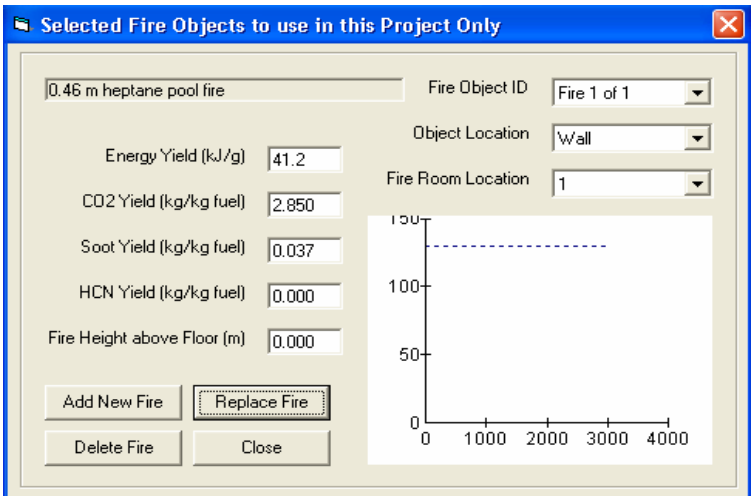

Figure 7.8: User interface for "fire specification"

7.1.4 Sprinkler setting

Commercial and residential sprinklers are the two types of sprinklers that are available for the users to select in BRANZFIRE. After selecting the types of sprinklers, parameters such as water spray density, sprinkler response time index (RTI), sprinkler C-factor, radial distance from fire to sprinkler, sprinkler's actuation temperature, and the distance of the sprinkler below the ceiling can be either specified by the users or utilise the default values pre-set in BRANZFIRE. In this study, the magnitude of these parameters was either obtained from literature or assumptions. Therefore, the selection of the sprinkler type was not important. "Residential sprinkler" was chosen for all simulations.

In the full scale fire tests, only 100 ml of water was used with each tested sprinkler. Bill and Heskestad (1995) suggests that "the sprinkler sprays occurring at actuation were sufficiently weak that no significant fire suppression or gas cooling took place." Therefore, "off" mode of the water spray density was used in all simulations.

The "nominal" RTI (See Table 2.3 in Chapter 2) of the sprinklers tested in the full scale fire tests were given by Bill and Heskestad (1995). It should be noted that the provided nominal RTI values were not obtained from the plunge tests conducted by Bill and Heskestad and the source of these values was not mentioned in the report (Bill and Heskestad 1995). However, it was considered that the given nominal RTI was the only data that could be obtained from the literature to specify the sprinklers investigated in the full scale fire tests. Therefore, the nominal RTI (See Table 2.3 in Chapter 2) values were used as the input in BRANZFIRE.

In addition, it should be noted that two (apparent) RTI values obtained from the wind tunnel experiments carried out in this study were used as the input in BRANZFIRE to specify the recessed sprinklers tested in the full scale fire tests (Test 9 and Test 12). The magnitude of the RTI used in Test 9 and Test 12 and the reasons described why they were chosen are presented in Section 7.2.2.1 of this chapter.

The C-factor of the sprinklers investigated in the full scale fire tests was not clarified by Bill and Heskestad (1995), therefore it was a variable that needed to be verified in this research. The sensitive analysis methodology used to specify the C-factor of the tested sprinklers in the full scale fire tests is described in Section 7.2.2.4 of this chapter. Further to this, the sensitivity analysis result is discussed in Chapter 8 of this report.

The actuation temperature of each sprinkler investigated in the full scale fire tests was given by Bill and Heskestad (1995) and shown in Table 2.3 in Chapter 2. Therefore, the input actuation temperature of each sprinkler simulated in BRANZFIRE was directly extracted from the reference (Bill and Heskestad 1995). It should be noted that the input actuation temperature in BRANZFIRE is the temperature at which the sprinkler will operate (the temperature specified by the supplier which is marked in the sprinkler) (Wade 2004a).

The radial distance in BRANZFIRE is defined as the horizontal distance between the vertical axis of fire to the position of the sprinkler sensing element (Wade 2004a). The radial distance measured in each corresponding full scale fire test was given by Bill

and Heskestad (1995) and tabulated in Table 7.4 below. The radial distances shown in this table were used as the input in BRANZFIRE simulations.

Table 7.4: radial distance measured in each corresponding full scale fire test

Test		Radial distance (m)	
		at near station	at far station
1 ~ 12, 16		1.64	4.55
Test	**Model**	**sidewall location**	**Comments**
13	K	2.32	At the near ceiling station
	E_s	2.24	Standard sidewall, deflector 0.1 m below ceiling
	E_r	2.32	Recessed sidewall, deflector 0.1 m below ceiling
	F_r	2.4	Recessed sidewall, deflector 0.1 m below ceiling
14	K	2.32	At the near ceiling station
	$E_s^{0.1}$	4.26	Standard sidewall, deflector 0.1 m below ceiling
	$E_r^{0.1}$	4.26	Recessed sidewall, deflector 0.1 m below ceiling
	$E_s^{0.3}$	4.26	Standard sidewall, deflector 0.3 m below ceiling
	$E_r^{0.3}$	4.26	Recessed sidewall, deflector 0.3 m below ceiling

The parameter “distance below the ceiling” indicates the vertical distance of the sprinkler below the ceiling (Wade 2004a). It should be noted that the sprinkler distance below the ceiling for the recessed sidewall sprinklers tested in the full scale fire tests were specified by Bill and Heskestad (1995). Therefore, the specified values (0.1 m and 0.3 m) were used as the input in BRANZFIRE for the recessed sidewall sprinklers. However, the sprinkler distance below the ceiling of the flush, recessed and concealed sprinklers were not given by Bill and Heskestad (1995). Hence, the sensitivity analysis was conducted to determine the best input sprinkler distance below the ceiling for the flush, recessed and concealed sprinklers in BRANZFIRE. The methodology and the result of this sensitivity analysis are presented in both Section 7.2.2.3 of this chapter and Chapter 8.

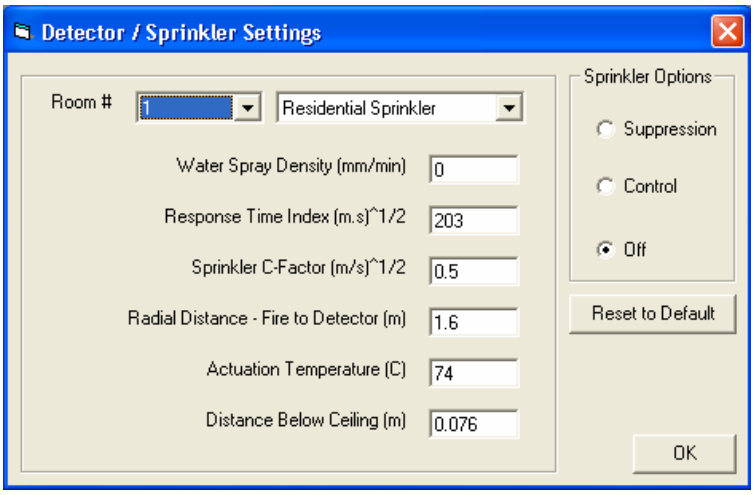

Figure 7.9: User interface for "sprinkler setting"

7.2 Modelled simulations

7.2.1 Parameter Variation

As mentioned in the previous sections, some of the input parameters are variable. The selection of them may affect the sprinkler response time predicted in BRANZFIRE. These varied parameters are summarized as follows:

- Input fire object location
- Input sprinkler distance below the ceiling
- Input C-factor of sprinklers

7.2.2 Methodology used to specify parameter variation

7.2.2.1 Baseline simulation scenario

In order to determine the input parameter variation in BRANZFIRE, a baseline simulation scenario was setup. During the sensitivity analysis, the input magnitudes of the variables (parameters) were modified based on the input of the baseline simulation scenario. By comparing all the simulation results from different inputs, the best input

of parameters in BRANZFIRE was determined when the most reliable and accurate results were obtained from the comparison.

Table 7.5 shows the input parameters in the baseline simulation scenario. It should be noted that the parameters not mentioned in this table were set to the values defined in the previous sections in this chapter.

Table 7.5: Input parameters in the baseline simulation scenario

Test	Model	Baseline simulation scenario input		
		Fire object location	Distance below ceiling (m)	C-factor $(m/s)^{1/2}$
2	I	Centre	0.076	0.96
3	D	Centre	0.076	0.89
4	H	Centre	0.076	0.96
5	G	Centre	0.076	0.89
6	C	Centre	0.076	0.89
7	H	Centre	0.076	0.96
8	A	Centre	0.076	0.89
9	A	Centre	0.076	0.89
10	J	Centre	0.076	0.96
11	B	Centre	0.076	0.89
12	B	Centre	0.076	0.89
13	E_s	Centre	0.1	0.89
	E_r	Centre	0.1	0.89
	F_r	Centre	0.1	0.89
14	$E_s^{0.1}$	Centre	0.1	0.89
	$E_r^{0.1}$	Centre	0.1	0.89
	$E_s^{0.3}$	Centre	0.3	0.89
	$E_r^{0.3}$	Centre	0.3	0.89
16	C	Centre	0.076	0.89

Since there was no flush, recessed and concealed sprinklers installed in Test 1, simulation was not conducted to model this full scale fire test. In addition to this, Test 15 was not modelled in BRANZFIRE. This is because there were no sprinklers installed in this full scale fire test.

The concealed sprinkler installed at the near ceiling station in Test 2 was not activated due to the experimental error during the full scale fire test. Therefore, simulations were not run to model the sprinkler activation at the near ceiling station for Test 2 in this work.

The experimental setup for Test 9 and Test 12 were very similar to Test 8 and Test 11 respectively. The only difference between them was that the recessed sprinklers' frame arms were orientated 90 ^{o} to the ceiling flow (ceiling jet) generated by the fire for Test 8 and Test 11. In contrast, the recessed sprinklers' frame arms were installed 0 ^{o} to the ceiling flow for Test 9 and Test 12. BRANZFIRE cannot specify the orientation of sprinklers' frame arms against the ceiling jet flow. However, it was found that the RTI of the (glass bulb) recessed sprinkler was significantly increased when the sprinkler's frame arms were orientated 0 ^{o} to the ceiling flow compared with the 90 ^{o} to the ceiling flow from the experimental result in this research (See Chapter 6). Therefore, it was considered that the increased RTI measured at the sprinkler's frame arms orientated 0 ^{o} to the ceiling flow in this study could be used to account for the affects of the different sprinkler installation orientations in the full scale fire tests (Test 9 and 12). As shown in Table 2.4 in Chapter 2, recessed sprinkler A and B was tested in Test 9 and Test 12 respectively. The type and size of heat-responsive element and the actuation temperature of sprinkler A and B are identical to sprinkler N_R and sprinkler M_R tested in the wind tunnel plunge test carried out in this study. Therefore, it is reasonable to assume that the apparent RTI of sprinkler N_R and M_R in the worst orientation (frame arm 0 ^{o} to the oncoming flow) obtained from this research (Table 6.2Table 6.3 and Table 6.2 in Chapter 6) could be used as the RTI for sprinkler A and B tested in Test 9 and Test 12. The RTI used in BRANZFIRE for simulating the recessed sprinklers (sprinkler A and B) in Test 9 and Test 12 was assumed to be 107.4 $(m.s)^{1/2}$ and 211.2 $(m.s)^{1/2}$ respectively.

The input parameters in BRANZFIRE used to model each full scale fire test shown in Table 7.5 above were made based on the following assumptions. With the exception of the recessed sidewall sprinklers, the sprinkler distance below the ceiling was assumed to be 0.076 m for the flush, recessed and concealed sprinklers in the baseline scenario. This assumption was made based on the approximate location of the heat-responsive element of the pendent sprinklers. In addition to this, 0.076 m below the

ceiling was the location (depth) of the thermocouple and flow probe used to measure the hot gas temperature and velocity in the full scale fire tests. The input C-factor of each sprinkler modelled in this scenario was assumed based on the experimental results provided by Annable (Annable 2006).

7.2.2.2 Input fire object location (Scenario 1)

Scenario 1 was conducted to determine the best input fire object location in BRANZFIRE for this study. Because the fire source in the full scale fire tests was placed close to a wall (not against a wall), the best input fire object location could be either selected from the "wall" option or the "centre" option in BRANZFIRE. As mentioned in Section 7.2.2.1, the input fire object location in the baseline simulation scenario was assumed to be the "centre". Therefore, the sensitivity analysis was conducted in BRANZFIRE by changing the fire object location to the "wall" in Scenario 1.

The ceiling jet temperatures recorded at the near and the far ceiling station in the full scale fire tests (Test 2 and Test 7) were given by Bill and Heskestad (1995). Therefore, comparisons of the ceiling jet temperatures between the full scale fire tests (Test 2 and Test 7) and the simulations in BRANZFIRE were made to determine the best input fire object location for this study.

In addition, the predicted sprinkler response times both from the baseline simulation scenario and Scenario 1 were also compared to determine the best input fire object location in BRANZFIRE.

7.2.2.3 Input sprinkler distance below the ceiling (Scenario 2 and 3)

As mentioned in Section 7.1.4, the sprinkler distance below the ceiling is defined as the vertical distance of the sprinkler below the ceiling. However, "the location of the sprinkler" is not specified in the user's guide of BRANZFIRE (Wade 2004a). Therefore, it was assumed that this distance was either measured from the lower plane

of the ceiling to the mid-point of the sprinklers' heat-responsive element (Scenario 2) or to the position of the sprinklers' deflector (Scenario 3) in this sensitivity analysis.

It should be noted that the vertical distance from the ceiling to the mid-point of the sprinkler's heat-responsive element (or to the position of the sprinklers' deflector) for the flush, recessed and concealed sprinklers depends on the installed recess distance of the sprinkler specified by the manufacturer. In order to be realistic, the recess distances of the flush, recessed and concealed sprinklers were used to assess the input sprinkler distance below the ceiling in both Scenario 2 and Scenario 3. However, the recess distances of the sprinklers investigated in the full scale fire tests were not given by Bill and Heskestad (1995). Therefore, it was assumed that the flush, recessed and concealed sprinklers' recess distances which are commonly used in New Zealand (Tyco Fire & Building Products 2006) were the same and adopted as the recess distances of the sprinklers tested in the full scale fire tests. By using the recess distances of the sprinklers required by the manufacturer, the maximum and the minimum input sprinkler distance below the ceiling in BRANZFIRE was obtained when the sprinklers were installed at the minimum and the maximum sprinkler recess distance respectively. The description of the sprinkler's recess distance is described in Chapter 5 of this thesis.

Table 7.6 shows the input sprinkler distance below the ceiling for Scenario 2 in BRANZFIRE. The maximum and the minimum input sprinkler distance below the ceiling for the concealed sprinklers was specified to be 0 m. This is because the heat-responsive element of the concealed sprinklers was hidden inside its recess housing and located above the lower plane of the ceiling despite the magnitude of the recess distance. Hence, it was assumed that the distance measured from the mid-point of the concealed sprinklers' heat-responsive element to the lower plane of the ceiling was 0 m. As described in Section 7.1.4, the vertical distance between the lower plane of the ceiling and the position of the sprinklers' deflector for the recessed sidewall sprinklers was given in the full scale fire tests (Bill and Heskestad 1995). Therefore, the input sprinkler distance below the ceiling for the recessed sidewall sprinklers was not modelled in Scenario 2. In addition to this, the distance from the lower plane of the ceiling to the mid-point of the sprinkler's heat-responsive element for the flush sprinkler is approximate identical to the distance from the ceiling to the position of the

sprinkler's deflector (Tyco Fire & Building Products 2006). Therefore, the input sprinkler distance below the ceiling for the flush sprinkler was only modelled in Scenario 3.

Table 7.6: Input sprinkler distance below the ceiling for Scenario 2

Test	Model	Distance from the lower plane of the ceiling to the mid-point of the sprinklers' heat-responsive element (m)	
		Minimum (Max. recess distance)	Maximum (Min. recess distance)
2	I	0	0
3	D	0.0033	0.016
4	H	0	0
6	C	0.0033	0.016
7	H	0	0
8	A	0.0033	0.016
9	A	0.0033	0.016
10	J	0	0
11	B	0.0033	0.016
12	B	0.0033	0.016
16	C	0.0033	0.016

Table 7.7 shows the input sprinkler distance below the ceiling for Scenario 3 in BRANZFIRE. It should be noted that the maximum and the minimum input sprinkler distance below the ceiling for the recessed sidewall sprinklers was identical. This is because the recessed sidewall sprinklers were placed horizontally to the ceiling. The sprinkler distance below the ceiling remained constant and was not affected by modifying the recess distance.

Table 7.7: Input sprinkler distance below the ceiling for Scenario 3

Test	Model	Distance from the lower plane of the ceiling to the position of sprinklers' deflector (m)	
		Minimum (Max. recess distance)	Maximum (Min. recess distance)
2	I	0.0127	0.0254
3	D	0.0223	0.035
4	H	0.0127	0.0254

5	G	0.0142	0.0236
6	C	0.0223	0.035
7	H	0.0127	0.0254
8	A	0.0223	0.035
9	A	0.0223	0.035
10	J	0.0127	0.0254
11	B	0.0223	0.035
12	B	0.0223	0.035
13	E_s	0.1	0.1
	E_r	0.1	0.1
	F_r	0.1	0.1
14	$E_s^{0.1}$	0.1	0.1
	$E_r^{0.1}$	0.1	0.1
	$E_s^{0.3}$	0.3	0.3
	$E_r^{0.3}$	0.3	0.3
16	C	0.0223	0.035

7.2.2.4 Input C-factor of sprinklers (Scenario 4)

Normally, the C-factor of sprinklers range from 0 $(m/s)^{1/2}$ to 2 $(m/s)^{1/2}$ (International Standard 2004). In order to determine the best input C-factor for the flush, recessed, concealed and recessed sidewall sprinklers in BRANZFIRE, a trial and error method was used. This method was approached by applying C-factor from 0 $(m/s)^{1/2}$ to 2 $(m/s)^{1/2}$ with an increment of 0.1 $(m/s)^{1/2}$ in BRANZFIRE to simulate each sprinkler investigated in the full scale fire tests. The best input C-factor for each sprinkler was determined when the predicted sprinkler response time in BRANZFIRE was closest to the experimental sprinkler response time recorded in the full scale fire test.

The simulation duration was assumed to be 3000 s in BRANZFIRE. “No operation” of sprinkler in simulations implied that the simulated sprinkler was not activated within 3000 s. It was also assumed that the simulated sprinkler had an infinite activation time if it did not operate during the 3000 s simulation time.

The sensitivity analysis of the input sprinkler C-factor was implemented based on the best result obtained from the baseline scenario, Scenario 1, Scenario 2 and Scenario 3.

7.2.3 The series of BRANZFIRE simulations

In this research, 549 simulations were conducted to analyse the input variables in BRANZFIRE. Simulations 1 ~ 30 shown in Table 7.8 were run to obtain the sprinkler response time in the baseline simulation scenario. It should be noted that only one sprinkler can be accommodated in BRANZFIRE for each simulation. Therefore, two simulations were run separately to model the sprinkler installed at the near and the far ceiling station for each full scale fire test.

Table 7.8: Simulations for the baseline scenario

Simulations for the baseline scenario						
Test	**Model**	**Simulation**		**Fire object location**	**C-factor $(m/s)^{1/2}$**	**Distance below ceiling (m)**
		Near station	**Far station**			
2	I	N/A	1	Centre	0.96	0.076
3	D	2	3	Centre	0.89	0.076
4	H	4	5	Centre	0.96	0.076
5	G	6	7	Centre	0.89	0.076
6	C	8	9	Centre	0.89	0.076
7	H	10	11	Centre	0.96	0.076
8	A	12	13	Centre	0.89	0.076
9	A	14	15	Centre	0.89	0.076
10	J	16	17	Centre	0.96	0.076
11	B	18	19	Centre	0.89	0.076
12	B	20	21	Centre	0.89	0.076
16	C	22	23	Centre	0.89	0.076
Test	**Model**	**Simulation**		**Fire object location**	**C-factor $(m/s)^{1/2}$**	**Distance below ceiling (m)**
		Sidewall location				
13	E_s	24		Centre	0.89	0.1
	E_r	25		Centre	0.89	0.1
	F_r	26		Centre	0.89	0.1
14	$E_s^{0.1}$	27		Centre	0.89	0.1
	$E_r^{0.1}$	28		Centre	0.89	0.1
	$E_s^{0.3}$	29		Centre	0.89	0.3
	$E_r^{0.3}$	30		Centre	0.89	0.3

Simulations 31 ~ 46 shown in Table 7.9 were run to assess the ceiling jet temperatures at distances of 0.006 m and 0.076 m below the ceiling at the near and the far ceiling station in BRANZFIRE (Scenario 1).

Table 7.9: Simulations for analysing the input fire object location with the ceiling jet temperatures (Scenario 1)

Simulations for analysing the input fire object location with the ceiling jet temperatures (Scenario 1)						
Test	Model	Simulation		Fire object location	C-factor $(m/s)^{1/2}$	Distance below ceiling (m)
		Near station	Far station			
2	I	31	32	Centre	0.96	0.006
2	I	33	34	Wall	0.96	0.006
2	I	35	36	Centre	0.96	0.076
2	I	37	38	Wall	0.96	0.076
7	H	39	40	Centre	0.96	0.006
7	H	41	42	Wall	0.96	0.006
7	H	43	44	Centre	0.96	0.076
7	H	45	46	Wall	0.96	0.076

Table 7.10 shows the input variables used to assess the sprinkler activation time in BRANZFIRE for analysing the input fire object location (Scenario 1).

Table 7.10: Simulations for analysing the input fire object location with the sprinkler response time (Scenario 1)

Simulations for analysing the input fire object location with the sprinkler response time (Scenario 1)						
Test	Model	Simulation		Fire object location	C-factor $(m/s)^{1/2}$	Distance below ceiling (m)
		Near station	Far station			
2	I	N/A	47	Wall	0.96	0.076
3	D	48	49	Wall	0.89	0.076
4	H	50	51	Wall	0.96	0.076
5	G	52	53	Wall	0.89	0.076
6	C	54	55	Wall	0.89	0.076
7	H	56	57	Wall	0.96	0.076
8	A	58	59	Wall	0.89	0.076
9	A	60	61	Wall	0.89	0.076
10	J	62	63	Wall	0.96	0.076

11	B	64	65	Wall	0.89	0.076
12	B	66	67	Wall	0.89	0.076
16	C	68	69	Wall	0.89	0.076
Test	**Model**	**Simulation**		**Fire object location**	**C-factor $(m/s)^{1/2}$**	**Distance below ceiling (m)**
		Sidewall location				
13	E_s	70		Wall	0.89	0.1
	E_r	71		Wall	0.89	0.1
	F_r	72		Wall	0.89	0.1
14	$E_s^{0.1}$	73		Wall	0.89	0.1
	$E_r^{0.1}$	74		Wall	0.89	0.1
	$E_s^{0.3}$	75		Wall	0.89	0.3
	$E_r^{0.3}$	76		Wall	0.89	0.3

Simulations 77 ~ 171 were used to assess the input sprinkler distance below the ceiling for the flush, recessed, concealed and recessed sidewall sprinklers. These simulations were run both at the minimum and maximum sprinkler distance below the ceiling by using the best input fire object location determined from Simulations 1 ~ 76.

Table 7.11 and Table 7.12 below show the input variables for analysing the input sprinkler distance below the ceiling if Scenario 2 and Scenario 3 respectively.

Table 7.11: Simulations for analysing the input sprinkler distance below the ceiling (Scenario 2)

Simulations for analysing the input sprinkler distance below the ceiling (Scenario 2)								
Test	**Model**	**Simulation**				**C-factor $(m/s)^{1/2}$**	**Sprinkler distance below the ceiling**	
		Near	**Far**	**Near**	**Far**		**Minimum (m)**	**Maximum (m)**
2	I	N/A	77	N/A	98	0.96	0	0
3	D	78	79	99	100	0.89	0.0033	0.016
4	H	80	81	101	102	0.96	0	0
6	C	82	83	103	104	0.89	0.0033	0.016
7	H	84	85	105	106	0.96	0	0
8	A	86	87	107	108	0.89	0.0033	0.016
9	A	88	89	109	110	0.89	0.0033	0.016
10	J	90	91	111	112	0.96	0	0
11	B	92	93	113	114	0.89	0.0033	0.016
12	B	94	95	115	116	0.89	0.0033	0.016
16	C	96	97	117	118	0.89	0.0033	0.016

Table 7.12: Simulations for analysing the input sprinkler distance below the ceiling (Scenario 3)

Simulations for analysing the input sprinkler distance below the ceiling (Scenario 3)								
Test	Model	Simulation				C-factor $(m/s)^{1/2}$	Sprinkler distance below the ceiling	
		Near	Far	Near	Far		Minimum (m)	Maximum (m)
2	I	N/A	119	N/A	142	0.96	0.0127	0.0254
3	D	120	121	143	144	0.89	0.0223	0.035
4	H	122	123	145	146	0.96	0.0127	0.0254
5	G	124	125	147	148	0.89	0.0142	0.0236
6	C	126	127	149	150	0.89	0.0223	0.035
7	H	128	129	151	152	0.96	0.0127	0.0254
8	A	130	131	153	154	0.89	0.0223	0.035
9	A	132	133	155	156	0.89	0.0223	0.035
10	J	134	135	157	158	0.96	0.0127	0.0254
11	B	136	137	159	160	0.89	0.0223	0.035
12	B	138	139	161	162	0.89	0.0223	0.035
16	C	140	141	163	164	0.89	0.0223	0.035
Test	Model	Simulation				C-factor $(m/s)^{1/2}$	Sprinkler distance below the ceiling (m)	
		Sidewall location						
13	E_s	165				0.89	0.1	
	E_r	166				0.89	0.1	
	F_r	167				0.89	0.1	
14	$E_s^{0.1}$	168				0.89	0.1	
	$E_r^{0.1}$	169				0.89	0.1	
	$E_s^{0.3}$	170				0.89	0.3	
	$E_r^{0.3}$	171				0.89	0.3	

Simulations 172 ~ 192 shown in Table 7.13 were run to determine the best input C-factor for the flush sprinkler. It should be noted that the best input C-factor of sprinklers was estimated based on the best sprinkler distance below the ceiling determined from Simulations 77 ~ 171.

Table 7.13: Simulations for analysing the input C-factor for the flush sprinkler

Simulations for analysing the input C-factor for flush sprinkler			
Test	Model	Simulation	
		Near station (sprinkler distance below ceiling 0.0236 m)	C-factor $(m/s)^{1/2}$
5	G	172	0
		173	0.1
		174	0.2

		175	0.3
		176	0.4
		177	0.5
		178	0.6
		179	0.7
		180	0.8
		181	0.89
		182	1
		183	1.1
		184	1.2
		185	1.3
		186	1.4
		187	1.5
		188	1.6
		189	1.7
		190	1.8
		191	1.9
		192	2

Simulations 193 ~ 549 were run to estimate the best input C-factor for the recessed, concealed and recessed sidewall sprinklers. The input variables in these simulations are shown in Appendix H.

In addition, the sprinkler response time correlation between BRANZFIRE and the full scale fire test for the flush, recessed, concealed and recessed sidewall sprinklers were determined after the best input C-factor values were obtained in this research (See Chapter 8).

CHAPTER 8

8 BRANZFIRE MODELLING RESULTS and DISCUSSION

This chapter of the report discusses the BRANZFIRE simulation results obtained in the investigation. Comparisons are also made between the predicted (BRANZFIRE) and the experimental (full scale fire test) sprinkler response times for the flush, recessed, concealed and recessed sidewall sprinklers in order to obtain the sprinkler response time correlation between the BRANZFIRE and the full scale fire tests. The BRANZFIRE simulation results for a particular simulation (Simulation 12) is given as an example and detailed in Appendix I.

In addition, the relationship of the sprinkler response time between the full scale fire test, wind tunnel test (plunge test) and BRANZFIRE modelling is described in Section 8.3.1 of this chapter.

8.1 Sensitivity analysis

The sensitivity analysis results are presented and discussed in this section to determine the best input fire object location, the best input sprinkler distance below the ceiling, and the best input C-factor for the flush, recessed, concealed and recessed sidewall sprinklers. The full set of the predicted sprinkler response times from the 549 simulations in BRANZFIRE are attached in Appendix J. In addition, it should be noted that the input parameters used in BRANZFIRE for each simulation and each scenario presented in this chapter are detailed in Chapter 7 of this report.

8.1.1 Baseline simulation scenario

Figure 8.1 below shows the predicted sprinkler response times in BRANZFIRE for the baseline simulation scenario (Simulation 1 ~ 30). As mentioned in Chapter 7, the simulation duration in each run of simulation carried out was 3000 s. Therefore, "∞"

shown in this figure indicates the sprinkler did not operate within the 3000 s simulation time and assumed had an infinite sprinkler response time. From this figure, it can be seen that only six sprinklers activated within 3000 s in this simulation scenario.

In order to help the visualisation of the predicted sprinkler response time simulation results, the results from different types of sprinklers simulated in BRANZFIRE are represented by using different colours (See Figure 8.1). Table 8.1 below tabulates the colour code used to represent the simulation result obtained from each corresponding sprinkler modelled in BRANZFIRE. It should be noted that the colour code shown in this table for each type of sprinkler is maintained throughout the rest of this report.

Table 8.1: Colour code used for different types of sprinklers

Colour code	Sprinkler type
Green	Flush
Blue	Recessed
Orange	Concealed
Pink	Recessed sidewall

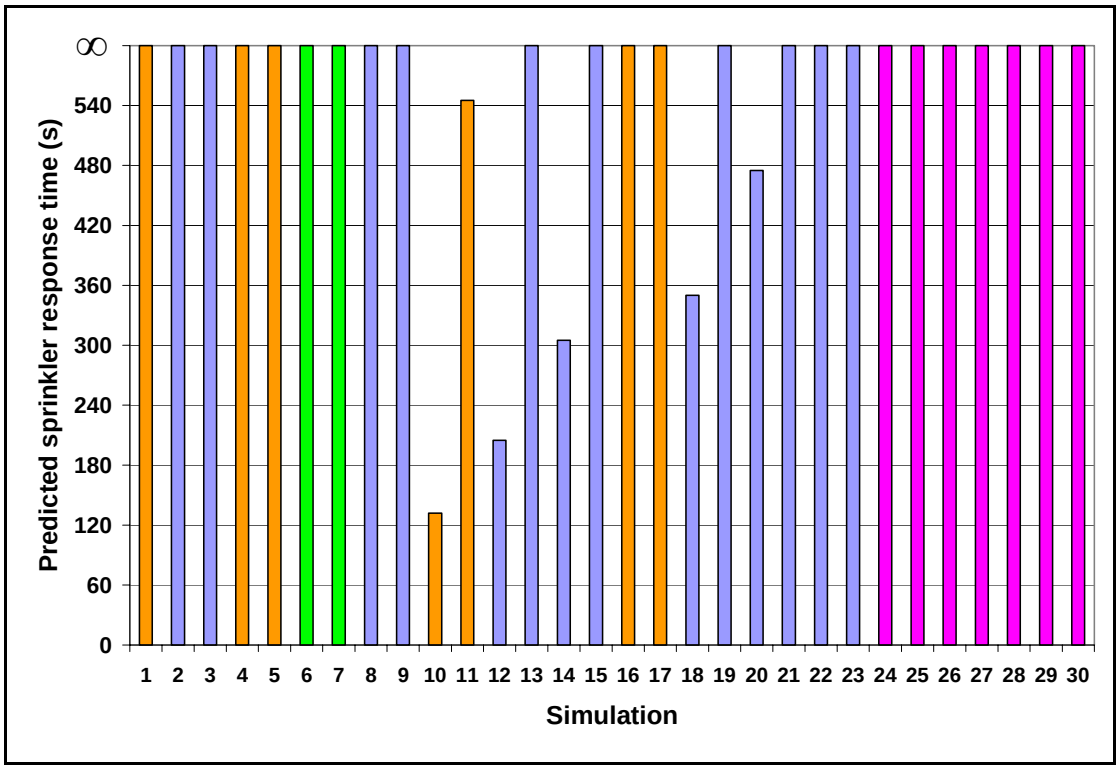

Figure 8.1: Sprinkler response time in BRANZFIRE for the baseline simulation scenario

8.1.2 Input fire object location (Scenario 1)

As described in Chapter 7, the best input fire object location in BRANZFIRE was determined based on the comparison of the ceiling jet temperatures between the full scale fire tests (Test 2 and Test 7) and the simulations in the BRANZFIRE. In addition to this, the predicted sprinkler response times both from the baseline simulation scenario and Scenario 1 were also compared to determine the best input fire object location in BRANZFIRE. It should be noted that the only difference between the baseline scenario and Scenario 1 was that the input fire object location of the former and latter was "centre" and "wall" respectively in BRANZFIRE.

Figure 8.2 below shows the predicted sprinkler response times in BRANZFIRE for Scenario 1 (Simulation 47 ~ 76). The simulated ceiling jet temperatures in BRANZFIRE for Scenario 1 (Simulation 31 ~ 46) are shown in Figure 8.3 and Figure 8.4 in Section 8.1.3 of this report.

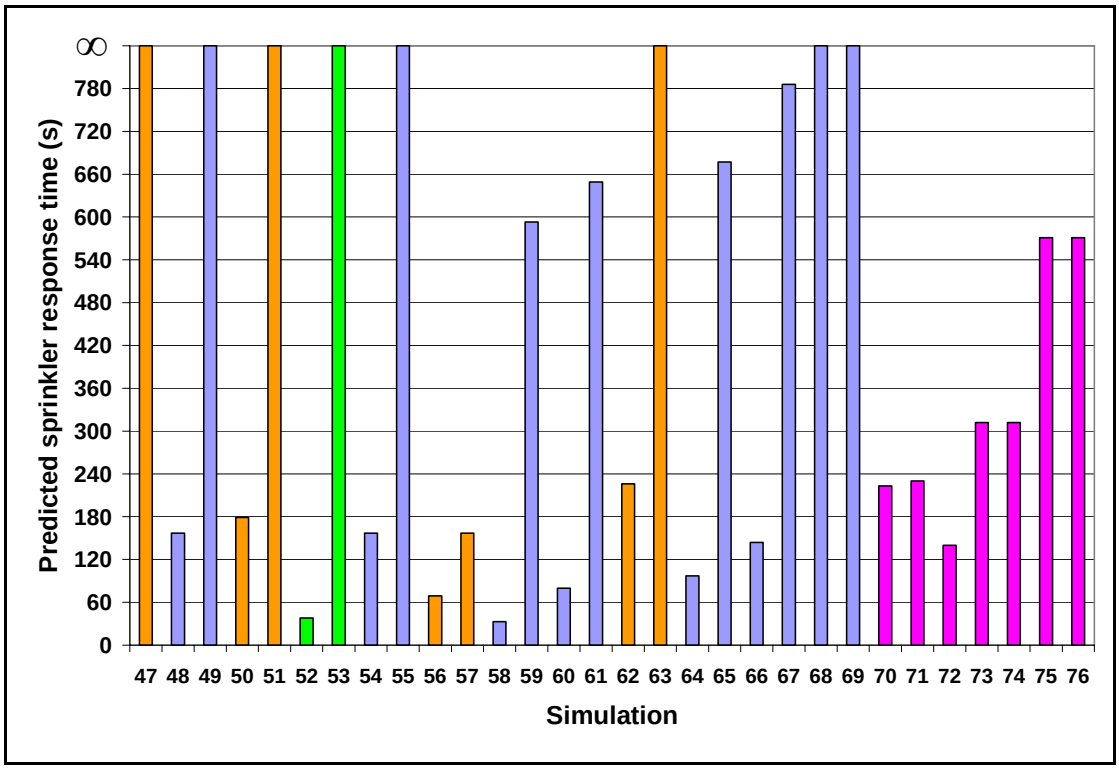

Figure 8.2: Sprinkler response time in BRANZFIRE for Scenario 1

8.1.3 Comparison of ceiling jet temperature (baseline scenario and Scenario 1)

Figure 8.3 and Figure 8.4 show the comparison of the ceiling jet temperatures between the BRANZFIRE (baseline scenario and Scenario 1) and the full scale fire test (Test 2) at a distance of 0.076 m and 0.006 m below the ceiling respectively.

As shown in Figure 8.3, the predicted ceiling jet temperatures at 0.076 m below the ceiling from Scenario 1 (at both the near and the far ceiling station) were closer to the experimental ceiling jet temperatures (Test 2) than the baseline scenario. In addition to this, Figure 8.4 shows that the ceiling jet temperature differences between Scenario 1 and Test 2 were smaller than the differences between the baseline scenario and Test 2 at a distance of 0.006 m below the ceiling (at both the near and far ceiling station). These comparisons show that Scenario 1 gave a closer ceiling jet temperature prediction to the full scale fire test (Test 2) than the baseline scenario.

The comparison of the ceiling jet temperatures between the BRANZFIRE (baseline scenario and Scenario 1) and the full scale fire test (Test 7) shows a similar result to the comparison between the BRANZFIRE and Test 2 as discussed above. Therefore, the comparison of the ceiling jet temperatures between BRANZFIRE (baseline scenario and Scenario 1) and the full scale fire test (Test 7) are not presented in this section graphically.

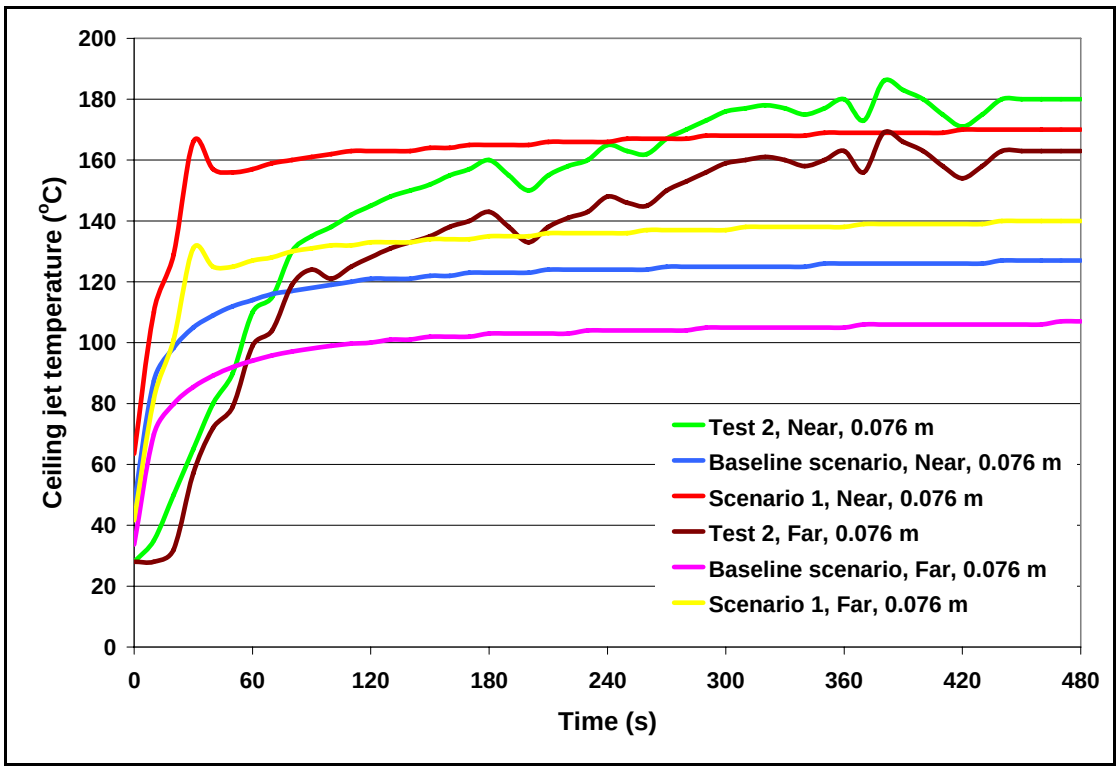

Figure 8.3: Comparison of the ceiling jet temperatures between the BRANZFIRE (baseline scenario and Scenario 1) and the full scale fire test (Test 2) at 0.076 m below ceiling

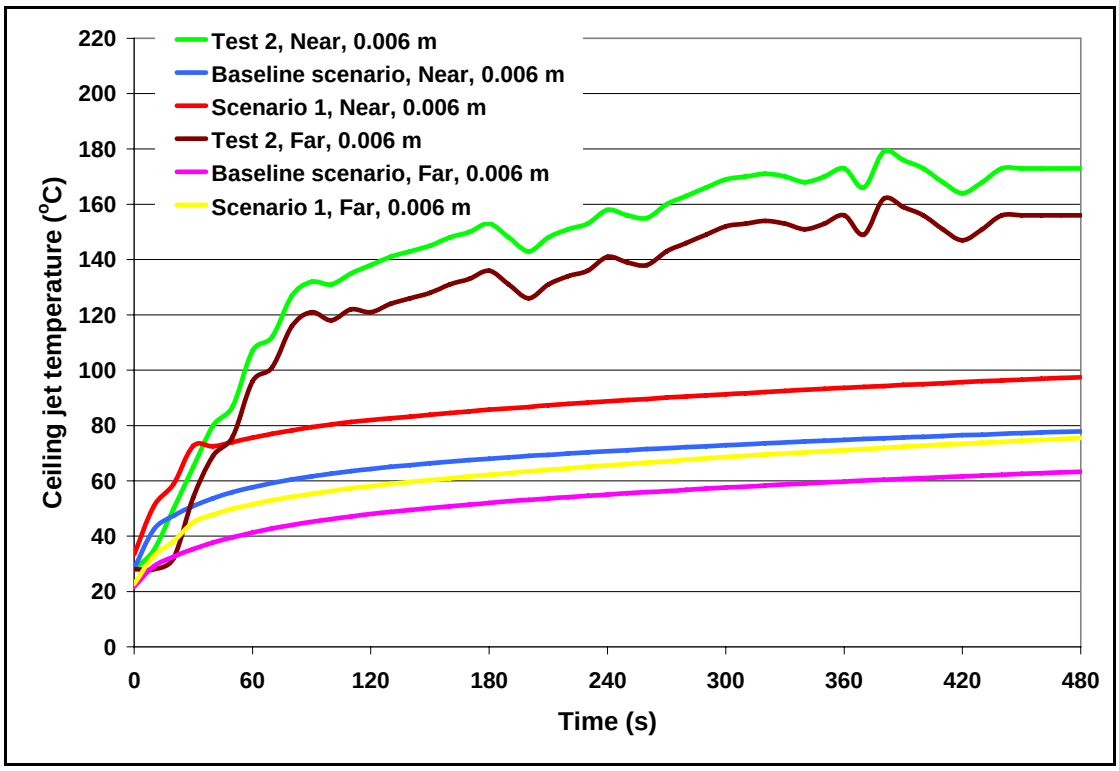

Figure 8.4: Comparison of the ceiling jet temperatures between the BRANZFIRE (Baseline scenario and Scenario 1) and the full scale fire test (Test 2) at 0.006 m below ceiling

8.1.4 Comparison of sprinkler response time (baseline scenario and Scenario 1)

By using the predicted sprinkler response times obtained from the baseline scenario (Figure 8.1) and Scenario 1 (Figure 8.2), Figure 8.5 was plotted to compare the sprinkler response times between the BRANZFIRE simulations and the full scale fire tests for both the scenarios.

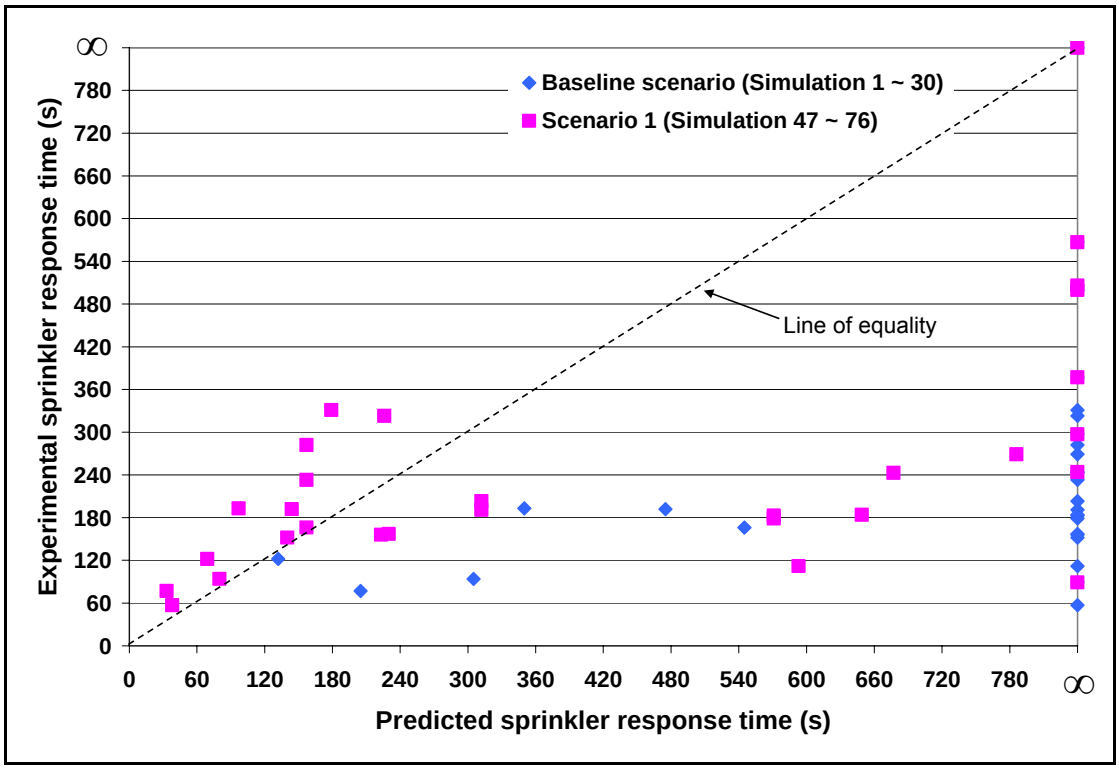

Figure 8.5: Comparison between the predicted and the experimental sprinkler response times for both the baseline scenario and Scenario 1

From this figure, it can be seen that more data points from Scenario 1 are scattered closer to the line of equality than the baseline scenario. This is because all of the sprinklers (with the exception of six sprinklers) were predicted to not operate in BRANZFIRE for the baseline scenario (See Figure 8.1). A data point dispersed closer to the line of equality implies that the difference between the predicted and the experimental sprinkler response time was smaller. Therefore, Scenario 1 gave a better prediction (sprinkler response time) than the baseline scenario.

By combining the analysed results from this section and Section 8.1.3, it was determined that the best input fire object location was “wall” (Scenario 1) in BRANZFIRE for this study. Therefore, the “wall” option was used as the input fire object location for simulations (77 ~ 549) in BRANZFIRE thereafter.

8.1.5 Input sprinkler distance below the ceiling (Scenario 2)

Scenario 2 was run to assess the input sprinkler distance below the ceiling in BRANZFIRE for this study. It should be noted that the input sprinkler distance below the ceiling in this scenario was assumed to be measured from the lower plane of the ceiling to the mid-point of the sprinklers’ heat-responsive element. The magnitude of the input sprinkler distance below the ceiling (for both the minimum and maximum) of each simulation for this scenario is detailed in Chapter 7 of this report.

Figure 8.6 shows the predicted sprinkler response times in BRANZFIRE at both the minimum and maximum sprinkler distance below the ceiling for Scenario 2. As mentioned in Chapter 7, the flush sprinkler and the recessed sidewall sprinklers were not modelled in Scenario 2. Therefore, there was no simulation result for the flush and recessed sidewall sprinklers shown in this figure.

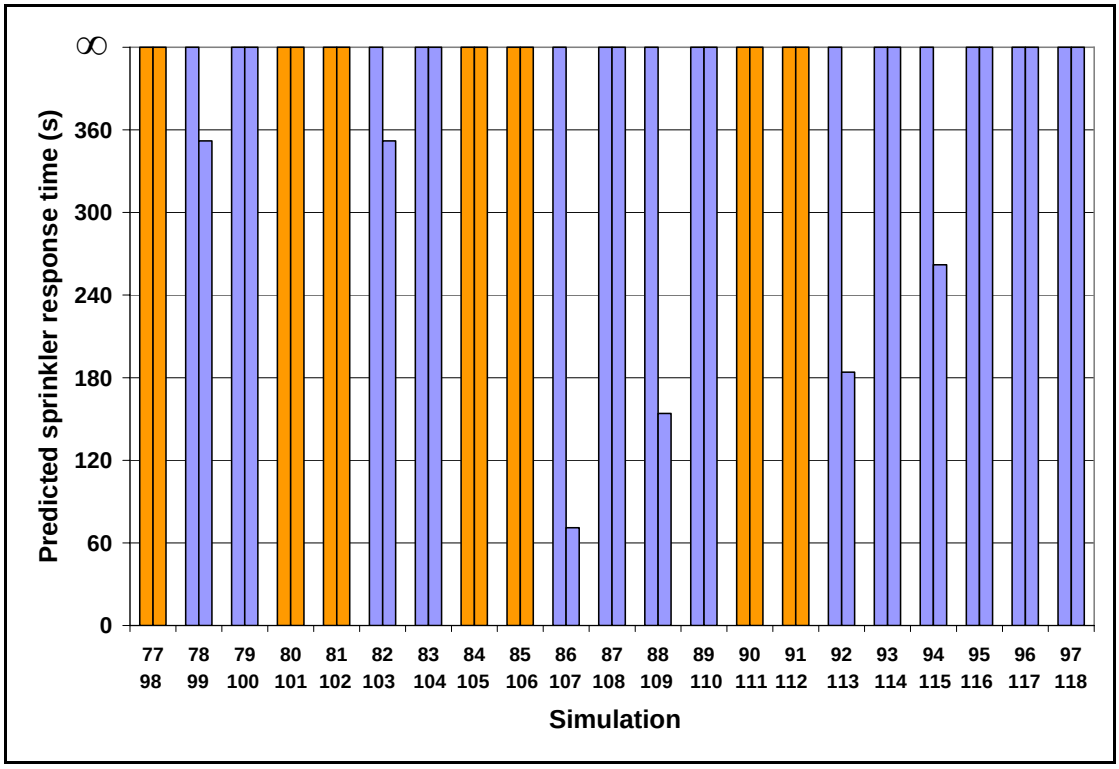

Figure 8.6: Sprinkler response time in BRANZFIRE for Scenario 2 at both the minimum (left hand bar) and maximum (right hand bar) sprinkler distance below the ceiling

As shown in this figure, the first and the second column of each pair of columns represents the predicted sprinkler response time in BRANZFIRE obtained at the minimum and the maximum input sprinkler distance below the ceiling respectively. In addition, the upper row of the number in the x-axis of this figure indicates the simulation identification run at the minimum sprinkler distance below the ceiling. In contrast, the lower row of the number indicates the simulation identification run at the maximum sprinkler distance below the ceiling.

From the simulation results shown in this figure, it was found that more sprinklers were activated within the simulation duration (3000 s) at the maximum sprinkler distance below the ceiling than the minimum sprinkler distance below the ceiling.

8.1.6 Input sprinkler distance below the ceiling (Scenario 3)

Scenario 3 was also run to assess the input sprinkler distance below the ceiling in this research. The simulation setup in BRANZFIRE for Scenario 3 and Scenario 2 was similar. The only difference between them was that the input sprinkler distance below the ceiling for Scenario 3 was assumed to be measured from the lower plane of the ceiling to the position of the sprinkler's deflector. The input sprinkler distance below the ceiling (for both the minimum and maximum) for this scenario is specified in detail in Chapter 7.

Figure 8.7 shows the predicted sprinkler response times in BRANZFIRE at both the minimum and maximum sprinkler distance below the ceiling for Scenario 3. It should be noted that the minimum and the maximum input sprinkler distance below the ceiling for the recessed sidewall sprinklers was identical (See Chapter 7). Therefore, the simulation results of the recessed sidewall sprinklers are illustrated separately from other sprinklers (flush, recessed and concealed sprinkles) and shown in Figure 8.8 in this section.

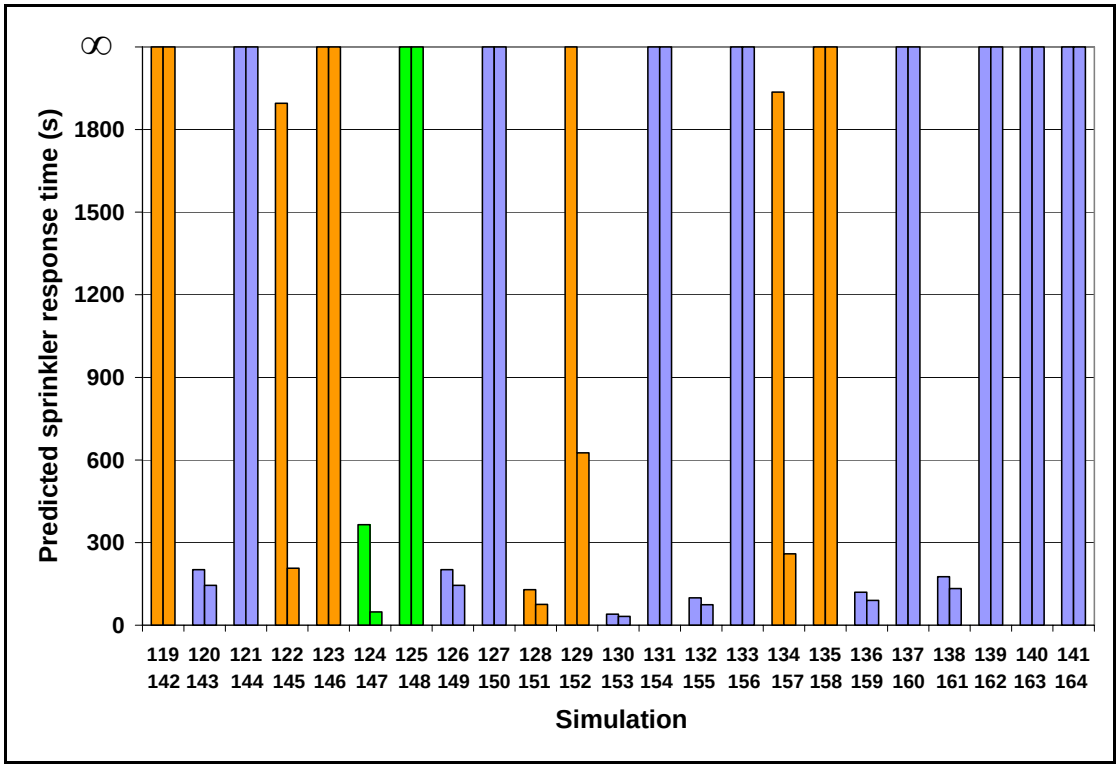

Figure 8.7: Sprinkler response time in BRANZFIRE for Scenario 3 at both the minimum and the maximum sprinkler distance below the ceiling

From the figure above, it can be seen that the maximum sprinkler response time predicted at the maximum sprinkler distance below the ceiling (despite the "no operation" activation time) was 626 s, which is smaller than the sprinkler response time (1936 s) predicted at the minimum sprinkler distance below the ceiling in this scenario.

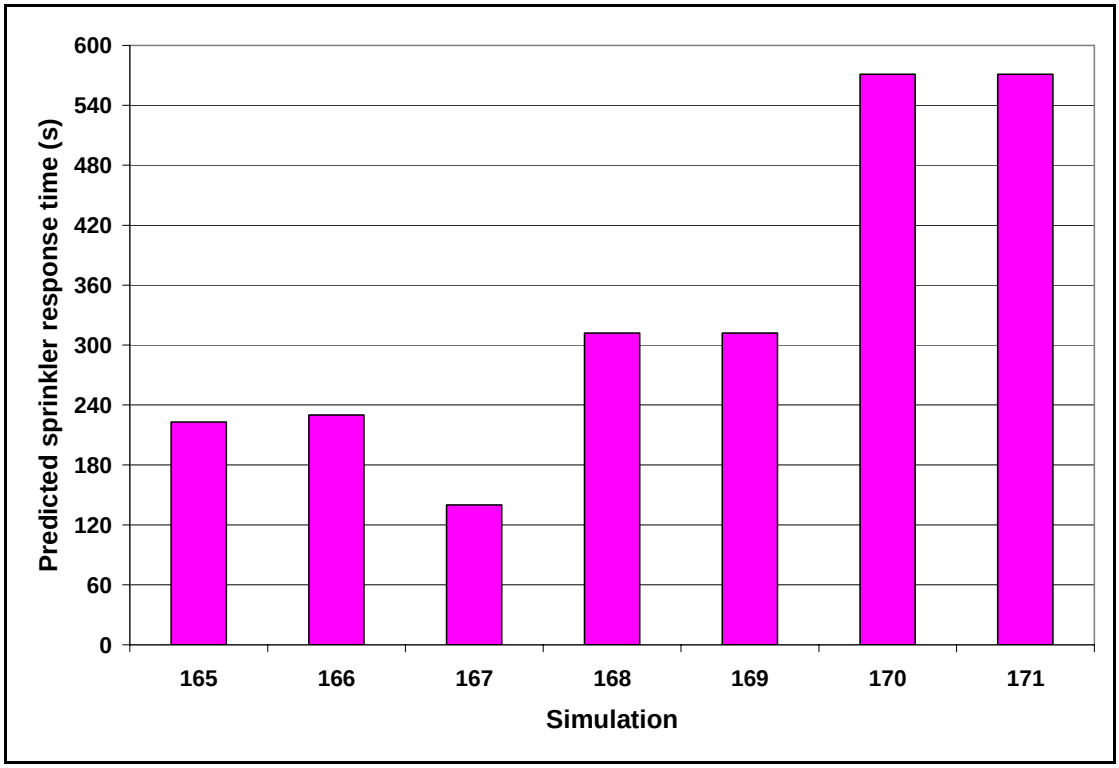

Figure 8.8: Sprinkler response time in BRANZFIRE for the recessed sidewall sprinklers

Figure 8.8 above shows the predicted sprinkler response times for the recessed sidewall sprinklers in BRANZFIRE. As described in Chapter 7, the sprinkler distance below the ceiling (from the lower plane of the ceiling to the sprinkler's deflector) of the recessed sidewall sprinklers was specified and given by Bill and Heskestad (1995). Therefore, the input sprinkler distance below the ceiling for the recessed sidewall sprinklers was directed referenced from Bill and Heskestad.

8.1.7 Comparison (Scenario 2 and Scenario 3)

In order to determine the best input sprinkler distance below the ceiling in BRANZFIRE, a comparison was made between the predicted (BRANZFIRE) and the experimental (full scale fire test) sprinkler response times for both Scenario 2 and Scenario 3 in this section.

Figure 8.9 below shows the comparison between the predicted and the experimental sprinkler response times for both Scenario 2 and Scenario 3 (at both the near and the far ceiling station). It should be noted that the flush sprinkler and the recessed sidewall sprinklers were only modelled in Scenario 3. Therefore, the simulation results (sprinkler response times) of these sprinklers from Scenario 3 were not incorporated to implement the comparison in this figure.

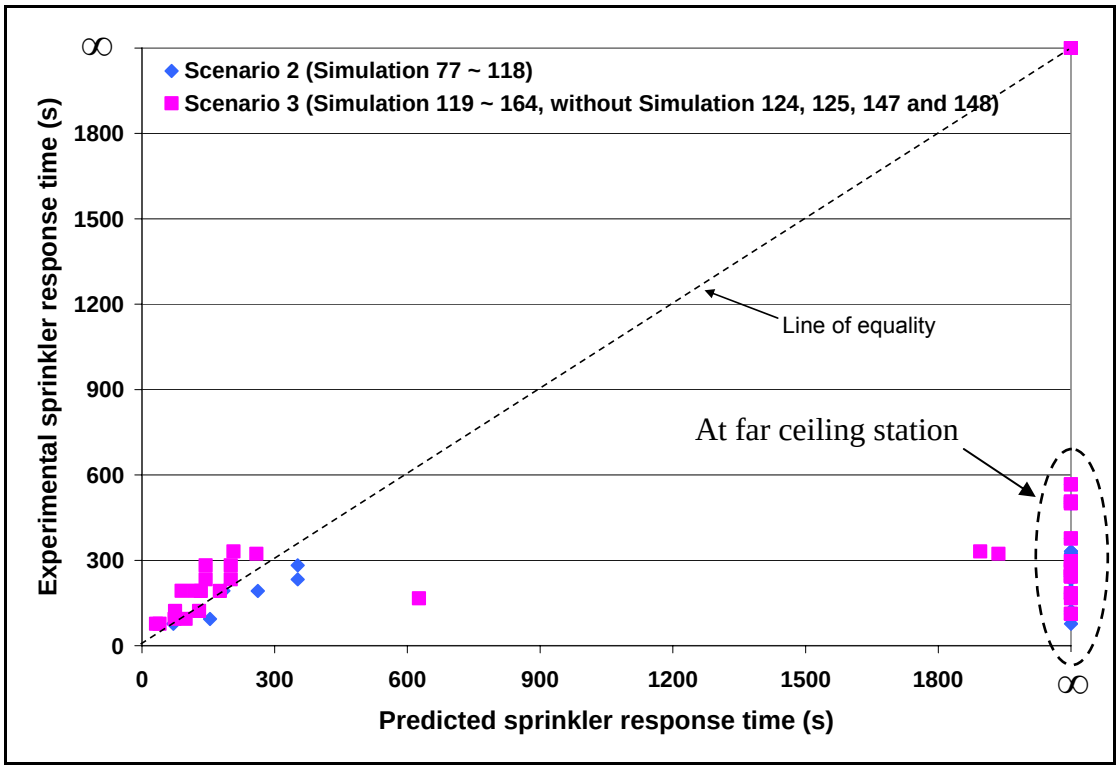

Figure 8.9: Comparison between the predicted and the experimental sprinkler response times for both Scenario 2 and Scenario 3 (at both the near and far ceiling station)

From this figure, it can be seen that the quantity of the data points distributed near the line of equality from Scenario 3 was greater than Scenario 2 (only six data points scattered near the line of equality from Scenario 2). This result implied that the

sprinkler response times predicted from simulations in Scenario 3 were more comparable to the experimental sprinkler response times than Scenario 2. Therefore, it was considered that a better sprinkler response time correlation between BRANZFIRE and the full scale fire tests could be obtained when the input sprinkler distance below the ceiling was specified from the lower plane of the ceiling to the point of the sprinklers' deflector (Scenario 3).

However, it should be noted that the sprinklers simulated in BRANZFIRE at the far ceiling station (the circled data points shown in Figure 8.9) were not predicted to operate within 3000 s. "No operation" for sprinklers simulated at the far ceiling station in BRANZFIRE may caused by the ceiling jet temperature differences between the prediction (BRANZFIRE) and the experiment (full scale fire test). As described in Section 8.1.3, the ceiling jet temperatures predicted in BRANZFIRE at the far ceiling station at a distance of 0.076 m and 0.006 m below the ceiling were lower than the experimental ceiling jet temperatures recorded from the full scale fire tests. This result implied that BRANZFIRE underestimated the ceiling jet temperatures at the far ceiling station. Due to this limitation of BRANZFIRE, the sprinkler activation time at the far ceiling station could not be determined from simulations. Therefore, it was decided that the sprinklers installed at the far ceiling station in the full scale fire tests would not be modelled in BRANZFIRE for the later simulations in this study.

The location of the ceiling station in BRANZFIRE was specified by inputting the radial distance between the vertical axis of the fire to the position of the sprinkler sensing element. The input radial distance for the near and the far ceiling station was 1.64 m and 4.55 m respectively and given by Bill and Heskestad (1995). As discussed in this section, the sprinklers installed at the far ceiling station in the full scale fire tests were not modelled in BRANZFIRE. Therefore, the best input radial distance for sprinklers modelled in BRANZFIRE was specified to be 1.64 m in this research. However, it should be noted that this value was only used as the input for the flush, recessed and concealed sprinklers in BRANZFIRE. This is because the recessed sidewall sprinklers investigated in the full scale fire tests were not installed at the near (or far) ceiling station. The installation locations of the recessed sidewall sprinklers in the full scale fire tests are illustrated in Chapter 2 of this thesis.

8.1.8 Best input sprinkler distance below the ceiling

From the discussion shown in the previous section, it was determined that the best input sprinkler distance below the ceiling could be obtained from Scenario 3 where the sprinkler distance below the ceiling was specified from the lower plane of the ceiling to the point of the sprinklers' deflector. However, it was considered that there were two specific (minimum and maximum) values of the sprinkler distance below the ceiling as specified in Scenario 3. For fire engineering design purposes, it is more convenient to provide a single value for fire engineers rather than a range of values. Therefore, a comparison was made between the predicted and experimental sprinkler response times for Scenario 3 at both the minimum and maximum sprinkler distance below the ceiling to determine the best input sprinkler distance below the ceiling (a single value) in this study.

Figure 8.10 below shows the comparison between the predicted and the experimental sprinkler response times for Scenario 3 at the minimum and the maximum sprinkler distance below the ceiling. It should be noted that this figure was a sub-set of Figure 8.9 by excluding the data points relative to the far ceiling station.

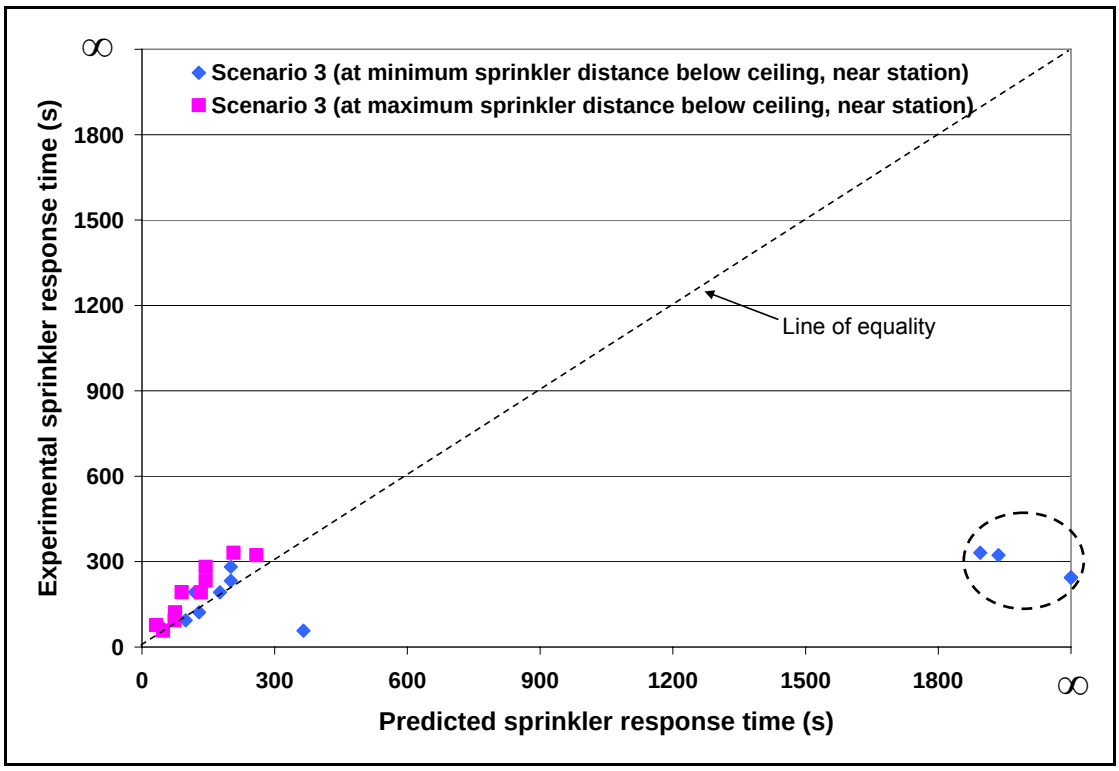

Figure 8.10: Comparison between the predicted and the experimental sprinkler response times for Scenario 3 at the minimum and maximum sprinkler distance below the ceiling

From this figure, it can be seen that there were still three data points (circled data points) dispersed far away from the line of equality. The three circled data points were plotted by using the predicted sprinkler response times obtained in BRNAZFIRE at the minimum input sprinkler distance below the ceiling. The differences between the predicted and the experimental sprinkler response times of the three circled data points were very large. Therefore, it was considered that BRANZFIRE gave a more accurate sprinkler response time prediction when the input in BRANZFIRE was the maximum sprinkler distance below the ceiling specified in Scenario 3. As a result, it was determined that the maximum sprinkler distance below the ceiling in Scenario 3 were the best input in BRANZFIRE for this study. The best input sprinkler distance below the ceiling for the flush, recessed, concealed and recessed sidewall sprinklers are tabulated in Table 8.2 below.

Table 8.2: Best input sprinkler distance below the ceiling

Sprinkler	Best input sprinkler distance below the ceiling (m)
Flush	0.024
Recessed	0.035
Concealed	0.025
Recessed sidewall	0.1 , 0.3

The magnitude of the best input sprinkler distance below the ceiling for each corresponding sprinkler was obtained from the sprinkler manufacturer (Tyco Fire & Tyco Fire & Building Products 2006). Therefore, they are realistic values and convenient for use in fire engineering design.

8.1.9 Input C-factor of sprinklers (Scenario 4)

The best input C-factor of the flush, recessed, concealed and recessed sidewall sprinklers was determined in this section by using the best input fire object location and the best input sprinkler distance below the ceiling as described in the previous sections.

Figure 8.11 below shows the typical predicted sprinkler response times in BRANZFIRE for the recessed sprinkler tested in the full scale fire test (Test 3) with different input C-factor. It should be noted that the trend of the predicted sprinkler response time as a function of the C-factor for each sprinkler (flush, recessed, concealed and recessed sidewall sprinklers) was similar to the result as shown in this figure. Therefore, the graphical results of other sprinklers tested in the full scale fire tests are not represented in this section and attached in Appendix K of this report.

From this figure, it was found that the predicted sprinkler response time increased linearly with a small increase rate when the C-factor was in a range from 0 $(m/s)^{1/2}$ to 0.6 $(m/s)^{1/2}$. However, the increase rate of the predicted sprinkler response time became larger when the input C-factor exceeded 0.6 $(m/s)^{1/2}$ in BRANZFIRE. For the C-factor ranges from 1.8 $(m/s)^{1/2}$ to 2 $(m/s)^{1/2}$, the sprinkler was not predicted to operate in BRANZFIRE.

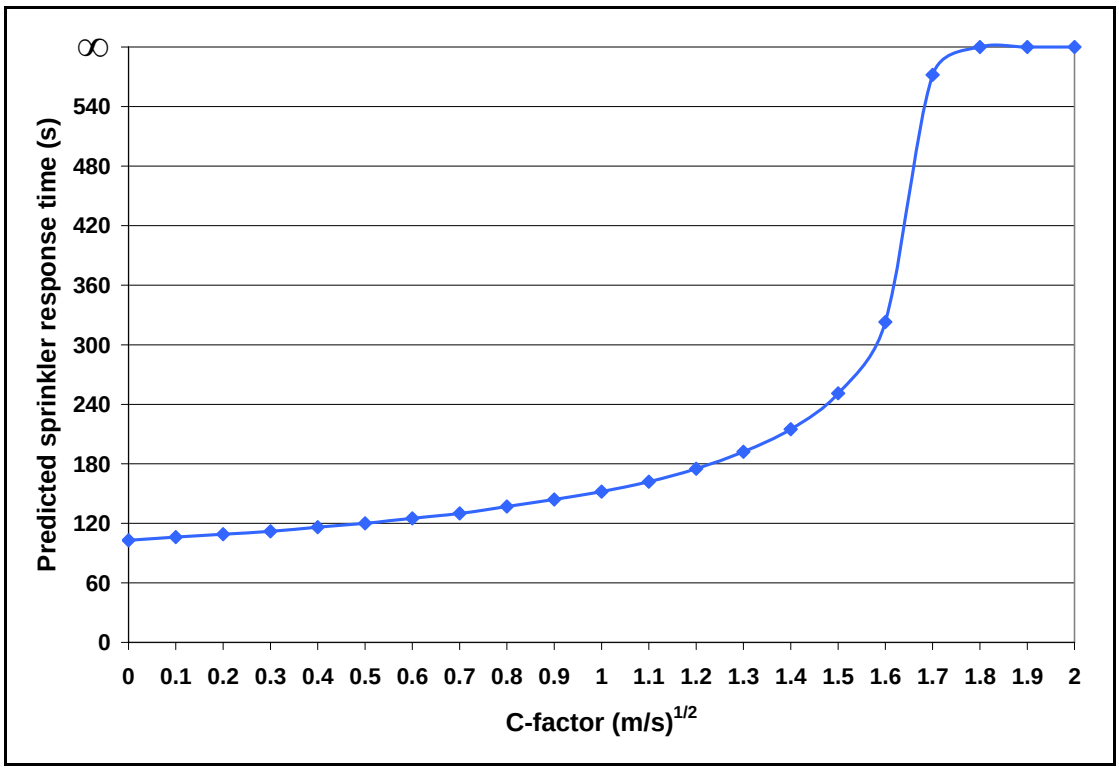

Figure 8.11: Sprinkler response time in BRANZFIRE for the recessed sprinkler (Simulation 193 ~ 213 for Test 3 in the full scale fire tests)

As mentioned in Chapter 7, the best input C-factor of each sprinkler was determined based on the magnitude of the discrepancy between the predicted and the experimental sprinkler response time and selected when the predicted sprinkler response time was closest to the experimental sprinkler response time.

Table 8.3 tabulates the best input C-factor in BRANZFIRE for the flush, recessed, concealed, and recessed sidewall sprinklers investigated in the full scale fire tests.

Table 8.3: Best input C-factor for flush, recessed, concealed and recessed sidewall sprinklers

Test	Sprinkler	Best input C-factor $(m/s)^{1/2}$
Flush sprinkler		
5	G	1.0
Recessed sprinkler		
3	D	1.5
6	C	1.5
8	A	1.8
9	A	1.4
11	B	1.8

12	B	1.6
16	C	0.4
Concealed sprinkler		
2	I	N/A
4	H	1.3
7	H	2
10	J	1.2
Recessed sidewall sprinkler		
13	Es	0.1
	Er	0.1
	Fr	1
14	$Es^{0.1}$	0.1
	$Er^{0.1}$	0.2
	$Es^{0.3}$	0
	$Er^{0.3}$	0

Note: N/A – Concealed sprinkler was not activated due to experimental error.

8.1.10 Verification of the best input C-factor for each type of sprinkler

In an attempt to provide further confidence in the best input C-factor found from this research, verification was conducted in this section. As mentioned in Chapter 1, the C-factor is a parameter that accounts for the heat loss due to conduction between the heat-responsive element and the fitting of the sprinkler (International Standard 2004). Therefore, the C-factor for the same types of sprinklers installed with identical tested room geometry, an identical piping system connected to the sprinklers, and the identical location and the heat release rate of the fire source should be similar.

8.1.10.1 Flush sprinkler

The flush sprinkler was only investigated in one single full scale fire test (Test 5). Therefore, the reliability of the best input C-factor for the flush sprinkler could not be examined due to the limitation of only knowing one best input C-factor. Therefore, it was assumed that the best input C-factor for the flush sprinkler obtained from Test 5

could be used as the input in BRANZFIRE to simulate the flush sprinkler tested in the full scale fire test.

8.1.10.2 Recessed sprinkler

For the full scale fire tests with the recessed sprinklers (Test 3, 6, 8, 9, 11, 12 and 16), with the exception of Test 16, the room geometry, the piping system connected to the sprinklers, and the location and the heat release rate of the fire source were the same. From Table 8.3, the best input C-factor values of Test 3, 6, 8, 9, 11 and 12 are very similar and vary from 1.4 $(m/s)^{1/2}$ to 1.8 $(m/s)^{1/2}$.

It should be noted that the room geometry of Test 16 was different than other tests, where the ventilation opening size connected to the outside environment of the tested compartment in Test 16 was much larger than other tests. This implied that the increase rate of the ceiling jet temperatures in Test 16 was lower than other tests. The sprinkler response time predicted in BRANZFIRE was significantly influenced by the ceiling jet temperatures. Therefore, the best input C-factor of Test 16 determined from the comparison between the predicted and the experimental sprinkler response time in this study was quite different that other tests.

From the analysis above, it was verified that the best input C-factor values for the recessed sprinklers obtained from this study were reasonable and could be used as inputs in BRANZFIRE to simulate the recessed sprinklers tested in the full scale fire tests.

8.1.10.3 Concealed sprinkler

Four of the full scale fire tests (Test 2, 4, 7 and 10) were conducted to investigate the sprinkler activation of the concealed sprinklers. For Test 2, the concealed sprinkler installed at the near ceiling station was not operated due to the experimental error. Therefore, the best input C-factor of this sprinkler in Test 2 could not be determined from the comparison between the predicted and the experimental sprinkler response times in this work.

For Test 4 and Test 10, the room geometry, the piping system connected to the sprinklers, and the location and the heat release rate of the fire source were identical. As seen from Table 8.3, the best input C-factor for Test 4 and Test 10 was very similar and specified as 1.3 $(m/s)^{1/2}$ and 1.2 $(m/s)^{1/2}$ respectively.

For Test 7, the experimental sprinkler response time was recorded to be 122 s. However, the maximum sprinkler response time was predicted to be 93 s in BRANZFIRE when the input C-factor was 2 $(m/s)^{1/2}$. The upper limit of the defined input C-factor range was 2 $(m/s)^{1/2}$ in this research, therefore the best input C-factor for the sprinkler in this test was assumed to be 2 $(m/s)^{1/2}$. It should be noted that the heat release rate of the fire source in Test 7 was approximately double the heat release rate of the fire source used in Test 4 and Test 10. This implied that the increase rate of the ceiling jet temperatures in Test 7 was larger than Test 4 and Test 10 and resulted in a faster sprinkler response time predicted in BRANZFIRE. Therefore, the best input C-factor of Test 7, determined from the comparison between the predicted and the experimental sprinkler response time in this study, was different than Test 4 and Test 10.

From the analysis above, it was verified that the best input C-factor values for the concealed sprinklers obtained from this study were reasonable and could be used as the input in BRANZFIRE to simulate the concealed sprinklers investigated in the full scale fire tests.

8.1.10.4 Recessed sidewall sprinkler

Test 13 and Test 14 were conducted in the full scale fire tests for investigating the recessed sidewall sprinklers. Sprinkler Es, Er and Fr were tested simultaneously in the full scale fire test (Test 13), therefore the tested room geometry, the piping system connected to the sprinklers, and the location and the heat release rate of the fire source were identical for each sprinkler. From Table 8.3, the best input C-factor for sprinkler Es and Er was the same and specified as 0.1 $(m/s)^{1/2}$. However, the best input C-factor for sprinkler Fr was larger than sprinkler Es and Er. This is because the distance between the vertical axis of the fire to the position of the sprinkler sensing element (radial distance) of sprinkler Fr was different than sprinkler Es and Er. As illustrated

in Figure 2.2 of Chapter 2, the sprinkler Fr had the largest radial distance and was located further away from the fire source when compared to sprinkler Es and Er. As shown in Section 8.1.3, the ceiling jet temperatures could be significantly changed when the input radial distance in BRANZFIRE was different. Since the radial distance of sprinkler Fr was largest, the ceiling jet temperatures at the location of sprinkler Fr were smallest when compared to at the location of sprinkler Es and Er. The smaller ceiling jet temperatures at the location of sprinkler Fr influenced the predicted sprinkler response time in BRANZFIRE. Therefore, the best input C-factor of sprinkler Fr determined from the comparison between the predicted and the experimental sprinkler response time in this study was different than sprinkler Es and Er.

For Test 14, sprinkler $Es^{0.1}$, $Er^{0.1}$, $Es^{0.3}$ and $Er^{0.3}$ were tested simultaneously. Therefore, the tested room geometry, the piping system connected to the sprinklers, and the location and the heat release rate of the fire source were identical for each tested sprinkler. From Table 8.3, it was found that the best input C-factor values of sprinkler $Es^{0.1}$, $Er^{0.1}$, $Es^{0.3}$ and $Er^{0.3}$ were very similar and varied from 0 $(m/s)^{1/2}$ to 0.2 $(m/s)^{1/2}$.

From the analysis above, it was verified that the best input C-factor values for the recessed sidewall sprinklers obtained from this study were reasonable and could be used as the input in BRANZFIRE to simulate the recessed sidewall sprinklers investigated in the full scale fire tests.

8.1.11 Apparent C-factor

As shown in Table 8.3, the best input C-factor values for each type of sprinkler were similar. In order to obtain a constant C-factor to represent each type of sprinkler, the "apparent C-factor" was determined in this section. The apparent C-factor of each type of sprinkler was calculated by averaging the best input C-factor values for the corresponding type of sprinkler as shown in Table 8.3. For example, the apparent C-factor for the concealed sprinklers was calculated to be 1.5 $(m/s)^{1/2}$, which is the average of the best input C-factor from Test 4, Test 7 and Test 10.

Table 8.4 tabulates the apparent C-factor for each type of sprinkler obtained in this study. It should be noted that the maximum decimal place of the input C-factor in BRANZFIRE was one. Therefore, the apparent C-factor of each type of sprinkler in this study was also displayed to one decimal place.

Table 8.4: Apparent C-factor for each type of sprinkler

Type of sprinkler	Apparent C-factor $(m/s)^{1/2}$
Flush	1.0
Recessed	1.4
Concealed	1.5
Recessed sidewall	0.2

In addition, the apparent C-factor shown in Table 8.4 was used to determine the sprinkler response time correlation between BRANZFIRE and the full scale fire tests for the flush, recessed, concealed and the recessed sidewall sprinklers in Section 8.2 of this chapter.

8.2 Sprinkler response time correlations

The sprinkler response time correlation between the BRANZFIRE and the full scale fire tests for the flush, recessed, concealed and recessed sidewall sprinklers is described in this section.

8.2.1 Flush sprinkler

As shown in Table 8.3 above, the flush sprinkler was only investigated in one single test in the full scale fire tests. Therefore, the sprinkler response time correlation was impossible to establish between BRANZFIRE and the full scale fire tests for the flush sprinkler in this study.

By using the best fire object location, the best input sprinkler distance below the ceiling and the apparent C-factor in BRANZFIRE for the flush sprinkler, the sprinkler response time was predicted to be 55 s, which is slightly smaller than the experimental sprinkler response time (57 s). The sprinkler response time difference between

BRANZFIRE and the full scale fire test is only 2 s. Therefore, it was considered that (for the user) if the inputs in BRANZFIRE are similar to this study (e.g. the geometry of the compartment, the location and heat release rate of the fire source, and the parameters used to specify a sprinkler), the sprinkler response time predicted in BRANZFIRE can be used to represent the response time of the flush sprinkler tested in the full scale fire tests. The parameters used to specify the flush sprinkler in BRANZFIRE were shown in Table 8.5.

Table 8.5: Input parameters in BRANZFIRE used to specify the flush sprinkler

Parameter	Input in BRANZFIRE
RTI	34 $(m.s)^{1/2}$
C-factor	1.0 $(m/s)^{1/2}$
Radial distance	1.64 m
Actuation temperature	74 ^{o}C
Sprinkler distance below ceiling	0.024 m

It should be noted that all of the input parameters (with the exception of the C-factor) tabulated in Table 8.5 above are obtained from literature. The input C-factor (apparent C-factor) used for the flush sprinkler in this study was obtained from the comparison between the predicted (BRANZFIRE) and the experimental sprinkler response times (full scale fire test). A more accurate input C-factor for a given type of sprinkler could be obtained by conducting more sprinkler tests in the full scale fire test. However, due to the limited number of the full scale fire test with the flush sprinkler, the input C-factor for the flush sprinkler obtained in this study was the best result that could be determined. Therefore, it was considered that this input C-factor for the flush sprinkler is reliable and could be used as the input in BRANZFIRE to model the flush sprinkler in the full scale fire test.

8.2.2 Recessed sprinkler

Figure 8.12 below shows the comparison of the sprinkler response times between the BRANZFIRE and the full scale fire tests for the recessed sprinklers. It should be noted that the predicted sprinkler response times in BRANZFIRE were obtained by

using the best input fire object location, the best input sprinkler distance below the ceiling and the apparent C-factor.

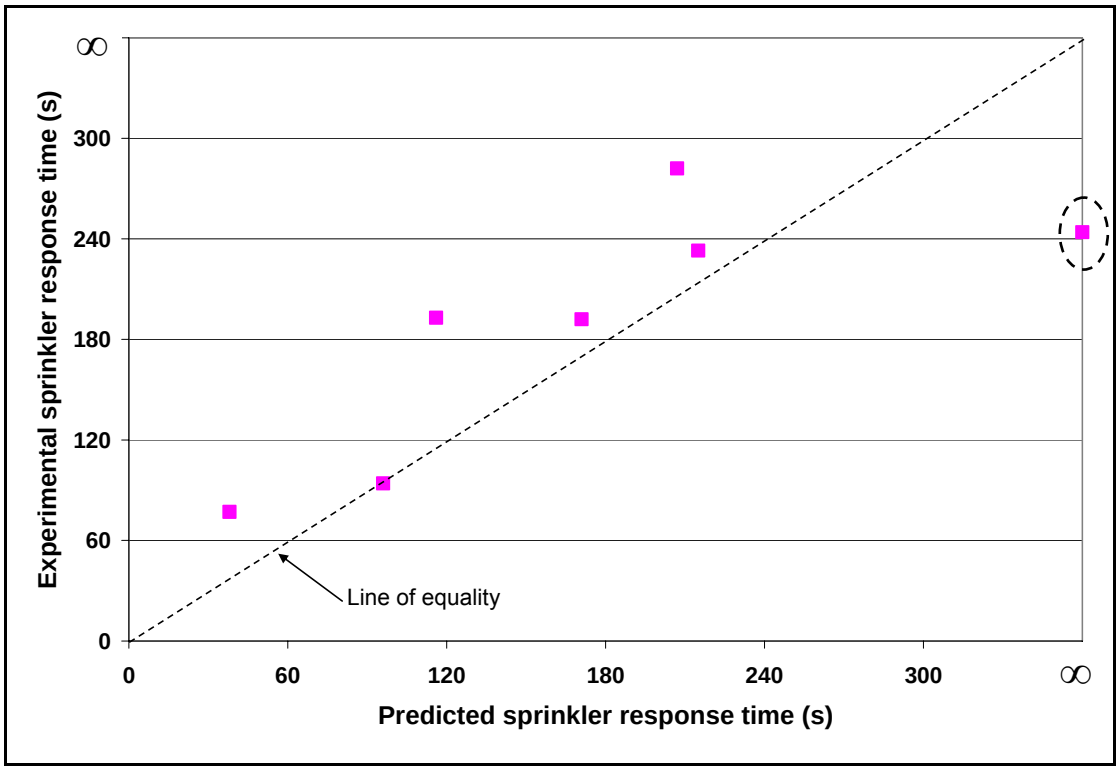

Figure 8.12: Comparison between the predicted and the experimental sprinkler response times for the recessed sprinklers by using the best input fire object location, the best sprinkler distance below the ceiling and the apparent C-factor

From this figure, it can be seen that all of the data points (with the exception of the circled data point) are located near the line of equality. This result implies that the sprinkler response times predicted in BRANZFIRE were similar to the sprinkler response times recorded in the full scale fire tests for the recessed sprinklers.

The circled data point was the comparison between the predicted and the experimental sprinkler response time from Test 16. As mentioned in Section 8.1.10, the tested room geometry of Test 16 (with much larger ventilation opening size) was different than other recessed sprinkler full scale tests. Therefore, the ceiling jet temperatures of Test 16 predicted in BRANZFIRE were influenced by the different input room geometry and smaller than the ceiling jet temperatures from other tests. The sprinkler activation in BRANZFIRE mainly depends on the ceiling jet temperatures at the location of the simulated sprinkler. Therefore, the predicted sprinkler response time of

Test 16 was larger than other tests. In addition to this (as seen from Figure 8.11 in Section 8.1.9) the predicted sprinkler response time became larger as the increase of the input C-factor in BRANZFIRE. The best input C-factor for Test 16 was 0.4 $(m/s)^{1/2}$ (See Table 8.3), which is smaller than the apparent C-factor (1.4 $(m/s)^{1/2}$) determined for the recessed sprinklers in this study. By approaching the apparent C-factor as the input to simulate the sprinkler tested in Test 16, BRANZFIRE failed to predict the sprinkler activation within the specified simulation duration (3000 s). Therefore, the circled data point from Test 16 was located far away from the line of equality in Figure 8.12.

Despite the outlying (circled) data point, Figure 8.12 shows a good sprinkler response time correlation between the prediction (BRANZFIRE) and the experiment (full scale fire test) for the recessed sprinklers. Therefore, it was considered that if the inputs in BRANZFIRE are similar to this study (e.g. the geometry of the compartment, the location and heat release rate of the fire source, and the parameters used to specify a sprinkler), the sprinkler response time predicted in BRANZFIRE can be used to represent the response time of the recessed sprinklers tested in the full scale fire tests. The parameters used to specify the recessed sprinklers in BRANZFIRE were shown in Table 8.6 below.

Table 8.6: Input parameters in BRANZFIRE to specify the recessed sprinklers

Parameter	Input in BRANZFIRE
RTI	35, 135, 183 $(m.s)^{1/2}$
C-factor	1.4 $(m/s)^{1/2}$
Radial distance	1.64 m
Actuation temperature	68, 74 ^{o}C
Sprinkler distance below ceiling	0.035 m

The input parameters tabulated in Table 8.6 (with the exception of the C-factor) were obtained from literature. The input C-factor for the recessed sprinklers was the apparent C-factor determined in Section 8.1.11 of this chapter. It should be noted that there are three different RTI values specified as possible inputs in BRANZFIRE for the recessed sprinklers (See Table 8.6). As mentioned in Chapter 2, there were four different models of the recessed sprinklers investigated in the full scale fire tests. In

addition to this, as described in Chapter 7, the nominal RTI of each tested recessed sprinkler was given by Bill and Heskestad and used as the input RTI in BRANZFIRE to simulate the corresponding recessed sprinkler tested in the full scale fire tests. The nominal RTI of the four different models (sprinkler A, B, C, and D in Table 2.3 of Chapter 2) of the recessed sprinklers are 35 $(m.s)^{1/2}$, 135 $(m.s)^{1/2}$, 183 $(m.s)^{1/2}$ and 183 $(m.s)^{1/2}$. Therefore, the recommended input RTI values were 35 $(m.s)^{1/2}$, 135 $(m.s)^{1/2}$, 183 $(m.s)^{1/2}$ for the recessed sprinklers in this study.

Additionally, the actuation temperature of sprinklers A, B, C, and D was provided by Bill and Heskestad (1995) and specified to be 68 ^{o}C, 68 ^{o}C, 74 ^{o}C and 74 ^{o}C respectively. Therefore, the input actuation temperatures obtained from this study for the recessed sprinklers were 68 ^{o}C and 74 ^{o}C (See Table 8.6).

8.2.3 Concealed sprinkler

Figure 8.13 shows the comparison between the predicted and the experimental sprinkler response times for the concealed sprinklers. It should be noted that the predicted sprinkler response times of the data points in this figure were obtained by using the best input fire object location, the best input sprinkler distance below the ceiling and the apparent C-factor in BRANZFIRE.

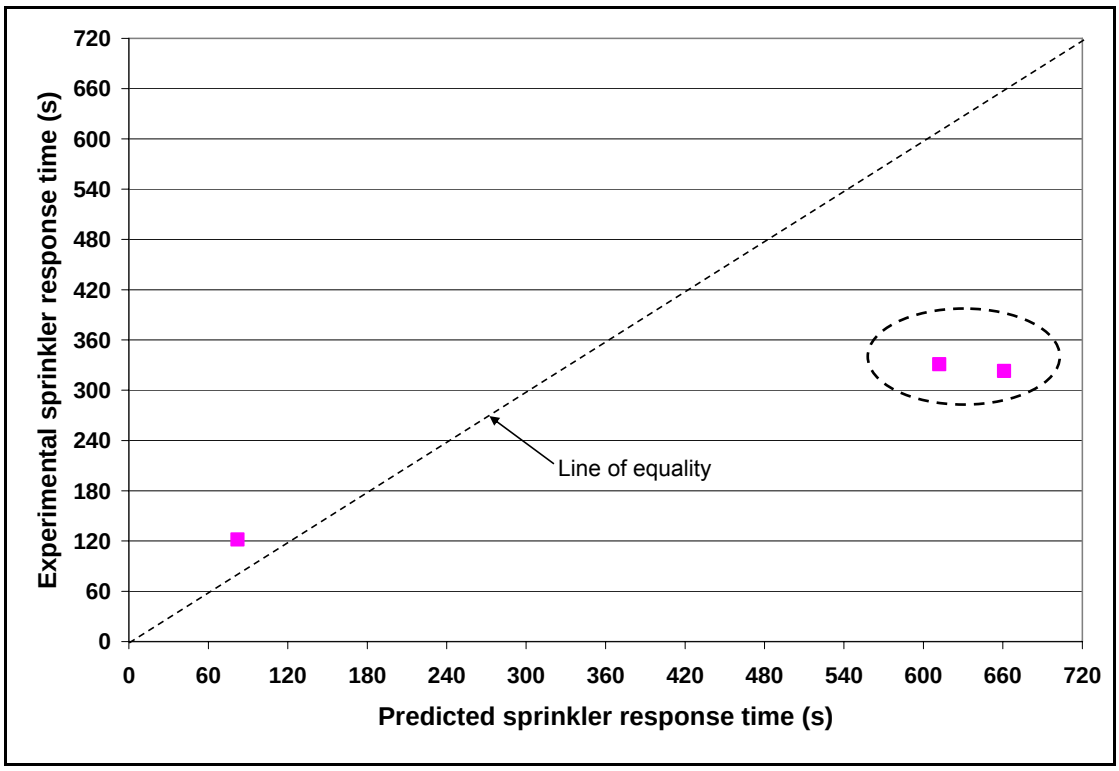

Figure 8.13: Comparison between the predicted and the experimental sprinkler response times for the concealed sprinklers by using the best input fire object location, the best sprinkler distance below the ceiling and the apparent C-factor

From this figure, it can be seen that there are two data points (circled data points) located far away at the right of the line of equality. This result implies that the predicted sprinkler response time in BRANZFIRE was larger than the experimental sprinkler response time recorded in the full scale fire tests. The best input C-factor values for the two circled data points were 1.3 $(m/s)^{1/2}$ and 1.2 $(m/s)^{1/2}$, which are smaller than the apparent C-factor (1.5 $(m/s)^{1/2}$) calculated for the concealed sprinklers in this study. Therefore, it was considered that the differences between the predicted and the experimental sprinkler response times may caused by using the different input C-factor values.

In order to examine the sensitivity of the input C-factor for the concealed sprinklers, another input apparent C-factor (1.3 $(m/s)^{1/2}$) was approached. This new apparent C-factor (1.3 $(m/s)^{1/2}$) was calculated by averaging the best input C-factor from Test 4 and Test 10 (See Table 8.3). This also implies that the best input C-factor of Test 7 was not incorporated to determine this new apparent C-factor.

Figure 8.14 shows the comparison between the predicted and the experimental sprinkler response times for the concealed sprinklers (Test 4, 7 and 10). It should be noted that the predicted sprinkler response times of the three data points plotted in this figure were obtained by using the best input fire object location, the best input sprinkler distance below the ceiling and the new apparent C-factor (1.3 $(m/s)^{1/2}$) in BRANZFIRE.

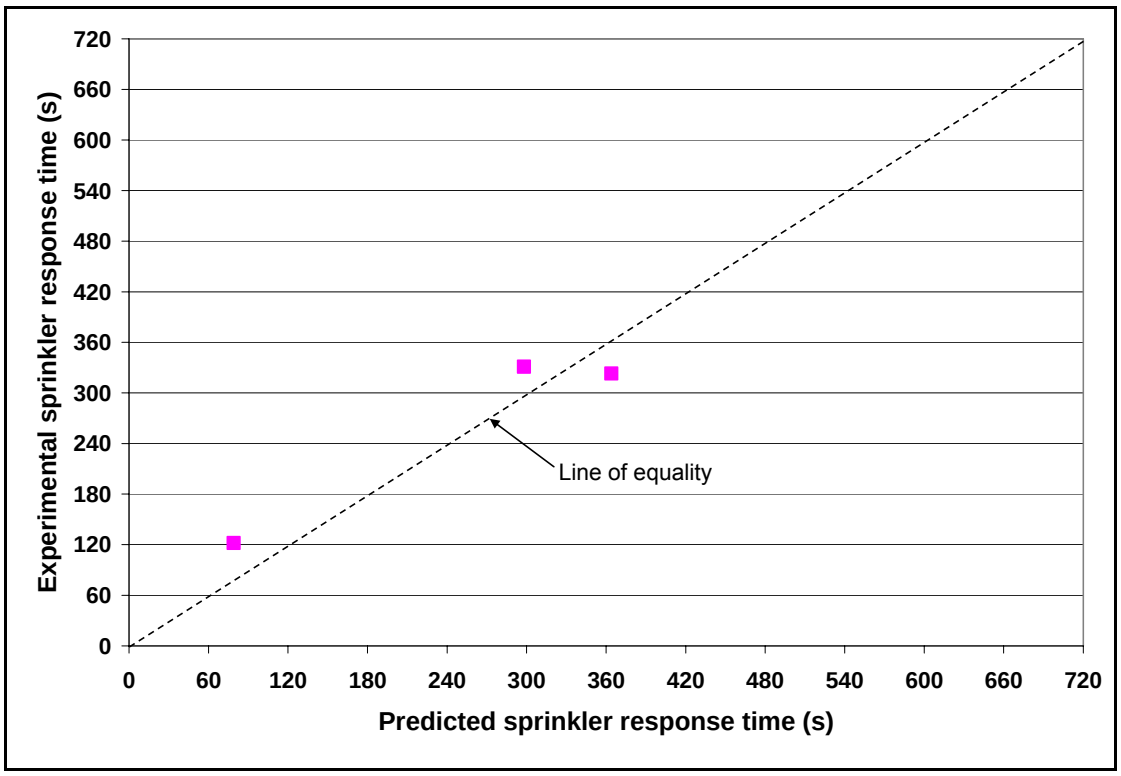

Figure 8.14: Comparison between the predicted and the experimental sprinkler response times for the concealed sprinklers by using the best input fire object location, the best sprinkler distance below the ceiling and the new apparent C-factor

As seen from this figure, the three data points were located near the line of equality. This result shows that the predicted sprinkler response times were very similar to the experimental sprinkler response times when the new apparent C-factor was used. By comparing the results shown in Figure 8.13 and Figure 8.14, it was found that the change of predicted sprinkler response time (circled data points) was large when the input apparent C-factor was modified from 1.5 $(m/s)^{1/2}$ to 1.3 $(m/s)^{1/2}$. This is because the relationship between the predicted sprinkler response time and the input C-factor in BRANZFIRE was non-linear.

Figure 8.15 shows the predicted non-linear sprinkler response times in BRANZFIRE for the concealed sprinkler tested in the full scale fire test (Test 4) with different input C-factor. The trend of the predicted sprinkler response time as a function of the C-factor for Test 10 was similar to the result as shown in this figure. Hence, the graphical result of Test 10 was not displayed here.

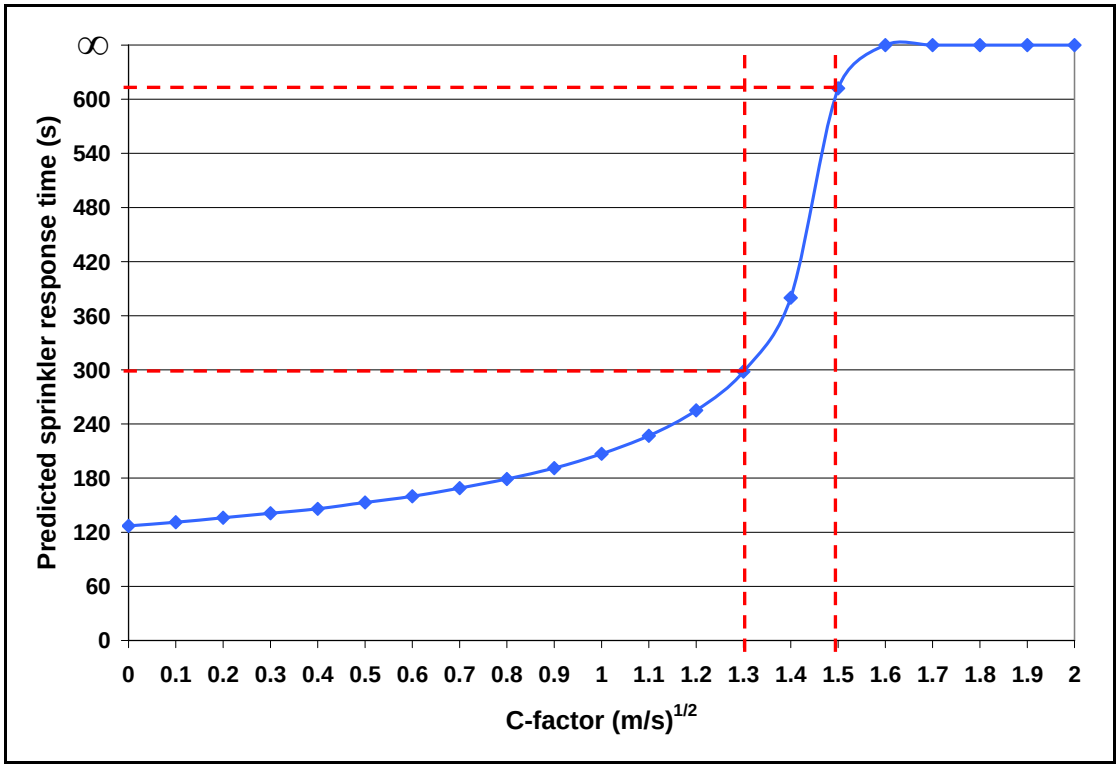

Figure 8.15: Sprinkler response time in BRANZFIRE for the concealed sprinkler (Simulation 340 ~ 360 for Test 4 in the full scale fire tests)

The comparison of the two C-factor values (the original 1.5 $(m/s)^{1/2}$ and the new 1.3 $(m/s)^{1/2}$) occurs at the most sensitive location on the graph. From this figure, it can be seen that the predicted sprinkler response time at the C-factor of 1.3 $(m/s)^{1/2}$ was 298 s, which is approximately half of the predicted sprinkler response time obtained at the C-factor of 1.5 $(m/s)^{1/2}$. This result also implies that the predicted sprinkler response time by using the apparent C-factor (1.5 $(m/s^{1/2})$) was much larger than by using the new apparent C-factor (1.3 $(m/s^{1/2})$).

By knowing the reason why the predicted sprinkler response times of the two circled data points were quite different than the experimental sprinkler response times, it was considered that the new apparent C-factor (1.3 $(m/s^{1/2})$) for the concealed sprinkler

obtained from the investigation is more appropriate and therefore should be used as the input in BRANZFIRE.

By obtaining the "best" apparent C-factor for the concealed sprinkler, it was considered that (for the user) if the inputs in BRANZFIRE are similar to this study (e.g. the geometry of the compartment, the location and heat release rate of the fire source, and the parameters used to specify a sprinkler), the sprinkler response time predicted in BRANZFIRE can be used to represent the response time of the concealed sprinklers tested in the full scale fire tests. The parameters used to specify the concealed sprinklers in BRANZFIRE were shown in Table 8.7 below.

Table 8.7: Input parameters in BRANZFIRE to specify the concealed sprinklers

Parameter	Input in BRANZFIRE
RTI	203, 264 $(m.s)^{1/2}$
C-factor	1.3 $(m/s)^{1/2}$
Radial distance	1.64 m
Actuation temperature	74 ^{o}C
Sprinkler distance below ceiling	0.025 m

The input parameters tabulated in Table 8.7 (with the exception of the C-factor) were obtained from literature. The input C-factor for the concealed sprinklers was the "best" apparent C-factor determined in this section. The input RTI shown in this table were the nominal RTI values provided by Bill and Heskestad (1995).

8.2.4 Recessed sidewall sprinkler

Figure 8.16 shows the sprinkler response time comparison between the BRANZFIRE and the full scale fire tests for the recessed sidewall sprinklers. It should be noted that the sprinkler response times predicted in BRANZFIRE were obtained by using the best input fire object location, the best input sprinkler distance below the ceiling and the apparent C-factor.

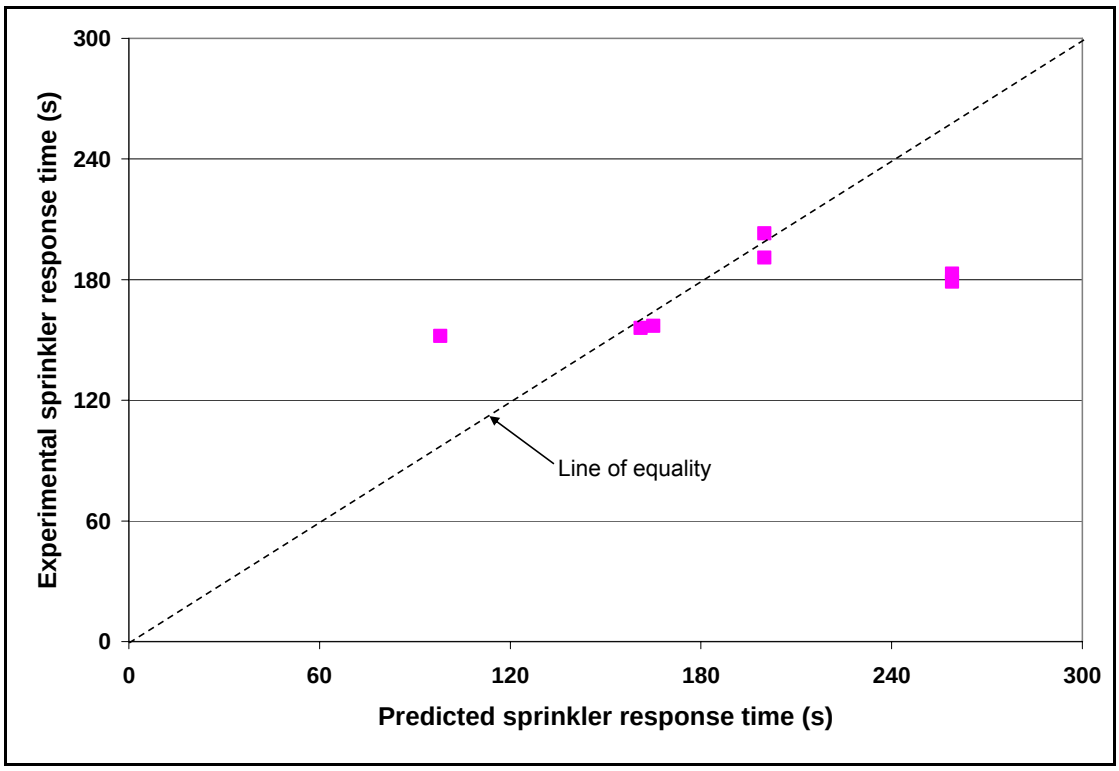

Figure 8.16: Comparison between the predicted and the experimental sprinkler response times for the recessed sidewall sprinklers by using the best input fire object location, the best sprinkler distance below the ceiling and the apparent C-factor

As seen from this figure, all the data points are scattered close to the line of equality. This result implies that the predicted sprinkler response times in BRANZFIRE were comparable and similar to the experimental sprinkler response times obtained in the full scale fire tests.

Figure 8.16 shows a good sprinkler response time correlation between the prediction (BRANZFIRE) and the experiment (full scale fire test) for the recessed sidewall sprinklers. Therefore, it was considered that (for the user) if the inputs in BRANZFIRE are similar to this study (e.g. the geometry of the compartment, the location and heat release rate of the fire source, and the parameters used to specify a sprinkler), the sprinkler response time predicted in BRANZFIRE could be used to represent the response time of the recessed sidewall sprinklers tested in the full scale fire tests. The parameters used to specify the recessed sidewall sprinklers in BRANZFIRE were shown in Table 8.8 below.

Table 8.8: Input parameters in BRANZFIRE to specify the recessed sidewall sprinklers

Parameter	Input in BRANZFIRE
RTI	135, 246 $(m.s)^{1/2}$
C-factor	0.2 $(m/s)^{1/2}$
Radial distance	2.24, 2.32, 2.4, 4.26 m
Actuation temperature	68 ^{o}C
Sprinkler distance below ceiling	0.1, 0.3 m

The input parameters tabulated in Table 8.8 (with the exception of the C-factor) were obtained from literature. The input C-factor for the recessed sidewall sprinklers was the apparent C-factor determined in Section 8.1.11 of this chapter. The input RTI and the input sprinkler distance below the ceiling shown in this table were the nominal RTI values and the actual distances provided by Bill and Heskestad (1995). It should be noted that there are four different radial distances specified as the input in BRANZFIRE for the recessed sidewall sprinklers (See Table 8.8). These radial distances were obtained from the data provided in the full scale fire tests by Bill and Heskestad (1995). In addition to this, the radial distances of the recessed sidewall sprinklers investigated in the full scale fire tests are illustrated in Chapter 2 of this thesis.

8.3 General discussion

The best input fire object location, the best input sprinkler distance below the ceiling and the input apparent C-factor in BRANZFIRE for the flush, recessed, concealed and the recessed sidewall sprinklers were determined in this chapter. However, since the experimental data from the full scale fire tests was limited (e.g. the sprinkler distance below the ceiling and the C-factor of sprinklers were not given), the sprinkler response time correlation equation between BRANZFIRE and the full scale fire tests could not be determined in this research.

It should be noted that the predicted sprinkler response time should give a conservative result for the fire engineering design purposes. Therefore, it is important that a safety factor be applied on the predicted sprinkler response time obtained in BRANZFIRE to generate a conservative result for the design purposes.

In the future, the full scale fire tests should be conducted at the University of Canterbury to obtain the sprinkler response time correlation for the flush, recessed, concealed and the recessed sidewall sprinklers.

8.3.1 Sprinkler response time relationship between full scale fire test, wind tunnel plunge test and BRANZFIRE modelling

As mentioned in Chapter 1, one of the objectives of this study was to find the relationship of the sprinkler response time between the full scale fire test, wind tunnel plunge test and BRANZFIRE modelling. In order to achieve this objective, the sprinkler relationship between the full scale fire test and the wind tunnel plunge test must first be determined. Since the full scale fire test was not conducted in this work, the experimental data used to obtain the relationship between the full scale fire test and the wind tunnel plunge test was extracted from Bill and Heskestad (1995). However, the experimental data provided by Bill and Heskestad was limited so that the sprinkler response time relationship between the full scale fire test and the wind tunnel plunge test could not be determined. Further to this, the sprinkler relationship between the full scale fire test, wind tunnel plunge test and the BRANZFIRE could not be determined. The descriptions listed below describe the reasons why the sprinkler response time relationship could not be obtained in this study.

- The comparison of the sprinkler response time between the full scale fire test and the wind tunnel plunge test was not made by Bill and Heskestad.

- One of the plunge test conditions (128 ^{o}C, 1 m/s and 0.007 mm Hg) used to investigate the recessed and concealed sprinklers in the wind tunnel by Bill and Heskestad were determined based on the comparison of the sprinkler response time between the full scale fire test and the wind tunnel plunge test. From this determination, the sprinkler response time difference between the full scale fire test and the wind tunnel plunge test was 35 s and was suggested to be reasonable. However, the process and methodology used to obtain other plunge test conditions was not given by Bill and Heskestad. In addition to this,

Bill and Heskestad did not define the acceptable range of the sprinkler response time difference when compared between the full scale fire test and the wind tunnel plunge test. Therefore, it was very difficult to determine the sprinkler response time relationship between the full scale fire test and the wind tunnel plunge test by having such limited data.

- The sprinkler response time relationship between the full scale fire test and the wind tunnel plunge test was also intended to be determined by comparing the RTI between the full scale fire test and the wind tunnel plunge test. However, the RTI values were not determined for the recessed and concealed sprinklers in the wind tunnel plunge test by Bill and Heskestad. Therefore, the sprinkler response time relationship between the full scale fire test and the wind tunnel plunge test was not determined in this study.

It should be noted that the recessed and concealed sprinklers investigated in the experiment (plunge test) of this research (See Chapter 5 and Chapter 6) was intended to be modelled in BRANZFIRE by approaching the sprinkler response time relationship between the full scale fire test, wind tunnel plunge test and the BRANZFIRE. However, this relationship was not determined and therefore the recessed and concealed sprinklers tested in the experiment of this study were not simulated in BRANZFIRE.

CHAPTER 9

9 CONCLUSIONS

A study on the activation time of the flush, recessed, concealed and recessed sidewall sprinklers was conducted in this investigation in order to achieve the primary objectives (See Chapter 1) set for this research. The conclusions and findings from each aspect of this work are described as follows.

9.1 UC3 wind tunnel

The calibration of the UC3 wind tunnel study provided the following conclusions:

- In general, the UC3 wind tunnel provides a very stable and uniform temperature profile in the tunnel test section. In addition to this, the UC3 wind tunnel produces consistent temperature and velocity results at different times by setting identical tunnel test conditions. However, the velocity uniformity of the UC3 wind tunnel needs to be improved in the future.

- The hot gas temperature in the UC3 wind tunnel can be heated up to 300 ^{o}C.

- The glue (used to glue the gaskets to the gaps between the wind tunnel sections) melted under the maximum calibrated hot gas temperature (300 ^{o}C). The maximum safely calibrated temperature was determined to be 200 ^{o}C, and therefore 200 ^{o}C was the highest temperature that was used in wind tunnel calibrating tests and plunge tests.

- At the sprinkler location in the test section, the selected hot gas temperature maintained a constant temperature with an accuracy of $\pm$ 1 ^{o}C for the hot gas temperature ranging from 129 ^{o}C to 141 ^{o}C and within $\pm$ 2 ^{o}C for the hot gas temperature ranging from 142 ^{o}C to 200 ^{o}C.

- Hot gas velocities of up to 2.94 m/s can be generated.

- At the sprinkler location in the test section, the selected hot gas velocity was constant with an accuracy of ± 0.20 m/s for range from 1 m/s to 2.94 m/s.

- The comparisons demonstrated good agreement between the calibration results in the experiment in this research, FMRC and the FRS in terms of temperature and velocity. Therefore, it was considered that the UC3 wind tunnel was reliable and could be used to conduct the plunge test for the sprinklers.

9.2 Plunge test

The plunge test (experiment) study provided the following conclusions:

- A suitable thermal sensitivity test (plunge test) for assessing the sprinkler response time and the RTI of the recessed and concealed sprinklers has been established at the University of Canterbury.

- The settings of the UC3 wind tunnel and the arrangement of the UC modified mounting plate provided consistent plunge test conditions for testing the recessed and concealed sprinklers.

- For the recessed sprinklers (sprinkler M_R and N_R), the sprinkler response times were not effected by the application of a vacuum during the plunge tests.

- The RTI values determined at the low hot gas temperature and velocity test conditions increase markedly compared to values at the high hot gas temperature and velocity test conditions.

- For sprinkler M_R, the RTI obtained in the worst orientation was larger than in the standard orientation (for both the “simple” RTI equation (without C-factor) and the “comprehensive” RTI equation (with C-factor)).

- For sprinkler M_R and N_R, the differences between the RTI from different plunge test conditions was found to be small in the standard orientation (for both the RTI equations). However, the variations of the RTI from different plunge test conditions became larger in the worst orientation (for both the RTI equations).

- For sprinkler O_C, the RTI in the worst orientation was smaller than in the standard orientation.

- For sprinkler P_C, the RTI in the standard orientation was smaller than in the worst orientation.

- Table 9.1 shows the apparent RTI for the recessed and concealed sprinklers investigated in this research in both the standard and the worst orientation. It should be noted that the apparent RTI of the recessed sprinklers and the concealed sprinklers were determined by using both the RTI equations and the "comprehensive" RTI equation respectively.

Table 9.1: Apparent RTI for recessed and concealed sprinklers

Sprinkler	The "simple" RTI equation (without C-factor)		The "comprehensive" RTI equation (with C-factor)	
	Standard orientation	Worst orientation	Standard orientation	Worst orientation
M_R	111.9 $(m.s)^{1/2}$	221 $(m.s)^{1/2}$	83.6 $(m.s)^{1/2}$	211.2 $(m.s)^{1/2}$
N_R	50.0 $(m.s)^{1/2}$	133.3 $(m.s)^{1/2}$	35.9 $(m.s)^{1/2}$	107.4 $(m.s)^{1/2}$
O_C	--	--	374.2 $(m.s)^{1/2}$	334.4 $(m.s)^{1/2}$
P_C	--	--	233.5 $(m.s)^{1/2}$	766 $(m.s)^{1/2}$

- By comparing the apparent RTI obtained from the experiments in this study with the RTI provided from FMRC (Bill and Heskestad 1995) and the BRE (Annable 2006), the results show significantly differences. However, the comparisons demonstrated good agreement between the apparent RTI in this study, FMRC and the BRE for the sprinkler N_R in the standard orientation

- The RTI is a parameter used to indicate how quickly a sprinkler can absorb heat from its surroundings sufficient to cause activation, and therefore the sprinkler response would be faster with a smaller RTI value for a given sprinkler. However, it should be noted that a larger RTI should be used to produce a conservative result for fire engineering design purposes.

9.3 BRANZFIRE and full scale fire test

The BRANZFIRE simulation and the full scale fire test studies provided the following conclusions:

- It was found that the ceiling jet temperatures predicted in BRANZFIRE were smaller than the recorded ceiling jet temperatures in the full scale fire tests (Bill and Heskestad 1995). Therefore, the accuracy of the simulation results is affected by this limitation of BRANZFIRE.

- The best input fire object location, the best input sprinkler distance below the ceiling and the input apparent C-factor in BRANZFIRE for the flush, recessed, concealed and the recessed sidewall sprinklers were determined in this research. The comparison shows a good sprinkler response time correlation between the prediction (BRANZFIRE) and the experiment (full scale fire test) for the flush, recessed, concealed, and the recessed sidewall sprinklers in the near ceiling station. Therefore, it was considered that (for the user) if the inputs in BRANZFIRE are similar to this study (e.g. the geometry of the compartment, the location and heat release rate of the fire source, and the parameters used to specify a sprinkler), the sprinkler response times predicted in BRANZFIRE can be used to represent the response time of all four sprinklers tested in the full scale fire tests.

- Table 9.2 shows the recommended inputs (parameters) used to specify each type of sprinkler in BRANZFIRE to simulate the sprinklers investigated in the full scale fire tests.

Table 9.2: Inputs (parameters) in BRANZFIRE for each type of sprinkler

Input in BRANZFIRE	Type of sprinkler			
	Flush	Recessed	Concealed	Recessed sidewall
RTI ($(m.s)^{1/2}$)	34	35, 135, 183	203, 264	135, 246
C-factor ($(m/s)^{1/2}$)	1	1.4	1.3	0.2
Radial distance (m)	1.64	1.64	1.64	2.24, 2.32, 2.4, 4.26
Actuation temperature (^{o}C)	74	68, 74	74	68
Sprinkler distance below ceiling (m)	0.024	0.035	0.025	0.1, 0.3

- All of the input parameters (with the exception of the C-factor) tabulated in table above are obtained from literature. The input RTI, the radial distances and the actuation temperatures shown in this table were referenced from Bill and Heskestad (1995). The input C-factor for the sprinklers was the apparent C-factor determined in Chapter 8 of the thesis. The magnitude of the input sprinkler distance below the ceiling shown in this table was obtained from the sprinkler manufacturer (Tyco Fire & Building Products 2006). Therefore, the input values shown in this table were considered to be reliable and convenient for use in fire engineering design.

- It should be noted that a predicted sprinkler response time should give a conservative result for the fire engineering design purposes. Therefore, it is important that a safety factor be applied on the predicted sprinkler response time obtained in BRANZFIRE to generate a conservative result for the design purposes.

- Since the experimental data from the full scale fire tests was limited (e.g. the sprinkler distance below the ceiling and the C-factor of sprinklers were not given), the sprinkler response time correlation equation between BRANZFIRE and the full scale fire tests could not be determined in this research. In addition, due to the fact that the experimental data provided by Bill and Heskestad (1995) was limited, the sprinkler response time relationship between the full scale fire test, the wind tunnel plunge test and BRANZFIRE modelling could not be determined in this study.

CHAPTER 10

10 FURTHER WORK

10.1 UC3 wind tunnel

Further work is required to develop the UC3 wind tunnel to meet the tunnel criteria represented by the FMRC as described in Chapter 3 of this report. In addition to this, further work is required to increase the maximum hot gas velocity generated inside the wind tunnel in order to carry out all the plunge test conditions for investigating the recessed and concealed sprinklers represented by the FMRC (Bill and Heskestad 1995). The recommendations shown below should be implemented in the future to improve the performance and the workability of the UC3 wind tunnel.

- The insulating material (glass wool fibre blankets) of the UC3 wind tunnel should be replaced with a high temperature (300 ^{o}C) resistance insulating material.
- The thickness of the flow straightener used in the UC3 wind tunnel should be increased to reduce the hot gas velocity variation level.
- A more powerful fan motor should be used in the wind tunnel so that the maximum hot gas velocity can be operated up to 3.48 m/s under the hot gas temperature of 289 ^{o}C.
- A more powerful vacuum pump should be used in the wind tunnel so that the maximum pressure difference between the plenum enclosure of UC modified mounting plate and test section of wind tunnel can reach 0.013 mm Hg under the hot gas temperature of 289 ^{o}C.
- More flow dividers should be installed at the upstream side of the test section of the UC3 wind tunnel to distribute the flow evenly in the tunnel. Further to this, the number of blades contained in one flow divider should be increased to distribute the hot gas flow more efficiently.

- In order to operate the wind tunnel at higher temperatures, operator safety and an assessment to determine whether existing wind tunnel explosion protection measures are adequate shall be investigated.

10.2 Plunge test

Further work is required to conduct more plunge tests with the recessed sprinklers and concealed sprinklers to investigate the influence of the sprinkler response time and the RTI in more specific areas. These specific areas are described below:

- More sprinkler frame arm orientations (e.g. 15 ^{o} and 45 ^{o}) against the oncoming hot gas flow in the wind tunnel should be implemented.
- The recessed and concealed sprinklers should be tested with different sprinkler distances below the ceiling. The sprinkler distance below the ceiling should be within the minimum and the maximum recess distance for the particular sprinkler required from the manufacturer.

- Further work is required to investigate the significance of sprinkler frame arm design relative to sprinkler thermal sensitivity and what impact this might have in respect of modelling.

Further investigation in the form of an error analysis should be considered to fully assess the accuracy of the calculated RTI of recessed and concealed sprinklers in this report by using the C factor from the BRE (Annable 2006).

Differences in wind tunnel boundary layer conditions are likely to have a significant influence on sprinkler activation. Further work is required to investigate the influence of the boundary layer condition of the UC3 wind tunnel on sprinklers (pendent, recessed and concealed sprinklers).

Further work is required to predetermine the conditions in the plunge test plenum for the recessed and concealed sprinklers before and after the concealer plate of the concealed sprinkler falls away.

10.3 BRANZFIRE modelling and full scale fire test

Further work is required to determine the sprinkler response time correlation between BRANZFIRE and the full scale fire test for the flush, recessed, concealed and the recessed sidewall sprinklers. Since the experimental data of the full scale fire test from literature was limited, it is suggested that the full scale fire tests be conducted at the University of Canterbury.

The setup of the full scale fire test should be identical to the setup of the full scale fire tests conducted by Bill and Heskestad (1995) at the FMRC. The details of the full scale fire test conducted at the FMRC can be either found from this report or the technical report presented by Bill and Heskestad (1995).

In this research, the sensitivity of the input C-factor in BRANZFIRE was investigated by using the "fixed" RTI values (either obtained from Bill and Heskestad (1995) or from the plunge test experiments in this study). Further work is required to examine the sensitivity of the input RTI in BRANZFIRE by fixing the input C-factor (e.g. input different RTI in BRANZFIRE by setting the C-factor equals 0 $(m/s)^{1/2}$).

In addition, further work is required to determine the relationship of the sprinkler response time between the full scale fire test, wind tunnel plunge test and BRANZFIRE.

CHAPTER 11

11 References

Annable K (2006). DCLG final research report, effectiveness of sprinklers in residential premises – an evaluation of concealed and recessed pattern sprinkler products, Section 5: thermal sensitivity. Building Research Establishment Ltd (BRE).

Alpert R L (2002). Ceiling jet flows. In: The SFPE Handbook of Fire Protection Engineering, Section 2/Chapter 2, National Fire Protection Association, Society of Fire Protection Engineers, Quincy, Massachusetts, Bethesda, MD.

Beever P E (1990). Estimating the response of thermal detectors. Journal of Fire Protection Engineering, Volume 2, Issue 1, pp 11 – 24.

Beyler C L (2002). Fire hazard calculations for large, open hydrocarbon fires. In: The SFPE Handbook of Fire Protection Engineering, Section 3/Chapter 11, National Fire Protection Association, Society of Fire Protection Engineers, Quincy, Massachusetts, Bethesda, MD.

Bill R G and Heskestad G (1995). Plunge test procedures for recessed, flush and concealed sprinklers. Factory Mutual Research Corporation, Norwood, Mass.

Buchanan A H (2001). Fire engineering design guide. Centre for Advanced Engineering, Christchurch, New Zealand.

Chin K S (2002). Development of bench-scale testing of sprinkler and smoke detector activation/response time. Thesis (M.E.F.E.) – University of Canterbury, Christchurch, New Zealand.

Cooper L Y (1998). Simulating the opening of fusible-link-actuated fire vents, NISTR 6227. National Institute of Standards and Technology (NIST).

Cox G and Kumar S (1987). Field modelling of fire in forced ventilated enclosures. Combustion Science Technology, Volume 52, pp 7 -23.

Cox G and Kumar S (2002). Modelling enclosure fires using CFD. In: The SFPE Handbook of Fire Protection Engineering, Section 3/Chapter 7, National Fire Protection Association, Society of Fire Protection Engineers, Quincy, Massachusetts, Bethesda, MD.

Davis W D (1999). Zone fire model jet: a model for the prediction of detector activation and gas temperature in the presence of a smoke layer, NISTIR 6324. National Institute of Standards and Technology (NIST).

Davis W D and Cooper L Y (1989). Estimating the environment and the response of sprinkler links in compartment fires with draft curtains and fusible link-actuated ceiling vents – Part II: user guide for the computer code LAVENT, NBSIR 89 – 4122. National Institute of Standards and Technology (NIST).

Evans D D (1998). Ceiling jet flows. In: Handbook of Fire Protection Engineering, Section 1/Chapter 9, National Fire Protection Association, Society of Fire Protection Engineers, Quincy, Massachusetts, Bethesda, MD.

Fleming R P (2002). Automatic sprinkler system calculations. In: The SFPE Handbook of Fire Protection Engineering, Section 4/Chapter 3, National Fire Protection Association, Society of Fire Protection Engineers, Quincy, Massachusetts, Bethesda, MD.

Fleming R P (2003). Principles of automatic sprinkler system performance. In: Fire Protection Handbook, Section 10/Chapter 9, National Fire Protection Association, Quincy, Massachusetts.

FM Approval Standard (2002). Approval standard for automatic sprinklers for fire protection, Class series 2000. FM Approvals LLC.

Forney G P, Cooper L Y and Moss W F (1990). The Consolidated Compartment Fire Model (CCFM) computer code application CCFM.VENTS, Part IV: user reference guide. National Institute of Standards and Technology (NIST).

Grant C C (1996). The birth of NFPA. National Fire Protection Association, Quincy, Massachusetts.

Grosshandler W L (1997). Towards the development of a universal fire emulator detector evaluation. Fire Safety Journal, Volume 29, pp 113 – 127.

Heskestad G and Bill R G (1987). Conduction heat-loss effects on thermal response of automatic sprinklers. Factory Mutual Research Corporation, Norwood, Mass.

Heskestad G and Bill R G (1988). Quantification of thermal responsiveness of automatic sprinklers including conduction effects. Fire Safety Journal, Volume 14, Issue 1, pp 113 – 125.

Heskestad G and Smith H F (1976). Investigation of a new sprinkler sensitivity approval test: the plunge test. Factory Mutual Research Corporation, Norwood, Mass.

Heskestad G and Smith H F (1980). Plunge test for determination of sprinkler sensitivity. Factory Mutual Research Corporation, Norwood, Mass.

Ingason H (1998). Investigation of thermal response of glass bulb sprinklers using plunge and ramp tests. Fire Safety Journal, Volume 30, Issue 1, pp 71 – 93.

International Standard (2004). Fire protection – automatic sprinkler system – Part 1: requirements and test methods for sprinklers. ISO Switzerland.

Isman K E (2003). Automatic sprinklers. In: Fire Protection Handbook, Section 10/Chapter 10, National Fire Protection Association, Quincy, Massachusetts.

Karlsson B and Quintiere J G (2000). Enclosure fire dynamic. CRC Press LLC.

Madrzykowski D and Fleming R P (2003). Residential sprinkler systems. In: Fire Protection Handbook, Section 10/Chapter 14, National Fire Protection Association, Quincy, Massachusetts.

McGrattan K B and Forney G P (2004). Fire dynamics simulator (Version 4) user's guide, NIST special publication 1019. National Institute of Standards and Technology (NIST).

Nelson H E (1990). Fire protection engineering tools for hazard estimation, NISTIR report 4380. National Institute of Standards and Technology (NIST).

Peacock R D, Jones W W, Reneke P A and Forney G P (2005). CFAST – Consolidated Model of Fire Growth and Smoke Transport (Version 6) user's guide. National Institute of Standards and Technology (NIST).

Puchovsky M T (2003). Automatic sprinkler systems. In: Fire Protection Handbook, Section 10/Chapter 11, National Fire Protection Association, Quincy, Massachusetts.

Purser D A (2005). Human physiology and toxicology in relation to fire hazards II cardiovascular function and asphyxiant gases. University of Canterbury, Christchurch, New Zealand.

Rohr K D (1998). U.S. experience with sprinklers "who has them? how well do they work?". National Fire Protection Association, Quincy, Massachusetts.

Saunders N M and Conder T (2002). Sprinklers for houses. BRANZ Ltd, Porirua city, New Zealand.

Solomon R E (1994). Automatic sprinkler systems handbook. National Fire Protection Association, Quincy, Massachusetts.

Standards New Zealand (2003). Automatic fire sprinkler systems. Standards New Zealand, Wellington, New Zealand.

Tewarson A (2002). Generation of heat and chemical compounds in fires. In: The SFPE Handbook of Fire Protection Engineering, Section 3/Chapter 4, National Fire Protection Association, Society of Fire Protection Engineers, Quincy, Massachusetts, Bethesda, MD.

Theobald C R (1987). Thermal response of sprinklers Part 1, FRS heated wind tunnel. Fire Safety Journal, Volume 12, Issue 1, pp 51 – 63.

Thompson N J (1964). Fire behaviour and sprinkler. National Fire Protection Association, Quincy, Massachusetts.

Tsai K (2004). Assessment of sprinkler activation prediction time in the BRANZFIRE zone model. University of Canterbury, Christchurch, New Zealand.

Tsui A (2002). Measuring the performance of a wind tunnel for testing fire sprinklers and smoke detectors. University of Canterbury, Christchurch, New Zealand.

Tsui A (2004). Statistical analysis of sprinkler response time index and conduction factor using the plunge test. Thesis (M.E.F.E.) – University of Canterbury, Christchurch, New Zealand.

Tyco Fire & Building Products (2006). World Wide Web address: http://www.tyco-gem.com/, date accessed: 17/08/06.

Wade C A (2004a). A user's guide to BRANZFIRE 2004. BRANZ, Wellington, New Zealand.

Wade C A (2004b). BRANZFIRE technical reference guide. BRANZ, Wellington, New Zealand.

Wade C A (2006). By personal communication. BRANZ, Wellington, New Zealand.

Wade C A, Spearpoint M and Tsai K (2006). Assessing the sprinkler activation predictive capability of the BRANZFIRE fire model. BRANZ Ltd and University of Canterbury, New Zealand.

Wakatsuki K (2005). High temperature radiation absorption of fuel molecules and an evaluation of its influence on pool fire modelling. University of Maryland, College Park, pp 55.

Walton W D (2002). Zone computer fire models for enclosures. In: The SFPE Handbook of Fire Protection Engineering, Section 3/Chapter 7, National Fire Protection Association, Society of Fire Protection Engineers, Quincy, Massachusetts, Bethesda, MD.

CHAPTER 12

12 Appendices

Appendix A Calibration results of the first model of the UC3 wind tunnel

Table 12.1: Test conditions for calibrating the first model of the UC3 wind tunnel

	Test 1	Test 2	Test 3	Test 4	Test 5	Test 6
Duration (mins)	10	10	10	10	10	10
Pre-set temperature (^{o}C)	50	50	128	128	200	200
Fan revolution frequency (Hz)	40	40	40	40	36	36
Blades orientation (flow divider)	Horizontal	Optimum	Horizontal	Optimum	Horizontal	Optimum

(Note: for the "horizontal" blades' orientation as shown in table above, the blades' orientation of the first flow divider was the same as the optimum blades' orientation. However, all blades of the second flow divider were set horizontal to the flow in the tunnel (0 ^{o} to the flow direction).)

Table 12.2: Calibration results of the first model of the UC3 wind tunnel

	Test 1	Test 2	Test 3	Test 4	Test 5	Test 6
Maximum hot gas velocity (m/s)	0.6	1.56	0.8	1.4	1.08	1.26
Variation range of the hot gas velocity (m/s)	+/- 0.4	+/- 0.2	+/- 0.5	+/- 0.2	+/- 0.5	+/- 0.22

Appendix B Velocity calibration results of the UC3 wind tunnel

Table 12.3: Test conditions for calibrating the (second model) UC3 wind tunnel

	Test 1	Test 2	Test 3	Test 4	Test 5	Test 6
Duration (mins)	10	10	10	10	10	10
Pre-set temperature (^{o}C)	20	20	128	128	200	200
Fan revolution frequency (Hz)	45	45	45	45	45	45
Blades orientation (flow divider)	Horizontal	Optimum	Horizontal	Optimum	Horizontal	Optimum

(Note: for the "horizontal" blades' orientation as shown in table above, the blades' orientation of the first flow divider was the same as the optimum blades' orientation. However, all blades of the second flow divider were set horizontal to the flow in the tunnel (0 ^{o} to the flow direction).)

Table 12.4: Calibration results of the UC3 wind tunnel

	Test 1	Test 2	Test 3	Test 4	Test 5	Test 6
Maximum hot gas velocity (m/s)	3.15	2.9	3.13	2.87	3.05	2.77
Variation range of the hot gas velocity (m/s)	+/- 0.25	+/- 0.2	+/- 0.25	+/- 0.2	+/- 0.29	+/- 0.2

Appendix C Configuration of sprinklers investigated in the research

(a) At the maximum recess distance

(b) At the minimum recess distance

Figure 12.1: Sprinkler M_R at the maximum and minimum recess distance

(a) At the maximum recess distance

(b) At the minimum recess distance

Figure 12.2: Sprinkler N_R at the maximum and minimum recess distance

(a): Top view

(b): Bottom view

(c): At the maximum recessed distance

(d) At the minimum recess distance

Figure 12.3: Sprinkler O_C at the maximum and minimum recess distance

(a): Top view

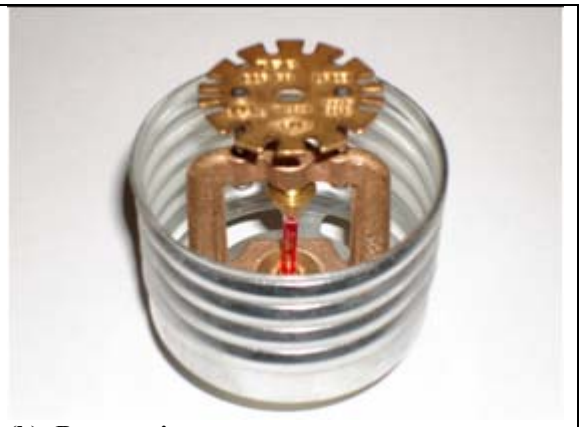

(b): Bottom view

(c): At the maximum recessed distance

(d) At the minimum recess distance

Figure 12.4: Sprinkler P_C at the maximum and minimum recess distance

Appendix D Plunge test conditions for sprinkler M_R, N_R, O_C and P_C (Test 1 ~ 108)

Table 12.5: Plunge test conditions for sprinkler M_R, N_R, O_C and P_C (Test 1 ~ 108)

Test	Sprinkler model	Frame arm orientation	Nominal hot gas temperature	Nominal hot gas velocity	Applied vacuum
1	M_R	90° to the hot gas flow	128 °C	1 m/s	No apply
2					
3					
4	M_R	90° to the hot gas flow	128 °C	1 m/s	0.007 mmHg
5					
6					
7	M_R	90° to the hot gas flow	197 °C	2.56 m/s	No apply
8					
9					
10	M_R	90° to the hot gas flow	197 °C	2.56 m/s	0.010 mmHg
11					
12					
13	M_R	90° to the hot gas flow	128°C	1 m/s	N/A
14					
15					
16	M_R	90° to the hot gas flow	128°C	2.56 m/s	N/A
17					
18					
19	M_R	90° to the hot gas flow	199°C	1 m/s	N/A
20					
21					
22	M_R	90° to the hot gas flow	197°C	2.56 m/s	N/A
23					
24					
25	M_R	0° to the hot gas flow	128°C	1 m/s	N/A
26					
27					
28	M_R	0° to the hot gas flow	128°C	2.56 m/s	N/A
29					
30					
31	M_R	0° to the hot gas flow	199°C	1 m/s	N/A
32					
33					
34	M_R	0° to the hot gas flow	197°C	2.56 m/s	N/A

35 36					
37 38 39	N_R	90^o to the hot gas flow	128^oC	1 m/s	N/A
40 41 42	N_R	90^o to the hot gas flow	128^oC	2.56 m/s	N/A
43 44 45	N_R	90^o to the hot gas flow	199^oC	1 m/s	N/A
46 47 48	N_R	90^o to the hot gas flow	197^oC	2.56 m/s	N/A
49 50 51	N_R	0^o to the hot gas flow	128^oC	1 m/s	N/A
52 53 54	N_R	0^o to the hot gas flow	128^oC	2.56 m/s	N/A
55 56 57	N_R	0^o to the hot gas flow	199^oC	1 m/s	N/A
58 59 60	N_R	0^o to the hot gas flow	197^oC	2.56 m/s	N/A
61 62 63	O_C	90^o to the hot gas flow	128^oC	1 m/s	0.007 mmHg
64 65 66	O_C	90^o to the hot gas flow	128^oC	2.56 m/s	0.007 mmHg
67 68 69	O_C	90^o to the hot gas flow	199^oC	1 m/s	0.010 mmHg
70 71 72	O_C	90^o to the hot gas flow	197^oC	2.56 m/s	0.010 mmHg
73 74 75	O_C	0^o to the hot gas flow	128^oC	1 m/s	0.007 mmHg
76 77	O_C	0^o to the hot gas flow	128^oC	2.56 m/s	0.007 mmHg

78					
79 80 81	O_C	0^o to the hot gas flow	199°C	1 m/s	0.010 mmHg
82 83 84	O_C	0^o to the hot gas flow	197°C	2.56 m/s	0.010 mmHg
85 86 87	P_C	90^o to the hot gas flow	128°C	1 m/s	0.007 mmHg
88 89 90	P_C	90^o to the hot gas flow	128°C	2.56 m/s	0.007 mmHg
91 92 93	P_C	90^o to the hot gas flow	199°C	1 m/s	0.010 mmHg
94 95 96	P_C	90^o to the hot gas flow	197°C	2.56 m/s	0.010 mmHg
97 98 99	P_C	0^o to the hot gas flow	128°C	1 m/s	0.007 mmHg
100 101 102	P_C	0^o to the hot gas flow	128°C	2.56 m/s	0.007 mmHg
103 104 105	P_C	0^o to the hot gas flow	199°C	1 m/s	0.010 mmHg
106 107 108	P_C	0^o to the hot gas flow	197°C	2.56 m/s	0.010 mmHg

Appendix E Experimental (plunge test) record data for recessed and concealed sprinklers in the research

Table 12.6: Experimental record data for recessed and concealed sprinklers

Test	Water (in the sprinkler waterway)		Ambient temperature(°C)	Activation time	
	Temperature (°C)	Pressure (Psi)		Cover plate (Concealed sprinkler only)	Sprinkler
1	14	6	17	N/A	1 min 20s
2	14	5.9	17	N/A	1 min 16s
3	14	6	17	N/A	1 min 13s
4	14	6	16	N/A	1 min 21s
5	14	6	16	N/A	1 min 13s
6	14	6	16	N/A	1 min 15s
7	14	6	15	N/A	25 s
8	14	6	15	N/A	25 s
9	14	6	15	N/A	23 s
10	14	6	15	N/A	23 s
11	14	6	15	N/A	23 s
12	14	6	15	N/A	24 s
13	14	6	17	N/A	1 min 20s
14	14	5.9	17	N/A	1 min 16s
15	14	6	17	N/A	1 min 13s
16	16	5.9	16	N/A	47 s
17	16	5.9	16	N/A	50 s
18	16	6	16	N/A	45 s
19	14	6	14	N/A	32 s
20	14	6	14	N/A	34 s
21	14	6	14	N/A	30 s
22	14	6	15	N/A	25 s
23	14	6	15	N/A	25 s
24	14	6	15	N/A	23 s
25	13	5.9	15	N/A	6 min 47s
26	13	5.8	15	N/A	6 min 00s
27	13	6	15	N/A	5 min 31s
28	16	6	16	N/A	1 min 55s
29	16	6	16	N/A	1 min 40s
30	16	6	16	N/A	1 min 49s

31	14	5.9	14	N/A	1 min 05s
32	14	5.9	14	N/A	1 min 05s
33	14	6	14	N/A	1 min 06s
34	14	6	16	N/A	42 s
35	14	6	16	N/A	41 s
36	14	6	16	N/A	44 s
37	13	5.9	15	N/A	56 s
38	13	6	15	N/A	40 s
39	13	6	15	N/A	41 s
40	16	6	17	N/A	21 s
41	16	5.9	17	N/A	20 s
42	16	5.9	17	N/A	19 s
43	13	5.8	13	N/A	12 s
44	13	5.1	13	N/A	13 s
45	13	5.9	13	N/A	12 s
46	14	6	17	N/A	9 s
47	14	6	17	N/A	9 s
48	14	6	17	N/A	9 s
49	13	6	17	N/A	8 min 27s
50	13	6	17	N/A	8 min 10s
51	13	6	17	N/A	8 min 44s
52	16	6	17	N/A	1 min 13s
53	16	6	17	N/A	1 min 17s
54	16	5.9	17	N/A	1 min 09s
55	14	6	14	N/A	42 s
56	14	5.7	14	N/A	38 s
57	14	6	14	N/A	41 s
58	14	6	18	N/A	20 s
59	14	6	18	N/A	21 s
60	14	6	18	N/A	19 s
61	14	5.3	15	1 min 1s	no operation
62	14	5.9	15	1 min 8s	no operation
63	14	6	15	48 s	no operation
64	12	6	17	33 s	15 min 38s
65	12	6	17	34 s	13 min 48s
66	12	5.9	17	35 s	15 min 41s
67	13	5.2	14	20 s	3 min 24s
68	13	5.9	14	21 s	2 min 58s
69	13	5.9	14	21 s	2 min 40s
70	11	5.9	14	17 s	2 min 55s
71	11	5.9	14	15 s	2 min 01s
72	11	5.9	14	18 s	2 min 21s
73	11	5.9	16	58 s	no operation

74	11	6	16	53 s	no operation
75	11	6	16	57 s	no operation
76	12	5.9	17	33 s	13 min 38s
77	12	5.9	17	39 s	14 min 51s
78	12	6	17	33 s	15 min 05s
79	13	5.9	15	18 s	2 min 26s
80	13	5.9	15	21 s	2 min 30s
81	13	6	15	22 s	3 min 06s
82	11	6	13	20 s	2 min 37s
83	11	5.9	13	17 s	2 min 06s
84	11	6	13	19 s	1 min 53s
85	14	5.9	14	1 min 10s	no operation
86	14	5.5	14	1 min 15s	no operation
87	14	5.8	14	59 s	no operation
88	10	5	14	52s	7 min 58s
89	10	6	14	44s	8 min 03s
90	10	5.9	14	48 s	7 min 40s
91	11	5	14	25 s	1 min 06s
92	11	5.9	14	23 s	1 min 14s
93	11	5	14	24 s	1 min 08s
94	11	5.9	13	17 s	1 min 14s
95	11	5.9	13	25 s	1 min 26s
96	11	5.9	13	16 s	50 s
97	11	6	15	1 min 13s	no operation
98	11	5.9	15	57s	no operation
99	11	6	15	1 min 17s	no operation
100	12	6	15	44 s	no operation
101	12	5.9	15	54 s	no operation
102	12	5.9	15	44 s	no operation
103	11	5.9	14	27 s	6 min 42s
104	11	5	14	18 s	4 min 02s
105	11	6	14	22 s	4 min 25s
106	11	5.1	13	18 s	2 min 50s
107	11	6	13	20 s	3 min 25s
108	11	6	13	21 s	2 min 55s

Appendix F Input file of Simulation 12 in BRANZFIRE (Example)

Simulation 12

```
=====================================================================
Description of Rooms
=====================================================================
Room  1  :
         Room Length (m) =                                  7.32
         Room Width (m) =                                   3.66
         Maximum Room Height (m) =                          2.44
         Minimum Room Height (m) =                          2.44
         Floor Elevation (m) =                              0.000
         Room  1  has a flat ceiling.

         Wall Surface is plasterboard, painted gypsum paper-faced
         Wall Density (kg/m3) =                             731.0
         Wall Conductivity (W/m.K) =                        0.170
         Wall Emissivity =                                  0.88
         Wall Thickness (mm) =                              12.7

         Ceiling Surface is plasterboard, painted gypsum paper-faced
         Ceiling Density (kg/m3) =                          731.0
         Ceiling Conductivity (W/m.K) =                     0.170
         Ceiling Emissivity =                               0.88
         Ceiling Thickness (mm) =                           12.7

         Floor Surface is concrete
         Floor Density (kg/m3) =                            2300.0
         Floor Conductivity (W/m.K) =                       1.200
         Floor Emissivity =                                 0.50
         Floor Thickness = (mm)                             100.0

=====================================================================
Description of Wall Vents
=====================================================================
From room  1  to outside, Vent No 1
                  Vent Width (m) =                          1.180
                  Vent Height (m) =                         2.060
                  Vent Sill Height (m) =                    0.000
                  Vent Soffit Height (m) =                  2.060
                  Opening Time (sec) =                      0
                  Closing Time (sec) =                      0

=====================================================================
Description of Ceiling/Floor Vents
=====================================================================
=====================================================================
Ambient Conditions
=====================================================================
Interior Temp (C) =                                         20.0
Exterior Temp (C) =                                         20.0
Relative Humidity (%) =                                     65

=====================================================================
```

```
Tenability Parameters
=====================================================================
Monitoring Height for Visibility and FED (m) =              2.00
Occupant Activity Level =                                   Light
Visibility calculations assume:                             reflective
signs
FED Start Time (sec)                                        0
FED End Time (sec)                                          10000

=====================================================================
Sprinkler / Detector Parameters
=====================================================================
Sprinkler installed in Room                                 1
         Sprinkler is off.
         Response Time Index (m.s)^1/2 =                    35.0
         Sprinkler C-Factor (m.s)^1/2 =                     0.9
         Radial Distance (m) =                              1.6
         Actuation Temperature (C) =                        68.0
         Water Spray Density (mm/min) =                     0.0
         Distance below ceiling (mm) =                      76
         Ceiling Jet model used is NIST JET.

=====================================================================
Mechanical Ventilation (to/from outside)
=====================================================================
Mechanical Ventilation not installed in Room 1

=====================================================================
Description of the Fire
=====================================================================
Radiant Loss Fraction =                                     0.40
Soot Alpha Coefficient =                                    2.50
Smoke Epsilon Coefficient =                                 1.20
Smoke Emission Coefficient (1/m) =                          13.32
Characteristic Mass Loss per Unit Area (kg/s.m2) =          0.021
Air Entrainment in Plume uses McCaffrey (default)

Burning Object No 1

              Located in Room                               1
              Energy Yield (kJ/g) =                         41.2
              CO2 Yield (kg/kg fuel) =                      2.850
              Soot Yield (kg/kg fuel) =                     0.037
              Fire Height (m) =                             0.000
              Fire Location (m) =                           Centre

              Time (sec)              Heat Release (kW)
               0                      130
               3000                   130

=====================================================================
Postflashover Inputs
=====================================================================
Postflashover model is OFF.

=====================================================================
Flame Spread Inputs
=====================================================================

=======
```

Appendix G Procedure of calculating the mass loss rate of the heptane

$$\dot{m}'' = \frac{\dot{Q}}{A_f \chi \Delta H_c}$$ Equation 12.1

Where:

$\dot{m}''$ = free burn mass loss rate (kg/m^2.s)

$\dot{Q}$ = heat release rate (kW)

A_f = horizontal burning area of the fuel (m^2)

χ = combustion efficiency

ΔH_c = complete heat of combustion (kJ/g)

For the 0.46 m heptane pool fire

$$\dot{Q} = 130 kW$$

$$A_f = \pi * \left(\frac{0.46}{2} \right)^2 = 0.166 m^2$$

ΔH_C = 44.6 (MJ/kg) --- obtained from Table 3.3 (Karlsson and Quintiere 2000)

χ = 0.85 --- obtained from Page 31 (Heskestad and Bill 1987)

$$\dot{m}'' = \frac{\dot{Q}}{A_f \chi \Delta H_c} = \frac{130}{0.166 * 0.85 * 44.6} = 0.021 (kg / m^2 s)$$

For the 0.6 m heptane pool fire

$$\dot{Q} = 260kW$$

$$A_f = \pi * \left(\frac{0.6}{2}\right)^2 = 0.283m^2$$

ΔH_C = 44.6 (MJ/kg) --- obtained from Table 3.3 (Karlsson and Quintiere 2000)

χ = 0.85 --- obtained from Page 31 (Heskestad and Bill 1987)

$$\dot{m}'' = \frac{\dot{Q}}{A_f \chi \Delta H_c} = \frac{260}{0.283 * 0.85 * 44.6} = 0.024(kg/m^2 s)$$

Appendix H Simulations for analysing the input C-factor in BRANZFIRE (Simulation 172 ~ 549)

Table 12.7: Simulations for analysis the input C-factor in BRANZFIRE (Simulation 172 ~ 549)

Simulations for analysing the input C-factor for flush sprinkler			
Test	**Model**	**Simulation**	
		Near station (sprinkler distance below ceiling 0.0236 m)	**C-factor $(m/s)^{1/2}$**
5	G	172	0
		173	0.1
		174	0.2
		175	0.3
		176	0.4
		177	0.5
		178	0.6
		179	0.7
		180	0.8
		181	0.89
		182	1
		183	1.1
		184	1.2
		185	1.3
		186	1.4
		187	1.5
		188	1.6
		189	1.7
		190	1.8
		191	1.9
		192	2
Simulations for analysing the input C-factor for recessed sprinkler			
Test	**Model**	**Simulation**	
		Near station (sprinkler distance below ceiling 0.035 m)	**C-factor $(m/s)^{1/2}$**
3	D	193	0
		194	0.1
		195	0.2
		196	0.3
		197	0.4
		198	0.5
		199	0.6
		200	0.7
		201	0.8

		202	0.89
		203	1
		204	1.1
		205	1.2
		206	1.3
		207	1.4
		208	1.5
		209	1.6
		210	1.7
		211	1.8
		212	1.9
		213	2
6	C	214	0
		215	0.1
		216	0.2
		217	0.3
		218	0.4
		219	0.5
		220	0.6
		221	0.7
		222	0.8
		223	0.89
		224	1
		225	1.1
		226	1.2
		227	1.3
		228	1.4
		229	1.5
		230	1.6
		231	1.7
		232	1.8
		233	1.9
		234	2
8	A	235	0
		236	0.1
		237	0.2
		238	0.3
		239	0.4
		240	0.5
		241	0.6
		242	0.7
		243	0.8
		244	0.89

		245	1
		246	1.1
		247	1.2
		248	1.3
		249	1.4
		250	1.5
		251	1.6
		252	1.7
		253	1.8
		254	1.9
		255	2
9	A	256	0
		257	0.1
		258	0.2
		259	0.3
		260	0.4
		261	0.5
		262	0.6
		263	0.7
		264	0.8
		265	0.89
		266	1
		267	1.1
		268	1.2
		269	1.3
		270	1.4
		271	1.5
		272	1.6
		273	1.7
		274	1.8
		275	1.9
		276	2
11	B	277	0
		278	0.1
		279	0.2
		280	0.3
		281	0.4
		282	0.5
		283	0.6
		284	0.7
		285	0.8
		286	0.89
		287	1

		288	1.1
		289	1.2
		290	1.3
		291	1.4
		292	1.5
		293	1.6
		294	1.7
		295	1.8
		296	1.9
		297	2
12	B	298	0
		299	0.1
		300	0.2
		301	0.3
		302	0.4
		303	0.5
		304	0.6
		305	0.7
		306	0.8
		307	0.89
		308	1
		309	1.1
		310	1.2
		311	1.3
		312	1.4
		313	1.5
		314	1.6
		315	1.7
		316	1.8
		317	1.9
		318	2
16	C	319	0
		320	0.1
		321	0.2
		322	0.3
		323	0.4
		324	0.5
		325	0.6
		326	0.7
		327	0.8
		328	0.89
		329	1
		330	1.1

		331	1.2
		332	1.3
		333	1.4
		334	1.5
		335	1.6
		336	1.7
		337	1.8
		338	1.9
		339	2
Simulations for analysing the input C-factor for concealed sprinkler			
Test	**Model**	**Simulation**	
		Near station (sprinkler distance below ceiling 0.0254 m)	**C-factor $(m/s)^{1/2}$**
4	H	340	0
		341	0.1
		342	0.2
		343	0.3
		344	0.4
		345	0.5
		346	0.6
		347	0.7
		348	0.8
		349	0.89
		350	1
		351	1.1
		352	1.2
		353	1.3
		354	1.4
		355	1.5
		356	1.6
		357	1.7
		358	1.8
		359	1.9
		360	2
7	H	361	0
		362	0.1
		363	0.2
		364	0.3
		365	0.4
		366	0.5
		367	0.6
		368	0.7
		369	0.8
		370	0.89

		371	1
		372	1.1
		373	1.2
		374	1.3
		375	1.4
		376	1.5
		377	1.6
		378	1.7
		379	1.8
		380	1.9
		381	2
10	J	382	0
		383	0.1
		384	0.2
		385	0.3
		386	0.4
		387	0.5
		388	0.6
		389	0.7
		390	0.8
		391	0.89
		392	1
		393	1.1
		394	1.2
		395	1.3
		396	1.4
		397	1.5
		398	1.6
		399	1.7
		400	1.8
		401	1.9
		402	2
Simulations for analysing the input C-factor for recessed sidewall sprinkler			
Test	**Model**	**Simulation**	**C-factor (m/s)$^{1/2}$**
13	E_s	403	0
		404	0.1
		405	0.2
		406	0.3
		407	0.4
		408	0.5
		409	0.6
		410	0.7
		411	0.8

		412	0.89
		413	1
		414	1.1
		415	1.2
		416	1.3
		417	1.4
		418	1.5
		419	1.6
		420	1.7
		421	1.8
		422	1.9
		423	2
13	E_r	424	0
		425	0.1
		426	0.2
		427	0.3
		428	0.4
		429	0.5
		430	0.6
		431	0.7
		432	0.8
		433	0.89
		434	1
		435	1.1
		436	1.2
		437	1.3
		438	1.4
		439	1.5
		440	1.6
		441	1.7
		442	1.8
		443	1.9
		444	2
13	F_r	445	0
		446	0.1
		447	0.2
		448	0.3
		449	0.4
		450	0.5
		451	0.6
		452	0.7
		453	0.8
		454	0.89

		455	1
		456	1.1
		457	1.2
		458	1.3
		459	1.4
		460	1.5
		461	1.6
		462	1.7
		463	1.8
		464	1.9
		465	2
14	$E_s^{0.1}$	466	0
		467	0.1
		468	0.2
		469	0.3
		470	0.4
		471	0.5
		472	0.6
		473	0.7
		474	0.8
		475	0.89
		476	1
		477	1.1
		478	1.2
		479	1.3
		480	1.4
		481	1.5
		482	1.6
		483	1.7
		484	1.8
		485	1.9
		486	2
14	$E_r^{0.1}$	487	0
		488	0.1
		489	0.2
		490	0.3
		491	0.4
		492	0.5
		493	0.6
		494	0.7
		495	0.8
		496	0.89
		497	1

		498	1.1
		499	1.2
		500	1.3
		501	1.4
		502	1.5
		503	1.6
		504	1.7
		505	1.8
		506	1.9
		507	2
14	$E_s^{0.3}$	508	0
		509	0.1
		510	0.2
		511	0.3
		512	0.4
		513	0.5
		514	0.6
		515	0.7
		516	0.8
		517	0.89
		518	1
		519	1.1
		520	1.2
		521	1.3
		522	1.4
		523	1.5
		524	1.6
		525	1.7
		526	1.8
		527	1.9
		528	2
14	$E_r^{0.3}$	529	0
		530	0.1
		531	0.2
		532	0.3
		533	0.4
		534	0.5
		535	0.6
		536	0.7
		537	0.8
		538	0.89
		539	1
		540	1.1

		541	1.2
		542	1.3
		543	1.4
		544	1.5
		545	1.6
		546	1.7
		547	1.8
		548	1.9
		549	2

Appendix I Simulation results of Simulation 12 in BRANZFIRE (Example)

Simulation 12

```
======================================================================
Results from Fire Simulation
======================================================================

0 min    00 sec
         (0 sec)                        Room 1    Outside

         Layer (m)                      2.440
         Upper Temp (C)                 20.0
         Lower Temp (C)                 20.0
         HRR (kW)                       12.4

0 min    10 sec
         (10 sec)                       Room 1    Outside

         Layer (m)                      1.855
         Upper Temp (C)                 58.5
         Lower Temp (C)                 20.7
         HRR (kW)                       130.0

0 min    20 sec
         (20 sec)                       Room 1    Outside

         Layer (m)                      1.564
         Upper Temp (C)                 65.0
         Lower Temp (C)                 22.0
         HRR (kW)                       130.0

0 min    30 sec
         (30 sec)                       Room 1    Outside

         Layer (m)                      1.440
         Upper Temp (C)                 70.4
         Lower Temp (C)                 23.8
         HRR (kW)                       130.0

0 min    40 sec
         (40 sec)                       Room 1    Outside

         Layer (m)                      1.394
         Upper Temp (C)                 74.5
         Lower Temp (C)                 25.8
         HRR (kW)                       130.0

0 min    50 sec
         (50 sec)                       Room 1    Outside

         Layer (m)                      1.377
         Upper Temp (C)                 77.2
         Lower Temp (C)                 27.7
         HRR (kW)                       130.0
```

```
1 min    00 sec
         (60 sec)                    Room 1    Outside

         Layer (m)                   1.377
         Upper Temp (C)              79.3
         Lower Temp (C)              29.4
         HRR (kW)                    130.0

1 min    10 sec
         (70 sec)                    Room 1    Outside

         Layer (m)                   1.383
         Upper Temp (C)              80.9
         Lower Temp (C)              30.9
         HRR (kW)                    130.0

1 min    20 sec
         (80 sec)                    Room 1    Outside

         Layer (m)                   1.391
         Upper Temp (C)              82.2
         Lower Temp (C)              32.2
         HRR (kW)                    130.0

1 min    30 sec
         (90 sec)                    Room 1    Outside

         Layer (m)                   1.399
         Upper Temp (C)              83.3
         Lower Temp (C)              33.2
         HRR (kW)                    130.0

1 min    40 sec
         (100 sec)                   Room 1    Outside

         Layer (m)                   1.410
         Upper Temp (C)              84.3
         Lower Temp (C)              34.0
         HRR (kW)                    130.0

1 min    50 sec
         (110 sec)                   Room 1    Outside

         Layer (m)                   1.418
         Upper Temp (C)              85.2
         Lower Temp (C)              34.7
         HRR (kW)                    130.0

2 min    00 sec
         (120 sec)                   Room 1    Outside

         Layer (m)                   1.423
         Upper Temp (C)              85.8
         Lower Temp (C)              35.3
         HRR (kW)                    130.0

2 min    10 sec
         (130 sec)                   Room 1    Outside

         Layer (m)                   1.427
```

```
         Upper Temp (C)              86.3
         Lower Temp (C)              35.8
         HRR (kW)                    130.0

2 min    20 sec
         (140 sec)                   Room 1    Outside

         Layer (m)                   1.430
         Upper Temp (C)              86.8
         Lower Temp (C)              36.2
         HRR (kW)                    130.0

2 min    30 sec
         (150 sec)                   Room 1    Outside

         Layer (m)                   1.432
         Upper Temp (C)              87.2
         Lower Temp (C)              36.5
         HRR (kW)                    130.0

2 min    40 sec
         (160 sec)                   Room 1    Outside

         Layer (m)                   1.433
         Upper Temp (C)              87.6
         Lower Temp (C)              36.8
         HRR (kW)                    130.0

2 min    50 sec
         (170 sec)                   Room 1    Outside

         Layer (m)                   1.434
         Upper Temp (C)              87.9
         Lower Temp (C)              37.0
         HRR (kW)                    130.0

3 min    00 sec
         (180 sec)                   Room 1    Outside

         Layer (m)                   1.435
         Upper Temp (C)              88.2
         Lower Temp (C)              37.2
         HRR (kW)                    130.0

3 min    10 sec
         (190 sec)                   Room 1    Outside

         Layer (m)                   1.436
         Upper Temp (C)              88.6
         Lower Temp (C)              37.4
         HRR (kW)                    130.0

3 min    20 sec
         (200 sec)                   Room 1    Outside

         Layer (m)                   1.437
         Upper Temp (C)              88.8
         Lower Temp (C)              37.5
         HRR (kW)                    130.0

3 min    30 sec
```

```
         (210 sec)                  Room 1    Outside

         Layer (m)                  1.438
         Upper Temp (C)             89.1
         Lower Temp (C)             37.7
         HRR (kW)                   130.0

3 min    40 sec
         (220 sec)                  Room 1    Outside

         Layer (m)                  1.438
         Upper Temp (C)             89.4
         Lower Temp (C)             37.8
         HRR (kW)                   130.0

3 min    50 sec
         (230 sec)                  Room 1    Outside

         Layer (m)                  1.439
         Upper Temp (C)             89.6
         Lower Temp (C)             37.9
         HRR (kW)                   130.0

4 min    00 sec
         (240 sec)                  Room 1    Outside

         Layer (m)                  1.439
         Upper Temp (C)             89.9
         Lower Temp (C)             38.0
         HRR (kW)                   130.0

4 min    10 sec
         (250 sec)                  Room 1    Outside

         Layer (m)                  1.440
         Upper Temp (C)             90.1
         Lower Temp (C)             38.1
         HRR (kW)                   130.0

4 min    20 sec
         (260 sec)                  Room 1    Outside

         Layer (m)                  1.440
         Upper Temp (C)             90.4
         Lower Temp (C)             38.2
         HRR (kW)                   130.0

4 min    30 sec
         (270 sec)                  Room 1    Outside

         Layer (m)                  1.441
         Upper Temp (C)             90.6
         Lower Temp (C)             38.3
         HRR (kW)                   130.0

4 min    40 sec
         (280 sec)                  Room 1    Outside

         Layer (m)                  1.441
         Upper Temp (C)             90.8
         Lower Temp (C)             38.4
```

```
         HRR (kW)                    130.0

4 min    50 sec
         (290 sec)                   Room 1    Outside

         Layer (m)                   1.441
         Upper Temp (C)              91.0
         Lower Temp (C)              38.5
         HRR (kW)                    130.0

5 min    00 sec
         (300 sec)                   Room 1    Outside

         Layer (m)                   1.442
         Upper Temp (C)              91.2
         Lower Temp (C)              38.5
         HRR (kW)                    130.0

5 min    10 sec
         (310 sec)                   Room 1    Outside

         Layer (m)                   1.442
         Upper Temp (C)              91.4
         Lower Temp (C)              38.6
         HRR (kW)                    130.0

5 min    20 sec
         (320 sec)                   Room 1    Outside

         Layer (m)                   1.442
         Upper Temp (C)              91.6
         Lower Temp (C)              38.7
         HRR (kW)                    130.0

5 min    30 sec
         (330 sec)                   Room 1    Outside

         Layer (m)                   1.442
         Upper Temp (C)              91.8
         Lower Temp (C)              38.7
         HRR (kW)                    130.0

5 min    40 sec
         (340 sec)                   Room 1    Outside

         Layer (m)                   1.443
         Upper Temp (C)              92.0
         Lower Temp (C)              38.8
         HRR (kW)                    130.0

5 min    50 sec
         (350 sec)                   Room 1    Outside

         Layer (m)                   1.443
         Upper Temp (C)              92.2
         Lower Temp (C)              38.9
         HRR (kW)                    130.0

.............................

49 min   00 sec
```

```
         (2940 sec)                    Room 1    Outside

         Layer (m)                     1.368
         Upper Temp (C)                99.0
         Lower Temp (C)                37.6
         HRR (kW)                      130.0

49 min   10 sec
         (2950 sec)                    Room 1    Outside

         Layer (m)                     1.368
         Upper Temp (C)                99.0
         Lower Temp (C)                37.6
         HRR (kW)                      130.0

49 min   20 sec
         (2960 sec)                    Room 1    Outside

         Layer (m)                     1.368
         Upper Temp (C)                99.0
         Lower Temp (C)                37.6
         HRR (kW)                      130.0

49 min   30 sec
         (2970 sec)                    Room 1    Outside

         Layer (m)                     1.368
         Upper Temp (C)                99.0
         Lower Temp (C)                37.6
         HRR (kW)                      130.0

49 min   40 sec
         (2980 sec)                    Room 1    Outside

         Layer (m)                     1.368
         Upper Temp (C)                99.0
         Lower Temp (C)                37.7
         HRR (kW)                      130.0

49 min   50 sec
         (2990 sec)                    Room 1    Outside

         Layer (m)                     1.368
         Upper Temp (C)                99.0
         Lower Temp (C)                37.7
         HRR (kW)                      130.0

50 min   00 sec
         (3000 sec)                    Room 1    Outside

         Layer (m)                     1.368
         Upper Temp (C)                99.0
         Lower Temp (C)                37.7
         HRR (kW)                      130.0


================================================================
Event Log
================================================================
Sprinkler/Detector Actuated at 205.0 Seconds.
```

```
=====================================================================
Summary of End-Point Conditions in Room of Fire Origin
=====================================================================
The FED narcotic gases did not reach an incapacitating dose of 0.1
FED Radiation (incap) of 1  Not Reached.
An Upper Layer Temperature of 600 deg C Not Reached.
Visibility at 2m above floor reduced to 10 m at 7.0 Seconds.
Temperature at 2m above floor has reached 80 deg C at 65.0 Seconds.

=====================================================================
Initial Time-Step = 1.00 seconds.
Computer Run-Time = 101.1 seconds.
=====================================================================
```

Appendix J Predicted sprinkler response time in BRANZFIRE (Simulation 1 ~ 549)

Baseline scenario	
Simulation	**Predicted sprinkler response time (s)**
1	No operation
2	No operation
3	No operation
4	No operation
5	No operation
6	No operation
7	No operation
8	No operation
9	No operation
10	132
11	545
12	205
13	No operation
14	305
15	No operation
16	No operation
17	No operation
18	350
19	No operation
20	475
21	No operation
22	No operation
23	No operation
24	No operation
25	No operation
26	No operation
27	No operation
28	No operation
29	No operation
30	No operation
Scenario 1	
Simulation	**Predicted sprinkler response time (s)**
47	No operation
48	157
49	No operation
50	179

51	No operation
52	38
53	No operation
54	157
55	No operation
56	69
57	157
58	33
59	593
60	80
61	649
62	226
63	No operation
64	97
65	677
66	144
67	786
68	No operation
69	No operation
70	223
71	230
72	140
73	312
74	312
75	571
76	571
Scenario 2	
Simulation	**Predicted sprinkler response time (s)**
77	No operation
78	No operation
79	No operation
80	No operation
81	No operation
82	No operation
83	No operation
84	No operation
85	No operation
86	No operation
87	No operation
88	No operation
89	No operation
90	No operation
91	No operation

92	No operation
93	No operation
94	No operation
95	No operation
96	No operation
97	No operation
98	No operation
99	352
100	No operation
101	No operation
102	No operation
103	352
104	No operation
105	No operation
106	No operation
107	71
108	No operation
109	154
110	No operation
111	No operation
112	No operation
113	184
114	No operation
115	262
116	No operation
117	No operation
118	No operation
Scenario 3	
Simulation	**Predicted sprinkler response time (s)**
119	No operation
120	201
121	No operation
122	1895
123	No operation
124	365
125	No operation
126	201
127	No operation
128	129
129	No operation
130	40
131	No operation
132	99

133	No operation
134	1936
135	No operation
136	120
137	No operation
138	176
139	No operation
140	No operation
141	No operation
142	No operation
143	144
144	No operation
145	207
146	No operation
147	48
148	No operation
149	144
150	No operation
151	75
152	626
153	32
154	No operation
155	74
156	No operation
157	259
158	No operation
159	90
160	No operation
161	133
162	No operation
163	No operation
164	No operation
165	223
166	230
167	140
168	312
169	312
170	571
171	571
Scenario 4	
Simulation	**Predicted sprinkler response time (s)**
172	31
173	32

174	33
175	34
176	35
177	36
178	38
179	41
180	44
181	48
182	55
183	66
184	90
185	176
186	398
187	1480
188	No operation
189	No operation
190	No operation
191	No operation
192	No operation
193	103
194	106
195	109
196	112
197	116
198	120
199	125
200	130
201	137
202	144
203	152
204	162
205	175
206	192
207	215
208	251
209	323
210	572
211	No operation
212	No operation
213	No operation
214	103
215	106
216	109

217	112
218	116
219	120
220	125
221	130
222	137
223	144
224	152
225	162
226	175
227	192
228	215
229	251
230	323
231	572
232	No operation
233	No operation
234	No operation
235	26
236	26
237	27
238	27
239	28
240	29
241	29
242	30
243	31
244	32
245	32
246	33
247	35
248	36
249	38
250	41
251	47
252	59
253	83
254	164
255	393
256	57
257	58
258	60
259	61

260	63
261	65
262	67
263	69
264	71
265	74
266	77
267	81
268	85
269	90
270	96
271	104
272	113
273	127
274	153
275	211
276	420
277	69
278	71
279	73
280	74
281	77
282	79
283	81
284	84
285	87
286	90
287	94
288	98
289	103
290	109
291	116
292	125
293	137
294	154
295	181
296	238
297	431
298	102
299	105
300	107
301	110
302	113

303	117
304	120
305	124
306	128
307	133
308	139
309	145
310	152
311	161
312	171
313	184
314	200
315	222
316	255
317	315
318	477
319	171
320	182
321	197
322	216
323	241
324	277
325	333
326	467
327	No operation
328	No operation
329	No operation
330	No operation
331	No operation
332	No operation
333	No operation
334	No operation
335	No operation
336	No operation
337	No operation
338	No operation
339	No operation
340	127
341	131
342	136
343	141
344	146
345	153

346	160
347	169
348	179
349	191
350	207
351	227
352	255
353	298
354	380
355	612
356	No operation
357	No operation
358	No operation
359	No operation
360	No operation
361	64
362	65
363	66
364	67
365	68
366	69
367	70
368	71
369	72
370	73
371	75
372	76
373	77
374	79
375	81
376	82
377	84
378	86
379	89
380	91
381	93
382	161
383	166
384	172
385	178
386	186
387	194
388	203

389	213
390	226
391	241
392	259
393	283
394	316
395	364
396	450
397	661
398	No operation
399	No operation
400	No operation
401	No operation
402	No operation
403	151
404	156
405	161
406	167
407	173
408	181
409	189
410	199
411	210
412	223
413	239
414	260
415	288
416	328
417	397
418	564
419	No operation
420	No operation
421	No operation
422	No operation
423	No operation
424	154
425	159
426	165
427	171
428	177
429	185
430	194
431	204

432	216
433	230
434	248
435	271
436	302
437	350
438	438
439	702
440	No operation
441	No operation
442	No operation
443	No operation
444	No operation
445	92
446	95
447	98
448	102
449	106
450	111
451	117
452	123
453	131
454	140
455	153
456	169
457	194
458	237
459	352
460	2477
461	No operation
462	No operation
463	No operation
464	No operation
465	No operation
466	185
467	192
468	200
469	209
470	220
471	232
472	247
473	264
474	287

475	312
476	357
477	421
478	550
479	No operation
480	No operation
481	No operation
482	No operation
483	No operation
484	No operation
485	No operation
486	No operation
487	185
488	192
489	200
490	209
491	220
492	232
493	247
494	264
495	287
496	312
497	357
498	421
499	550
500	No operation
501	No operation
502	No operation
503	No operation
504	No operation
505	No operation
506	No operation
507	No operation
508	233
509	245
510	259
511	275
512	294
513	318
514	350
515	393
516	457
517	571

518	1099
519	No operation
520	No operation
521	No operation
522	No operation
523	No operation
524	No operation
525	No operation
526	No operation
527	No operation
528	No operation
529	233
530	245
531	259
532	275
533	294
534	318
535	350
536	393
537	457
538	571
539	1099
540	No operation
541	No operation
542	No operation
543	No operation
544	No operation
545	No operation
546	No operation
547	No operation
548	No operation
549	No operation

Appendix K Predicted sprinkler response times in BRANZFIRE with different input C-factor

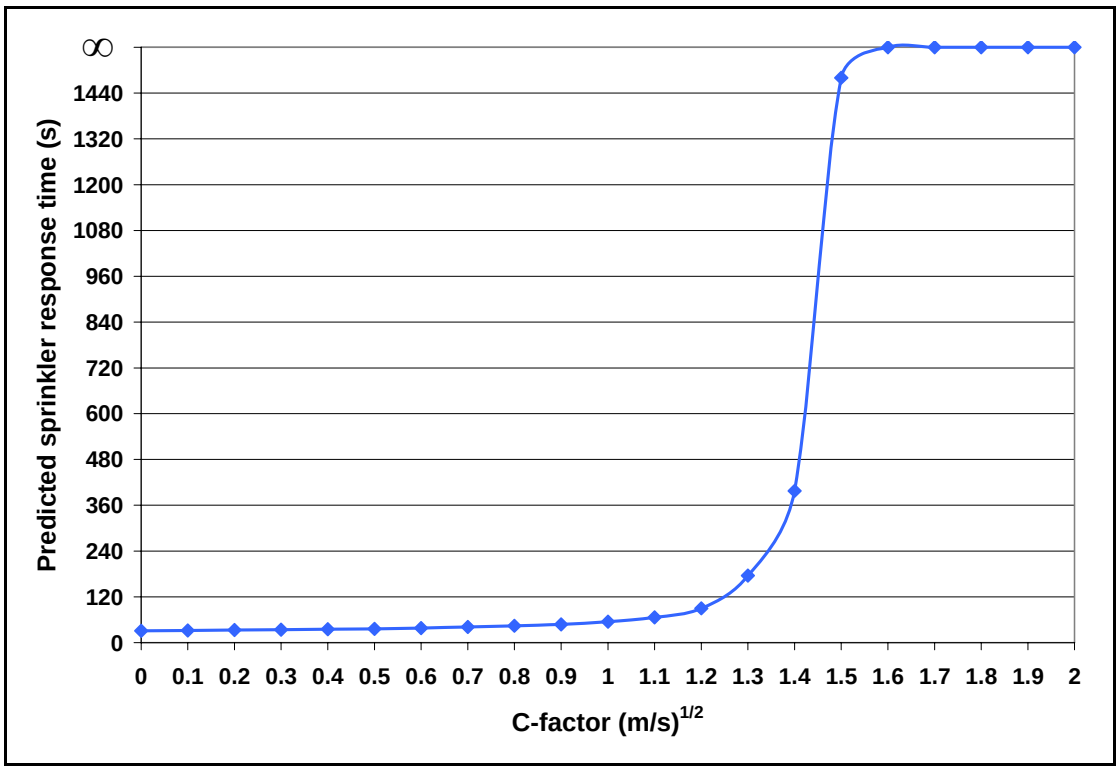

Figure 12.5: Sprinkler response times in BRANZFIRE for flush sprinkler (Simulation 172 ~ 192)

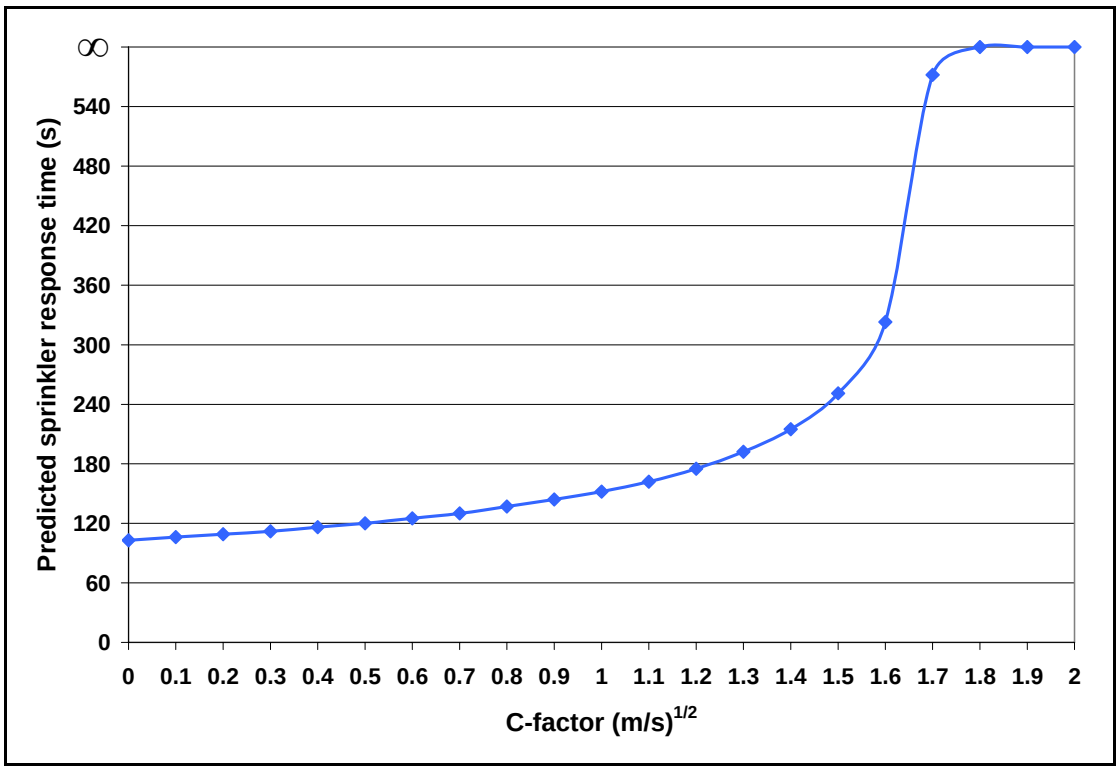

Figure 12.6: Sprinkler response times in BRANZFIRE for recessed sprinkler (Simulation 193 ~ 213)

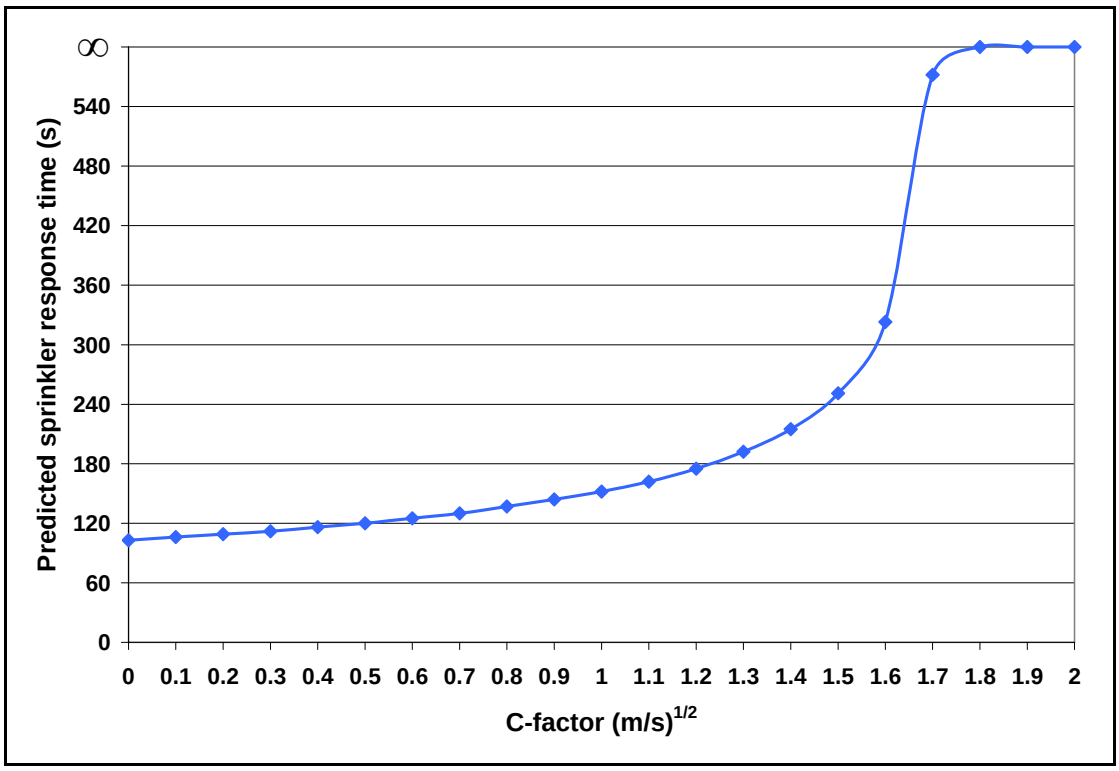

Figure 12.7: Sprinkler response times in BRANZFIRE for recessed sprinkler (Simulation 214 ~ 234)

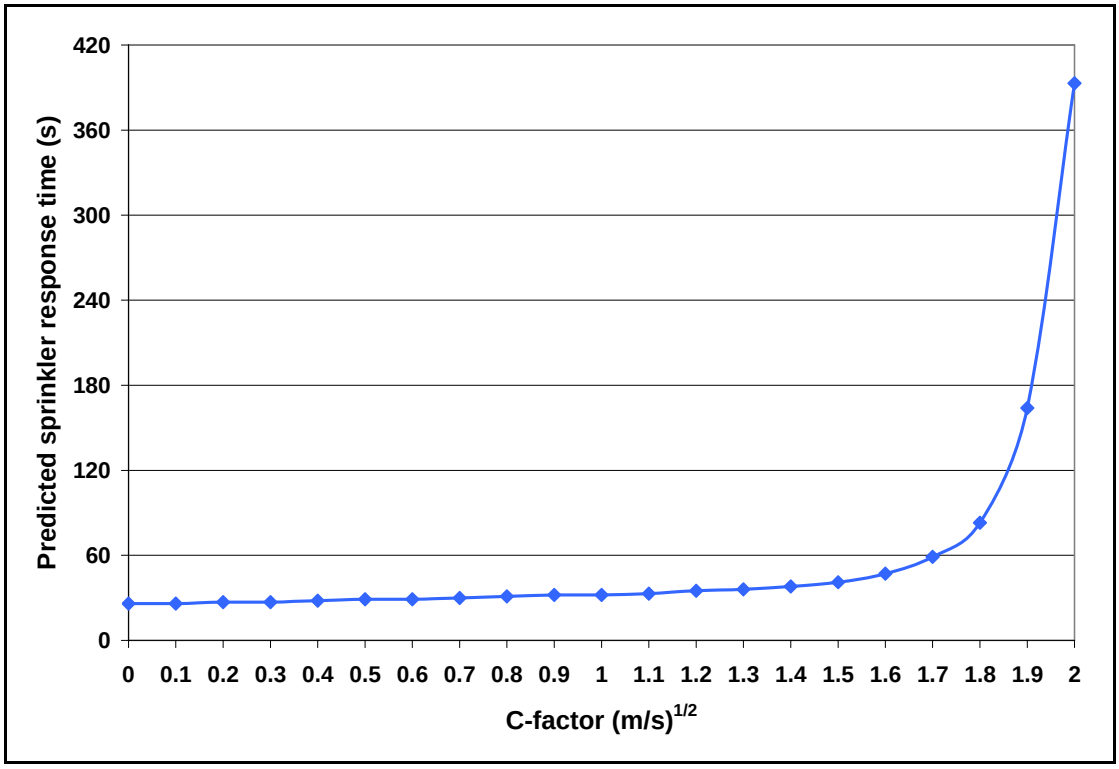

Figure 12.8: Sprinkler response times in BRANZFIRE for recessed sprinkler (Simulation 235 ~ 255)

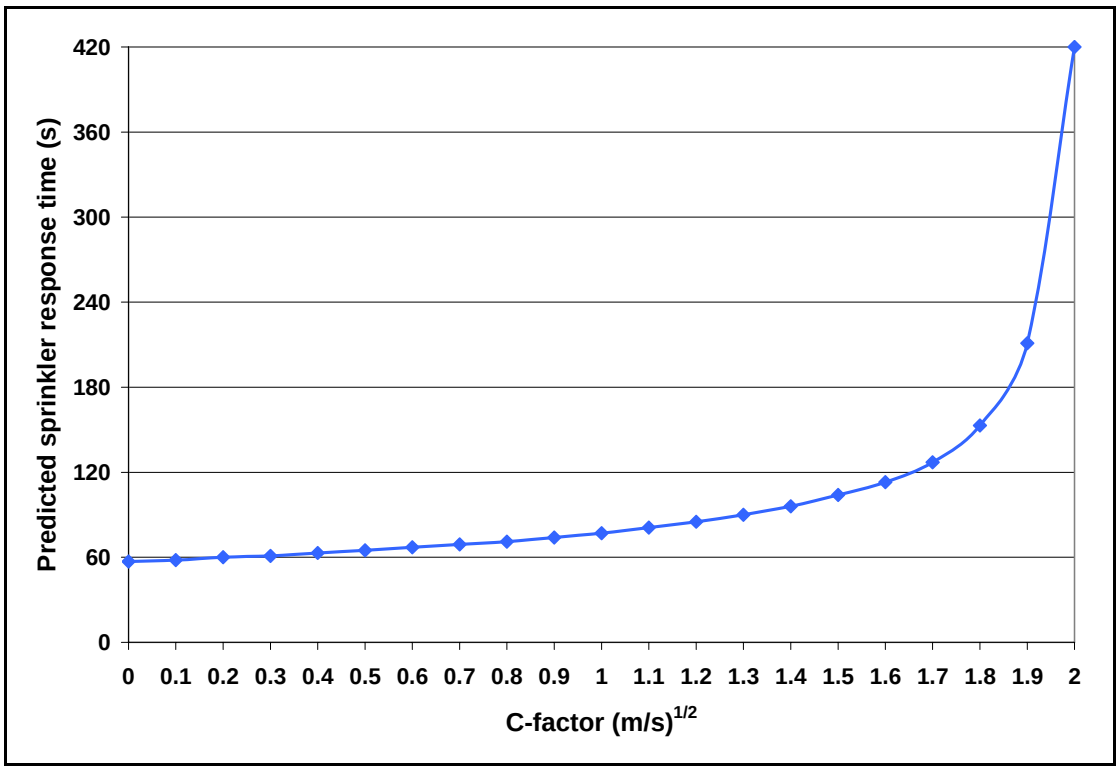

Figure 12.9: Sprinkler response times in BRANZFIRE for recessed sprinkler (Simulation 256 ~ 276)

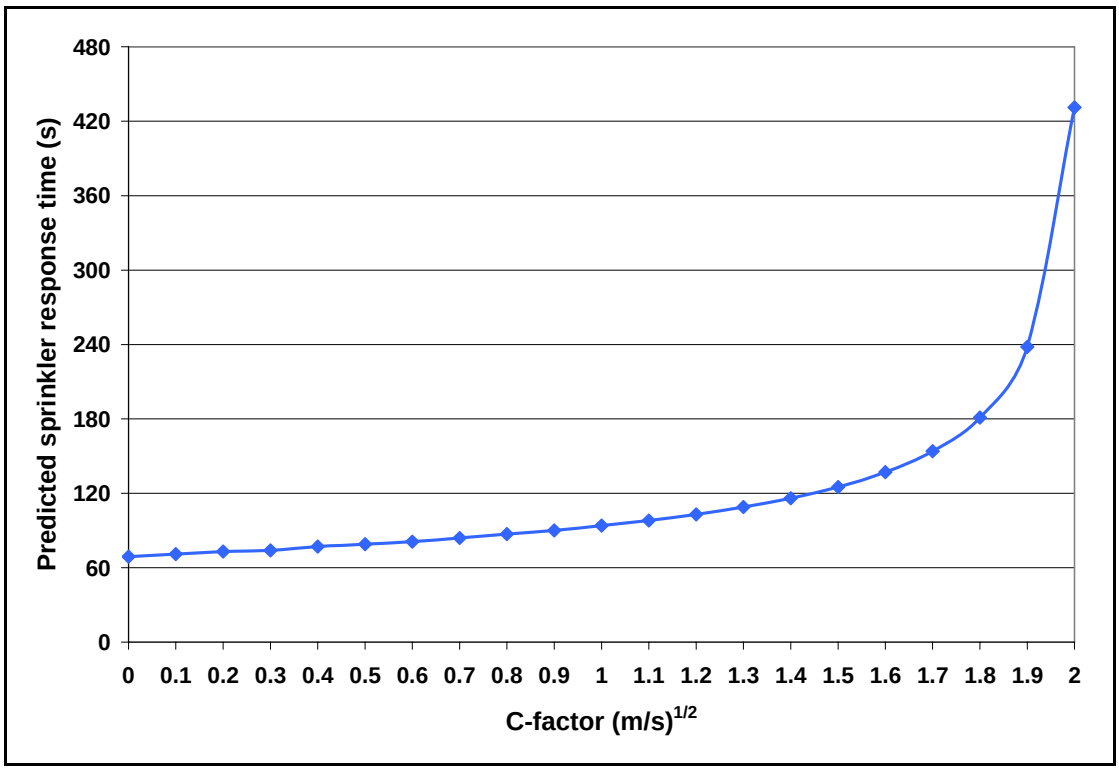

Figure 12.10: Sprinkler response times in BRANZFIRE for recessed sprinkler (Simulation 277 ~ 297)

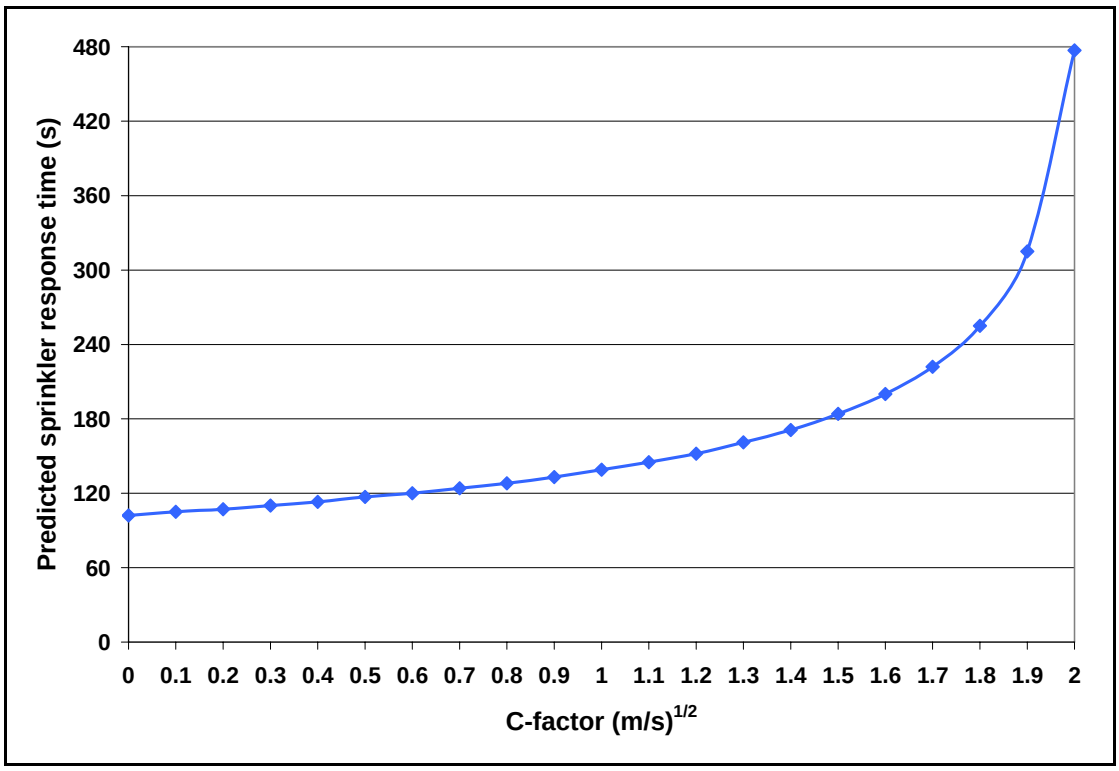

Figure 12.11: Sprinkler response times in BRANZFIRE for recessed sprinkler (Simulation 298 ~ 318)

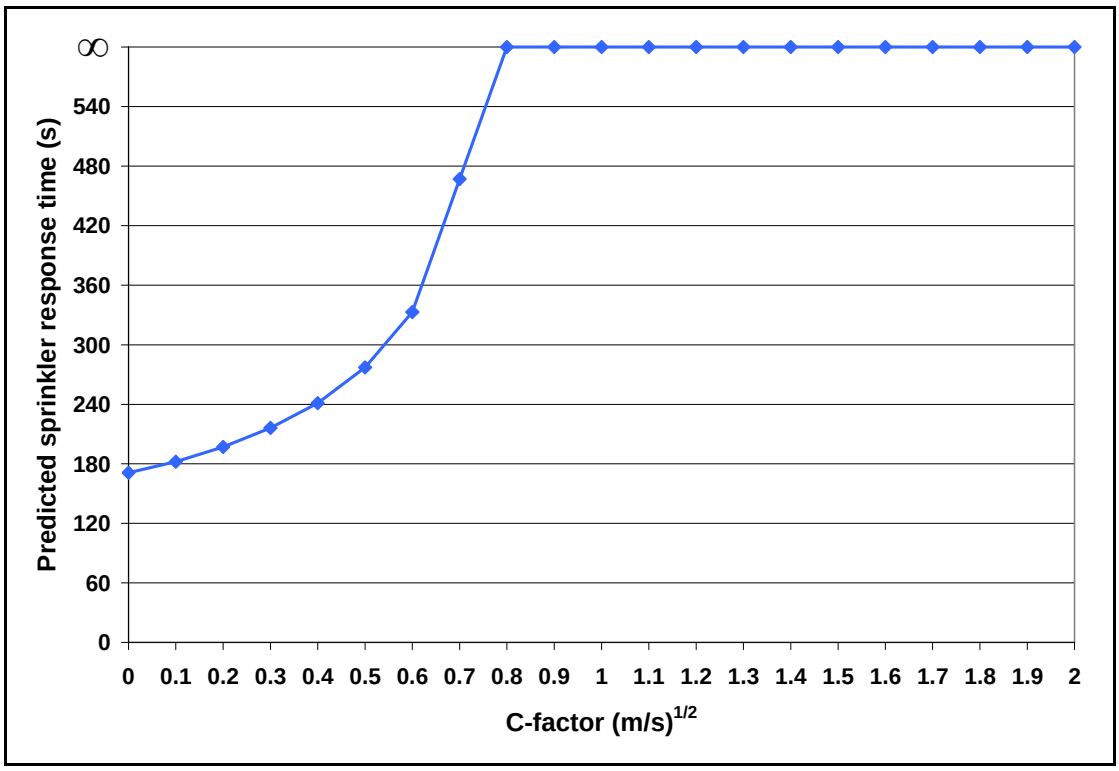

Figure 12.12: Sprinkler response times in BRANZFIRE for recessed sprinkler (Simulation 319 ~ 339)

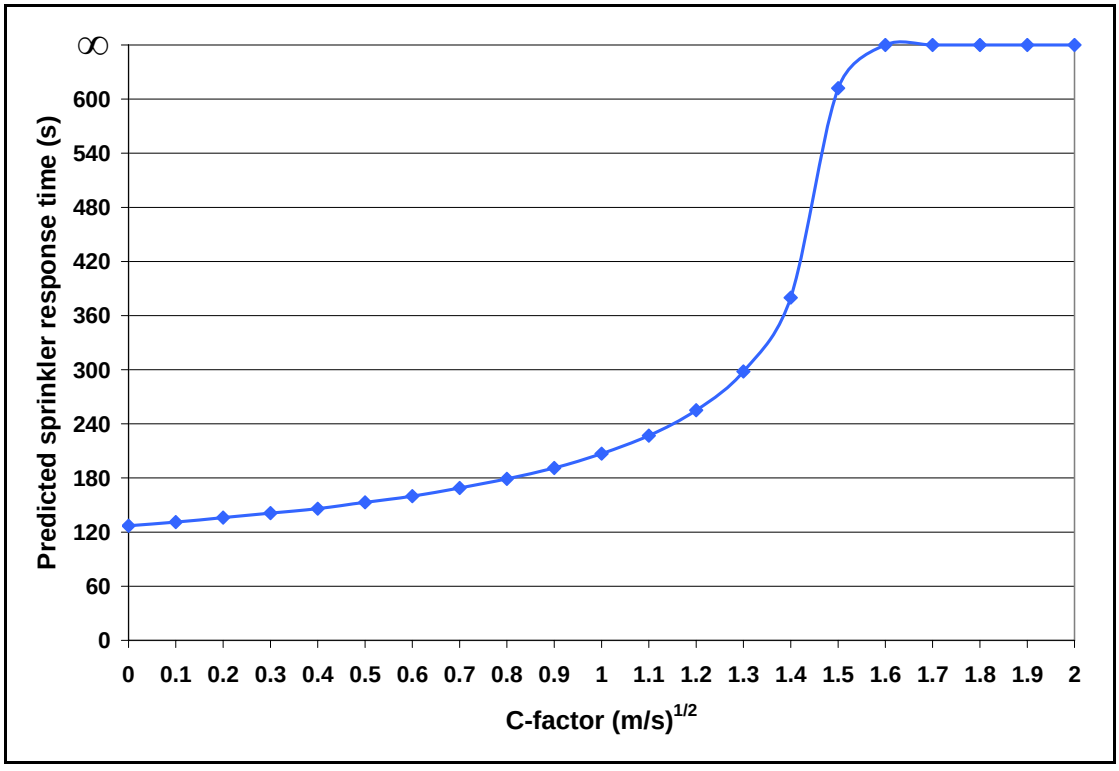

Figure 12.13: Sprinkler response times in BRANZFIRE for concealed sprinkler (Simulation 340 ~ 360)

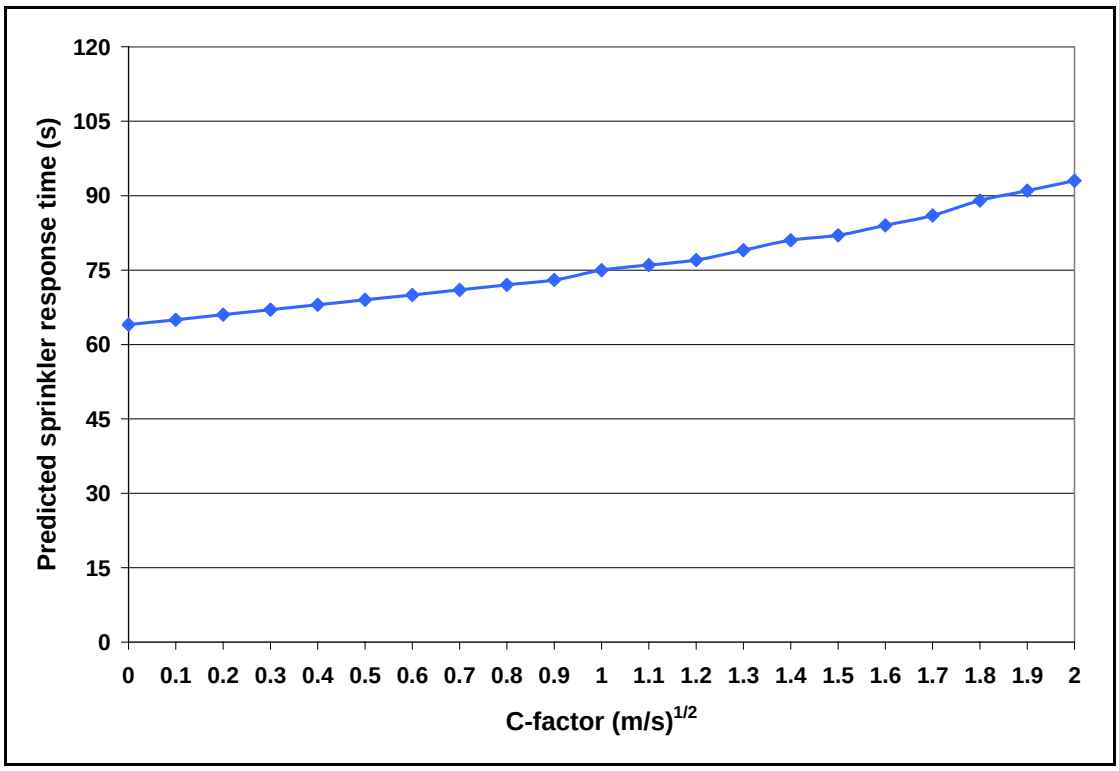

Figure 12.14: Sprinkler response times in BRANZFIRE for concealed sprinkler (Simulation 361 ~ 381)

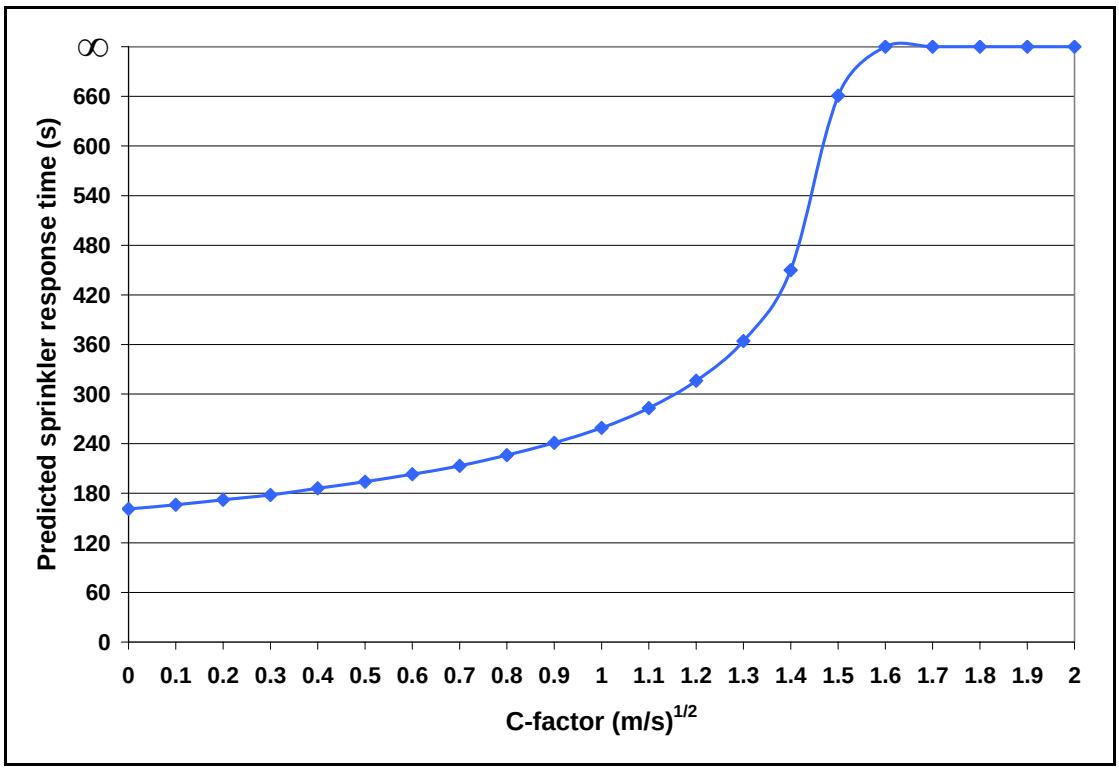

Figure 12.15: Sprinkler response times in BRANZFIRE for concealed sprinkler (Simulation 382 ~ 402)

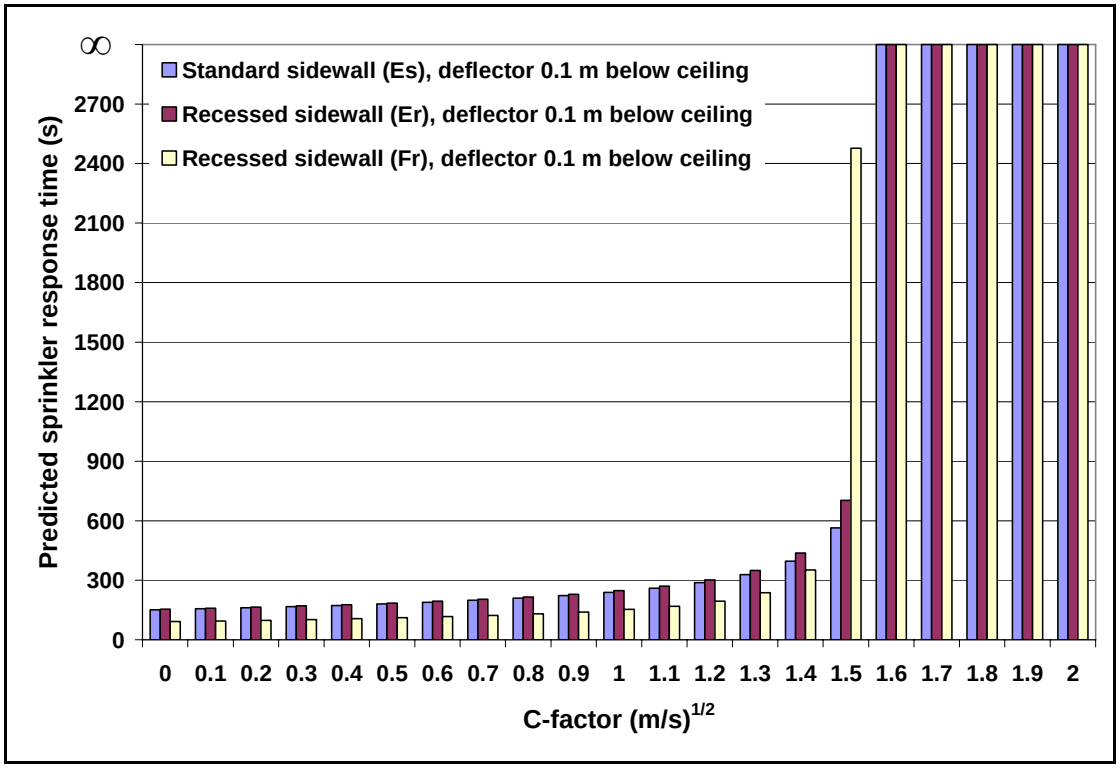

Figure 12.16: Sprinkler response times in BRANZFIRE for recessed sidewall sprinkler (Simulation 403 ~ 465)

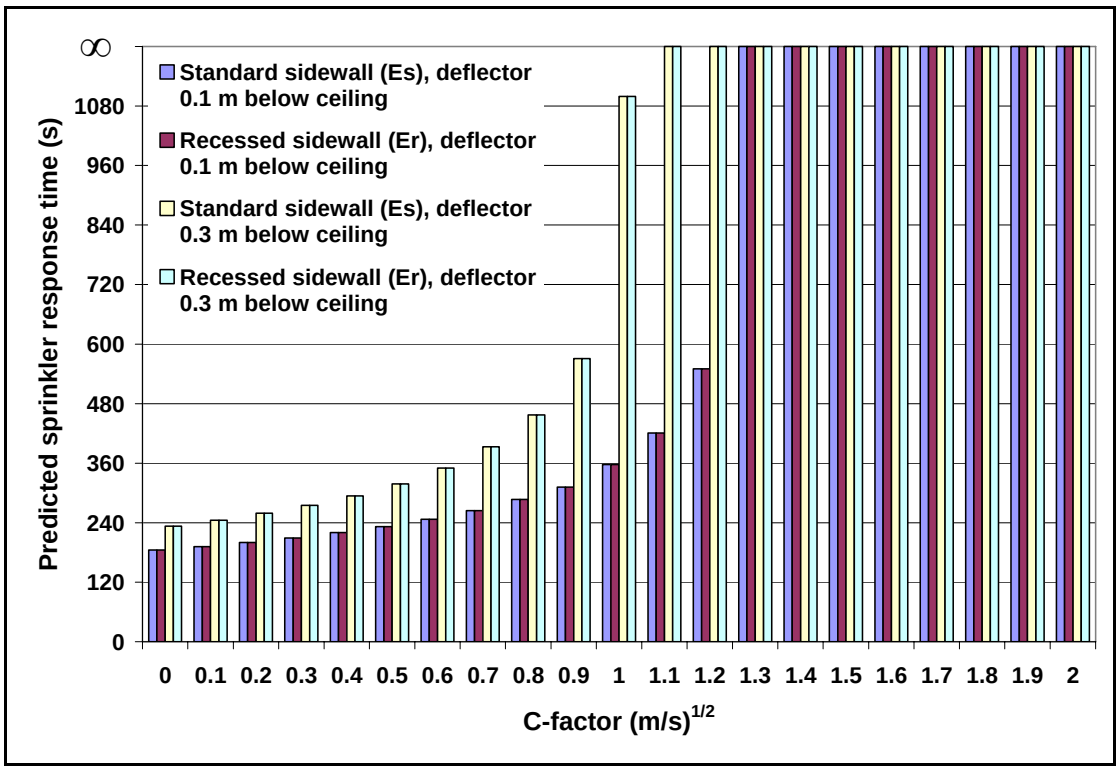

Figure 12.17: Sprinkler response times in BRANZFIRE for recessed sidewall sprinkler (Simulation 466 ~ 549)